# Synthesis of Glycomaterials for Multivalent Interactions

**Gokhan Yilmaz**

**A thesis submitted in partial fulfilment of the requirements for the degree of**

**Doctor of Philosophy in Chemistry**

**Department of Chemistry**


**September 2016**

# Declaration

I hereby declare that experimental work contained in this thesis is original research carried out by the author, unless otherwise stated, in the Department of Chemistry at the University of Warwick and Queen Mary University of London, October 2012 and September 2016. No material contained herein has been submitted for any other degree, or at any other institution.

Results from other authors are referenced in the usual manner throughout the text.

Date: 23 September 2016

**Gokhan Yilmaz**

# Table of Contents

# List of Figures

# List of Schemes

# List of Tables

# Abbreviations

| | |
|---|---|
| ACPA or V-501 | 4,4’-azobis(4-cyanopentanoic acid) |
| DLS | Dynamic Light Scattering |
| MTT | 3-(4,5-Dimethylthiazolyl-2)-2,5-diphenyltetrazolium bromide |
| WGA | Wheat germ agglutinin |
| AcGEA | 2-(2',3',4',6'-Tetra-O-acetyl-β-D-glucopyranosylxy) ethyl acrylate |
| ACN | Acetonitrile |
| AEMA | N-(2-aminoethyl)methacrylamide |
| AFM | Atomic force microscopy |
| AGET | Activators generated by electron transfer |
| AGET | Activators generated by electron transfer |
| AIBN | 4,4’-azobis-(2-methylpropionitrile) |
| APA | 3-azidopropylacrylate |
| ATRP | Atom transfer radical polymerization |
| BF3-OEt2 | Boron trifluoride diethyl etherate |
| ButenOx | 2-Butenyl-2-oxazoline |
| CB | Cucurbiturils |
| CD | Cyclodextrins |
| ConA | Concavalin |
| CPBDT | 2-Cyano-2-propyl benzodithioate |
| CROP | Cationic ring opening polymerization |
| CRP | C-reactive protein |

| | |
|---|---|
| CTP | (4-Cyanopentanoic acid)-4-dithiobenzoate |
| CuAAC | Copper-catalyzed azide-alkyne cycloaddition |
| DC-SIGN | Dendritic cell-specific intercellular adhesion molecule-3-grabbing non-integrin |
| DecenOx | 2-decenyl-2-oxazoline |
| DEGMA | Di(ethylene glycol) methyl ether methacrylate |
| DMA | N,N-dimethylacrylamide |
| DMF | Dimethylformamide |
| DMSO | Dimethyl sulfoxide |
| DOSY | Diffusion-ordered spectroscopy |
| DOX | Doxorubicin |
| eATRP | Electrochemically mediated ATRP |
| ECA | Erythrina cristagalli agglutinin |
| EDC | 1-[3-(dimethylamino)- propyl]-3-ethyl carbodiimide |
| EPR | Enhanced permeability and retention |
| ESI-MS | Electrospray ionization-mass spectrometry |
| EtOx | 2-ethyl-2-oxazoline |
| GC | Gas Chromotography |
| GPC | Gel Permeation Chromatography |
| GSK-3 | Glycogen synthase kinase-3 |
| HCV | Hepatitis C virus |
| HEMA | 2-hydroxyethyl methacrylate |
| HIV | Human immunodeficiency virus |
| IgA | Immunoglobulin A |

| | |
|---|---|
| iPOx | 2-isopropenyl-2-oxazoline |
| ITC | Isothermal titration calorimetry |
| LCST | Lower critical solution temperature behavior |
| MA | Methyl acrylate |
| MAA | Methacrylic acid |
| MAIpGLc | 3-O-methacryloyl-1,2:5,6-di-O-isopropylidine-D-glucofuranose |
| MALDI-ToF MS | Matrix assisted laser desorption/ionisation-time of flight mass spectroscopy |
| MC-SPR | Multichannel surface plasmon resonance |
| MeOTs | Methyl p-toluenesulfonate |
| MMA | Methyl methacrylate |
| MPH | Metalloid polymer hybrid |
| MUA | 11-mercaptoundecanoic acid |
| NCA | N-carboxyanhydrides |
| Neu5Ac | N-acetylneuramic acid |
| NHS | N-hydroxysuccinimide |
| NMP | Nitroxide-mediated polymerization |
| NOESY | 2D nuclear overhauser enhancement spectroscopy |
| OEGMA | Poly(ethylene glycol) methyl ether methacrylate |
| PA-IL | Paeruginosa lectin |
| PDI | Polydispersity index |
| PEG | Poly(ethylene glycol) |
| PEGMA | Poly(ethylene glycol) methacrylate |
| PNA | Peanut agglutinin |

| | |
|---|---|
| PTX3 | Pentraxin 3 |
| QCM | Quartz crystal microbalance |
| RAFT | Reversible addition-fragmentation chain transfer |
| RCA120 | Ricinus communis agglutinin |
| RES | Reticuloendothelial system |
| RID | Refractive index detector |
| ROMP | Ring-opening metathesis polymerization |
| SB-216763 | 3-(2,4-Dichlorophenyl)-4-(1-methyl-1H-indol-3-yl)-1H-pyrrole-2,5-dione |
| SEC | Size-exclusion chromatography |
| SET-LRP | Single electron transfer-living radical polymerization |
| SPR | Surface plasmon resonance |
| SPRmax | Surface plasmon resonance maximum band |
| TEM | Transmission Electron Microscopy |
| TGA | Thermal gravimetric analysis |
| TLC | Thin-layer chromatography |
| TMM-LRP | Transition metal-mediated living radical polymerization |
| VWD | Variable Wavelength Detector |
| β-CD | β-cyclodextrin |

# Acknowledgements

Firstly, I would like to thank Dr Remzi Becer for giving me this opportunity to work in our group. He always encourages us to learn more and more about chemistry. He provided an excellent support during my PhD. He was not only my supervisor, but also my friend. I will never forget his excellent guidance and advices.

I would also like to thank Professor David M. Haddleton for his generous support. He is always helpful and supportive for my research.

I am grateful to my funding sponsor, Turkish Military Academy, allowed me to study at University Warwick and Queen Mary University.

I thank all my friends in Becer group who are fantastic guys. Firstly, I would like to thank Dr Edward Malins who is the first graduated PhD student in our group. He was always very kind and helpful throughout my research. Secondly, I would like to thank my close friend (kardesim) Resat. We did not share only fume hood, but also our food, money, place, etc. I still remember taste of menemen when you cooked for breakfast in your place. I would like to special thank Suzan who is like a mummy in the lab. She always tries to keep lab clean and tidy. However, it is impossible because of us. Additionally, I would like to thank her again for lunches she brought from home for me when my wife was not here. I would also like to thank Manuel for his help and advices about chemistry since he is a good chemist. I would like thank Jackie who is the funniest Chinese guy I have met. I would like thank to Valentin for keeping the lab noise and also active. I will remember how to dance together. Many thanks is going to Yamin, he always brings fantastic Belgium chocolate from there. I also would like to thank Dr Ben Gridley, Elham, Martin, Dominic, Norlaily, Thian, Cigdem, Frederico and Martina for their valuable collaboration.

Lastly, I would like to thank my wife (Dilek'ime) and my parents for their endless patience and love. Without their support, I cannot make this happen. This thesis is dedicated to my wife and family.

# Abstract

Carbohydrates have attracted much attention to insert their biological properties into nanostructured materials due to their use for bio-mimetic purposes, their crucial role in bio-recognition processes at molecular level and their functional role in living systems. Glycopolymers, which are synthetic macromolecules with sugar moieties, exhibit a crucial role for many biological processes such as signal transmission, intercellular recognition and fertilization. The interaction between carbohydrates and lectins could be greatly enhanced by the multivalent effect of densely packed carbohydrate molecules with unique functionalities, which is known as the “glycocluster effect”. Therefore, the investigation of this specific interaction between glycopolymer and protein is very important to create more complex and biologically relevant carbohydrate mimics.

Well-defined amphiphilic block glycopolymers with the same mannose content have been self-assembled in aqueous solution to form glyconanoparticles with different morphologies (spherical, worm-like micelles and vesicles). The size and shape of nanoparticles have significant effects on the binding affinities with dendritic cell-specific intercellular adhesion molecule-3-grabbing non-integrin (DC-SIGN). Moreover, the obtained glyco-micelles have a great potential for drug delivery applications.

Glycopolymer-coated gold nanoparticles (glyco-AuNPs) which were synthesized with reversible addition-fragmentation chain transfer (RAFT) polymerization were combined with doxorubicin (DOX) as a model anticancer drug by creating a pH-sensitive hydrazone linkage in the presence of cysteine (Cys) and a cross-linker for both chemotherapy and radiation therapy.

The reversible single-chain glycopolymer folding structures in α-shape with different sugar moieties were created to investigate the influence of this folded collapse on the binding capability with different lectins. The single-chain folding structures were achieved by the host-quest interaction of β-cyclodextrin and adamantane in very high diluted aqueous solution. The binding results evidenced

that these single-chain folded structures enhanced greatly the multivalent interaction.

A new *S*-glucosyl substituted 2-oxazoline glycomonomer was synthesized via thiol-ene "*click*" chemistry and then polymerized using cationic ring-opening polymerization (CROP) technique. In order to investigate the effect of *S*-glucosyl substituent linker length on the cloud point and binding ability systematically, A series of well-defined glyco-copolymers with different sugar linker length to the polymer backbone was prepared. The obtained results showed that it has a significant influence on the cloud point and binding capability.

# Chapter 1 Introduction on the preparation of glycomaterials and their interactions with lectins

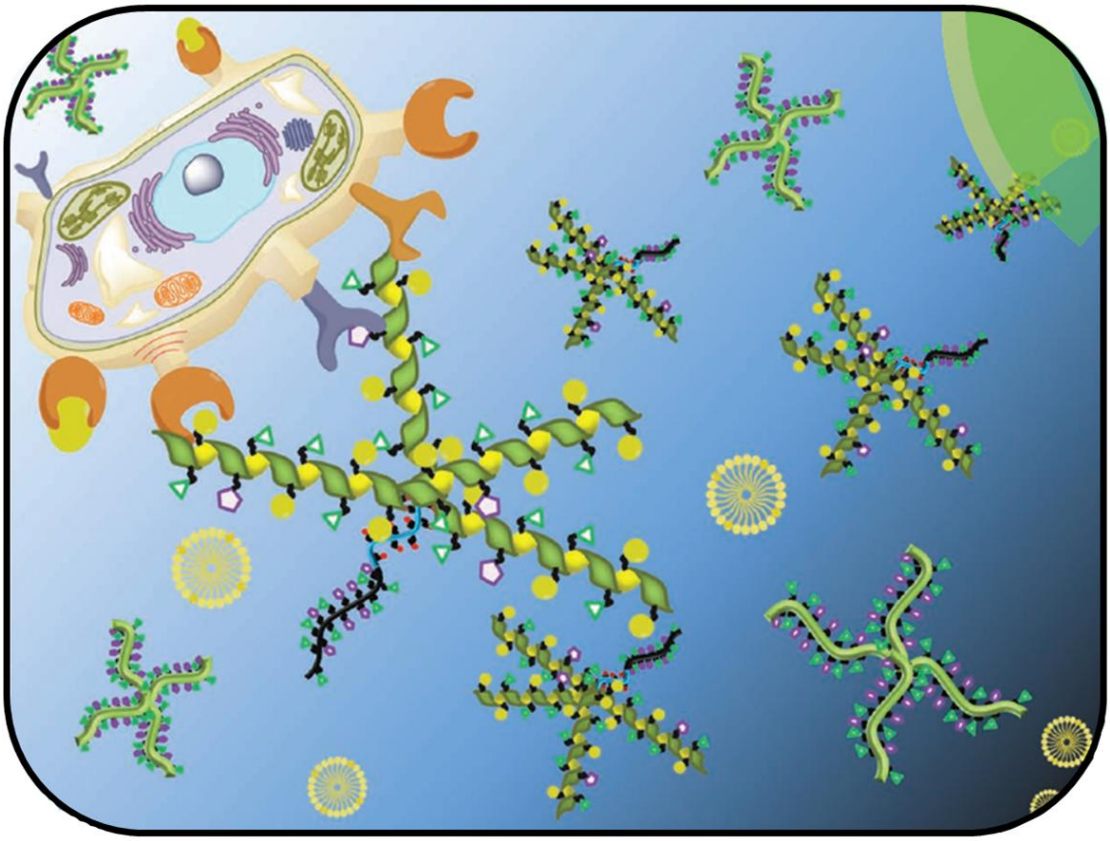

*Advances in the controlled radical polymerization and click reaction techniques have allowed the preparation of more complex and well-defined glyco-polymers/particles in various architectures, such as micelles, dendrimers and nanogels. In the last decade, functionalized and self-assembled nano-objects and scaffolds containing glycopolymers were designed to utilize in several biological and biomedical applications (i.e. pathogen detection, inhibitors of toxins and lectin-based biosensors). These studies facilitated the understanding and investigation of the sugar code based on the carbohydrate-lectin interactions that are significantly influenced by the glycopolymeric architecture, valency, size, and density of binding elements. In this chapter, the synthesis of functionalized glyco-polymers/particles, their interactions with lectins and their potential applications are highlighted.*

## 1.1 Multivalent carbohydrate-lectin interactions of glycomaterials

Carbohydrates differ from other biological molecules in terms of their monomeric units and their ability to form precisely branched macromolecules as in glycoproteins.[1-3] Polymer chemists and biologists are still investigating in order to answer two critical questions that established the natural sugar code: How are carbohydrates involved in lectin specific recognition events? How do carbohydrates influence the properties of the lectins to which they are attached?

Oligosaccharides have a high-density coding capacity due to the variations in anomeric status, linkage positions, ring size, branching, and introduction of site specific substitutions.[4,5] Their major function in biological environment is to serve as recognition markers.[6] A wide range of oligosaccharide structures allow them to specifically bind to catalytically active sites of lectins, to modulate the interactions of glycoconjugates with other molecules, and to affect the rate of binding and recognition processes which involve conformational changes due to naturally evolved sugar code.[7,8] This special sugar coding system let oligosaccharides to have crucial biological roles with unusual oligosaccharide sequences and presentations of common terminal sequences as well as further modifications of the sugars themselves.[9,10] However, the detailed understanding in terms of functions of oligosaccharides is rather limited due to demanding synthesis requirements of such structures. Although there have been major developments on chemical synthesis of oligosaccharides, such as introduction of good anomeric leaving groups and advances in the solid phase synthesis techniques, it is still demanding to isolate, purify, and analyze the exact structure of oligosaccharides.[11]

Glycopolymers, which are synthetic macromolecules with sugar moieties, have been considered as alternative structures to oligosaccharides.[12,13] In general, they exhibit a crucial role for many biological processes such as signal transmission, intercellular recognition and fertilization.[14-17] Although the interactions between carbohydrates and lectins are weak, it could be greatly enhanced by the multivalent effect of densely packed carbohydrate molecules with unique functionalities, which is also known as the “glycocluster effect”.[18,19] Hence, fundamental understanding

and investigation of these specific interactions between glycopolymers and proteins with high selectivity and strength are becoming more attractive for polymer chemists due to their potential use in biomimetic applications and human therapeutics. Despite the fact that many different types of glycopolymers including linear and spherical structures and glycodendrimers in the form of micelles, vesicles and micro/nano particles have been prepared to date, it is still challenging to synthesize designed glycopolymers with precisely controlled chain lengths, carbohydrate compositions and chain architectures. Nevertheless, some recent literature reports have demonstrated a reasonable control in chain length, architecture, monomer sequence, chain folding, and tertiary structures to achieve the preparation of precision glycopolymers.

During the last decade, there has been a great deal of interest in the integration of nanotechnology and carbohydrates.[20,21] The advances in glyconanotechnology have allowed creation of different bioactive glyconanostructures for various medical applications such as drug delivery, biomaterials, gene therapy, pathogen detection, inhibitors of toxins and lectin-based biosensors.[22-25] Nanoparticles functionalized with carbohydrates presented a highly multivalent vehicle for interaction with lectins and allowed the immobilization of ligands at relatively high local concentrations on small surfaces.[26] Carbohydrates have attracted much attention to insert their biological properties into nanostructured materials due to their utilization for biomimetic purposes, their crucial role in bio-recognition processes at molecular level and their functional role in living systems.[27] Glyconanoparticles as carbohydrate-based systems provide in a similar manner to mimic the behavior of naturally existing glycocalyx.[28] Therefore, the fabrication and engineering of highly innovative glyconanoparticles with unique physiochemical properties help to further enhance their specific recognition properties on multivalent scaffolds in glycoscience.

One of the first reports on the synthesis of glycopolymers was published in 1944.[29] The formation of a viscous polymer solution after heating tetra-allyl-α methyl glucosides was firstly introduced by Nichols and Yanovsky. Further reports on the

polymerization of allyl ethers of carbohydrates emerged in a short time after this report.[30,31] However, until the last decade, there had been limited attempts to react a functional polymeric backbone with a carbohydrate to obtain a glycopolymer because of the difficulty of introducing sufficiently reactive pendant groups onto the polymer backbone to react with carbohydrates. This obstacle has been overcome in the last decade by combination of living polymerization techniques and click reactions.

Generally, there are two advanced synthesis methods to prepare well-defined glycopolymers, which are the polymerization of carbohydrate-bearing monomers without the deprotection step and post-polymerization modifications of functional polymers with carbohydrates prepared *via* combination of controlled/living polymerization techniques and click reactions. The widely used controlled/living radical polymerization techniques to obtain well-defined glycopolymers can be listed as nitroxide-mediated polymerization (NMP), atom transfer radical polymerization (ATRP), reversible addition-fragmentation chain transfer (RAFT), single electron transfer-living radical polymerization (SET-LRP), ring-opening metathesis polymerization (ROMP), and ionic ring-opening polymerization.[32-34] Besides, a large number of reports have emerged on the synthesis of glycopolymers *via* conventional free-radical polymerization in both aqueous and non-aqueous media. These techniques are relatively more tolerant to prepare well-defined glycopolymers with different functionalities. Moreover, the most important advantage of these techniques is their applicability to use a very wide range of monomers under various experimental conditions. According to these promising recent approaches on the preparation of sequenced glycopolymers as well as studying their interactions with lectins, polymer scientists have contributed massively in the last decade to the design of the new generation of sequence controlled glycopolymers and also complex glyconanoparticles with different architectures. Selected glycopolymer synthesis techniques that were used in this thesis were discussed in the following sections.

## 1.2 Synthesis of glycopolymers

### 1.2.1 Conventional free radical polymerization

Conventional free-radical polymerization has been one of the most widely used polymerization techniques since the 1940s. Even though there are many elegant control/living radical polymerization techniques, free radical polymerization is still one of the most preferred techniques to generate glycopolymers. The polymerization is initiated by free radical initiators and generally used to polymerize vinyl saccharides to obtain glycopolymers. The first paper published by Kimura *et al.* in 1961 based on the free radical homo- and copolymerization of 3-O-methacryloyl-1.2,5.6-diisopropylidene-D-glucose.[35] In the following years, the interest on the free radical polymerization of glycomonomers increased significantly due to its advantages, which are the tolerance to impurities and the wide range of reaction conditions in terms of the solvents and temperatures. At the same time, high dispersities of the obtained polymers and insufficient controlling of terminal functionalities are the most critical disadvantages. Therefore, this technique is not recommended to synthesize well-defined glycopolymers with high molar masses, low dispersities and functional end groups. It was highlighted here to provide controversial review for readers.

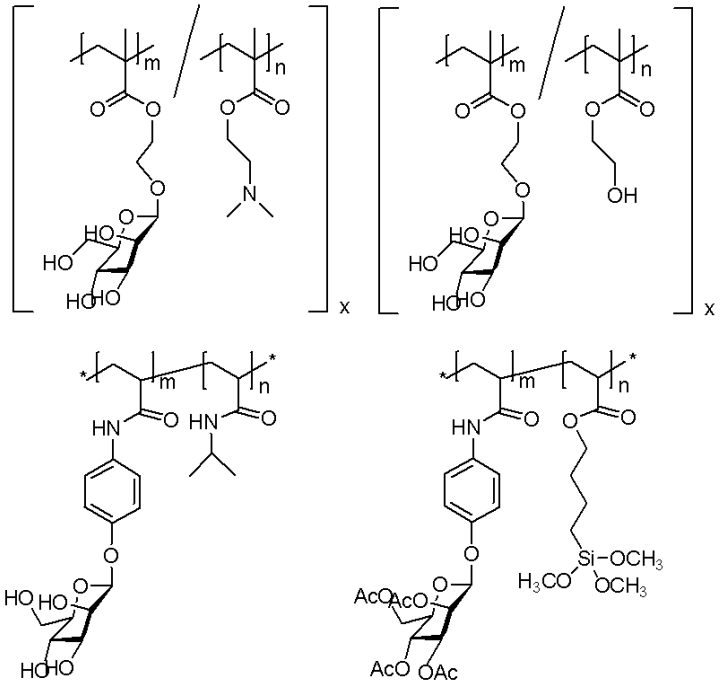

**Figure 1.1.** The glycopolymers synthesized *via* free-radical polymerization.

A small library of statistical copolymers, poly[2-(α-D-mannopyranosyloxy)ethyl-co-2-dimethylaminoethyl methacrylate]s, poly(ManEMA-co-DMAEMA), were prepared by free radical polymerization.[36] (Figure 1.1 top left) The resulting glycopolymers demonstrated the binding affinity with plasmid DNA while displaying a cluster glycoside effect. Further research was done to better understand the cellular uptake of these polymers, the same monomer was copolymerized with HEMA.[37] (Figure 1.1 top right) The glycopolymers were then quickly taken up by HeLa cells, a cell lines that has a high affinity to mannose.

The glycomonomer, p-acrylamidophenyl-α-D-mannopyranoside (Man), was copolymerized with NIPAm *via* emulsion polymerization in the presence of a crosslinker.[38] (Figure 1.1 bottom left) Even though the resulting nanoparticles showed the specific interaction with Con A, the binding kinetics could be enhanced by swelling of the nanoparticles. A similar monomer was also copolymerized with 3-(trimethoxysilyl) propyl methacrylate in another work.[39] (Figure 1.1 bottom right) Furthermore, an acetyl protected monomer was employed to accommodate the solubility of the hydrophobic 3-(trimethoxysilyl) propyl methacrylate. The immobilization of these glycopolymers on a silica surface could allow the development of a sensor that could selectively detect ConA or other proteins.

### 1.2.2 Ring-opening polymerization (ROP)

Ring opening polymerization (ROP), one of the earliest controlled/living radical polymerization techniques, usually provides a sufficient control for cyclic monomers. Even though the polymerizations of 6-membered ring monomers are thermodynamically unfavorable, 3-,4-,5-,7- and 8-membered rings can be polymerized successfully *via* ROP. Ring-opening polymerizations depending on the catalyst type can be listed as cationic, anionic and enzymatic ring-opening. It is also possible to synthesize complex architectures such as star polymers.[40-42]

The synthesis of glycopolymers was firstly reported in the 1980s by using the anhydride form of various sugars.[43,44] Glycomonomers based on *N*-carboxyanhydrides (NCA) were used to obtain well-defined glycopolymers in many studies.[45,46] Recently, Heise and co-workers reported the synthesis of polypeptide

block copolymers with different block length ratios using sequential ring opening metathesis polymerization (ROMP) of benzyl-L-glutamate and propargylglycine (PG) *N*-carboxyanhydrides (NCA).[47] (Figure 1.2 left)

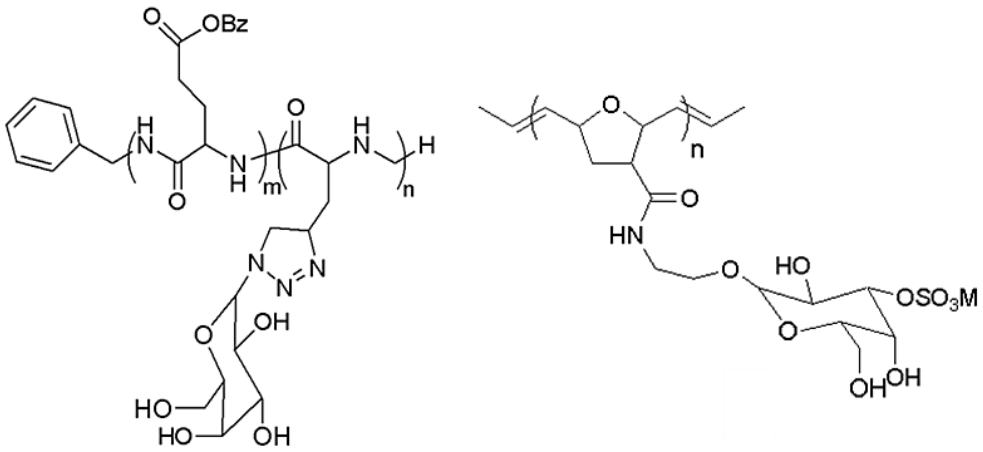


**Figure 1.2.** A schematic representation of of glycopolymers synthesized *via* ROP.

Kiessling *et al.* succeeded to prepare mannose- and galactose-containing glycopolymers *via* ROMP in water in the presence of $RuCl_3$ at 55 °C.[48] These glycopolymers showed the control of multivalent interactions by altering the binding epitope density. (Figure 1.2 right) Then, this work was extended to investigate the effect of the simultaneous existence of cis- and trans-isomers in the backbone. Moreover, they have discussed several mechanisms of multivalent ligand binding, which are chelate effect, subsite binding, steric stabilization, statistical effect, and receptor clustering. More work has been carried out by the group of Kiessling on sulfated saccharides.[49] By using a similar strategy, ROMP was used to synthesize sulfated glycopolymers showing efficient binding towards L- or P-selectin. Furthermore, they observed that glycopolymers synthesized in the presence of high content of ruthenium trichloride resulted in discoloration of polymers thhat indicated the contamination of materials.

The cationic ring opening polymerization (CROP) has only been performed a few times in glycopolymer synthesis because the direct polymerization of carbohydrate-containing oxazoline-monomers is still very limited. Therefore, it is really necessary to develop new strategies to prepare different types of glycopolymers with various tuneable properties *via* CROP. 2-Substituted-2-oxazolines are the most commonly

used monomers for CROP and they are promising candidates for biological applications due to their biocompatibility and low cytotoxicity. There are only two reports dealing with the direct cationic ring opening polymerization of a sugar-functionalized 2-oxazoline so far. Đ The first study was performed in 2010 by Kojima *et al.* and two different S-galactosyl substituted oxazolines were prepared in three steps and polymerized *via* CROP (Đ = 1.20-1.24).[50] After the deprotection, the obtained poly(2-oxazoline)s having pendant sugar showed the specific interaction with the $RCA_{120}$. After a very short time, Schubert and his coworkers reported the synthesis of glucose-substituted 2-oxazoline monomer and its co-polymerization by CROP in the presence of 2-oxazoline-based monomers.[51] This new glucose-substituted 2-oxazoline monomer was prepared by using copper-catalyzed azide-alkyne cycloaddition (CuAAC) click chemistry after many multi-step reactions. A series of well-defined block glycocopolymers with different chain lengths was prepared in acetonitrile at 120 °C.

Basically, even though ROP polymerization has had a long history and has been widely used for the polymerization of different functional cyclic monomers, the use of it in the direct polymerization of carbohydrate-containing cyclic monomers is rather limited. Another critical disadvantage of using ROMP polymerization is that the toxic heavy metals used in polymerization could potentially contaminate the final polymers; hence the removal of these catalysts has to be scrutinized, especially for biological applications.

### 1.2.3 Reversible addition-fragmentation transfer (RAFT) polymerization

RAFT polymerization of various monomers using dithioesters and trithiocarbonates as chain transfer agents were reported by the scientists in CSIRO in early 1998.[52] After its discovery, it has become one of the most popular living polymerization processes. There are many articles reporting the synthesis of glycopolymers *via* RAFT. The main advantages of this technique are; (i) it can be applied to a wide range of functional monomers and allows the preparation of polymers in various architectures such as random, block, gradient and star shaped copolymers, (ii) higher molar masses, are easily achievable while maintaining low molar mass

distributions, (iii) it does not require the use of metal catalysts which is important in bio-applications. RAFT polymerization is controlled by a reversible transfer reaction between growing radicals as active species and RAFT agents as dormant species. The chemical structures of the RAFT agents are crucial to provide the delicate balance to precisely control the chain length. However, due to the use of free radical initiators as a radical source the chain end fidelity of the polymers are generally lower than 90%. As the chemical nature of the glycopolymers has a crucial importance on the bioactivity more suitable reaction conditions are required. Besides, RAFT polymerizations are usually carried out in the range of 60 to 70 °C. However, recent literature reports show that it is also possible to perform RAFT polymerizations at room temperature in aqueous solutions. Therefore, RAFT polymerization could easily been employed for polymerization of glycomonomers in aqueous medium by many research groups.[53,54]

The first report published by Lowe and co-workers based on the RAFT polymerization of a glycomonomer.[55] The glycomonomer (2-methacryloxyethyl glucoside) was polymerized in aqueous solution using the most widely employed RAFT agent (4-cyanopentanoic acid)-4-dithiobenzoate (CTP) and 4,4'-azobis(4-cyanopentanoic acid) (ACPA) as the water-soluble initiator. Basic polymerization conditions were used to enhance the solubility of the RAFT agent and the initiator. Despite of the low monomer conversion, the pseudo-first-order kinetics confirmed the sufficient control over the polymerization. However, chain extension with 3-sulfopropyl methacrylate (SPMA) increased the dispersity to 1.63 with a loss of active RAFT end groups. In contrast to this, the chain extension of poly(SPMA) that was used as a macro-RAFT agent with the glycomonomer provided a narrow molar mass distribution of 1.18.

Mawhinney and co-workers developed a RAFT-based one-step polymerization method to prepare tri-component statistical fluorescent glycopolymers.[56] Three different monomers including *N*-(2-hydroxyethyl) acrylamide (HEAA), *N*-(2-aminoethyl)methacrylamide (AEMA) and *N*-(2-glyconamidoethyl)-methacrylamide possessing varied pendant carbohydrates were used for the one-step tri-component RAFT copolymerization (Figure 1.3). The binding abilities of these tri-

component glycopolymers were analyzed with *Paeruginosa* lectin (PA-IL) bacteria and *Galanthus nivalis* plant lectin (GNL). While the α-mannose-containing polymer showed very strong binding with GNL, β-D-galactose-containing polymer showed enhanced binding ability with PA-IL.

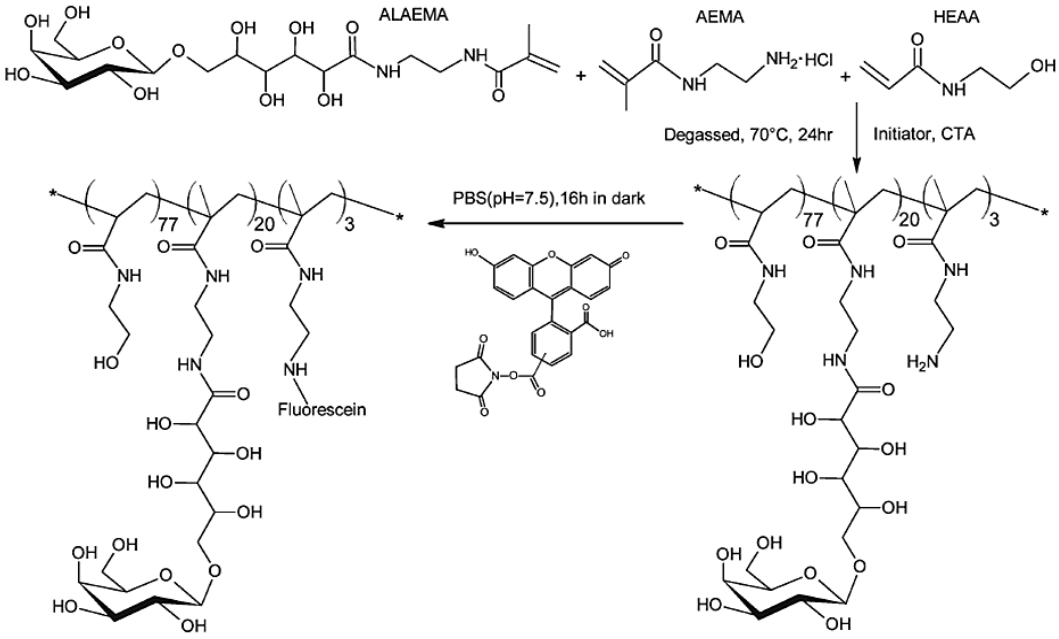


**Figure 1.3.** Illustration of the synthesis of fluorescent glycopolymers PMA-ALAEMA-Fluorescein containing β-galactoside as the pendant sugar.[56]

Recently, Bulmus and collaborators developed a gene delivery system *via* the synthesis of spermine-like glycopolymer *via* RAFT polymerization.[57] After the RAFT polymerization of BocAEAEMA, P(BocAEAEMA) was used as a macro-RAFT agent for chain extension with glycomonomer, mannose acrylate, (ManAc). This chain extension reaction was undertaken in DMF at 70 °C for 12 hours using AIBN. The ability of this well-defined glycopolymer to form polyplex with DNA was investigated. The glycopolymer block decreased this interaction between p(AEAEMA) and DNA regardless of their specific binding affinity with proteins. Another interesting result was that the size of p(AEAEMA)-*b*-p(ManAc) and DNA formed polyplex particles are smaller than the size of p(AEAEMA) and DNA formed particles in according to DLS measurements due to the hydrophilic property of the glycopolymer.

The synthesis of self-assembled porphyrin-glycopolymer conjugates have been developed by Chen *et al.*[58] The combination of RAFT polymerization and one-pot conjugation reaction was introduced. These porphyrin-p((methacrylamido) glucopyranose) conjugates showed the self-assembly behavior to form micelles in the water due to hydrophobic porphyrin in the middle and hydrophilic glycopolymer at both ends. Binding properties to ConA and anti-cancer effect for cancer cells (K562) were studied for these glycopolymers. As expected, glycoparticles showed high and specific binding ability towards ConA. Moreover, *in vitro* studies and cytotoxicity tests of the glycomicelles against K562 cells in dose revealed that these self-assembled micelles killed these cancer cells under light irradiation and in light treatment length dependent manners. Therefore, this report has a high potential for the development of applications for cancer imaging and therapy.

### 1.2.4 Copper-mediated control/living radical polymerization

Transition metal-mediated living radical polymerization, (TMM-LRP), is another widely employed route to synthesize glycopolymers, which are well-defined in terms or chain length and functionalities. Functional groups can be introduced easily into polymers *via* TMM-LRP by utilizing functional initiators.[59] TMM-LRP process is based on a rapid exchange of a halide atom (especially Cl or Br) between a growing radical and a dormant species. To gain an excellent control over the polymerization, the equilibrium is slightly shifted towards the dormant species.[60] (Figure 1.4)

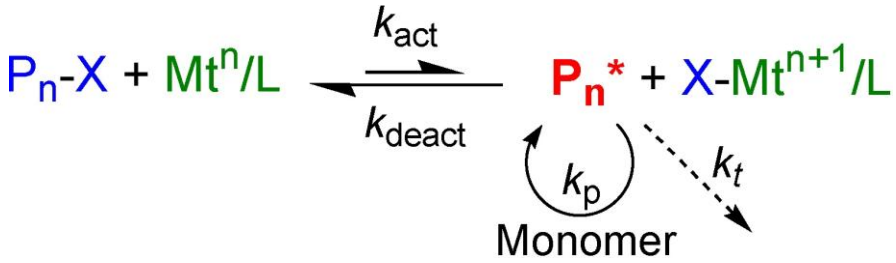


**Figure 1.4.** Activation-deactivition equilibrium in Cu-mediated living/radical polymerization.

As the equilibrium in this mechanism is mainly towards dormant species side, these stable dormant species could easily avoid side reactions, such as chain transfer reactions or termination. Various transition metals can be employed in TMM-LRP such as Cu, Ru, Fe and Ni. However, copper has been the most commonly used transition metal because of its high efficiency and availability. Another important parameter on the degree of control over the polymerization is the type of the ligand. Nitrogen-containing multidentate ligands have been commonly used for copper mediated living/radical polymerizations. Highly polar solvents such as alcohols, DMSO, DMF, N-methyl-2-pyrrolidone (NMP) and mixtures with water are usually employed for the synthesis of glycopolymer in this technique because of the solubility of glycomonomer and the copper-ligand complex.

Cu-catalyzed living/radical polymerization techniques such as ATRP and SET-LRP are relatively more tolerant to different reaction solvents and conditions in controlling the kinetic chain length and macromolecular architecture. The most well-known technique is probably ATRP that utilizes the lower oxidation state copper(I) halide and nitrogen-based ligand complexes as the catalyst system. Recently, improved ATRP processes have been developed, namely activators generated by electron transfer (AGET), activators regenerated by electron transfer (ARGET), electrochemically mediated ATRP (eATRP) and initiators for continuous activator regeneration (ICAR) ATRP.[61] However, simultaneous reverse and normal initiation (SR&NI) ATRP takes advantage as Cu(II), an alkyl halide and a radical initiator are initially present in the reaction medium. Therefore, it is possible to reduce the amount of copper complex used as well as to prepare different types of macromolecular architectures. One of the most important issue with Cu mediated living/radical polymerizations is the purification of copper completely for biomedical applications.

The first paper that was reported in 1998 by Ohno *et al.* was based on the polymerization of a protected glycomonomer *via* ATRP.[62] The glycomonomer, 3-*O*-methacryloyl-1,2:5,6-di-*O*-isopropylidine-D-glucofuranose (MAIpGLc), was polymerized in the presence of CuBr/4,4′-di-*n*-heptyl-2,2′-bipyridine catalyst in 1,2-dimethoxybenzene at 80 °C to yield the glycopolymers. (Figure 1.5 left) The ATRP

polymerizations of MAIpGLc were approximately linear due to the first-order kinetic plots. Liang and colleagues have also reported the synthesis of glycopolymers *via* ATRP.[63] The polymerization of 2-(2′,3′,4′,6′-tetra-*O*-acetyl-β-D-glucopyranosylxy) ethyl acrylate, (AcGEA) was carried out in chlorobenzene using CuBr/2,2′-bipyridine catalyst and 1-phenylethyl bromide initiator at 80 °C. The conversion was reached to 70% with the low dispersities. (Figure 1.5 right)

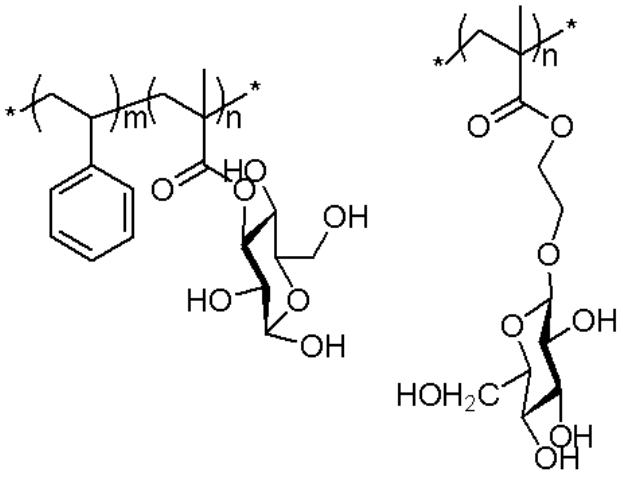


**Figure 1.5.** The first examples of glycopolymers synthesized *via* ATRP.

The synthesis of different types of precision multi-block glycopolymers was reported by Haddleton *et al. via* SET-LRP.[64] The click chemistry of 3-azidopropylacrylate (APA) to alkylated mannose, glucose, and fucose was employed to prepare several types of glycomonomers, respectively. The obtained glycopolymers showed high chain end fidelity to allow for polymerization of more of the same or different glycomonomers in one pot. As depicted in Figure 1.6, chain extension was carried out by addition of mannose monomer (ManAc) dissolved in DMSO into the polymerization reaction mixture *via* cannula under nitrogen. Fucose monomer (FucA) was added in the same way after reaching to full monomer conversion. This sequential addition of subsequent monomers were added sequentially one more time and continued until the glycopolymer reached to six short blocks (DP = 2 for each block; $M_n$ = 7.6 kDa; $Đ$ = 1.13).

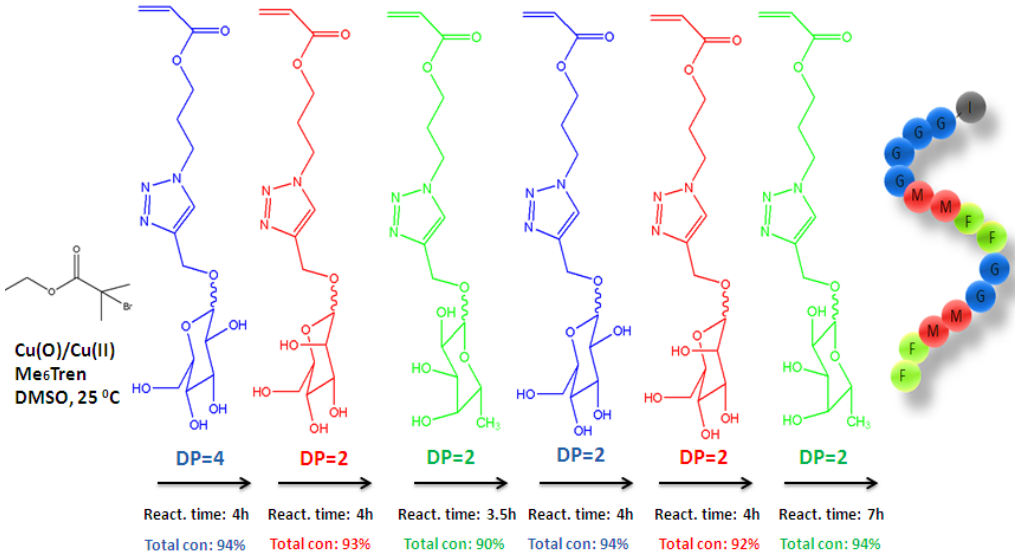


**Figure 1.6.** Schematic representation of the synthesis of multiblock glycopolymers by iterative addition of glycomonomers at defined time period.

The binding abilities of these precision glycopolymers were investigated with the human lectin dendritic cell-specific intercellular adhesion molecule-3-grabbing non-integrin (DC-SIGN) by using surface plasmon resonance (SPR). Even though the binding ability of the synthesized multi-block glycopolymers exhibited a clear dependence with the number-average degree of polymerization of each glycomonomer, the glycopolymers with different sugar units did not present sufficient binding affinity.

Another versatile method was developed to synthesize well-defined and site specific protein–glycopolymer bioconjugates.[65] ATRP of Lactobionamidoethyl methacrylate (LAMA) was carried out in *N*-methyl-2-pyrrolidinone at 20 °C by using a biotinylated poly(ethylene glycol) (biotin–PEG ATRP) initiator and CuBr/2,2'-bipyridine as a catalyst. The interactions of these biotin-terminated glycopolymers with streptavidin were analyzed. The most important benefit of this method is the direct preparation of glycopolymers in the presence of free hydroxyl groups of sugars and without a number of protection and deprotection steps that are required in many other techniques.

## 1.3 Synthesis of glyconanoparticles

Glyconanoparticles as carbohydrate-based systems provide in a similar manner to mimic the behavior of naturally existing glycocalyx.[23,26,27] Therefore, the fabrication and engineering of novel glyconanoparticles with unique physiochemical properties help to further enhance their specific recognition properties on multivalent scaffolds in glycoscience. According to recent developments in the routine synthetic methods of glyconanoparticles, it is nowadays possible to design new multivalent systems providing multivalent carbohydrate-receptor interactions. Basically, there are several types of glyconanoparticles, namely, metallic, semiconductor glyco-quantum dots, magnetic, and self-assembled glyconanoparticles. In this part, recent examples of selected glyconanoparticles showing specific interactions with various lectins that are related to the work in this thesis were summarized.

### 1.3.1 Polymeric glyconanoparticles

A wide range of polymeric glyconanoparticles that were prepared in the last years exhibited excellent and significant recognition properties towards lectins. Very recent and elegant synthetic routes have allowed polymer chemists to prepare polymeric glyconanoparticles with different chemical functional groups and a broad variety of morphologies. These polymeric glyconanoparticles are promising on the creation of different bioactive glycopolymer structures for various health related applications such as drug delivery, biomaterials, bio- and nanotechnologies, and gene therapy.

Chen *et al.* have reported the synthesis of self-assembled porphyrin-glycopolymer conjugates *via* the combination of RAFT polymerization and one-pot conjugation reaction.[58] These porphyrin-PMAG conjugates showed the desired self-assembly behavior to form micelles in the water due to hydrophobic porphyrin groups in the middle and hydrophilic sugar groups at both ends. The binding abilities of the synthesized glyconanoparticles were tested with ConA and anti-cancer effect for cancer cells (K562) was studied. AS expected, these glycopolymers showed high and specific binding ability with ConA. Moreover, the cytotoxicity assay of the glycomicelles against K562 cells in dose revealed that these self-assembled micelles

killed the cancer cells under light irradiation and light treatment length dependent manners.

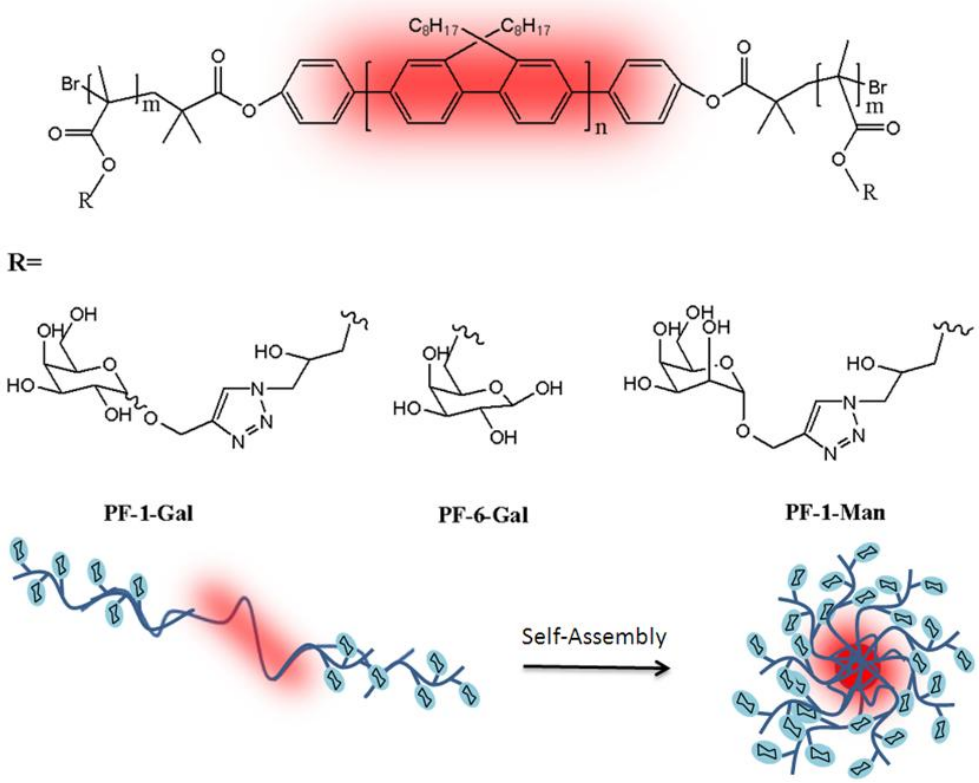


**Figure 1.7.** Chemical structures of galactose and mannose functionalized glycopolymers and schematic representation of the self-assembled nanoparticles.

Jiang and co-workers have performed three self-assembled nanoparticles from triblock copolymers with the same polymeric backbone but different sugar regioisomers as pendant groups.[66] Firstly, rod-block of poly(9,9-dioctylfluorene) macroinitiator was conjugated with the bromine-functionalized polyfluorene (PF) initiator from the two ends of it to exist in the middle block of the glycopolymers. As illustrated in Figure 1.7, well-dispersed spheres were obtained from the polymer self-assembled into nanoparticles with the glyco block as the shell and the rod block as the core. The bioactivity of these formed nano-objects was analyzed with PNA and Erythrina cristagalli agglutinin (ECA) utilizing a quartz crystal microbalance (QCM).

Fernàndez-Garcìa and collaborators reported to prepare a various amphiphilic block glycopolymers based on *n*-butyl acrylate (BA) and methyl methacrylate (MMA) *via*

ATRP.[67] A small library of the well-defined amphiphilic block glycopolymers having di- and triblock glycopolymers with different hydrophobic blocks and varying the hydrophilic block lengths was demonstrated. The different architectures of glyconanoparticles did not show any significant influence on their interaction with ConA.

In another study, the same group have proposed the synthesis of different amphiphilic glycopolymers *via* free radical polymerization.[68] Poly(ethylene glycol) methacrylate (PEGMA) was prepared and copolymerized with methyl acrylate (MA). The free radical copolymerization of the glycomonomer and MA was undertaken using AIBN as an initiator in DMSO at 70 °C. The different amphiphilic glycopolymers with the different ratio of monomers were prepared by using this approach. The binding affinity of these polymer-coated particles with ConA was analyzed *via* Fluorescence Microscopy. It was found that the number of glycol units in the glycopolymer stabilizers affected the binding ability directly and significantly.

### 1.3.2 Metallic glyconanoparticles

A metallic core (noble metals, magnetic elements, semiconductors) can be functionalized with different types of glycopolymers to form a carbohydrate shell. Conjugation of sugar derivatives onto these metal-based nanoclusters present interesting properties, which include a wide array of assembling model and size-related electronic, magnetic and optical properties. Moreover, metallic glyconanoparticles opened new avenues to develop carbohydrate-based multivalent systems due to their easy modification in size and composition. In this way, multifunctional behavior can be directly inserted in the organic shell. The interaction with suitably functionalized biological ligands onto metallic glyconanoparticles is promising for their use in bio-mimetic purposes and also some medicinal applications. Glyconanoparticles can create a glycocalyx-like shell with globular shape and chemically defined composition to understand the main functions of the carbohydrates at cell surface in a better way.

Gold and silver metallic nano platforms are most commonly used as a metallic surface because of their covalent and chemoselective immobilization and ease of

preparation and unique optoelectronic properties. The group of Penadés firstly presented gold nanoclusters coated with the thiol-ended disaccharide lactose (Galβ1-4Glcβ1) or the trisaccharide Lewis X (Galβ1-4[Fucα1-2]GlcNAcβ1, $Le^X$ ) to study the calcium-dependent $Le^x$ self-aggreagtion in 2001.[69] In another work, a single step reaction was succeeded to prepare gold nanoclusters coated with sugar derivatives *via* reducing a gold salt ($HAuCl_4$) in the presence of an excess of thiol-armed glycoconjugates.[70]

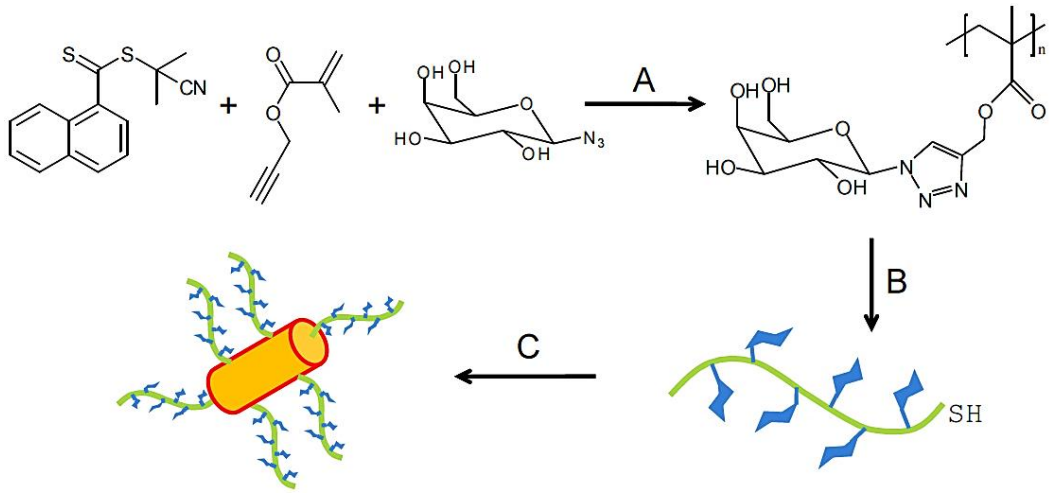


**Figure 1.8.** Synthesis of a glycopolymer-coated gold nanoparticle. Conditions: (A) copper powder, methyl 2-bromopropionate, DMSO, 25 °C; (B) 2 equiv of R-$NH_2$ /$NEt_3$, DMF, 50 C, 24h; (C) gold nanorods, $H_2O$, 12h.[71]

Recently, Cu(0)-catalyzed one-pot reaction for the synthesis of glycopolymers was developed to prepare gold glyconanoparticles for the first time.[71] As depicted in Figure 1.8, the end-group reduction was performed to enable the glycopolymers being grafted to gold nanorods. Lastly, these thiol-terminated glycopolymers covered the surface of gold nanorods to form a self-assembled monolayer due to the interaction of Au-S bond. The obtained glyco-nanorods were examined *via* Transmission Electron Microscopy (TEM) and Dynamic Light Scattering (DLS). These glycopolymer substituted gold nanoparticles showed have a great binding affinity with PNA due to the sufficient numbers of galactose groups on the surface of the nanoparticles.

Biotinylated gold glyconanoparticles were prepared from well-defined biotinylated glycopolymers, poly(*N*-isopropylacrylamide), poly(ethyleneglycol), and $HAuCl_4$ *via* the *in-situ* photochemical reduction of $HAuCl_4$ and glycopolymers in the presence of Irgagure-2959, a water-soluble benzoin photo initiator.[72] These biotinylated gold glyconanoparticles with a high colloidal stability showed high affinity for bioconjugation to streptavidin. Multivalent gold nanoparticles coated with sulfated ligands and glucose derivatives succeeded to neutralize the direct infection of T-lymphocytes with HIV in the nanomolar range. The adsorption and fusion process of the virus infection were targeted by these gold glyconanoparticles *via* the binding to Gp120 with high affinity. For further investigations, gold glyconanoparticles having sulfated ligands and high mannose containing oligosaccharides have been tested in inhibition experiments of HIV and trans-infection to verify their potential synergetic effect.

## 1.4 "Click" chemistry for polymer synthesis

The term "click" chemistry was firstly introduced by Sharpless and co-workers in 2001 and then it has received a significant attention for the preparation of structurally complex molecules, not only in polymer chemistry but also in other research fields such as biochemistry, medicinal and surface chemistry.[73] The "click" reactions that are usually one-pot reaction have become very powerful and commonly used pathway due to very high yields and inoffensive byproducts.[74-77] The required reaction process includes simple reaction conditions such as ambient temperature, pressure and the presence of air/oxygen. Carbohydrates with various functionalities can be incorporated into a polymer either by clicking onto the polymeric backbone or by direct polymerizing them as glycomonomers. Over the past few years, different sugars with azide, alkyne, and thiol functional groups have been used for the synthesis of new glycomonomers *via* efficient "click" reactions.[78] In this section, "click" reactions that were used to prepare different types of glycomonomers in this thesis were highlighted.

### 1.4.1 Copper(I) catalyzed azide-alkyne cycloaddition (CuAAC) reaction

Copper(I) catalyzed azide-alkyne cycloaddition (CuAAC) is one of the most important and frequently used "click" reactions since it can be incorporated into a variety of new routes to synthesize glycopolymers. This type of click reaction is very unique as organic azides are relatively reactive and selective compounds and they can easily undergo a dipolar cycloaddition reaction with alkynes and olefins.[79,80] As shown in Figure 1.9, Cu(I) is used as a catalyst to accelerate the reaction and also eliminate the thermal dipolar azide-alkyne cycloaddition due to stepwise mechanism. The stepwise catalytic cycle starts with the formation of a Cu(I) acetylide species *via* the π complex. Nevertheless, the use of a toxic metal catalyst, copper(I), remains as a main drawback, especially for bio-related applications.

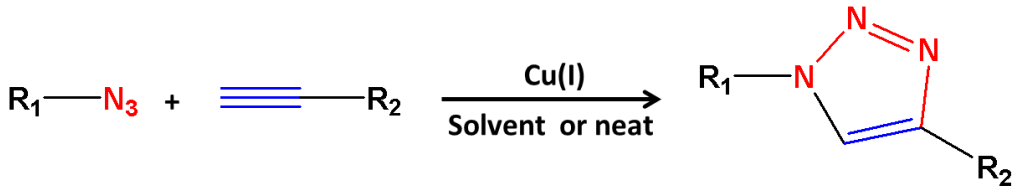


**Figure 1.9.** Copper(I) catalyzed azide-alkyne cycloaddition reaction.

Stenzel and collaborators have reported the synthesis and RAFT polymerization of a novel glycomonomer *via* CuAAC. The azide-functional sugar was clicked with 4-trimethylsilyl-1-buten-3-yne to yield a glycomonomer without protecting groups. The deprotection of the alkyne by tetra-n-butylammonium fluoride (TBAF) and the CuAAC "click" reaction were performed in a one-pot reaction, where the copper(I) was produced in situ by the reduction of $CuSO_4$ using sodium ascorbate.

Another two versatile strategies to prepare well-defined glycopolymers were reported by Haddleton *et al. via* a combination of transition metal-mediated living radical polymerization (TMM-LRP) and Cu(I)-catalyzed click chemistry.[81,82] In the first route, the monomer bearing mannose units was synthesized by Huisgen 1,3-dipolar cycloaddition of the mannose azide and propargyl methacrylate using $(PPh_3)_3CuBr$ as the catalyst. The polymerization of the glycomonomer was initiated with the maleimide-functionalized initiator in the presence of Rhodamine B methacrylate using *N*-(ethyl)-2-pyridylmethanimide and Cu(I)Br as the catalytic

system at ambient temperature. The post-functionalization method was chosen as the second approach that allowed synthesizing well-defined neoglycopolymer protein biohybrid materials. Firstly, trimethylsilyl-protected alkyne side-chain polymeric scaffold were prepared *via* ATRP using again *N*-(ethyl)-2-pyridylmethanimide/Cu(I)Br as the catalytic system in toluene at 70 °C. Its subsequent deprotection in THF with TBAF at room temperature was performed and alkyne groups were clicked with azido sugar derivatives to yield end-functionalized fluorescent glycopolymers.

### 1.4.2 Thiol-ene "click" reaction

The high reactivity of thiols due to their high polarizability and available d-orbitals on the sulfur atom allows thiols being used for wide range thiol-based reactions with plenty of available and useful substrates.[76,83] Hence, the thiol-ene "click" chemistry, another popular "click" reaction, is actually known for over 100 years.[73] The addition of a thiol to an alkene bond can proceed *via* two different mechanistic pathways, namely a radical and an ionic pathway.[76,84] As illustrated in Figure 1.10, the radical thiol-ene "click" reaction involves three steps: initiation, propagation and finally termination. Initiation starts with the treatment of a thiol with photoinitiator under irradiation to yield a thiyl radical. Following the formation of radicals, propagation step takes place in two steps. The first one is the direct addition of the thiyl radical across the C=C bond yielding an intermediate carbon centered radical. The second part of propagation involves chain transfer to a second molecule of thiol to give the thiol-ene addition product and a new thiyl radical. The propagation terminates instantly since two radicals react with each other by combination (coupling). Additionally, radical thiol-ene (photo) polymerization is becoming more attractive for polymer chemists due to rapid polymerization rate, solvent free reaction and good mechanical properties and also it is emerging as an important conjugation reaction that is suitable for in a biological setting.

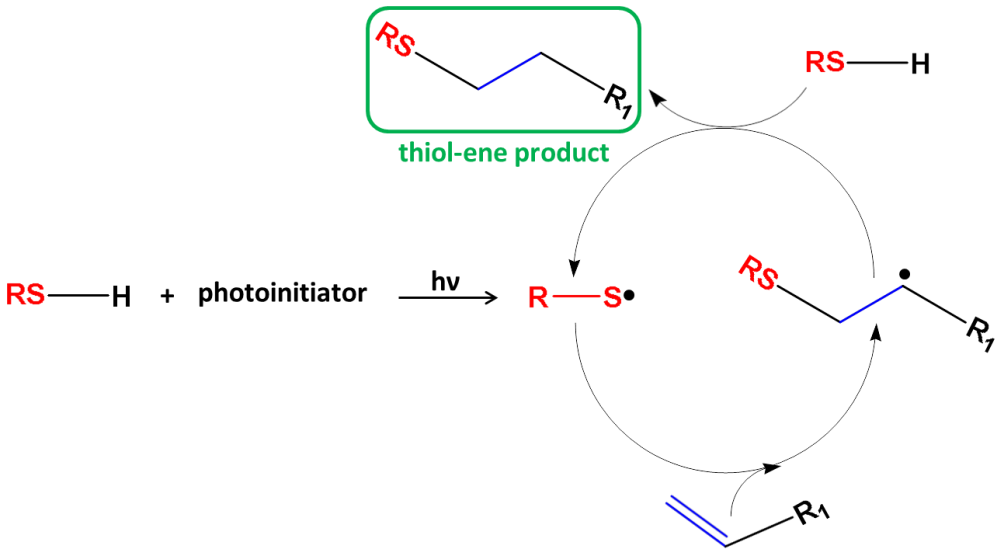


**Figure 1.10.** The mechanism for the hydrothiolation of a C=C bond in the presence of a photoinitiator and UV light.

Chen *et al*. have developed the synthesis of glycopolymers *via* thiol-ene coupling reaction between ene-functional precursor (co)polymers and glucothiose under photochemical conditions with 2,2-dimethoxy-2-phenylacetophenone (DMPA) as the photoinitiator.[85] Firstly, poly(2-(methacryloyloxy)-ethyl pent-4-enoate) having ene side groups was prepared by the treatment of poly(2-hydroxyethyl methacrylate) with 4-pentenoic anhydride. Then, glucothiose was clicked to alkyne functional groups under photochemical conditions. Block copolymerization of di(ethylene glycol) methyl ether methacrylate (DEGMA) and 2-hydroxyethyl methacrylate (HEMA) was performed and followed by a post-polymerization modification of the hydroxyl groups of HEMA to clickable vinyl units. The obtained glycopolymers are used to form thermoresponsive glycomicelles as a potential drug carrier.

Schlaad and collaborators performed a post-polymerization modification of a well-defined poly(2(-3-isobutenyl)-2-oxazoline) with an acetylated thioglucose (2,3,4,6-tetra-O-acetyl-1-thio-β-D-glucopyranose) to yield protected glycopolymers.[86] Following this report, Schubert *et al* reported the synthesis of glycopolymers by using the same approach. However, in this case, poly(2-decenyl-2-oxazoline) was clicked with an acetylated thioglucose to prepare a small library of glycopolymers.[87]

## 1.5 Lectins

Lectins (latin: legere (to select)) that have first been described at the end of the 19th century are defined as carbohydrate-binding proteins.[88] Lectins are fundamental to many important biological process and living organisms.[89,90] They are ubiquitously spread in nature and also they are major components of the outer surface of mammalian cells.[91] Lectins have a specific and reversible interaction with carbohydrates non-covalently, that is known as cell agglutination.[2] Furthermore, many bacteria have the ability to agglutinate erythrocytes by own lectins. The major attribute of the activity of lectins is obtained by using the agglutination and precipitation processes. Even though there are a wide variety of lectins in terms of their structure and size, all these different lectins are highly specific for sugar moieties. Sharon and co-workers have pioneered to study the binding between lectins and carbohydrates and also did a classification based on the monosaccharide ligand toward which they exhibit the highest affinity. This classification is losing its usefulness slowly due to marked differences in the fine specificities of lectins within a single category. Moreover, an increasing number of lectins that have now been isolated from organisms such as plants, animals and microorganisms do not show high affinities toward simple saccharides. Another way to make a classification of lectins is based on their molecular structure. First group named simple lectins consist of a small number of subunits with molecular weights typically below 40 kDa. Secondly, mosaic lectins are very diverse in structure from different sources such as viral hemagglutinins, animal lectins of C-, P- and I-types consist of different types of protein domains. Last group is macromolecular assembly lectins, which are filamentous, heteropolymeric organelles. They are very common in bacteria. However, their structure has a minor component site for the interaction with carbohydrate.

### 1.5.1 Plant lectins

Plant lectins are very commonly used lectins for the examination of the multivalent binding of carbohydrates. Even though many different biological functions of lectins in plants have not still been investigated certainly, it is known that they play

important roles in external and internal activities of plants such as to protect the plant from fungal attack and herbivorous animals, storage of proteins, modulation of enzymatic activities, and adjustment to altered environmental conditions.[92] Legume lectins are the biggest family and the most studied among the simple plant lectins. More than 100 lectins have been isolated and characterized structurally from the seeds of the plants in which they are present. Concanavalin A (ConA) was the first member of this family since its discovery in 1919.[93] ConA is the most popular and the cheapest plant lectin and also it has high binding affinity with mannose and glucose. Therefore, it is usually used as a model lectin to investigate the multivalent binding of glycopolymers. ConA was originally extracted and isolated from the jack bean and its molecular weight is between 104-112 kDa. Like most other lectins, ConA binds to metallic atoms ($Mn^{+2}$ and $Ca^{+2}$) and also these cations enhance significantly the binding ability of ConA with carbohydrates. Moreover, ConA is a tetramer at neutral pH with four subunits in a tetrahedral orientation where the binding sites are 72 Å apart from each other.

Peanut agglutinin (PNA) that is another legume lectin binds to galactose, preferably to galactosyl (β,1-3) *N*-acetylgalactosamine, and has wide range of applications.[94] Moreover, a partially unfolded intermediate of PNA retains its carbohydrate binding ability with affinities that are 75–85% of those of native PNA. Although not always directly necessary for binding, the divalent cations improve their carbohydrate binding. *Triticum vulgare* (wheat germ agglutinin, WGA) is in Gramineae family and a dimeric lectin with eight binding sites for GlcNAc that are separated by distances of 14 Å.[95] It exists in three isoforms, WGA1, WGA2 and WGA3 with a high specificity to *N*-acetylglucosamine and *N*-acetylneuraminic acid. WGA has the ability to recognize specifically the pathogen for plant defense mechanisms. Ricinus communis (ricin) is isolated from castor bean and binds selectively to galactose.[96] Ricin is a ribosome-inactivating protein and also used for generating immunotoxins. Ricin and Ricinus communis agglutinin (RCA) are closely related to be one of the most toxic lectins and can cause rapid death.[97] Jacalin from the Moraceae family that was extracted from the Jackfruit (Artocarpus integrifolia) can recognize to galactose (β,1-3) *N*-acetylgalactosamine and Immunoglobulin A (IgA).

### 1.5.2 Animal lectins

Animal lectins were originally listed in five families, which are C-, I-, P-type lectins, pentraxins, and galectins.[91,98] Despite of the increased knowledge about their structures and functionalities, animal lectins are still more complicated in comparison to plant lectins. C-type lectins that are the most commonly used in animal lectins need $Ca^{+2}$ ions for their interaction with carbohydrates. The large family of C-type lectins includes collectins, selectins, endocytic receptors, and proteoglycans.[99] They differ significantly in the types of glycans that they recognize with high affinity because of their carbohydrate-recognition domains. C-type lectins serve for many different functions in animal, such as cell-cell adhesion, immune response to pathogens, the control of protein levels in the blood and apoptosis. Proteins use the C-type lectin fold to bind other proteins, lipids, and inorganic molecules. C-Type lectins can have a variable number of subunits with 1–8 binding sites per subunit. The C-type lectin fold is unique and a compact domain of 110–130 amino acid residues with a double-looped, two-stranded antiparallel β-sheet formed by the amino-and carboxy-terminal residues connected by two α-helices and a three-stranded antiparallel β-sheet. As depicted in Figure 1.11, $Ca^{+2}$ cations in the carbohydrate-recognition domains often coordinated to amino acid residues with carbonyl side chains and these residues directly bind to sugars when $Ca^{+2}$ is bound in site 2.

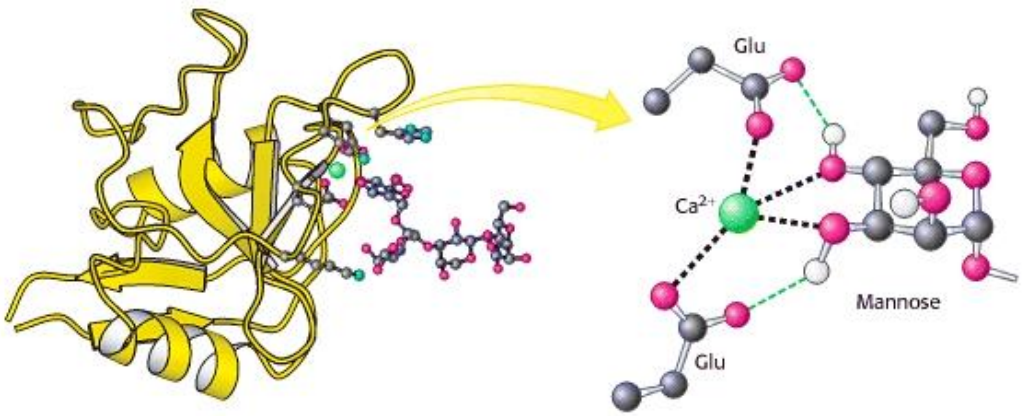


**Figure 1.11.** Structure of a C-Type carbohydrate-binding domain from an animal lectin.[99]

C-type lectins are endocytic lectins as the hepatic galactose/*N*-acetylglucosamine receptor. Moreover, many C-type lectins exist as trimers, including the trimeric rat mannose-binding protein-A in complex with α-methyl mannoside. Interestingly, some C-type lectins are extremely small; for example, hepatic intestinal pancreatic protein and pancreatic stone protein.[100,101] The selectins are the best characterized family of C-type lectins in terms of their extensively documented roles as cell-adhesion molecules. Specific interaction between the selectins and cell-surface glycoconjugate ligands play a key role in adhesive interactions among these cells. Dendritic cell-specific intercellular adhesion molecule-3-grabbing non-integrin (DC-SIGN; CD209) and its closely related homolog DC-SIGNR lectin are human C-type lectins present on both macrophages and also dendritic cell subpopulations.[102] Dendritic cells that are the most antigen presenting cells form a major component of the immune system. They act as messengers between the innate and adaptive immunity in order to process antigen material and present it on the surface to other cells of immune systems such as T-cells.[103] DC-SIGN binds to microorganisms and host molecules by recognizing surface rich in mannose containing glycans through multivalent glycan-protein interactions and notably serves a target molecule for several viruses such as human immunodeficiency virus (HIV) and hepatitis C virus (HCV). Langerin, another C-type lectin, binds ligands with specificity for mannose, *N*-acetyl-glucosamine and fucose.[104] Dectin-1 that was discovered over a decade ago, therefore, has been gained interest in investigation of its intracellular signalling mechanisms.[105]

Selectins are classified into four subtypes: E-selectin (in endothelial cells), PSGL-1-seleection (in hematopoietic cells), L-selectin (in leukocytes) and P-selectin (in platelets and endothelial cells).[106] They show a specific affinity to mannose, but also fucose and *N*-acetylglucosamine.

I-type lectins are from the immunoglobulin superfamily, excluding antibodies and T-cell receptors.[107] The Siglec family of sialic acid–binding lectins is the only well-characterized group of I-type lectins regarding both structurally and functionally. P-type lectins play an important role in the generation of functional lysosomes within the cells of higher eukaryotes by directing newly synthesized lysosomal enzymes

bearing the mannose 6-phosphate signal to lysosomes. The only two members of the P-type lectin family, the cation-dependent mannose 6-phosphate receptor and the insulin-like growth factor II/mannose 6-phosphate receptor, have the great ability to recognize phosphorylated mannose residues.[107]

Pentraxins that are a family of evolutionarily conserved pattern-recognition proteins are divided into two groups: short pentraxins and long pentraxins.[108] The two short pentraxins are C-reactive protein (CRP) and serum amyloid P-component (SAP). The prototype protein of the long pentraxin group is pentraxin 3 (PTX3). CRP and SAP are produced primarily in the liver while PTX3 is produced in a variety of tissues during inflammation.[109] The short pentraxins performs several functions to recognize a variety of pathogenic agents and then to either eliminate them or neutralize their harmful effects by utilizing the complement pathways and macrophages in the host. The first galectin was found as a noncovalent dimer and isolated from chick muscle aa well as from extracts of calf heart and lung in 1976. Generally, galectins have the binding ability with β-galactosides, preferably as lactose and *N*-acetyl lactosamine, and a significant sequence similarity in the carbohydrate-binding site. Galectins can contribute to cell–cell and cell–matrix interactions and regulate immune and inflammatory responses. Some galectins have shown the importance and necessity in cancer progression.

## 1.6 Analysis of the interactions of glyco-polymers/particles and lectins

Various analytical methods have been developed to study multivalent carbohydrate -lectin interactions.[110-113] The most widely applied and the oldest technique is turbidimetry that is based on the determination of the turbidity of the solution upon aggregation of lectin and polymer chains. UV-vis spectrometer can be utilized to determine the turbidity of the solution at varying ratio of lectin to glycopolymers. Alternatively, quantitative precipitation and quenching of fluorescence emission techniques have been employed to distinguish effect arising from receptor clustering and receptor proximity, respectively. More advanced techniques such as ITC, atomic force microscopy (AFM), quartz crystal microbalance (QCM), and surface plasmon resonance (SPR) spectroscopy have also been used widely to

investigate carbohydrate-lectin interactions.[114-118] This section will briefly describe these techniques with the selected examples as well as their cons and pros.

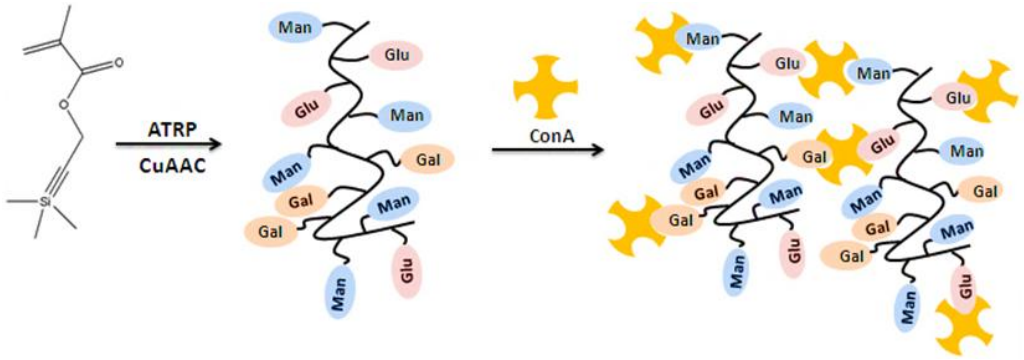


**Figure 1.12.** Schematic representation of the glycopolymer lectin binding.

Haddleton *et al.* have recently reported a library of well-defined glycopolymers with different sugar azides (mannose, galactose, and glucose) and their ability to form cluster with ConA *via* five different assays analysis (quantitative precipitation, turbidimetry, fluorescence quenching assays, inhibitory potency assays, reversal aggregation assays).[119] ConA was chosen as a model lectin due to the interactions with a wide range of saccharides, especially mannose and glucose. The influence of the nature and densities of different sugars residues on the stoichiometry of the cluster, the rate of the cluster formation, the inhibitory potency of the glycopolymers, and the stability of the turbidity were investigated *via* using these different assays. The glycopolymer that was substituted with one mannose residue per repeat unit showed the highest and strongest binding ability as multivalent ligand for clustering ConA. Therefore, mannose residues seem to be the main factor to enhance multiple interactions for the binding stoichiometry, the rate of binding, the potency and the stability of ConA clustering. The other factor is that an increasing the chain length provided enhanced binding, but it was less benefit after a certain length. Based on these results, this work is a crucial example to demonstrate how well-defined glycopolymers with various pendant epitopes have a big influence on the lectin-multivalent interaction and the stability of glycopolymer-ConA cluster.

It is possible to measure the sedimentation velocity related to the binding rate of lectins and carbohydrates by using a more advanced technique such as analytical

ultracentrifugation. Moreover, the thermodynamics of binding between lectins and multivalent ligands can be determined using isothermal titration calorimetry (ITC). Single molecule force spectroscopy has recently developed into a highly sensitive tool for the investigation of single biomolecule interactions.[115] Atomic Force Microscopy (AFM) or optical tweezers have been used to measure dissociation forces of single ligand-receptor complexes in the pico newton range.[116]

Quartz crystal microbalance (QCM) is a simple, cost effective, high-resolution mass sensing technique, which has been employed to study a wide range of molecular systems at the solution-surface interface.[117] Quartz crystal microbalance with dissipation monitoring (QCM-D) technique is a special type of QCM based on the ring-down technique relevant to the piezoelectric effect in quartz crystals, whose frequency of oscillation changes in proportion to the amount of mass adsorbed onto their surface.

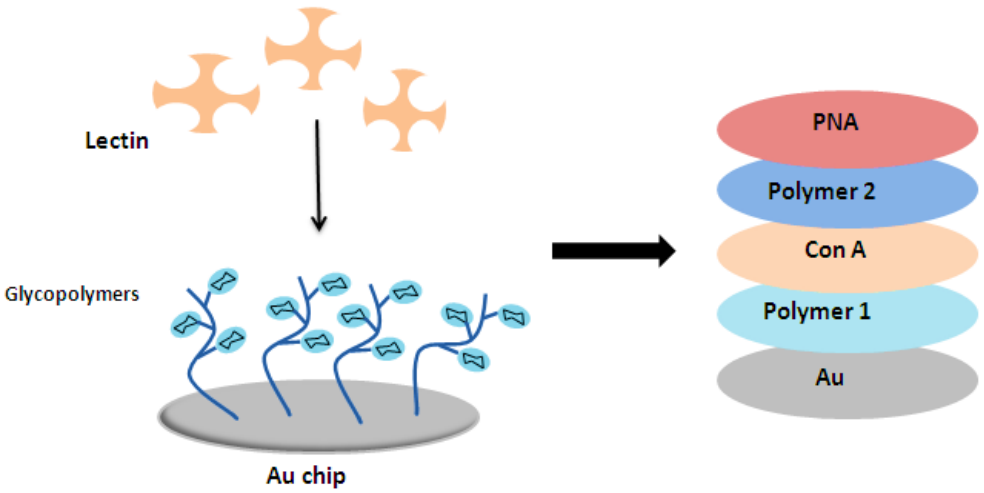


**Figure 1.13.** Formation of layer-by-layer assembly of glycopolymers and lectins followed by quartz crystal microbalance technique.[120]

As seen in Figure 1.13, the layer-by-layer formation of glycopolymer and lectin was confirmed by using QCM-D.[120] Firstly, gold chip was chemically modified with 11-mercaptoundecanoic acid (MUA), followed by 1-[3-(dimethylamino)- propyl]-3-ethyl carbodiimide (EDC) hydrochloride and *N*-hydroxysuccinimide (NHS). Subsequently, ConA was bound to the surface *via* nucleophilic substitution of lysine and ethanolamine hydrochloride was used to block unreacted NHS groups to prevent their interaction with glycopolymers. Mannose glycopolymer was flown

over the surface to determine the rate of binding. The sufficient binding was achieved because of the existing galactose units in the glycopolymer.

Surface plasmon resonance (SPR) spectrometer monitors the interactions of two or more molecules or molecular assemblies in real time. Basically, SPR is based on the measurement of adsorption of material onto planar metal surfaces.[118] SPR utilizes the flow of analyte solution over a functionalized gold surface resulting in a change in the refractive index. This technique is very sensitive and can be used to detect association of glycoproteins or glycopolymers in pico-molar concentrations. There is a good example for the use of this technique to investigate the potential of mannose containing glycopolymers to interact with human DC- SIGN and the ability of these glycopolymers to inhibit the interactions between DC-SIGN and the HIV envelope glycoprotein gp120.[121] Multichannel surface plasmon resonance (MC-SPR) was used to investigate the binding affinity of a library of glycopolymers with bacterially expressed soluble recombinant human DC-SIGN tetramers. DC- SIGN was immobilized onto an SPR sensor chip and the interactions between DC-SIGN and the glycopolymers were probed as a function of glycopolymer concentration. The homopolymer of mannose exhibited the highest binding affinity.

To conclude, many methods have been developed to study multivalent carbohydrate-lectin interactions. In particular, QCM and SPR techniques are highly sensitive in detection and provide more reliable data because the ligands or analytes can be immobilized on a surface. Indeed, there is a need for combination of different techniques and development of precisely sequence controlled synthesis techniques to have a better understanding in glycopolymer-lectin binding activities and to create the synthetic glycopolymer code.

## 1.7 Biomedical applications of glyco-polymers/particles

### 1.7.1 Drug and gene delivery

As mentioned above, glyco-polymers and particles can be used on the development of various drug/gene delivery systems for the treatment of different diseases in an efficient way. In the last decade, significant progression in carbohydrate science

provided a major research area for the preparation of advanced glycomaterials including targeted delivery of drugs and biological molecules in the field of drug/gene delivery devices. However, achieving a high selectivity and significant drug/gene drug and release profile are still in need of improvement in terms of some complications and side effects for their vitality during the duration of pharmacological action. Especially, glyco-micelles have a great potential to develop drug delivery systems as nanocarriers in which the drug release occurs due to a change in the environment conditions such as pH, temperature, ionic strength, presence or absence of chemical species, electric fields and irradiation with UV/visible light.[122,123]

For a long time, cancer has been one of the leading causes of death in the world and huge amount of people are still suffering of cancer today. The most common chemotherapeutic reagents used to treat cancer, such as Doxorubicin (DOX), Cisplatin, Methotrexate and Cytarabine, are generally associated with non-localized systemic toxicity.[124] However, the cytotoxic drugs used for treatment of different types of cancer have also some side effects, for example nausea, hair loss, and pulmonary disorders. Therefore, the use of more biocompatible carriers with high loading capacity, low overall toxicity and receptor-mediated endocytosis specificity is urgently required. The swift sequestration of anticancer drugs by mononuclear phagocytes of the reticuloendothelial system (RES) is another challenge for the use of drug carriers.[125] Wang and collaborators have reported hepatocytes-targeted delivery of Doxorubicin by using glycopolymers with reducible ionic cores.[126] They succeeded an encapsulation of DOX into the galactose-decorated reduction-sensitive cystamine cross-linked micelles and these glyco-micelles showed rapid release of the drug under reductive cancer environment as evidenced by the stronger fluorescence intensity from DOX compared to micelles lacking galactose molecules.

Li *et al.* have developed the synthesis of pH-sensitive pullulan-DOX conjugated nanoparticles.[127] The obtained nanoparticles showed a release profile of more than 75% of DOX within 2 hours at pH 5 and with less than 15% release after 12 hours at pH 7.4.

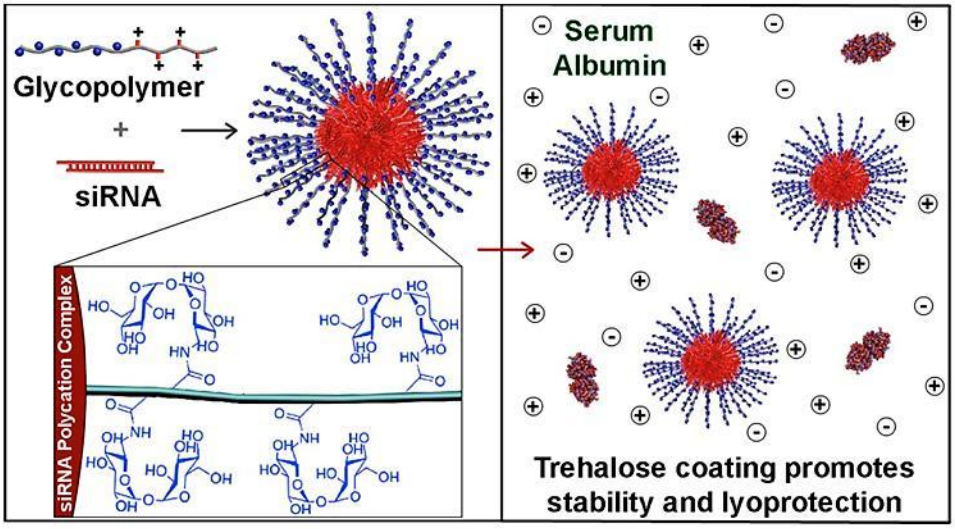


**Figure 1.14**. Schematic illustration of glycopolymer based polyplexes containing siRNA for release.[128]

As depicted in Figure 1.14, Reineke and co-workers synthesized a new methacrylamido trehalose monomer and polymerized to create polyplexes containing siRNA.[128] These siRNA nanocomplexes showing excellent stability was tracked to undergo cytoplasmic trafficking and siRNA-induced down regulating of the target gene was achieved at $IC_{50}$ of 19nM.

### 1.7.2 Bioimaging and biosensing

Metallic glyconanoparticles are emerging as an efficient platform for diagnostic and therapeutic purposes since they have several unique features such as chemical inertness, facile surface functionalizability, electronic structure amenable for plasmon resonance and optical properties suitable as imaging agents.[129] Especially, the optical properties of gold nanoparticles can be manipulated using spectroscopic techniques to determine successful binding of biorecognizable molecules to receptors or by colloidal aggregation.[130] Therefore, glyco-gold nanoparticles have a great potential to use as biosensors due to the inherent multivalency of the particles and lectins. Gibson *et al.* developed a system that is able to discriminate different strains of *Escherichia coli* by multivalent thioglucose-conjugated AuNPs based on their variable expression and binding to lectin receptor FimH on the cell surface.[131]

Zhou and coworkers have reported the novel synthesis of TEMPO-oxidized chitin nanocrystals labelled with fluorescent imidazoisoquinolinone dye and simultaneously functionalized them with mannose carbohydrate ligands (Figure 1.15).[132] These carbohydrate functionalized nanocrystals showed a selective and specific binding ability to lectins and bacteria *via* carbohydrate-protein interactions.

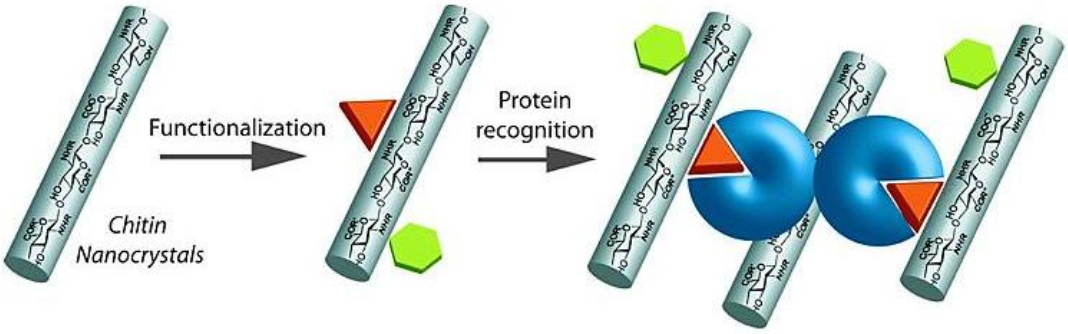


**Figure 1.15.** Schematic illustration of carbohydrate and fluorescent dye functionalized nanocrystals and their selective binding.[132]

Amperometric glucose biosensor developed from the functional graphene oxide (FGO) nanosheet was investigated by Veerapandian and collaborators.[133] The FGO nanosheet was composed of metalloid polymer hybrid (MPH) nanoparticles and a gold-printed circuit board electrode on the surface of a grapheme oxide nanosheet. As a biosensor, this FGO nanosheet performed with a correlation efficiency of 0.9981 and also showed long term stability and in close agreement with current commercialized glucose sensors.

### 1.7.3. Pathogen inhibitions

The important mechanism of pathological events is based on molecular interactions between cell surface carbohydrates of the host and specialised carbohydrate-specific bacterial proteins called adhesins or lectins, respectively.[134] Hence, pathological recognition has been trying to be investigated in terms of bacterial and viral infections. Microbial colonisation of the body can be interpreted with the glycoconjugate decoration of the host cells according to multivalence interaction of carbohydrate among microbes and cell surfaces.[135] Ogata and coworkers have recently developed the design of artificial sulfated sialoglycopolypeptides carrying Neu5Acα2,3Galβ1,4 (6-sulfo)GlcNAc and Neu5Acα2,6Galβ1,4(6-sulfo)GlcNAc

residues in the side chain that were designed as hemagglutinin inhibitors against influenza viruses.[136] They used a hemagglutination assay to binding affinity. The results showed the binding affinity to influenza virus was approximately $1.2x10^3$ fold higher than a fetuin control.

Luczkowiak *et al.* reported that glycofullerenes decorated with up to 36 mannose or galactose moieties which were able to competitively bind and inhibit DC-SIGN-dependent cell entry of Ebola virus (Figure 1.16).[137] The binding studies proved the multivalence interaction due to blocking viral infectivity. This versatile could potentially be used as tools for developing more efficient models for inhibiting bacterial and viral infection.

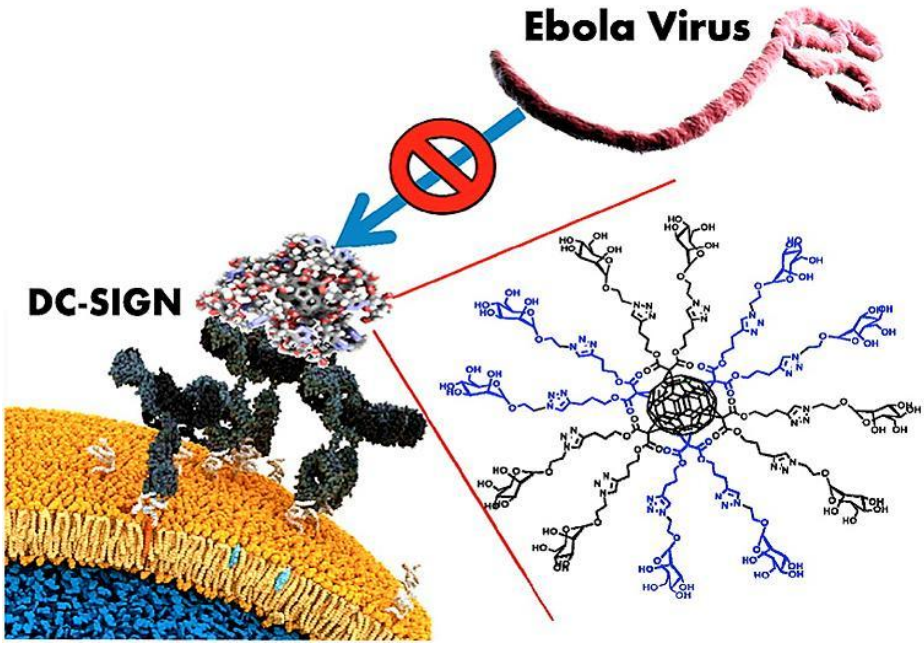


**Figure 1.16.** Representation of the interaction between glycofullerenes and DC-SIGN and blocking of Ebola virus.[137]

Poly(ethylene oxide)-b-polycaprolactone polymersomes were created to interact and inhibit the influenza virus at two different stages of infectivity by Gillies and coworkers.[138] At the primary level, the polymersomes are conjugated with sialic acid *N*-acetylneuramic acid (Neu5Ac) multivalent dendrons for the binding with viral hemagglutinin gp120 protein to prevent entry into host cell. At the secondary level, the encapsulation of a neuraminidase inhibitor zanamivir into the

polymersomes was aimed be released upon aggregation and prevent progeny virion release that further decreases host cell interaction and replication potential. While the sialodendron had a 17-fold (per sialoside) enhancement, the dendritic sialopolymersome showed a 2000 fold increase in binding avidity. Moreover, the zanamivir loaded polymersomes having a high loading capacity profiled a slowly-sustained release and usability for a long-time.

## 1.8 Conclusion

In this chapter, the synthesis of the various well-defined glyco-polymer/particle architectures and their interaction with corresponding lectins for different biorelated applications such as drug delivery purposes, biomaterials, bio- and nanotechnologies and gene therapy were highlighted. Very recent and elegant synthetic routes have allowed polymer chemists to prepare a wide range of glyco-polymers/particles that show really excellent and significant recognition properties towards lectins. These novel methodologies for synthesizing and studying well-defined glycopolymers have a potential for future investigations to enhance their unique recognition properties and develop therapeutic agents and biological probes. It is likely that a forthcoming close interdisciplinary collaboration between glyco-polymer/particle synthesis and the medical/pharmaceutical research area for therapeutic purposes and for many more bio-related devices.

In chapter two and three, self-assembly and gold glyconanoparticles were prepared for the development of drug delivery and release system and the investigation of their binding with DC-SIGN.

In chapter four, single-chain folding of glycopolymer was achieved to enhance the lectin binding ability.

In chapter five, the new *S*-glucosyl substituted 2-oxazoline glycomonomer was synthesized and polymerized *via* the living cationic ring-opening polymerization.

## 1.9 References

(1) Houseman, B. T.; Mrksich, M. *Chem. Biol.* **2002**, *9*, 443.

(2) Ghazarian, H.; Idoni, B.; Oppenheimer, S. B. *Acta histochemica* **2011**, *113*, 236.
(3) Gabius, H.-J.; Siebert, H.-C.; André, S.; Jiménez-Barbero, J.; Rüdiger, H. *ChemBioChem* **2004**, *5*, 740.
(4) Gabius, H.-J.; André, S.; Kaltner, H.; Siebert, H.-C. *Biochimica et Biophysica Acta (BBA) - General Subjects* **2002**, *1572*, 165.
(5) Kiessling, L. L.; Splain, R. A. *Annual Review of Biochemistry* **2010**, *79*, 619.
(6) Gamblin, D. P.; Scanlan, E. M.; Davis, B. G. *Chemical Reviews* **2009**, *109*, 131.
(7) Garegg, P. J.; Lindberg, A. A. *Carbohydrate Antigens*; American Chemical Society, 1993; Vol. 519.
(8) Kiessling, L. L.; Cairo, C. W. *Nat Biotech* **2002**, *20*, 234.
(9) Ilyas, R.; Wallis, R.; Soilleux, E. J.; Townsend, P.; Zehnder, D.; Tan, B. K.; Sim, R. B.; Lehnert, H.; Randeva, H. S.; Mitchell, D. A. *Immunobiology* **2011**, *216*, 126.
(10) Bertozzi, C. R.; Kiessling; L., L. *Science* **2001**, *291*, 2357.
(11) Kiessling, L. L.; Gestwicki, J. E.; Strong, L. E. *Angewandte Chemie International Edition* **2006**, *45*, 2348.
(12) Jones, M. W.; Otten, L.; Richards, S. J.; Lowery, R.; Phillips, D. J.; Haddleton, D. M.; Gibson, M. I. *Chemical Science* **2014**, *5*, 1611.
(13) Yilmaz, G.; Becer, C. R. *Frontiers in Bioengineering and Biotechnology* **2014**, *2*.
(14) Deng, Z.; Li, S.; Jiang, X.; Narain, R. *Macromolecules* **2009**, *42*, 6393.
(15) Becer, C. R. *Macromolecular Rapid Communications* **2012**, *33*, 742.
(16) Spain, S. G.; Cameron, N. R. *Polymer Chemistry* **2011**, *2*, 60.
(17) Miura, Y. *Journal of Polymer Science Part a-Polymer Chemistry* **2007**, *45*, 5031.
(18) Arnaud, J.; Audfray, A.; Imberty, A. *Chemical Society Reviews* **2013**, *42*, 4798.
(19) Spain, S. G.; Gibson, M. I.; Cameron, N. R. *Journal of Polymer Science Part A: Polymer Chemistry* **2007**, *45*, 2059.
(20) de la Fuente, J. M.; Penadés, S. *Biochimica et Biophysica Acta (BBA) - General Subjects* **2006**, *1760*, 636.
(21) Yilmaz, G.; Becer, C. R. *Polymer Chemistry* **2015**, *6*, 5503.
(22) Marradi, M.; Martín-Lomas, M.; PenadÉs, S. In *Advances in Carbohydrate Chemistry and Biochemistry*; Derek, H., Ed.; Academic Press: 2010; Vol. Volume 64, p 211.
(23) Marradi, M.; Chiodo, F.; Garcia, I.; Penades, S. *Chemical Society Reviews* **2013**, *42*, 4728.
(24) Mudshinge, S. R.; Deore, A. B.; Patil, S.; Bhalgat, C. M. *Saudi Pharmaceutical Journal* **2011**, *19*, 129.
(25) Ahmad, Z.; Shah, A.; Siddiq, M.; Kraatz, H.-B. *RSC Advances* **2014**, *4*, 17028.
(26) Chiodo, F.; Marradi, M.; Calvo, J.; Yuste, E.; Penadés, S. *Beilstein Journal of Organic Chemistry* **2014**, *10*, 1339.

(27) Penadés, S.; de la Fuente, J. M.; Barrientos, Á. G.; Clavel, C.; Martínez-Ávila, O.; Alcántara, D. In *Nanomaterials for Application in Medicine and Biology*; Giersig, M., Khomutov, G. B., Eds.; Springer Netherlands: Dordrecht, 2008, p 93.
(28) García, I.; Marradi, M.; Penadés, S. *Nanomedicine* **2010**, *5*, 777.
(29) Nichols, P. L.; Yanovsky, E. *Journal of the American Chemical Society* **1944**, *66*, 1625.
(30) Nichols, P. L.; Wrigley, A. N.; Yanovsky, E. *Journal of the American Chemical Society* **1946**, *68*, 2020.
(31) Talley, E. A.; Vale, M. D.; Yanovsky, E. *Journal of the American Chemical Society* **1945**, *67*, 2037.
(32) Yilmaz, G.; Becer, C. R. In *Carbohydrate Nanotechnology*; John Wiley & Sons, Inc: 2015, p 137.
(33) Yilmaz, G.; Becer, C. R. *European Polymer Journal* **2013**, *49*, 3046.
(34) Zhang, Q.; Haddleton, D. M. In *Hierarchical Macromolecular Structures: 60 Years after the Staudinger Nobel Prize II*; Percec, V., Ed.; Springer International Publishing: Cham, 2013, p 39.
(35) Kimura, S.; Imoto, M. *Die Makromolekulare Chemie* **1961**, *50*, 155.
(36) Obata, M.; Kobori, T.; Hirohara, S.; Tanihara, M. *Polymer* **2012**, *53*, 4672.
(37) Obata, M.; Shimizu, M.; Ohta, T.; Matsushige, A.; Iwai, K.; Hirohara, S.; Tanihara, M. *Polymer Chemistry* **2011**, *2*, 651.
(38) Hoshino, Y.; Nakamoto, M.; Miura, Y. *Journal of the American Chemical Society* **2012**, *134*, 15209.
(39) Seto, H.; Ogata, Y.; Murakami, T.; Hoshino, Y.; Miura, Y. *ACS Applied Materials & Interfaces* **2012**, *4*, 411.
(40) Blencowe, A.; Tan, J. F.; Goh, T. K.; Qiao, G. G. *Polymer* **2009**, *50*, 5.
(41) Wiltshire, J. T.; Qiao, G. G. *Macromolecules* **2006**, *39*, 9018.
(42) Wiltshire, J. T.; Qiao, G. G. *Macromolecules* **2006**, *39*, 4282.
(43) Good, F. J.; Schuerch, C. *Macromolecules* **1985**, *18*, 595.
(44) Uryu, T.; Yamaguchi, C.; Morikawa, K.; Terui, K.; Kanai, T.; Matsuzaki, K. *Macromolecules* **1985**, *18*, 599.
(45) Rüde, E.; Westphal, O.; Hurwitz, E.; Fuchs, S.; Sela, M. *Immunochemistry* **1966**, *3*, 137.
(46) Aoi, K.; Tsutsumiuchi, K.; Okada, M. *Macromolecules* **1994**, *27*, 875.
(47) Huang, J.; Bonduelle, C.; Thévenot, J.; Lecommandoux, S.; Heise, A. *Journal of the American Chemical Society* **2012**, *134*, 119.
(48) Mortell, K. H.; Weatherman, R. V.; Kiessling, L. L. *Journal of the American Chemical Society* **1996**, *118*, 2297.
(49) Schuster, M. C.; Mortell, K. H.; Hegeman, A. D.; Kiessling, L. L. *Journal of Molecular Catalysis A: Chemical* **1997**, *116*, 209.
(50) Takasu, A.; Kojima, H. *Journal of Polymer Science Part A: Polymer Chemistry* **2010**, *48*, 5953.

(51) Kempe, K.; Weber, C.; Babiuch, K.; Gottschaldt, M.; Hoogenboom, R.; Schubert, U. S. *Biomacromolecules* **2011**, *12*, 2591.
(52) Chiefari, J.; Chong, Y. K.; Ercole, F.; Krstina, J.; Jeffery, J.; Le, T. P. T.; Mayadunne, R. T. A.; Meijs, G. F.; Moad, C. L.; Moad, G.; Rizzardo, E.; Thang, S. H. *Macromolecules* **1998**, *31*, 5559.
(53) McCormick, C. L.; Lowe, A. B. *Accounts of Chemical Research* **2004**, *37*, 312.
(54) Lowe, A. B.; McCormick, C. L. *Progress in Polymer Science* **2007**, *32*, 283.
(55) Lowe, A. B.; Sumerlin, B. S.; McCormick, C. L. *Polymer* **2003**, *44*, 6761.
(56) Wang, W.; Chance, D. L.; Mossine, V. V.; Mawhinney, T. P. *Glycoconj J* **2014**, *31*, 133.
(57) Kurtulus, I.; Yilmaz, G.; Ucuncu, M.; Emrullahoglu, M.; Becer, C. R.; Bulmus, V. *Polymer Chemistry* **2014**, *5*, 1593.
(58) Lu, W.; Ma, W.; Lu, J.; Li, X.; Zhao, Y.; Chen, G. *Macromolecular Rapid Communications* **2014**, *35*, 827.
(59) Kamigaito, M.; Ando, T.; Sawamoto, M. *Chemical Reviews* **2001**, *101*, 3689.
(60) Ouchi, M.; Terashima, T.; Sawamoto, M. *Chemical Reviews* **2009**, *109*, 4963.
(61) Matyjaszewski, K. *Macromolecules* **2012**, *45*, 4015.
(62) Ohno, K.; Tsujii, Y.; Fukuda, T. *Journal of Polymer Science Part A: Polymer Chemistry* **1998**, *36*, 2473.
(63) Liang, Y.-Z.; Li, Z.-C.; Chen, G.-Q.; Li, F.-M. *Polymer International* **1999**, *48*, 739.
(64) Zhang, Q.; Collins, J.; Anastasaki, A.; Wallis, R.; Mitchell, D. A.; Becer, C. R.; Haddleton, D. M. *Angewandte Chemie International Edition* **2013**, DOI:10.1002/anie.201300068.
(65) Narain, R. *Reactive and Functional Polymers* **2006**, *66*, 1589.
(66) Sun, P.; He, Y.; Lin, M.; Zhao, Y.; Ding, Y.; Chen, G.; Jiang, M. *ACS Macro Lett.* **2014**, *3*, 96.
(67) Muñoz-Bonilla, A.; León, O.; Bordegé, V.; Sánchez-Chaves, M.; Fernández-García, M. *Journal of Polymer Science Part A: Polymer Chemistry* **2013**, *51*, 1337.
(68) Alvárez-Paino, M.; Juan-Rodríguez, R.; Cuervo-Rodríguez, R.; Muñoz-Bonilla, A.; Fernández-García, M. *Journal of Colloid and Interface Science* **2014**, *417*, 336.
(69) de la Fuente, J. M.; Barrientos, A. G.; Rojas, T. C.; Rojo, J.; Cañada, J.; Fernández, A.; Penadés, S. *Angewandte Chemie International Edition* **2001**, *40*, 2257.
(70) Barrientos, Á. G.; de la Fuente, J. M.; Rojas, T. C.; Fernández, A.; Penadés, S. *Chemistry – A European Journal* **2003**, *9*, 1909.
(71) Lu, J.; Zhang, W.; Richards, S.-J.; Gibson, M. I.; Chen, G. *Polymer Chemistry* **2014**, *5*, 2326.
(72) Narain, R.; Housni, A.; Gody, G.; Boullanger, P.; Charreyre, M.-T.; Delair, T. *Langmuir* **2007**, *23*, 12835.

(73) Kolb, H. C.; Finn, M. G.; Sharpless, K. B. *Angewandte Chemie International Edition* **2001**, *40*, 2004.
(74) Tang, W.; Becker, M. L. *Chemical Society Reviews* **2014**, *43*, 7013.
(75) Tiwari, V. K.; Mishra, B. B.; Mishra, K. B.; Mishra, N.; Singh, A. S.; Chen, X. *Chemical Reviews* **2016**, *116*, 3086.
(76) Lowe, A. B. *Polymer Chemistry* **2010**, *1*, 17.
(77) Hein, C. D.; Liu, X.-M.; Wang, D. *Pharmaceutical research* **2008**, *25*, 2216.
(78) Slavin, S.; Burns, J.; Haddleton, D. M.; Becer, C. R. *European Polymer Journal* **2011**, *47*, 435.
(79) Lutz, J.-F.; Schlaad, H. *Polymer* **2008**, *49*, 817.
(80) Johnson, J. A.; Finn, M. G.; Koberstein, J. T.; Turro, N. J. *Macromolecular Rapid Communications* **2008**, *29*, 1052.
(81) Geng, J.; Lindqvist, J.; Mantovani, G.; Haddleton, D. M. *Angewandte Chemie International Edition* **2008**, *47*, 4180.
(82) Besenius, P.; Slavin, S.; Vilela, F.; Sherrington, D. C. *Reactive and Functional Polymers* **2008**, *68*, 1524.
(83) Acosta Ortiz, R.; García Valdez, A. E.; Navarro Tovar, A. G.; Hilario de la Cruz, A. A.; González Sánchez, L. F.; García Trejo, J. H.; Espinoza Muñoz, J. F.; Sangermano, M. *Journal of Polymer Research* **2014**, *21*, 1.
(84) Koo, S. P. S.; Stamenović, M. M.; Prasath, R. A.; Inglis, A. J.; Du Prez, F. E.; Barner-Kowollik, C.; Van Camp, W.; Junkers, T. *Journal of Polymer Science Part A: Polymer Chemistry* **2010**, *48*, 1699.
(85) Chen, G.; Amajjahe, S.; Stenzel, M. H. *Chemical Communications* **2009**, 1198.
(86) Gress, A.; Völkel, A.; Schlaad, H. *Macromolecules* **2007**, *40*, 7928.
(87) Kempe, K.; Neuwirth, T.; Czaplewska, J.; Gottschaldt, M.; Hoogenboom, R.; Schubert, U. S. *Polymer Chemistry* **2011**, *2*, 1737.
(88) Sharon, N.; Lis, H. *Glycobiology* **2004**, *14*, 53R.
(89) Sharon, N.; Lis, H. *Science* **1989**, *246*, 227.
(90) Kumar, K.; Chandra, K.; Sumanthi, J.; Reddy, G.; Shekar, P.; Reddy, B. *Journal of Orofacial Sciences* **2012**, *4*, 20.
(91) Kilpatrick, D. C. *Biochimica et Biophysica Acta (BBA) - General Subjects* **2002**, *1572*, 187.
(92) Etzler, M. E. *Annual Review of Plant Physiology* **1985**, *36*, 209.
(93) Pieters, R. J. *Org. Biomol. Chem.* **2009**, *7*, 2013.
(94) Loris, R.; Casset, F.; Bouckaert, J.; Pletinckx, J.; Dao-Thi, M.-H.; Poortmans, F.; Imberty, A.; Perez, S.; Wyns, L. *Glycoconj J* **1994**, *11*, 507.
(95) Mario Sánchez, M.; Cabezas, J. A. *Biochemical Education* **1998**, *26*, 309.
(96) Endo, Y.; Tsurugi, K. *Journal of Biological Chemistry* **1987**, *262*, 8128.
(97) Kumar, J.; McDowall, L.; Chen, G.; Stenzel, M. H. *Polymer Chemistry* **2011**, *2*, 1879.

(98) Gabius, H.-J. *Biochimica et Biophysica Acta (BBA) - General Subjects* **2002**, *1572*, 163.
(99) Taylor, P. R.; Martinez-Pomares, L.; Stacey, M.; Lin, H.-H.; Brown, G. D.; Gordon, S. *Annual Review of Immunology* **2005**, *23*, 901.
(100) Geijtenbeek, T. B. H.; Gringhuis, S. I. *Nat Rev Immunol* **2009**, *9*, 465.
(101) Dambuza, I. M.; Brown, G. D. *Current Opinion in Immunology* **2015**, *32*, 21.
(102) Su, S. V.; Hong, P.; Baik, S.; Negrete, O. A.; Gurney, K. B.; Lee, B. *Journal of Biological Chemistry* **2004**, *279*, 19122.
(103) Banchereau, J.; Steinman, R. M. *Nature* **1998**, *392*, 245.
(104) Flacher, V.; Douillard, P.; Aït-Yahia, S.; Stoitzner, P.; Clair-Moninot, V.; Romani, N.; Saeland, S. *Immunology* **2008**, *123*, 339.
(105) Plato, A.; Willment, J. A.; Brown, G. D. *International Reviews of Immunology* **2013**, *32*, 134.
(106) McEver, R. P. *Current Opinion in Cell Biology* **2002**, *14*, 581.
(107) Agrawal, A.; Singh, P. P.; Bottazzi, B.; Garlanda, C.; Mantovani, A. *Advances in Experimental Medicine and Biology* **2009**, *653*, 98.
(108) Mantovani, A.; Garlanda, C.; Doni, A.; Bottazzi, B. *Journal of Clinical Immunology* **2008**, *28*, 1.
(109) Lee, R. T.; Lee, Y. C. *Glycoconj J* **2000**, *17*, 543.
(110) Smith, E. E.; Smith, Z. H. G.; Goldstein, I. J. *Biochemical Journal* **1968**, *107*, 715.
(111) Roy, R.; Page, D.; Figueroa Perez, S.; Verez Bencomo, V. *Glycoconj J* **1998**, *15*, 251.
(112) Islam Khan, M.; Mandal, D. K.; Brewer, C. F. *Carbohydrate Research* **1991**, *213*, 69.
(113) Burke, S. D.; Zhao, Q.; Schuster, M. C.; Kiessling, L. L. *Journal of the American Chemical Society* **2000**, *122*, 4518.
(114) Ambrosi, M.; Cameron, N. R.; Davis, B. G.; Stolnik, S. *Org. Biomol. Chem.* **2005**, *3*, 1476.
(115) Chiad, K.; Stelzig, S. H.; Gropeanu, R.; Weil, T.; Klapper, M.; Müllen, K. *Macromolecules* **2009**, *42*, 7545.
(116) Zlatanova, J.; Lindsay, S. M.; Leuba, S. H. *Progress in Biophysics and Molecular Biology* **2000**, *74*, 37.
(117) Marx, K. A. *Biomacromolecules* **2003**, *4*, 1099.
(118) Homola, J.; Yee, S. S.; Gauglitz, G. *Sensors and Actuators B: Chemical* **1999**, *54*, 3.
(119) Gou, Y.; Geng, J.; Richards, S.-J.; Burns, J.; Remzi Becer, C.; Haddleton, D. M. *Journal of Polymer Science Part A: Polymer Chemistry* **2013**, *51*, 2588.
(120) Gou, Y.; Slavin, S.; Geng, J.; Voorhaar, L.; Haddleton, D. M.; Becer, C. R. *ACS Macro Lett.* **2012**, *1*, 180.

(121) Becer, C. R.; Gibson, M. I.; Geng, J.; Ilyas, R.; Wallis, R.; Mitchell, D. A.; Haddleton, D. M. *Journal of the American Chemical Society* **2010**, *132*, 15130.
(122) Kedar, U.; Phutane, P.; Shidhaye, S.; Kadam, V. *Nanomedicine: Nanotechnology, Biology and Medicine* **2010**, *6*, 714.
(123) Miyata, K.; Christie, R. J.; Kataoka, K. *Reactive and Functional Polymers* **2011**, *71*, 227.
(124) Laitala-Leinonen, T. *Recent Patents on DNA & Gene Sequences* **2010**, *4*, 113.
(125) Owens Iii, D. E.; Peppas, N. A. *International Journal of Pharmaceutics* **2006**, *307*, 93.
(126) Wang, A.; Gao, H.; Sun, Y.; Sun, Y.-l.; Yang, Y.-W.; Wu, G.; Wang, Y.; Fan, Y.; Ma, J. *International Journal of Pharmaceutics* **2013**, *441*, 30.
(127) Li, H.; Bian, S.; Huang, Y.; Liang, J.; Fan, Y.; Zhang, X. *Journal of Biomedical Materials Research Part A* **2014**, *102*, 150.
(128) Sizovs, A.; Xue, L.; Tolstyka, Z. P.; Ingle, N. P.; Wu, Y.; Cortez, M.; Reineke, T. M. *Journal of the American Chemical Society* **2013**, *135*, 15417.
(129) Li, X.; Takashima, M.; Yuba, E.; Harada, A.; Kono, K. *Biomaterials* **2014**, *35*, 6576.
(130) Schleh, C.; Semmler-Behnke, M.; Lipka, J.; Wenk, A.; Hirn, S.; Schäffler, M.; Schmid, G.; Simon, U.; Kreyling, W. G. *Nanotoxicology* **2012**, *6*, 36.
(131) Richards, S.-J.; Fullam, E.; Besra, G. S.; Gibson, M. I. *Journal of Materials Chemistry B* **2014**, *2*, 1490.
(132) Zhou, J.; Hao, N.; De Zoyza, T.; Yan, M.; Ramström, O. *Chemical communications (Cambridge, England)* **2015**, *51*, 9833.
(133) Kim, H. Y.; Jang, K. J.; Veerapandian, M.; Kim, H. C.; Seo, Y. T.; Lee, K. N.; Lee, M.-H. *Biotechnology Reports* **2014**, *3*, 49.
(134) Ribeiro-Viana, R.; Sánchez-Navarro, M.; Luczkowiak, J.; Koeppe, J. R.; Delgado, R.; Rojo, J.; Davis, B. G. *Nat. Commun.* **2012**, *3*, 1303.
(135) Varki, A. *Journal of Molecular Medicine* **2012**, *90*, 481.
(136) Ogata, M.; Uzawa, H.; I. P. J. Hidari, K.; Suzuki, T.; Y. Park, E.; Usui, T. *Journal of Applied Glycoscience* **2014**, *61*, 1.
(137) Luczkowiak, J.; Muñoz, A.; Sánchez-Navarro, M.; Ribeiro-Viana, R.; Ginieis, A.; Illescas, B. M.; Martín, N.; Delgado, R.; Rojo, J. *Biomacromolecules* **2013**, *14*, 431.
(138) Nazemi, A.; Haeryfar, S. M. M.; Gillies, E. R. *Langmuir* **2013**, *29*, 6420.

# Chapter 2 Self-assembled glyconanoparticles with controlled morphologies for dendritic cell lectin DC-SIGN binding and drug delivery

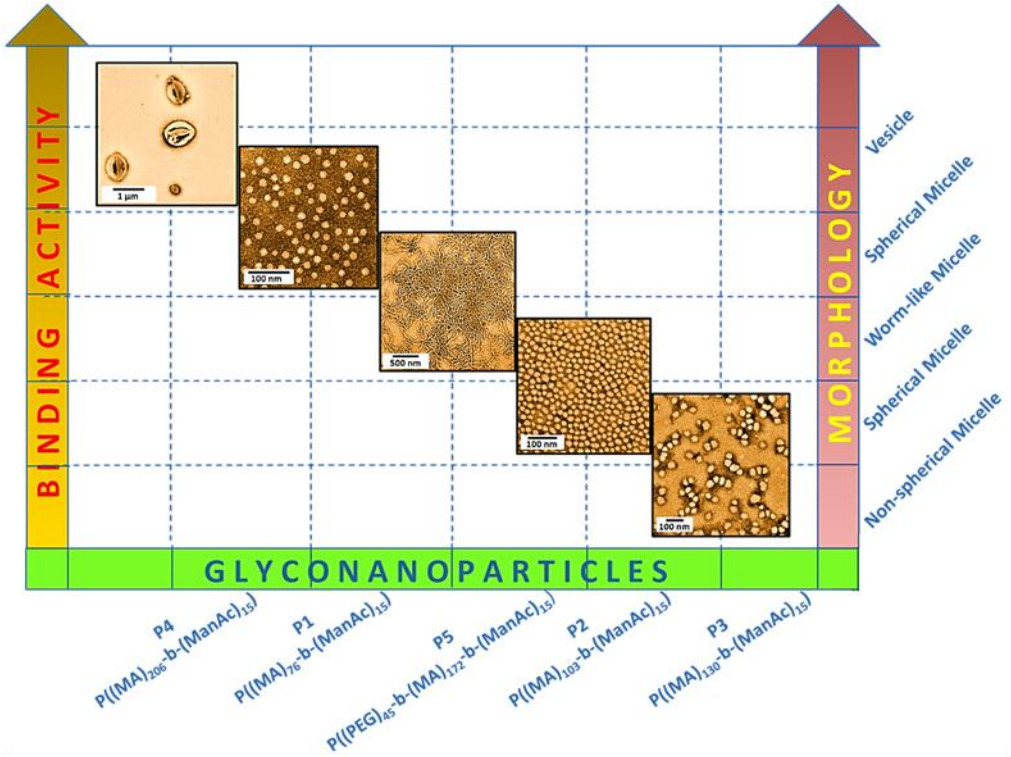


*Well-defined amphiphilic block glycopolymers with the same mannose content have been self-assembled in aqueous solution to form glyconanoparticles with different morphologies (spherical, worm-like micelles and vesicles) and narrow size distributions between 0.144 and 0.367. Transmission electron microscopy (TEM) and dynamic light scattering (DLS) were used to characterize these self-assembled glyconanoparticles. The size and shape of nanoparticles have significant effects on the binding affinities with dendritic cell-specific intercellular adhesion molecule-3-grabbing non-integrin (DC-SIGN; CD209), which is measured utilizing a surface plasmon resonance spectrometer. Additionally, SB-216763 (GSK-3 inhibitor) loaded glyco-micelles were developed via the combination of solvent-evaporation and dialysis techniques, which exhibited a slow and sustained release of the hydrophobic drug.*

## 2.1 Introduction

Protein-carbohydrate interactions play an important role in many biological processes including cell interactions with immune systems, tumor metastasis, adhesion of infectious agents to host cells and many more.[1,2] Proteins involved in these signalling and processing pathways are known as lectins.[3,4] These carbohydrate binding proteins are wide-spread in nature and they differ from antibodies or enzymes entities.[5] For example, it has been shown that some viruses such as HIV express many carbohydrate entities at their surface. These glycosylated surfaces enable them to bind to specific lectins of the immune system cells. Therefore, one of the promising strategies for infectious diseases would be to design competing systems with higher lectin affinity than pathogens, thus preventing their adhesion. Although the binding between single carbohydrates and lectins is weak, it could be greatly enhanced by the multivalent effect of densely packed carbohydrate molecules with unique functionalities, which is also known as the "glycocluster effect".[6] Glyconanoparticles as carbohydrate-based systems provide in a similar manner to mimic the behavior of naturally existing glycocalyx. Therefore, the fabrication and engineering of innovative glyconanoparticles with unique physiochemical properties help to further enhance their specific recognition properties on multivalent scaffolds in glycoscience.

Recent and elegant synthetic routes have allowed polymer chemists to prepare a wide range of glyconanoparticles that provide strong and selective recognition properties towards lectins.[7-11] In particular, amphiphilic block glycopolymers have attracted a great attention in terms of their ability to form various types of glyconanoparticles. These amphiphilic glycopolymers are generally composed of biocompatible, biodegradable hydrophobic polymer blocks covalently bonded to a biocompatible hydrophilic block.[12-14] Some recent studies have shown that amphiphilic block glycopolymers with different carbohydrate compositions were used to produce nanoparticles, such as micelles, nanospheres, core-shell nanoparticles, micelle-like nanoparticles, crew cut micelles, nanocapsules and polymersomes.[15-19] These studies facilitate the understanding and investigation of

glycopolymer-lectin-binding activities that are significantly influenced by glycopolymer architecture, valency, size, and density of binding elements. Furthermore, they offer a promising route for the creation of a broad variety of bioactive self-assembled glyco-nanostructures for biomedical applications such as drug delivery, biomaterials, bio- and nano-technologies, and gene therapy.[20-24] During the last few of years, a number of strategies devoted to prepare glycopolymers *via* single electron transfer living radical polymerization (SET-LRP) technique has exploded.

In this chapter, SET-LRP was used to synthesize several types of amphiphilic block co-glycopolymers bearing mannose moieties by using methyl acrylate (MA), glycomonomer (ManAc) and/or poly(ethylene glycol) (PEG) as hydrophobic and hydrophilic blocks, respectively. Mannose glycomonomer was prepared according to the procedure reported by Qiang *et al.*[25] Poly(ethylene glycol) bis(2-bromoisobutyrate) (PEG-Br) was used as an initiator to prepare amphiphilic triblock glycocopolymer. The self-assembly of these well-defined amphiphilic glycopolymers was investigated in aqueous solution to obtain glyconanostructures with various size and morphologies. The resulting glyconanoparticles were further investigated for their binding affinities with lectins, in particular with DC-SIGN, which is a human C-type lectin present on both macrophages and also dendritic cell subpopulations. DC-SIGN binds to micro organisms and host molecules by recognizing surface rich in mannose containing glycans through multivalent glycan-protein interactions and notably serves a target molecule for several viruses such as human immunodeficiency virus (HIV) and hepatitis C virus (HCV).[26,27]

Various analytical methods have been developed to study multivalent carbohydrate-lectin interactions.[8] Surface plasmon resonance (SPR) spectrometer that was used to analyze the interaction between DC-SIGN and the glyconanoparticles in this study monitors the interaction of two or more molecules or molecular assemblies in real time. This technique is very sensitive and can be used to detect association of glycoproteins or glycopolymers in even pico-molar concentrations. In the first part of this chapter, we reported the synthesis of well-

defined amphiphilic glycopolymers *via* SET-LRP technique, their spontaneous self-assembly behavior and binding studies of the resulting nanoparticles with DC-SIGN. Polymeric micelles have a great potential for the contribution on the development of various drug delivery and release systems in pharmacological applications.[28-32] Very recent and robust strategies have allowed polymer chemists to prepare polymeric micelles with different chemical functional groups and a broad variety of morphologies. In particular, the ability of glyco-micelles in terms of molecular recognition events and biological interaction processes could play a crucial role in order to develop cell specific targeted drug delivery systems. Therefore, they have attracted increasing attention due to their potential in biomimetic applications and human therapeutics.

Jiang and co-workers have performed three types of self-assembled nanoparticles from triblock copolymers with the same polymeric backbone but different sugar regioisomers as pendant groups.[33] Well-dispersed spheres were obtained from the polymer that is self-assembled into nanoparticles with the glyco block as the shell and the rod block as the core. The bioactivity of these nano-objects was analyzed with PNA and Erythrina cristagalli agglutinin (ECA) *via* quartz crystal microbalance (QCM). Similarly, Huang *et al* prepared glycosylated peptide-based block copolymers to form glycoparticles with well-defined morphologies in an aqueous solution.[34]

Hence, in the second part of this chapter, the synthesized amphiphilic glycopolymers were employed to prepare SB-216763 loaded glyco-micelles as nanocarriers. SB-216763, 3-(2,4-Dichlorophenyl)-4-(1-methyl-1H-indol-3-yl)-1H-pyrrole-2,5-dione, is a potent and selective inhibitor of the J and K isozymes of glycogen synthase kinase-3 (GSK-3).[35,36] GSK-3 is a serine/threonine protein kinase, the activity of which is liked to some pathological conditions, such as diabetes and/or insulin resistance, and Alzheimer's disease and also it is active in a number of central intracellular signalling pathways.[37] It has not been performed for the encapsulation and also the development of delivery and release systems so far. To the best of our knowledge, this is the first attempt to load SB-216763 into micelles

successfully and also to investigate the *in vitro* release of SB-216763 from glyco-micelles with sufficient control. The results showed that SB-216763 loaded glyco-micelles can be utilized for the further investigations in cellular microenvironment due to a sustained drug release.

## 2.2 Results and Discussion

### 2.2.1 Synthesis of mannose glycomonomer (ManAc)

In general, there are two advanced synthesis methods to prepare well-defined glycopolymers, which are polymerization of carbohydrate-bearing monomers without the deprotection steps and chemical modifications of functional polymers with carbohydrates via controlled/living polymerization techniques in combination with click reactions. The most important and frequently employed click reaction is undoubtedly the Copper-catalyzed azide-alkyne cycloaddition (CuAAC) that could be used either to prepare different types of glycomonomer or to efficiently modify polymer chains after the polymerization. Firstly, one-pot Fischer type glycosylation reaction was performed to prepare alkyne functionalized mannose and then CuAAC of this with azide functionalized acrylate yielded a mannose glycomonomer.

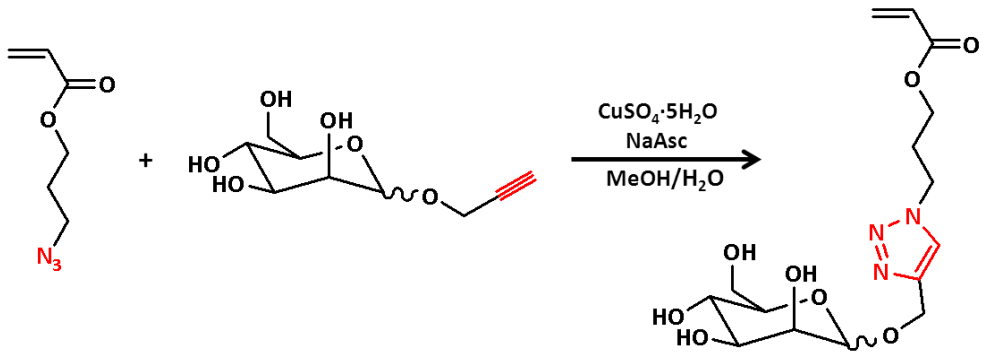


**Scheme 2.1.** Schematic representation of the synthesized D-Mannose glycomonomer *via* CuAAC.

As depicted in Scheme 2.1, CuAAC "*click*" reaction was carried out in the presence of $CuSO_4 \cdot 5H_2O$ and (+)-sodium L-ascorbate as a catalyst system in $MeOH/H_2O$ mixture at the room temperature for 24 h. This reaction was monitored and confirmed by $^{1}H$- NMR, $^{13}C$-NMR, FT-IR, and ESI-MS. As shown in Figure 2.1, the

appearance of the new peak at 8.05 ppm indicates the formation of a triazole ring that confirms the glycomonomer structure. Besides, the existence of D-mannose C-1 peaks at 99.6 & 103.6 ppm in the $^{13}C$ NMR showed that the glycomonomer is an anomeric mixture. In the ESI-MS spectra, there is a clear peak at 374.3 m/z that corresponds to the calculated molecular weight of the mannose glycomonomer with 374.2 m/z. Finally, the product was obtained as a white solid with a 58.2% yield.

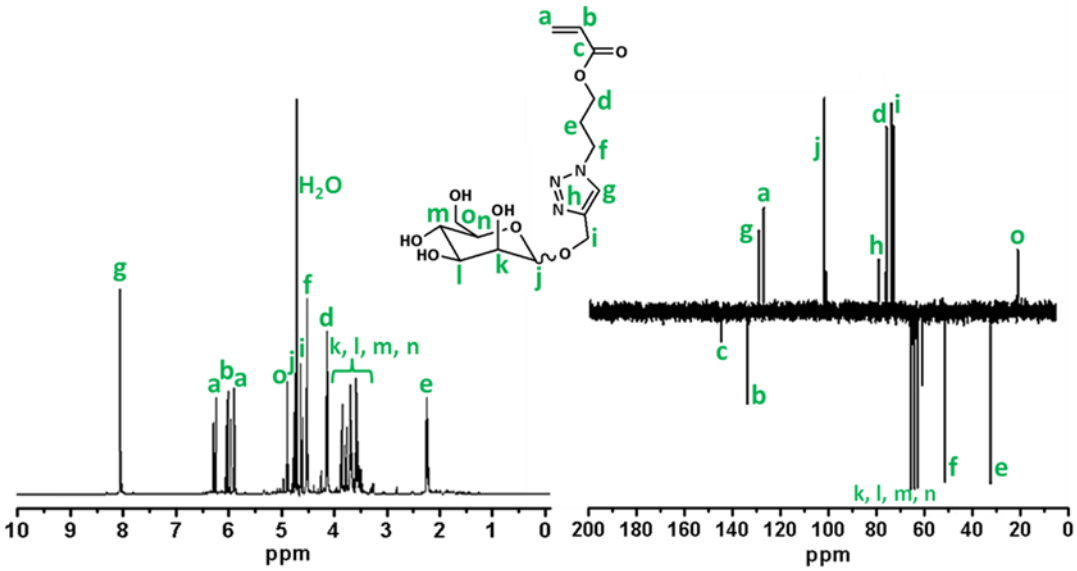


**Figure 2.1.** $^{1}H$-NMR and $^{13}C$-NMR spectrum of D-mannose glycomonomer.

### 2.2.2 Synthesis of PEG-Br initiator

Poly(ethylene glycol) (PEG) is one of the most widely used polymers in biorelated applications such as drug delivery purposes, biomaterials, bio- and nanotechnologies, and gene therapy. This usefulness can mainly be attributed to its low toxicity, water solubility, stability and also good relevance with various biological molecules. In addition, it has been widely used as the hydrophilic block of amphiphilic block copolymers to prepare particles. In according to all these important properties of PEG, it was used to prepare triblock co-glycopolymer in order to create worm-like micelles.

The synthesis of PEG-Br initiator was performed through an esterification reaction. PEG was esterified by the addition of 2-bromoisobutyryl bromide (BiBB) in the

presence of TEA and THF. After purification, PEG-Br was obtained as a white powder in high yield. The reaction was monitored by $^{1}$H-NMR and the esterification was confirmed by the appearance of the peaks at 2.0 ppm from the methyl groups of the product. Furthermore, the structure was also confirmed by comparing the ratios of the integral of $CH_3$-O to the integral of $C(CH_3)_2Br$ (expected 3:6) and the integral ratios of $CH_3$-O-$CH_2$-R to $C(CH_3)_2Br$ (expected 2:6).

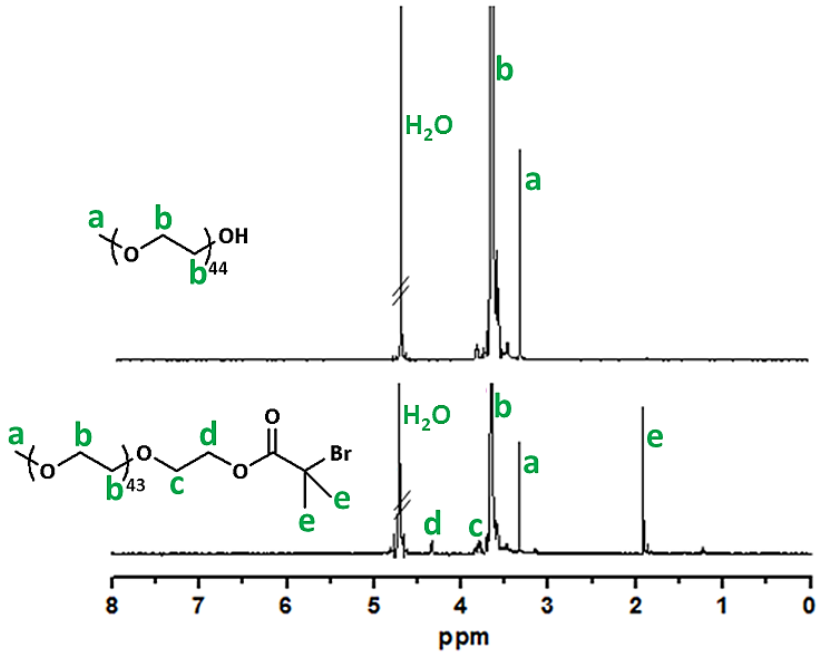


**Figure 2.2.** $^{1}$H NMR of the PEG-Br initiator showing the appearance of the methyl peak (e) at 1.96 ppm in $D_2O$.

### 2.2.3 Homopolymerization of MA using PEG-Br initiator

PEG-Br was synthesized as described above and employed as an initiator for homopolymerization of MA to optimize polymerization conditions. The SET-LRP of MA was carried out in the presence of PEG-Br in DMSO at 25$^{o}$C using a Cu(0)/Cu(II) and $Me_6$Tren as a catalyst. To optimize the polymerization, chain extension reaction was performed. In order to obtain targeted $M_n$ values and low dispersities, kinetic study of the homopolymerization of MA and one-pot chain extension was investigated at periodic intervals.

The conversion was measured by $^{1}H$ NMR and calculated according to the integral of vinyl groups with that of the O-$CH_3$ groups at 3.80 ppm. The molar mass and dispersity index were determined by Gel Permeation Chromatography (GPC). The reaction displayed a living nature and full conversion was obtained in 3 hours with a measured $M_n$ of 8300 g.mol$^{-1}$ and dispersity of 1.11. In order to investigate the chain end fidelity of the synthesized polymers, chain extension of MA with DP = 30 was carried out. As expectedly, the time required to reach quantitative conversion has increased. After 6 hours, the conversion of 97% was achieved without any significant tailing or shoulder at either high or low molar mass regions of the GPC. As seen in Figure 2.3, GPC traces confirmed the successful chain growth as clear shifts to higher molar mass with increased polymerization time has been observed. The $M_n$ increased to 10900 g.mol$^{-1}$ and the $Đ$ did not show any considerable change.

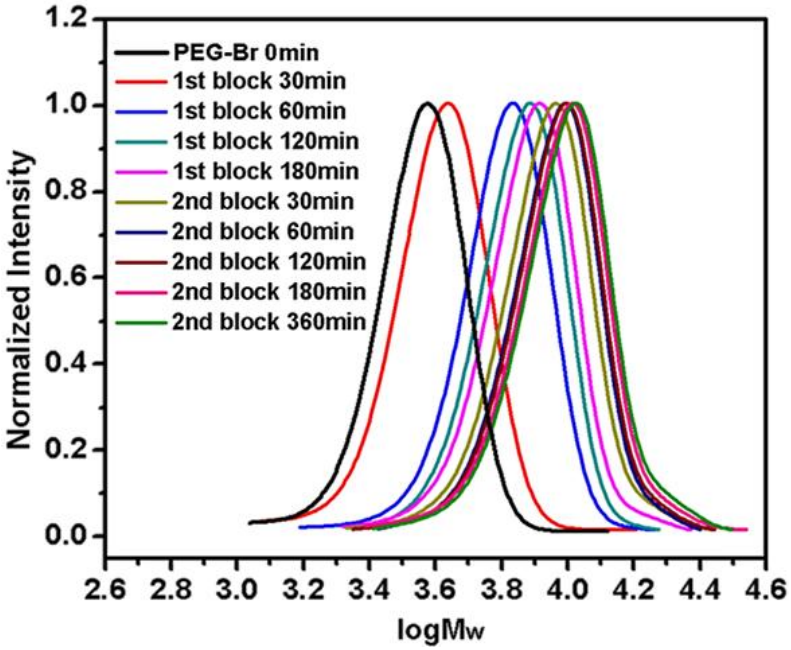


**Figure 2.3.** GPC traces of the SET-LRP of MA and chain extension using PEG-Br initiator.

Semi-logarithmic kinetic plot displayed a linear increase of conversion with time as expected, indicating the livingness of the polymerization. The increase in the molar mass with conversion over time was hence also linear. It was obvious that the polymerization of MA has been achieved with a good control. It was also shown

that the polymerization showed living characteristics throughout the whole polymerization without any termination or side reaction. To retain chain end fidelity of the living polymers, chain extension reaction was carried out up to 97% conversion.

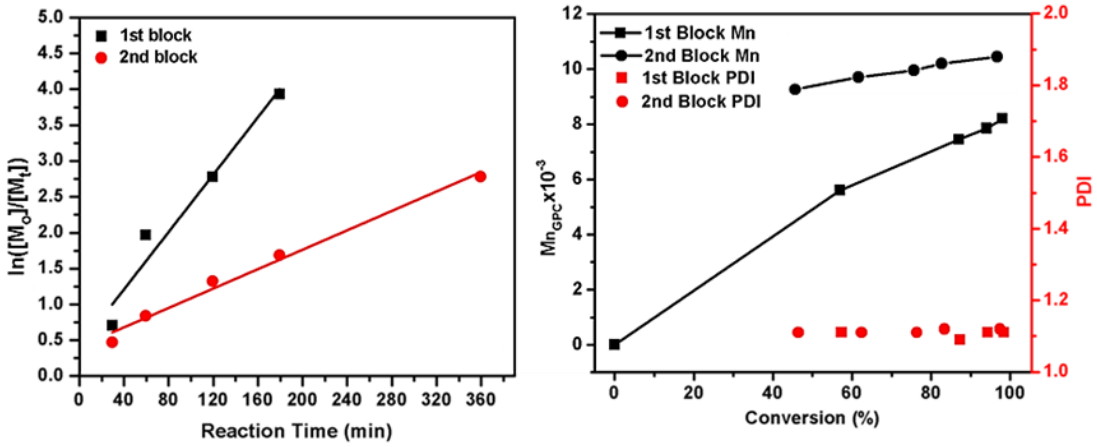


**Figure 2.4.** Semi-logarithmic kinetic plot (left) and molar mass/dispersity data (right) of SET-LRP of MA and chain extension reaction.

### 2.2.4 Synthesis of amphiphilic block co-glycopolymers

A series of well-defined amphiphilic block glycopolymers were prepared *via* SET-LRP by using EBiB or PEG-Br as an initiator. PEG initiator was used to provide increased hydrophilic behavior and also stability to fabricate vesicle assemblies. The molar ratio of [MA]/[ManAc] has been varied to yield amphiphilic block copolymers with increasing ratios between their hydrophobic and hydrophilic moieties.

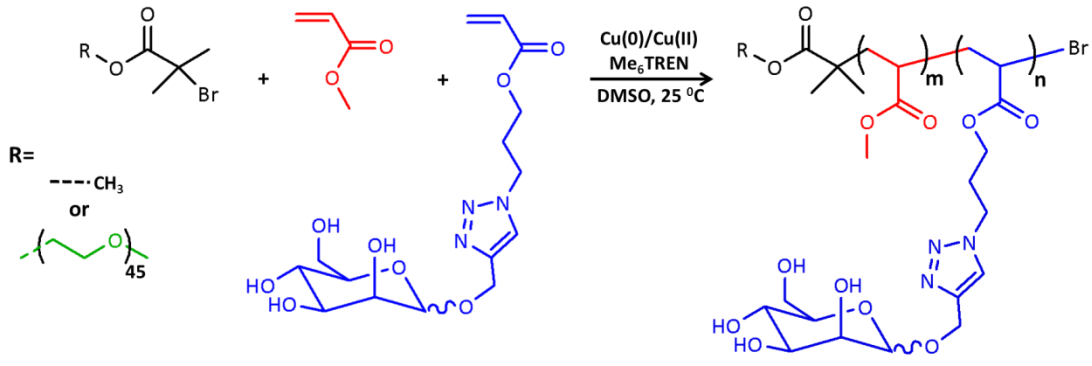


**Scheme 2.2.** Schematic representation of copolymerization of MA and ManAc *via* SET-LRP with EBiB or PEG-Br initiator.

The average molecular shape of nanoparticles is most simply a reflection of the hydrophilic fraction. One-pot polymerization approach has been employed to ensure excellent block formation. Firstly, MA was polymerized up to 96-97% conversion and subsequently; the chain extension of the second block with glycomonomer (DP = 15, dissolved and degassed in 1 mL of DMSO) was carried out after 3 h based on the information obtained from the kinetic study of MA. The conversion of both monomers was followed by using $^{1}$H NMR, which showed the disappearance of the vinyl groups completely between 5.8-6.4 ppm after 3 hours. Both monomers reached to full conversion. The purified glycopolymers were analyzed by GPC and $^{1}$H NMR. Based on these results, it was clear that the copolymerization of MA and ManAc has been achieved with an excellent control as indicated by low dispersity indices and increasing molar mass. Summary of analysis of all P((MA)$_m$-b-(ManAc)$_n$) polymers (**P1, P2, P3, P4**) were presented in Table 2.1.

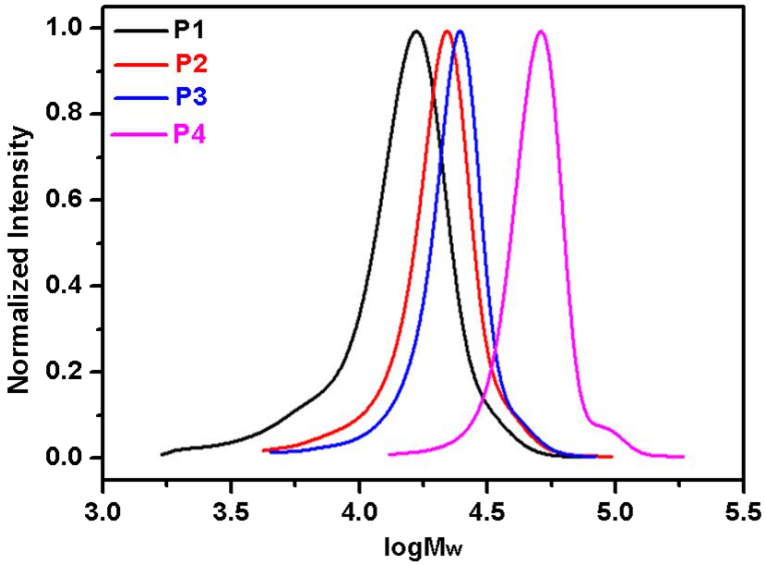


**Figure 2.5.** GPC traces of amphiphilic block co-glycopolymers, P((MA)$_m$-b-(ManAc)$_n$) (**P1, P2, P3, P4**).

**Table 2.1.** Summary of monomer conversions, number average molar mass ($M_n$) and molar mass distributions ($Đ$) of all block co-glycopolymers.

| Polymer | [MA]:[ManAc]:[I][a] | $\rho$[b] (%) | | $M_{n,NMR}$[c] (g.mol$^{-1}$) | $M_{n,GPC}$[d] (g.mol$^{-1}$) | $Đ$ |
|---|---|---|---|---|---|---|
| | | MA | ManAc | | | |
| **P1 = P($(MA)_{76}$-b-$(ManAc)_{15}$)** | 80:15:1 | 96 | 98 | 11850 | 12400 | 1.16 |
| **P2 = P($(MA)_{103}$-b-$(ManAc)_{15}$)** | 105:15:1 | 97 | 99 | 14150 | 14800 | 1.18 |
| **P3 = P($(MA)_{130}$-b-$(ManAc)_{15}$)** | 135:15:1 | 96 | 99 | 16400 | 17600 | 1.17 |
| **P4 = P($(MA)_{206}$-b-$(ManAc)_{15}$)** | 210:15:1 | 97 | 98 | 22800 | 26900 | 1.20 |
| **P5 = P($(PEG)_{45}$-b-$(MA)_{172}$-b-$(ManAc)_{15}$)** | 180:15:1 | 96 | 99 | 23800 | 24600 | 1.17 |

**[a] Initial molar ratio of monomers to initiator; [b] Conversion ($\rho$) obtained from $^1$H NMR analysis; [c] Calculated according to eq. $M_{n,NMR}$= $[M]_0/[I]$ x conv% (from NMR) x $M_w$ of MA and ManAc + $M_w$ of initiator; [d] Determined by DMF GPC (relative to PMMA stn.).**

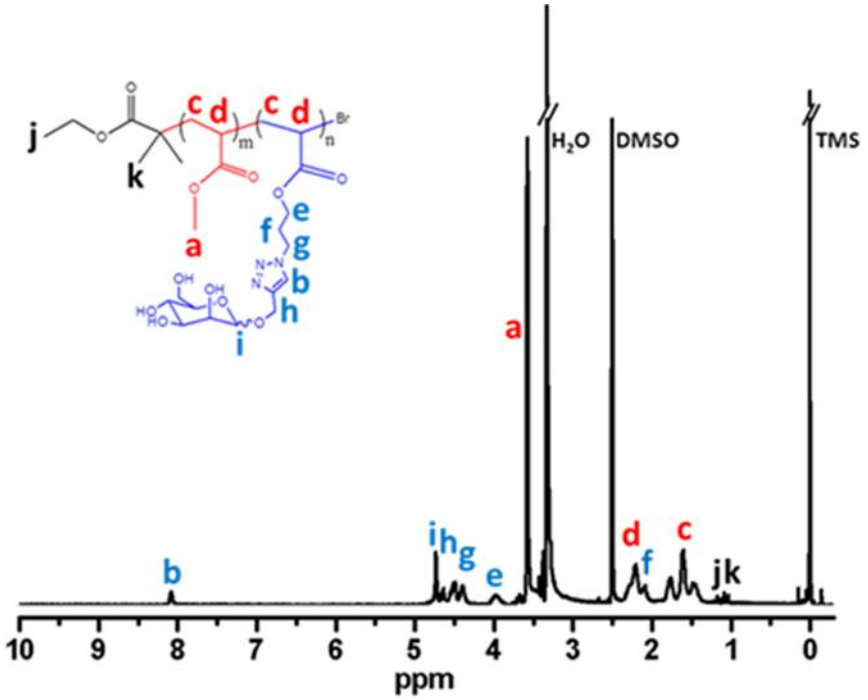


**Figure 2.6.** $^1$H NMR spectra of the purified P($(MA)_m$-b-$(ManAc)_n$)**.**

Chain end fidelity of P((PEG)-b-(MA)) has been confirmed by chain extension with MA prior to the synthesis of the triblock co-glycopolymer, **P5**, using the same approach in the presence of PEG-Br initiator. GPC analysis revealed a clear baseline shift of elution traces after each monomer addition with increasing molar mass and final $Đ$ of 1.17. Depending on the polymerization rate of glycomonomer, the reaction was kept for 24 hours after addition in order to reach to full conversion.

No significant tailing or shoulder has been observed in the GPC traces throughout the polymerization. Moreover, the measured $M_n$ by GPC and the theoretical molar mass calculated based on the monomer conversions are in good agreement.

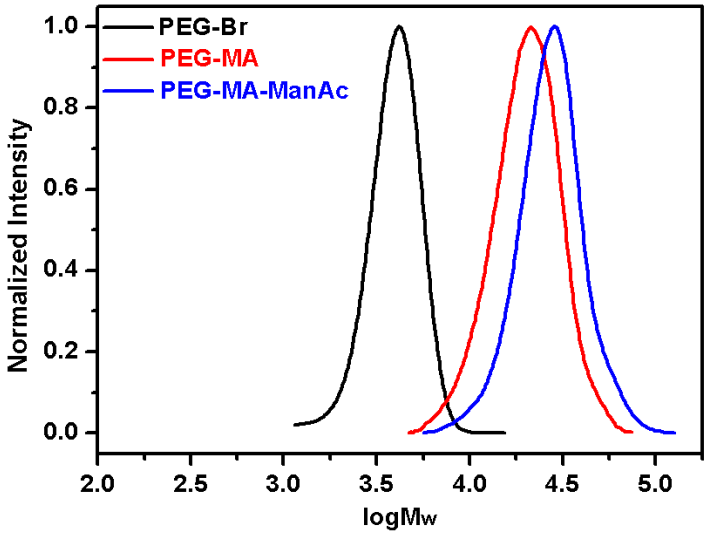


**Figure 2.7.** GPC traces of triblock co-glycopolymer, P((PEG)$_{45}$-b-(MA)$_{172}$-b-(ManAc)$_{15}$) (**P5**).

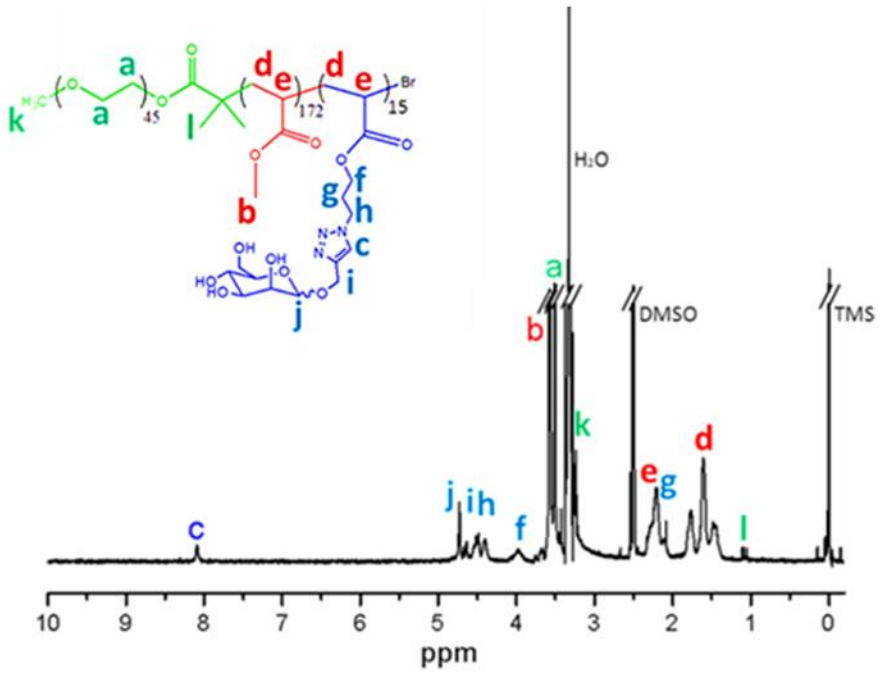


**Figure 2.8.** $^1$H NMR of the obtained amphiphilic triblock co-glycopolymer after purification.

### 2.2.5 Preparation and characterization of glyconanoparticles *via* TEM and DLS

Nanoparticles of these amphiphilic glycopolymers having PEG block and/or carbohydrate group as hydrophilic block and MA as hydrophobic one were prepared using a nanoprecipitation (solvent-switch) method. Briefly, each glycopolymer (≈ 7 mg) was dissolved in 1 mL DMF to give an initial concentration of 0.5 µM. To this solution, 2 mL of ultra-pure water was added at a rate of 5 µL /min using a programmable syringe pump. Slow-injection of water droplets into glycopolymer DMF solution ensured that thermodynamically stable self-assembled structures were obtained. The morphology and size of the resulting nanoparticles were systematically characterized by TEM and DLS, respectively. All block co-glycopolymers showed the self- assembly behavior in the water to create nanoparticles. PTA solution was used for the preparation of TEM samples in order to increase positively staining on the film coated copper grid. Amphiphilic block copolymers, **P1**, **P2** and **P3** yielded well-dispersed nanoparticles around 25 nm with a regular spherical shape and a narrow size distribution according to TEM imaging and DLS measurements.

**Table 2.2.** Physicochemical properties of the glyconanoparticles.

| Polymer | Molar ratio of [MA] to [ManAc] | DLS | | TEM | |
|---|---|---|---|---|---|
| | | $D_h$ (nm) | Đ | Size (nm) | Observed Morphology |
| **P1** | 1.17:1 | 22±1.2 | 0.144 | 17±3 | spherical micelles |
| **P2** | 1.58:1 | 23±1.3 | 0.173 | 18±5 | spherical micelles |
| **P3** | 2.00:1 | 26±1.1 | 0.221 | 25±6 | non-spherical micelles |
| **P4** | 3.16:1 | 380±2.6 | 0.356 | 420±25 | vesicles |
| **P5** | 2.64:1 | 65±1.6 | 0.376 | 35±8 | worm-like micelles |

These features were typical of spherical micelles. Further TEM analysis was conducted on each suspension measuring the average diameter of more than 50 single particles. Most of particles displayed an average diameter of 20 nm, which was slightly smaller than the obtained by DLS due to the air-dried TEM samples.

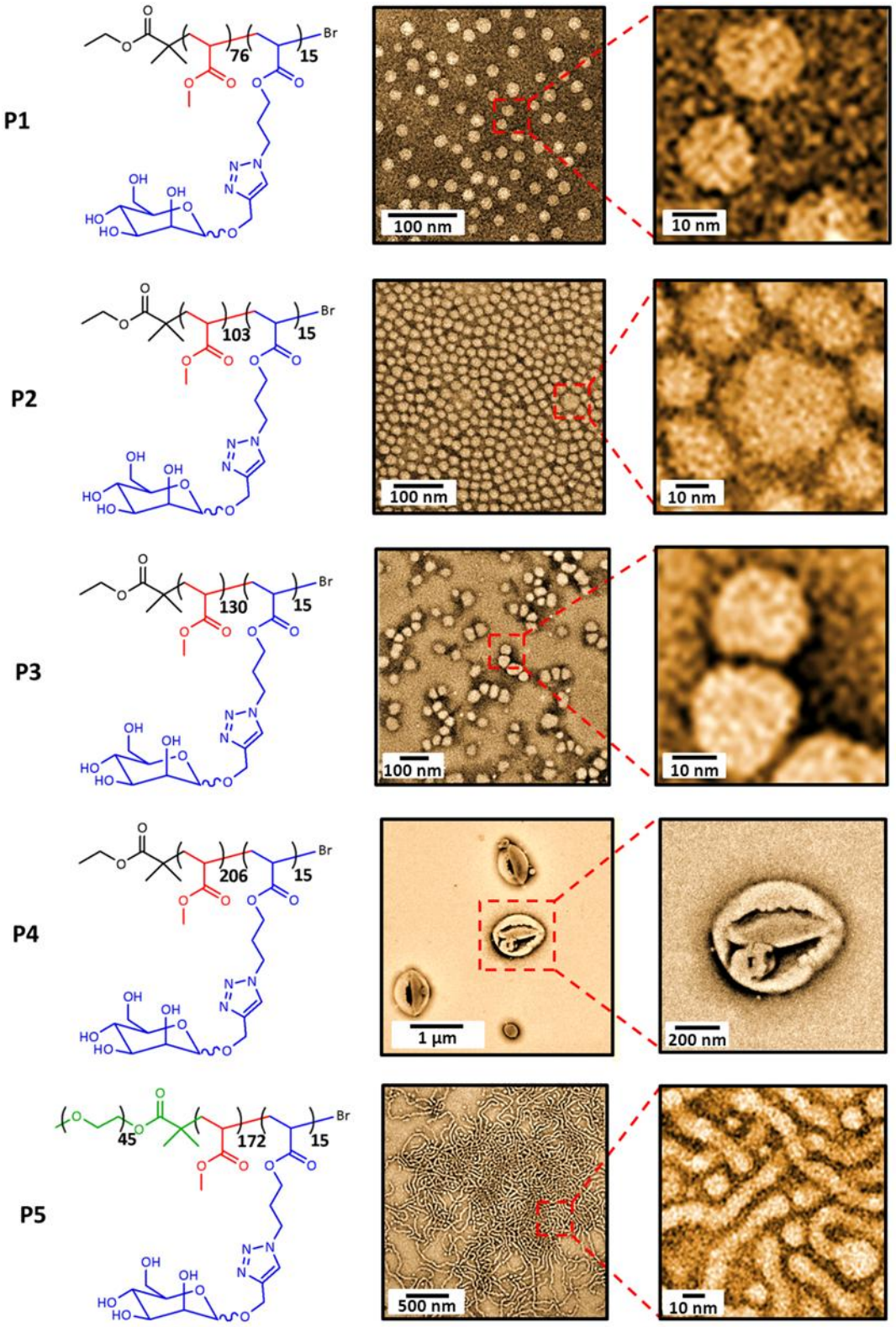


**Figure 2.9.** Chemical structures of polymers and TEM images of the obtained glyconanoparticles.

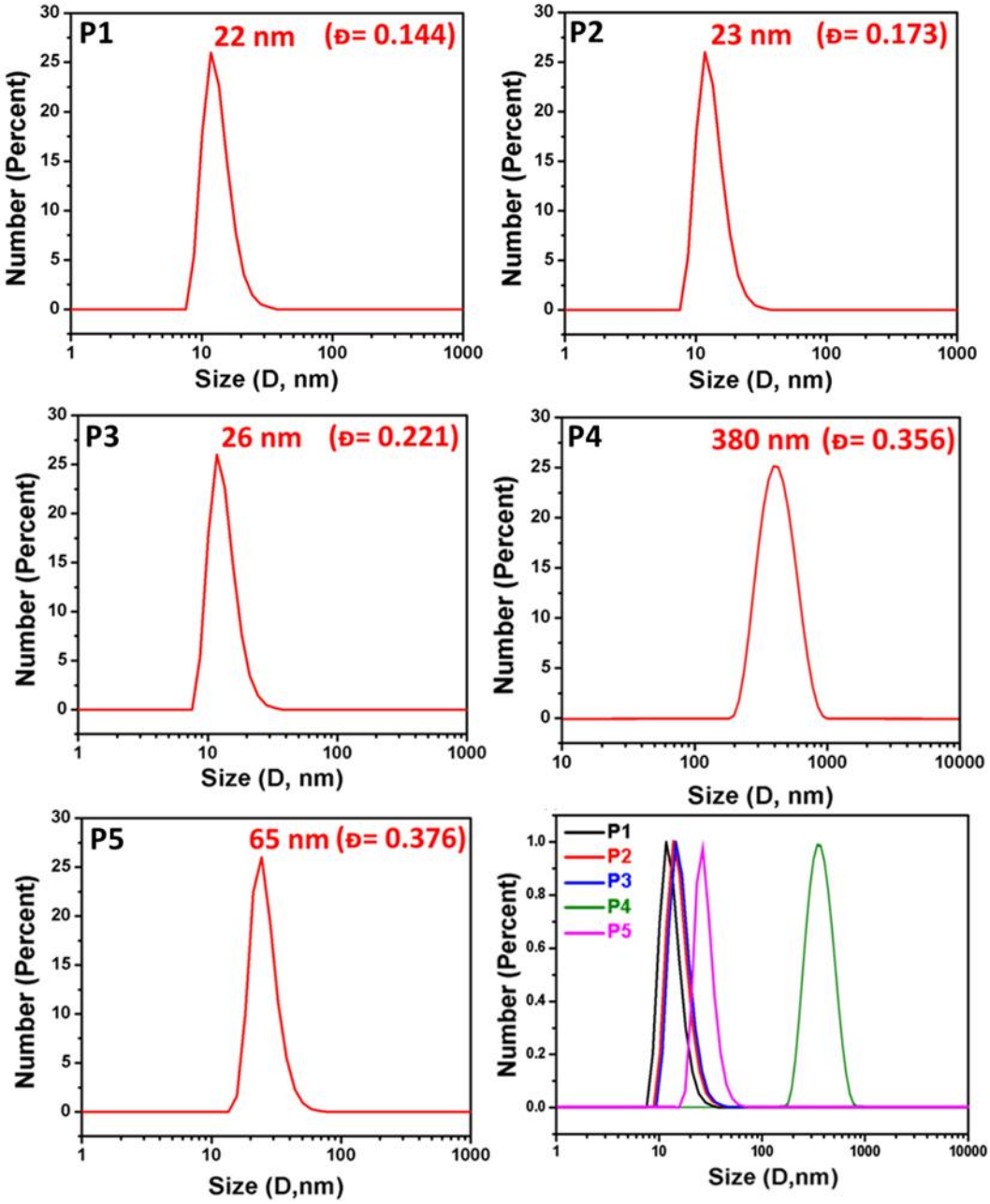


**Figure 2.10.** DLS measurements of all glyconanoparticles.

Furthermore, TEM imaging showed that most of the particles were not clustered, which was promising, as micelles generally tend to cluster together. It was also observed that **P2** and **P3** gave small amount of bigger aggregates. Increasing the hydrophobic content revealed the formation of self-assembled nanoparticles with higher hydrodynamic diameter. Indeed, the TEM image **P4** showed the formation of vesicular structures and DLS measurements a narrow size distribution centered at

380 nm. According to TEM and DLS results, size of glyconanoparticles was increasing with increase of polymer length.

Depending on the increase of MA fraction on the polymer, the existence region of nanoparticles became broader each time. This was possibly due to dependency on composition, molecular geometry, relative block lengths of the constitutive copolymers and the preparation methods on the formation of nanoparticles. Another attempt was conducted on **P4** to obtain a higher number of vesicular particles, decreasing the injection rate of the aqueous solution into the polymer one. The self-assembly of amphiphilic triblock glycopolymer, **P5**, has lower hydrophobic fraction than **P1**-**P4,** P($(MA)_m$-b-$(ManAc)_n$), due to the increasing molecular weight ratio of the hydrophobic block. According to TEM measurement, the majority of nanoparticles were worm-like micelles but with a small fraction of spherical micelles. The length of these worm-like micelles was in the range of 45 to 60 nm and their width was 24 nm, which was in agreement with unimer chain scaling. Further increase of molar ratio of hydrophobic block (for **P4** and **P5**) allowed creating different aggregates such as vesicles and worm-like micelles. In according to TEM images, they did not show any aggregation, which is very good because generally micelles like aggregation because of hydrophilic part of the surface of the nanoparticles.

### 2.2.6 Interaction between glyconanoparticles and DC-SIGN

C-type lectins that are one of the largest families of the animal lectins need $Ca^{+2}$ ions for their interaction with carbohydrates. Commonly, they consist of complex structures with carbohydrate recognition domains of about 120 amino acids and can have a variable number of subunits with 1-8 specific binding sites.[2,38] In here, DC-SIGN was employed for binding purposes, which is a human lectin on cell surfaces that binds preferentially to N-linked high-mannose oligosaccharides. DC-SIGN plays a critical role in human immunodeficiency virus (HIV) and hepatitis C virus (HCV) trafficking ability to interaction with the highly mannosylated gp120 glycoprotein present on the envelope of HIV.[39]

Surface Plasmon Resonance (SPR) is a very sensitive technique and can be used to detect association of glycoproteins or glycopolymers in pico-molar concentrations. It is employed here to investigate the binding ability of the glycopolymers. SPR was based on the measurement of adsorption of material onto planar metal surfaces has been employed to study a wide range of molecular systems at the solution-surface interface.[40]

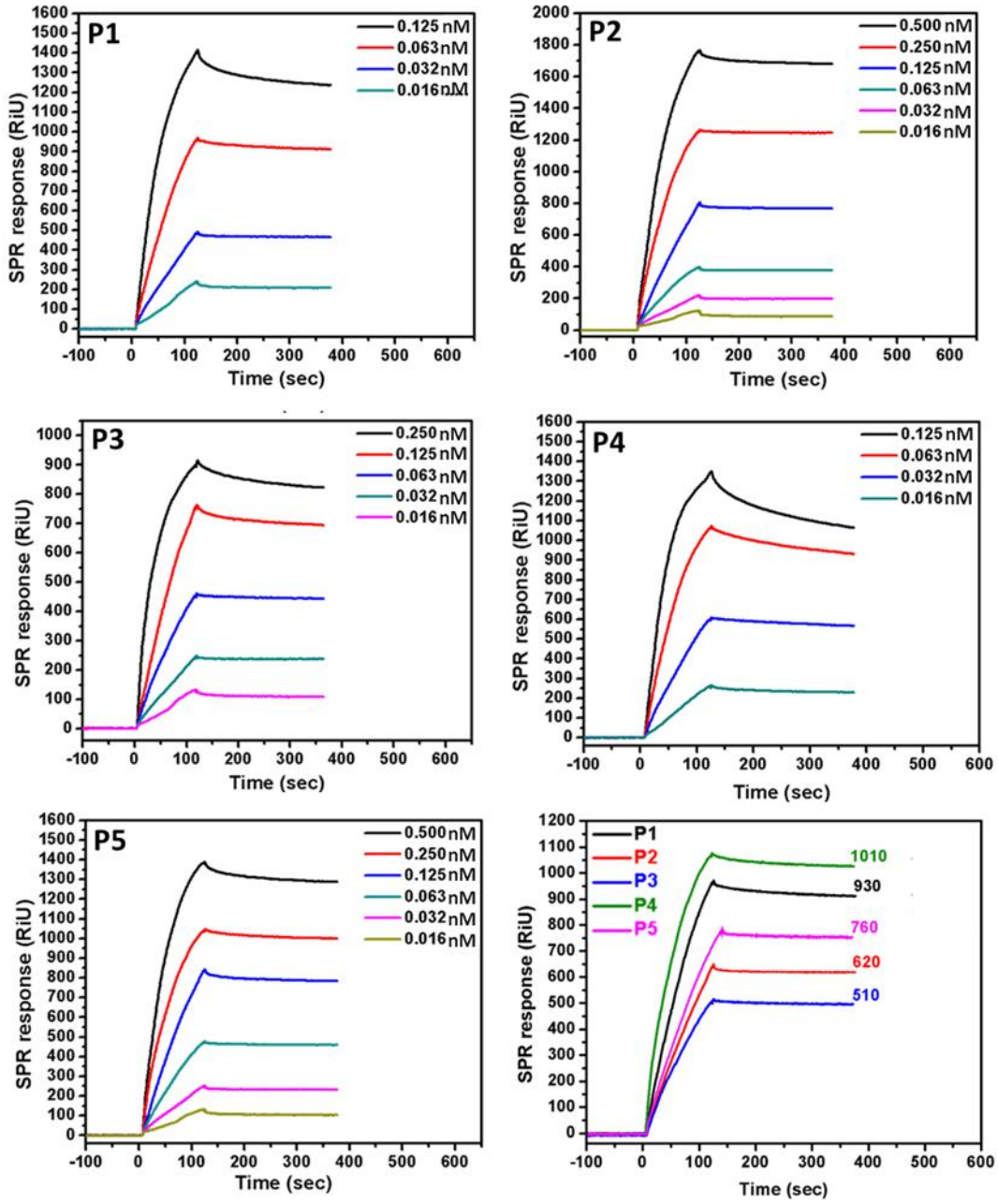


**Figure 2.11.** SPR sensorgrams showing the binding of glyconanoparticles onto DC-SIGN functionalized surfaces. The concentration ranges for nanoparticles were 0.5-

0.016 nM. In addition, competition experiment was carried out at the same nanoparticle concentration (0.063 nM).

The “glyco-cluster effect” that is known as the multivalent effect of densely packed saccharides with unique functionalities saccharides creates to provide high affinities for proteins owing to their multivalency. Therefore, it is very important to achieve effective lecting binding and affect signal transduction. Even though different types of glycopolymers with different carbohydrate, sugar number, density, ligand shape, linker structure, spacing between carbohydrate units, and the nature of the polymer backbone were investigated by several research groups in the last decade, glyconanoparticles have not yet been investigated systematically. This motivated us to investigate how the glyconanoparticles in different size and morphology could change and enhance binding affinity with lectins. Therefore, this study could be a good starting point for further investigations.

In general, all glyconanoparticles showed good signals during binding events with DC-SIGN. As expected, the binding of each nanoparticle to DC-SIGN decreased with decreased nanoparticle concentration. Most of the glyconanoparticles showed relatively high binding value at higher concentrations and in good agreement with concentration. In order to observe the binding levels of the various glyconanoparticles comparatively, all nanoparticle solutions were analyzed with DC-SIGN at the same molar nanoparticle concentration (Figure 2.11). According to the SPR data, vesicle nanoparticles of **P4** had a much higher affinity in comparison to other GNPs. Interestingly, **P1** showed the second highest binding level in this series after **P4**. This may be due to the mannose groups on the surface of **P1** glyconanoparticles being more accessible in order to mediate strong interactions with DC-SIGN. Another interesting result is that the worm-like micelles **P5** showed higher level of interaction than **P2** and **P3**. The possible reason can be that the formation of worm-like micelles in clustered structures may enhance the binding capability of nanoparticles with the natural oligomeric structure of DC-SIGN. As a result, the small increase in the size of a nanoparticle showed a dramatic decrease on binding with DC-SIGN.

### 2.2.7 Preparation and characterization of SB216763-loaded micelles

Micro/nano-materials have a great potential for the contribution on the development of various drug delivery systems for the treatment of diseases such as acne, asthma, cancers and others in efficient way.[41,42] Obviously, advances in the nanotechnology have allowed the preparation of more complex and defined several architecture materials including targeting drugs and biological molecules in the field of drug delivery devices. In particular, polymeric nanoparticles are the most common used materials for the drug delivery devices in the pharmacological applications.[43] Therefore, although they are becoming more attractive for scientists due to their potential ability for useful in biomimetic applications and human therapeutics, there are still some obstacles regarding some implications and also inefficient delivery and release behaviors. Hence, the use of more biocompatible carriers with high loading capacity, low overall toxicity and receptor-mediated endocytosis specificity is required. The abilities and capabilities of glyconanoparticles in terms of molecular recognition events and biological interaction processes could play a crucial role in order to develop the drug delivery and release systems. This perspective encouraged us to try the incorporation of hydrophobic drug molecules into glyco-micelles to investigate loading capacity and also to develop a targeted drug delivery system.

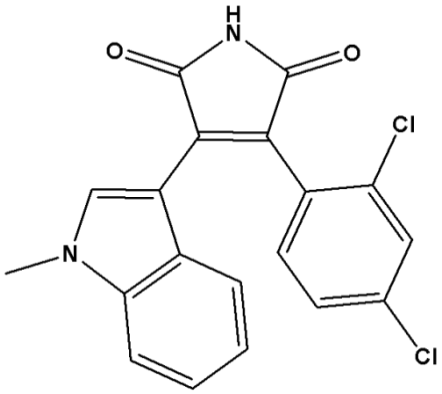


**Scheme 2.3.** Chemical structure of 3-(2,4-Dichlorophenyl)-4-(1-methyl-1H-indol-3-yl)-1H-pyrrole-2,5-dione (SB-216763).

As depicted in Scheme 2.3, 3-(2,4-Dichlorophenyl)-4-(1-methyl-1H-indol-3-yl)-1H-pyrrole-2,5-dione (SB-216763) was employed to use for encapsulation as a potent and selective inhibitor of the J and K isozymes of glycogen synthase kinase-3 (GSK-3).[35] GSK-3 is a serine/threonine protein kinase, the activity of which is linked to some pathological conditions, such as diabetes and/or insulin resistance, and Alzheimer's disease and also it is active in a number of central intracellular signaling pathways.[37]

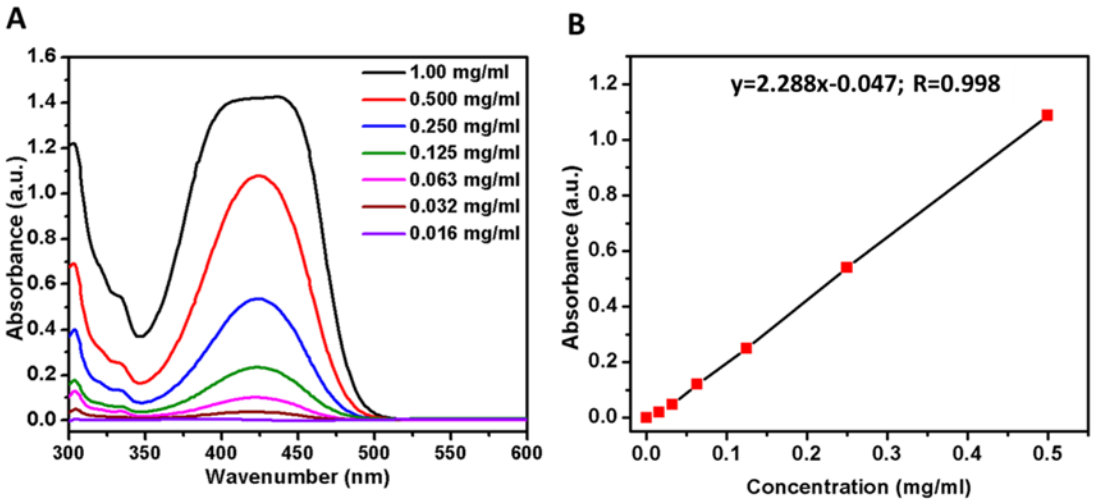


**Figure 2.12. A)** UV absorbance of SB-216763 in THF at different concentrations; **B)** Calibration curve of SB-216763 in THF by UV-vis spectroscopy ($\lambda_{max}$=425 nm).

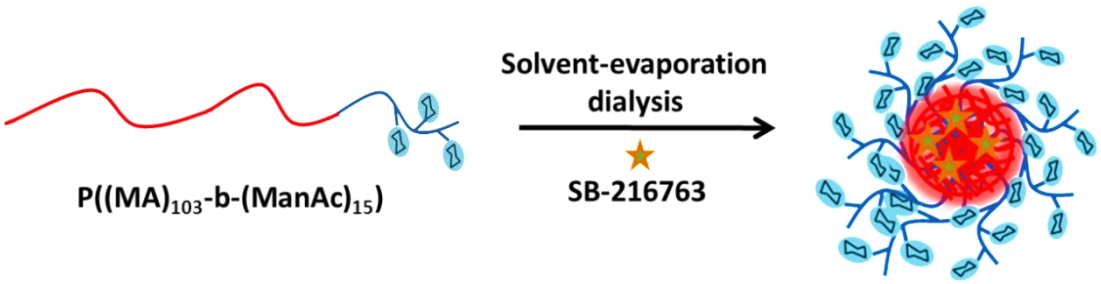


**Scheme 2.4.** Schematic illustration of SB-216763 encapsulation.

SB-216763 loaded glyconanoparticles were prepared by using **P2** amphiphilic glycopolymer *via* the combination of solvent-evaporation and dialysis techniques that is an ideal approach for the encapsulation of hydrophobic drugs. UV-vis spectroscopy was used to determine the amount of SB-216763 encapsulated in glyco-micelles. For this purpose, the UV absorbance of SB-216763 in THF was

measured at different concentrations to obtain a calibration curve (Figure 2.12). SB-216763 free micelles solution was measured firstly in order to revise its UV absorbance at 425 nm. However, it did not show any considerable absorbance. Nevertheless, the UV absorbance of SB-216763 loaded micelles was obtained. According to the calibration curve of SB-216763 in THF, the concentration of the encapsulated SB-216763 was calculated as 0.12 $mg.mL^{-1}$.

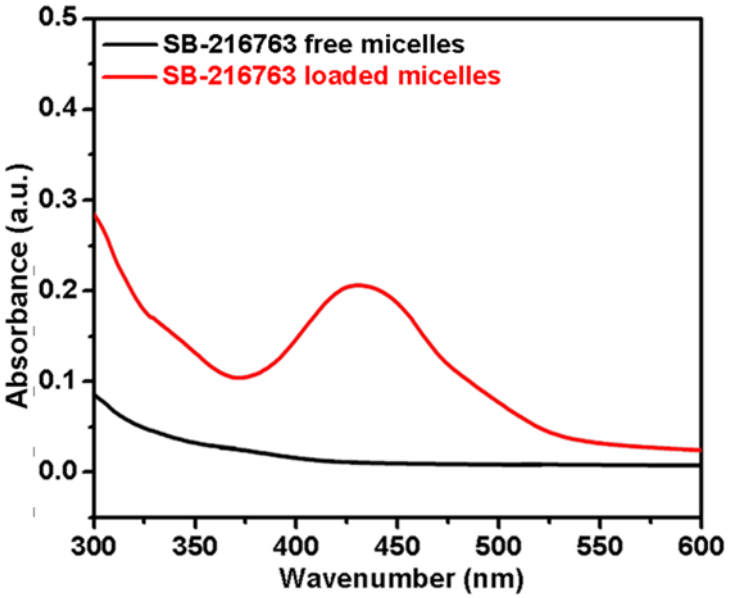


**Figure 2.13.** The UV absorbance of SB-216763 free and loaded glyco-micelles in water.

The loading efficiency (DLE) and content (DLC) was calculated as the following formulas:

$$DLE(wt\%) = Me/Mf \times 100\%$$

$$DLC(wt\%) = Me/Mp \times 100\%$$

where *M*e is the weight of the encapsulated in glyco-micelles, *M*f is the weight of drug in feed and *M*p is the weight of the polymer used. *M*f = 0.5 mg, *M*p = 5 mg.

As seen in Table 2.3, DLE was calculated as 23.6 wt% which is an acceptable quantitative loading capacity for hydrophobic drugs and 2.36 wt % was obtained for

DLC. Theoretically, the drug loading efficiency mainly depends on the extent of hydrophobic interaction between the drug and micellar core.

Furthermore, SB-216763 loaded glyco-micelles were characterized in terms of the size and zeta potential by using DLS. A dramatic increase in the hydrodynamic volume was obtained between SB-216763 free and loaded glyco-micelles that indicated successful encapsulation of SB-216763. As shown in Figure 2.14, the size of the glyco-micelles after the SB-216763 loading increased from 23±0.6 nm to 37.±1.2 nm with dispersity index (*Đ*) as 0.27, signifying a narrow particle size distribution. This increase in micelle size after the incorporation of SB-216763 was attributed to the encapsulation of the drug molecules in the hydrophobic core of polymeric micelle. Additionally, the negative zeta potential of glyco-micelles showed a slight increase from -19.6±2.4 mV to -21.4±3.8 mV after the SB-216763 loading.

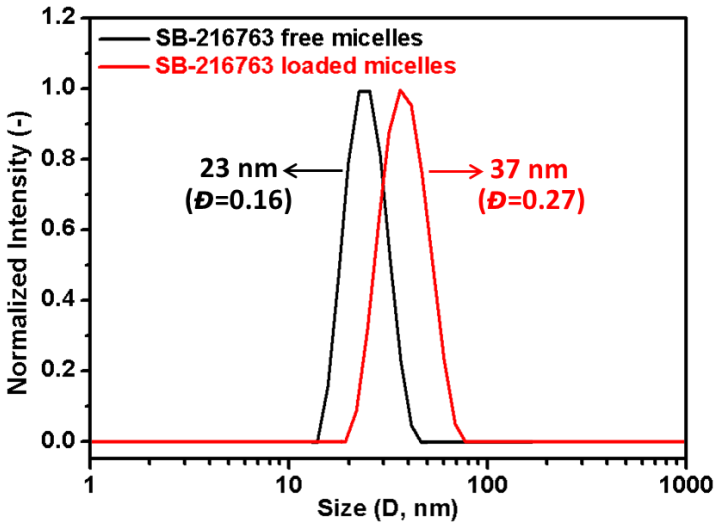


**Figure 2.14** DLS measurement of SB-216763 free and loaded glyco-micelles.

Corresponding TEM studies showed that the micelles were spherical with a core-shell morphology. However, after the loading of SB-216763, some adverse effect on the particle morphology was observed due to less monodisperse population of glyco-micelles. According to TEM imaging, the size of SB-216763 loaded glyco-micelles ranged between 28±1.8 and 43±3.2 nm. The average size of SB-216763 loaded micelles was calculated as 36±2.6 nm.

**Table 2.3.** Characterization of SB-216763 free and loaded glyco-micelles.

| Sample | $D_h$ (nm) | Đ | ζ potential (mV) | DLE (wt%) | DLC (wt%) |
|---|---|---|---|---|---|
| **SB-216763 free micelles** | 23±0.6 | 0.16 | -19.6±2.4 | - | - |
| **SB-216763 loaded micelles** | 37±1.2 | 0.27 | -21.4±3.8 | 23.6 | 2.36 |

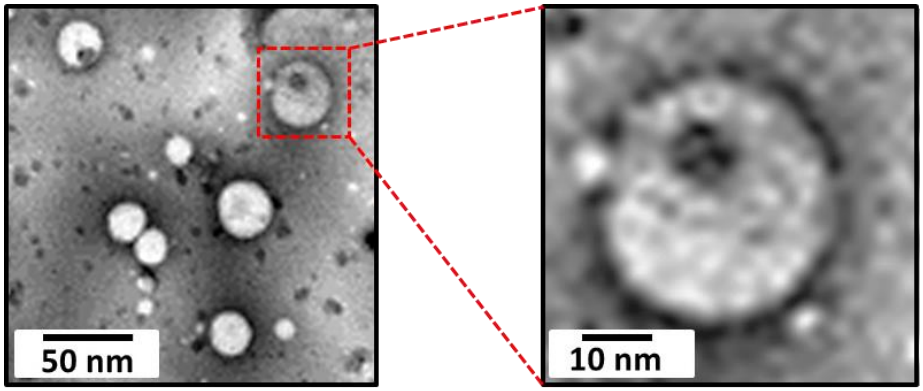


**Figure 2.15** TEM images of SB-216763 loaded glyco-micelles.

### 2.2.8 *In vitro* drug release

As mentioned above, polymeric micelles have a great potential to develop drug delivery systems as nanocarriers in which the drug release occurs due to a change in the environment conditions such as pH, temperature, ionic strength, presence or absence of chemical species, electric fields and irradiation with UV/visible light. To provide a highly selective and significant drug release process in terms of sufficient control over drug release is very important due to some absorption barriers and dosage limitations. Bioactive molecule or drug release from polymeric micellar core can be undertaken by two main strategies that are dissociation of the micelle followed by the separation of the drug from monomers and drug-hydrophobic core bond breakage in the micelle followed by diffusional escape from the micelle system. After the loading of SB-216763 successfully into glyco-micelles, release profiles of these SB-216763 loaded glyco-micelles were generated in order to investigate the potential use of these particles as delivery carriers.

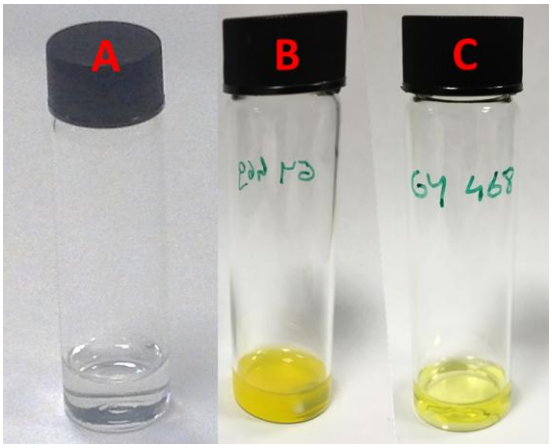


**Figure 2.16.** Appearance of blank glyco-micelles (**A**); free SB-216763 in water (**B**); SB-216763 loaded glyco-micelles (**C**).

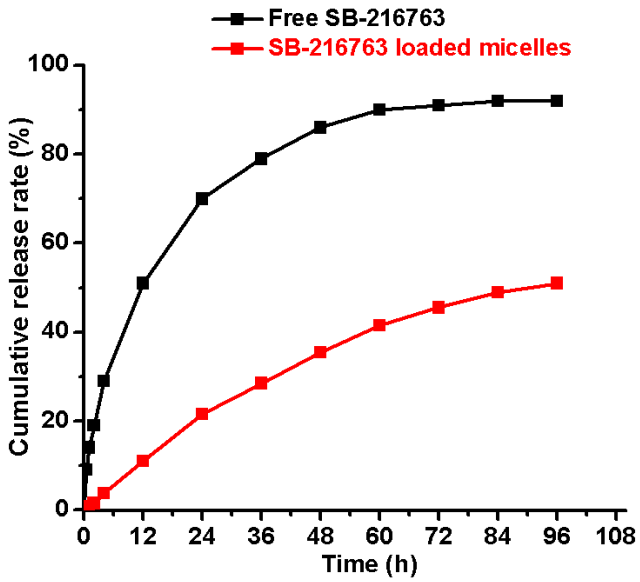


**Figure 2.17.** Cumulative drug release profiles of free SB-216763 and SB-216763 loaded glyco-micelles at pH 7.4 for 96 h at 37 °C.

The release studies of free SB-216763 and SB-216763 loaded glyco-micelles were carried out by a dialysis method. Our release studies were performed in phosphate buffer solution (PBS) at pH 7.4 and 37 °C with 2 wt% albumin to mimic a biological environment. SB-216763 released from free SB-216763 and SB-216763 loaded glyco-micelles were continuously monitored in 4 days. As illustrated in Figure 2.17, SB-216763 loaded glyco-micelles presented very slow release behavior compared

with much faster cumulative release rate of free SB-216763. As expectedly, free SB-216763 showed an initial burst of drug release in the first 24 h of incubation with 71%, while only 8% of the loaded SB-216763 was released from glyco-micelles during the same period. The dissolution and diffusion of the loaded SB-216763 from micelles were really more controllable according to slow degradation of the glyco-micelles, representing an advantage of this system compared to other similar systems. The cumulative release rate of SB-216763 from the glyco-micelles was 48% over the period of 4 days. Hence, *in vitro* release profile of SB-216763 loaded glyco-micelles was very promising for the development of future sustained delivery in in vivo biological systems.

## 2.3 Conclusion

In the first part of chapter 2, several types of amphiphilic block glycocopolymers with optimal molar masses and relatively narrow molar mass distributions were synthesized *via* SET-LRP to prepare different glyconanostructures. These synthesized amphiphilic glycopolymers with the same number of mannose units self-assembled in water to generate glyconanoparticles with different morphologies such as spherical and worm-like micelles as well as spherical vesicles. The shape and size of these self-assembled glyconanopartices were characterized *via* TEM and DLS. Then, the interaction of these glyconanoparticles of different size and shape with DC-SIGN was monitored by SPR. The SPR results indicate that the size and shape of nanoparticles have significant effects on the binding level with DC-SIGN. According to the binding performance of these glyconanoparticles, they can be potentially utilized in biomedical applications for inhibition of viral infection such as HIV. In the second part, glyco-micelles were loaded with SB-216763 by the combination of solvent-evaporation and dialysis techniques. After the successful characterization steps, the *in vitro* release profile of SB-216763 from the glyco-micelles was defined. The obtained results suggest a great potential of SB-216763 loaded glyco-micelles for the development of drug delivery and release systems for therapeutic applications.

## 2.4 Experimental

### 2.4.1 Materials

α-bromoisobutyryl bromide (EBiB, 98%), triethylamine (BioUltra, ≥99.5%), poly(ethylene glycol) methyl ether (average $M_n$ ≈ 2000 g.mol$^{-1}$) (MeO-PEG), methyl acrylate (MA) (99%, contains ≤100 ppm MEHQ as inhibitor), phosphotungstic acid (PTA), SB-216763 (98%) and albumin (≥98%) were purchased from Sigma Aldrich Chemical Company (Dorset, UK) and used as received unless stated otherwise. tris(2-(Dimethylamino)ethyl)amine ($Me_6$TREN), $H_2SO_4$-silica catalyst, N-(ethyl)-2-pyridylmethanimine ligand (ethyl ligand) used were previously synthesized within the group. All other reagents and solvents were obtained at the highest purity available from Sigma Aldrich Chemical Company. MA was passed through a basic alumina column to remove inhibitors prior to reactions. Dialysis tube (1kDa and 3.5 kDa MWCO) was purchased from Spectrum Laboratories (California, USA). Human Dendritic Cell-specific ICAM-3 Grabbing Non-integrin lectin (DC-SIGN) was purchased from Elicityl OligoTech Company (Crolles, France). Carbon coated copper grids with a mesh size of 400 were purchased from Agar Scientific.

### 2.4.2 Instruments and Analysis

$^{1}$H-NMR and $^{13}$C-NMR nuclear magnetic resonance spectroscopy (Bruker DPX-400) were used to determine the chemical structure of the synthesized polymers. Samples were dissolved at 5 mg/mL concentration in $D_2O$ or $(CD_3)_2SO$.

Size-exclusion chromatography (SEC) measurements were conducted on an Agilent 1260 infinity system operating in DMF with 5.0 mM $NH_4BF_4$ and equipped with refractive index detector (RID) and variable wavelength detector (VWD), 2 PLgel 5 µm mixed-C columns (300×7.5mm), a PLgel 5 mm guard column (50x7.5mm) and an autosampler. The instrument was calibrated with linear poly(methyl methacrylate) standards in range of 550 to 46890 g/mol. All samples were passed through 0.2 µm PTFE filter before analysis.

The particle size distributions and zeta potential of the nanoparticles were determined by using a Malvern Zetasizer Nano ZS instrument equipped with a He-

Ne laser at 633 nm. DLS measurements were performed by taking 1mL of nanoparticle solution from the dialyzed solution directly. Samples were introduced into the cells after filtration through 0.45 µm PTFE microfilters to determine the size of nanoparticles in aqueous solutions. All measurements were carried out at 25 °C and repeated three times. The averaged correlation function from these 3 measurements was analyzed using CONTIN method to obtain the distribution of diffusion coefficients (*D*) of the solutes. From these data, the Stokes– Einstein equation allows us to obtain the apparent equivalent hydrodynamic radius ($R_H$):

$$R_H = k_B T / 6\pi\eta_S D$$

$k_B$ is the Boltzmann constant, T is the temperature of the sample, $\eta_S$ is the viscosity of the fluid and *D* is the translational diffusion coefficient at a finite dilution.

UV-visible spectra were recorded on a PerkinElmer Lamda 25 UV/VIS spectrometer equipped with a (PTP-1) temperature control unit at a certain temperatures in the range of 200 nm and 600 nm using quartz microcuvettes.

The morphologies of the self-assembled structures were analyzed by Transmission Electron Microscopy (TEM), using a JEOL 2100 instrument operating at an acceleration voltage of 200kV and equipped with a CCD camera from Gatan. Each TEM sample was prepared by dropping 5µL of the nanoparticle aqueous solution on a Fresh glow-discharged carbon-coated copper grid for 1 min. The residue of aqueous solution was blotted away with a strip of filter paper and the grid was subsequently dipped into 20 µL of a 0.75 % PTA aqueous solution, pH 7, for 10 seconds in order to positively stain the sample. After removing the excess of PTA solution by a strip of filter paper, the grid was dried under vacuum and stored at room temperature until imaging.

Beckman DU Series 700 UV/Vis Scanning Spectrophotometer was used to analyze the binding ability of the nanoparticles. SPR Sensorgrams were recorded in a Biorad ProteOn XPR36 SPR biosensor (Biorad, Hercules CA). Soluble DC-SIGN was immobilized to 6000 response units (RU) on discrete channels within Biorad GMC sensor chips *via* amine coupling. Soluble-phase analytes were prepared in 25 mM

HEPES pH 7.4, 150 mM NaCl, 5 mM CaCl2, 0.01% Tween-20 and flowed over the immobilized materials at a rate of 25 µL/min at 25˚C. Regeneration of the sensor chip surfaces was performed using 10 mM glycine pH 2.5.

FT-IR spectra were recorded on a Bruker FT-IR spectrometer TENSOR II with Diamond-ATR module. The scanning range was 600-4000 $cm^{-1}$ with a resolution of 1 $cm^{-1}$.

Electrospray ionization-mass spectrometry (ESI-MS) spectra were recorded on a Thermo Finnigan LCQ Decaquadrupole ion trap mass spectrometer (Thermo Finnigan, San Jose, CA), equipped with an atmospheric pressure ionization source operating in the nebulizer assisted electrospray mode and was used in positive ion mode.

### 2.4.3 Synthesis of mannose glycomonomer

1-(2'-propargyl) D-mannose (2.46 g, 12.6 mmol) and 3-azidopropyl acrylate (2.85 g, 11.8 mmol) were dissolved in MeOH/$H_2O$ (2:1 vol/vol, 60 mL), aqueous solution of $CuSO_4 \cdot 5H_2O$ (246 mg, 0.9 mmol) and (+)-sodium L-ascorbate (284 mg, 1.2 mmol) were added into the reaction solution. The reaction mixture was stirred at ambient temperature for 24 h. Methanol was then removed under vacuum and the residue mixture was freeze dried to remove water. The obtained product was purified through silica gel column chromatography using DCM-MeOH (8:1) as eluent. After removing of solvent, the product was obtained as white (1.62 g, yield: 58.2%).

$^1$H NMR ($D_2O$, 298 K, 400 MHz): δ =8.06 (s, 1 H, NCH=C), 6.37 (dd, J=1.8, 15.5 Hz), 6.36 (dd, J=1.6, 15.7 Hz) (anomeric 1 H, $CH_2$=C), 6.14 (dd, J=10.4, 6.9 Hz), 6.13(dd, J=10.4, 7.0 Hz) (anomeric, 1 H, $CH_2$=CHC=O), 5.89 (dd, 1 H, J=1.5, 8.9 Hz, $CH_2$=C), 4.70-5.05 (m, $CH_2$-OH, H-1 of mannose , overlap with $H_2O$), 4.64 (d, 1 H, J=12.3 Hz, $CH_2$-OH), 4.55 (t, 2 H, J=6.9 Hz, $CH_2$-N), 4.19 (t, 2 H, J=6.0 Hz, C=O-O-$CH_2$), 3.40-3.92 (m, H residues of mannose), 2.30 (m, 2H, $CH_2$-$CH_2$-$CH_2$) ppm.

$^{13}$C NMR ($D_2O$, 298 K, 400 MHz): δ =146.4 (C=O), 145.4 (N-CH=C), 131.9 ($CH_2$=C), 129.2 ($CH_2$=C), 125.6 (N-CH=C), 100.8 (β anomeric, C 1 of mannose), 100.7 (α

anomeric, C 1 of mannose), 78.4,75.2, 75.0, 72.5, 72.3, 72.0, 68.6, 68.4 (carbons of anomeric mannose), 63.0($CH_2$-OH), 62.6 (C=O-O-$CH_2$), 60.7 (C-$CH_2$-O), 48.5 ($CH_2$-$CH_2$-N), 28.5($CH_2$-$CH_2$-$CH_2$) ppm.

ESI-MS m/z: calculated for $C_{15}H_{23}N_3O_8$ ($M+H^+$), 372.2; found, 374.3.

### 2.4.4 Synthesis of PEG-Br initiator

This synthesis of PEG-Br macroinitiator was performed through an esterification reaction. In a 250 mL round-bottom flask, 5 gr (2.5 mmol) of MeO-PEG and 1.046 mL (7.5 mmol) of TEA were stirred in 50 mL of THF and cooled down to 0°C. Then, a mixture of 0.775 mL (6.25 mmol) of BIBB and 5 mL of THF was added dropwise to the reaction mixture over an hour. The reaction was allowed to warm up to room temperature and stirred overnight. The formed salt was filtered and excess volatiles were removed from the filtrate. The filtrate was then precipitated twice in cold hexane to yield a white powder.

$^1$H-NMR ($CDCl_3$, 400 MHz) δ: 4.42 (m, 2H, $CH_3$-O-$CH_2$-R), 3.74 (b, 176H, R-O-$CH_2$-$CH_2$-O-R PEG repeating unit), 3.42 (s, 3H, $CH_3$-O-R), 2.00 (s, 6H, $C(CH_3)_2Br$).

### 2.4.5 General procedure for SET-LRP

Amphiphilic copolymers were synthesized according to the following experimental procedure. Schlenk tube was charged with different ratio of MA monomer (relevant eq), pre-activated Cu(0) wire (5 cm), $CuBr_2$ (0.04 eq) and DMSO (6 ml) and then the mixture was degassed by gentle bubbling of argon gas for 30 min. Pre-degassed $Me_6$TREN (0.19 eq) and EBiB or PEG-Br initiator (1 eq) were then added *via* gas tight syringe sequentially. The Schlenk tube was sealed and the reaction mixture was allowed to polymerize at 25$^o$C. Sampling was carried out using a degassed syringe to check the conversion of MA. After it reached to full conversion, the glycomonomer solution (15 eq. in 1 mL DMSO) was then degassed with argon for 20 min and subsequently transferred *via* cannula to the Schlenk tube under argon protection to polymerize. After 18 h polymerization, a sample was taken for $^1$H NMR and GPC analysis to check full monomer conversion. The $^1$H NMR result

confirmed >98% conversion according to integral of vinyl groups with that of the triazole groups (NCH=C) at 8.06-8.07 ppm. Catalyst residues were removed by filtering through a column of neutral alumina prior to DMF GPC analysis. The reaction was stopped *via* exposure to the air and then the reaction mixture was dialyzed against a mixture of distilled water and methanol for 3 days, while changing the water at least three times. The final product was freeze-dried under vacuum and characterized by $^{1}$H NMR.

### 2.4.6 Preparation and characterization of glyconanoparticles

Glyconanoparticles were prepared using the nanoprecipitation (solvent-switch) method. The same procedure was used for all amphiphilic glycopolymers. Briefly, each glycopolymer (7 mg) was dissolved in 1 mL DMF to yield an initial concentration of 0.5 µM. To this solution, 2 mL of ultra-pure water was progressively added at a rate of 5 µL /min using a master dual pump from Worked Precision Instruments. This procedure takes 6 hours, thus avoiding forming any kinetically trapped self-assembled structures. The final mixture was diluted with 7 mL of ultrapure water to freeze the self-assembled structures (final ratio DMF/H2O of 1/10; [glycopolymer] =0.05 µM). Excess of DMF was removed through 3 days dialysis against ultra-pure water, using membranes with a MW cut off 3.5 kDa. The final suspensions were characterized by DLS and TEM.

### 2.4.7 Determination of Binding Ability of Glyconanoparticles by SPR

Interactions between the glyconaoparticles and DC-SIGN were measured using SPR in a high-throughput multichannel mode. In the concentration experiments, all glyconanoparticles were measured at different concentrations, in which the buffer was flowed over the chip alone before (90 s) and after (240 s) injection of the analyte (120 s). Buffer solution was prepared in 25 mM HEPES pH 7.4, 150 mM NaCl, 5 mM $CaCl_2$, 0.01% Tween-20. Regeneration of the sensor chip surfaces was performed using 10 mM glycine pH 2.5. Before measurements, star-shaped (5 arms) glycopolymer at different concentrations was used as control for binding. It showed higher affinities during binding with DC-SIGN because of higher mannose content.

### 2.4.8 SB-216763 loaded glyco-micelles preparation

SB-216763 loaded micelles were prepared *via* the combination of solvent evaporation and dialysis methods. 5 mg block copolymer and 0.5 mg drug were dissolved in THF:MeOH (3:2) 5 mL mixture and then this solution was mixed with 2 mL water and stirred until complete evaporation of the organic solvent mixture had taken place at room temperature. The remaining aqueous solution was then transferred into dialysis tube and dialyzed against HPLC water for 24 h. Finally the formulation was passed through a 0.25 µm membrane before DLS and UV measurements.

### 2.4.9 *In vitro* drug release

*In vitro* drug release of the SB-216763 from SB-216763 loaded glyco-micelles was evaluated by the dissolution technique. The *in vitro* release studies of free SB-216763 and SB-216763 loaded glyco-micelles were performed at 37 °C in phosphate buffer solution (PBS) (pH = 7.4) with 2 wt% albumin to mimic a biological environment. Dialysis bags (MW 3500 Da) containing 1 mL of sample were submerged in 50 mL buffer medium under mild stirring. To investigate the in vitro release profiles of the samples, 1 mL of each of the samples was collected at regular time intervals and replaced with an equal volume of fresh medium. The concentration of SB-216763 in each sample was calculated using a calibration curve. Probing the released SB-216763, the cumulative drug release percentage ($E_r$) was calculated according to the following equation:

$$E_r = \frac{Ve \sum_{1}^{n-1} Ci + Vo\, Cn}{M(Dox)}$$

where M(SB-216763) represents the amount of SB-216763 in the micelles, Vo is the whole volume of the release media (Vo = 50 mL), Ve is the volume of the replace media (Ve = 1 mL), and Cn represents the concentration of SB-216763 in the $n^{th}$ sample.

## 4.5 References

(1) Ambrosi, M.; Cameron, N. R.; Davis, B. G. *Org. Biomol. Chem.* **2005**, *3*, 1593.
(2) Kumar, K.; Chandra, K.; Sumanthi, J.; Reddy, G.; Shekar, P.; Reddy, B. *Journal of Orofacial Sciences* **2012**, *4*, 20.
(3) Bertozzi, C. R.; Kiessling; L., L. *Science* **2001**, *291*, 2357.
(4) Ghazarian, H.; Idoni, B.; Oppenheimer, S. B. *Acta histochemica* **2011**, *113*, 236.
(5) Arnaud, J.; Audfray, A.; Imberty, A. *Chemical Society Reviews* **2013**, *42*, 4798.
(6) Ahmed, M.; Wattanaarsakit, P.; Narain, R. *European Polymer Journal* **2013**, *49*, 3010.
(7) Wang, L.; Williams, G. R.; Nie, H.-l.; Quan, J.; Zhu, L.-m. *Polymer Chemistry* **2014**, *5*, 3009.
(8) Yilmaz, G.; Becer, C. R. *Frontiers in Bioengineering and Biotechnology* **2014**, *2*.
(9) Yilmaz, G.; Becer, C. R. *Polymer Chemistry* **2015**, *6*, 5503.
(10) Wang, W.; Chance, D.; Mossine, V.; Mawhinney, T. *Glycoconj J* **2014**, *31*, 133.
(11) Yilmaz, G.; Becer, C. R. *European Polymer Journal* **2013**, *49*, 3046.
(12) Muñoz-Bonilla, A.; León, O.; Bordegé, V.; Sánchez-Chaves, M.; Fernández-García, M. *Journal of Polymer Science Part A: Polymer Chemistry* **2013**, *51*, 1337.
(13) Alvárez-Paino, M.; Juan-Rodríguez, R.; Cuervo-Rodríguez, R.; Muñoz-Bonilla, A.; Fernández-García, M. *Journal of Colloid and Interface Science* **2014**, *417*, 336.
(14) Suriano, F.; Pratt, R.; Tan, J. P. K.; Wiradharma, N.; Nelson, A.; Yang, Y.-Y.; Dubois, P.; Hedrick, J. L. *Biomaterials* **2010**, *31*, 2637.
(15) Peyret, A.; Trant, J. F.; Bonduelle, C. V.; Ferji, K.; Jain, N.; Lecommandoux, S.; Gillies, E. R. *Polymer Chemistry* **2015**, *6*, 7902.
(16) Jones, M. W.; Otten, L.; Richards, S. J.; Lowery, R.; Phillips, D. J.; Haddleton, D. M.; Gibson, M. I. *Chemical Science* **2014**, *5*, 1611.
(17) Kurtulus, I.; Yilmaz, G.; Ucuncu, M.; Emrullahoglu, M.; Becer, C. R.; Bulmus, V. *Polymer Chemistry* **2014**, *5*, 1593.
(18) Godula, K.; Bertozzi, C. R. *Journal of the American Chemical Society* **2012**, *134*, 15732.
(19) Lou, S.-F.; Wang, L.; Williams, G. R.; Nie, H.; Quan, J.; Zhu, L. *Colloids and Surfaces B: Biointerfaces* **2014**, *113*, 368.
(20) Babiuch, K.; Wyrwa, R.; Wagner, K.; Seemann, T.; Hoeppener, S.; Becer, C. R.; Linke, R.; Gottschaldt, M.; Weisser, J. r.; Schnabelrauch, M.; Schubert, U. S. *Biomacromolecules* **2011**, *12*, 681.
(21) Luo, Y.; Liu, L.; Wang, X.; Shi, H.; Lv, W.; Li, J. *Soft Matter* **2012**, *8*, 1634.
(22) Zhang, C.-Y.; Yeh, H.-C.; Kuroki, M. T.; Wang, T.-H. *Nat Mater* **2005**, *4*, 826.
(23) Iversen, T.-G.; Skotland, T.; Sandvig, K. *Nano Today* **2011**, *6*, 176.

(24) Lim, D. W.; Yeom, Y. I.; Park, T. G. *Bioconjugate Chemistry* **2000**, *11*, 688.
(25) Zhang, Q.; Collins, J.; Anastasaki, A.; Wallis, R.; Mitchell, D. A.; Becer, C. R.; Haddleton, D. M. *Angewandte Chemie International Edition* **2013**, *52*, 4435.
(26) Geijtenbeek, T. B. H.; Kwon, D. S.; Torensma, R.; van Vliet, S. J.; van Duijnhoven, G. C. F.; Middel, J.; Cornelissen, I. L. M. H. A.; Nottet, H. S. L. M.; KewalRamani, V. N.; Littman, D. R.; Figdor, C. G.; van Kooyk, Y. *Cell* **2000**, *100*, 587.
(27) Ilyas, R.; Wallis, R.; Soilleux, E. J.; Townsend, P.; Zehnder, D.; Tan, B. K.; Sim, R. B.; Lehnert, H.; Randeva, H. S.; Mitchell, D. A. *Immunobiology* **2011**, *216*, 126.
(28) Miller, T.; van Colen, G.; Sander, B.; Golas, M. M.; Uezguen, S.; Weigandt, M.; Goepferich, A. *Pharmaceutical Research* **2013**, *30*, 584.
(29) Cai, K.; He, X.; Song, Z.; Yin, Q.; Zhang, Y.; Uckun, F. M.; Jiang, C.; Cheng, J. *Journal of the American Chemical Society* **2015**, *137*, 3458.
(30) Ahmad, Z.; Shah, A.; Siddiq, M.; Kraatz, H.-B. *RSC Advances* **2014**, *4*, 17028.
(31) Miyata, K.; Christie, R. J.; Kataoka, K. *Reactive and Functional Polymers* **2011**, *71*, 227.
(32) Kedar, U.; Phutane, P.; Shidhaye, S.; Kadam, V. *Nanomedicine: Nanotechnology, Biology and Medicine* **2010**, *6*, 714.
(33) Sun, P.; He, Y.; Lin, M.; Zhao, Y.; Ding, Y.; Chen, G.; Jiang, M. *ACS Macro Lett.* **2014**, *3*, 96.
(34) Huang, J.; Bonduelle, C.; Thévenot, J.; Lecommandoux, S.; Heise, A. *Journal of the American Chemical Society* **2012**, *134*, 119.
(35) Liu, H.; Mi, S.; Li, Z.; Lv, X.; Li, K.; Hua, F.; Hu, Z. *Acta Pharmaceutica Sinica B* **2013**, *3*, 226.
(36) Kirby, L. A.; Schott, J. T.; Noble, B. L.; Mendez, D. C.; Caseley, P. S.; Peterson, S. C.; Routledge, T. J.; Patel, N. V. *PLoS ONE* **2012**, *7*, e39329.
(37) Coghlan, M. P.; Culbert, A. A.; Cross, D. A. E.; Corcoran, S. L.; Yates, J. W.; Pearce, N. J.; Rausch, O. L.; Murphy, G. J.; Carter, P. S.; Roxbee Cox, L.; Mills, D.; Brown, M. J.; Haigh, D.; Ward, R. W.; Smith, D. G.; Murray, K. J.; Reith, A. D.; Holder, J. C. *Chemistry & Biology* **2000**, *7*, 793.
(38) Dambuza, I. M.; Brown, G. D. *Current Opinion in Immunology* **2015**, *32*, 21.
(39) Su, S. V.; Hong, P.; Baik, S.; Negrete, O. A.; Gurney, K. B.; Lee, B. *Journal of Biological Chemistry* **2004**, *279*, 19122.
(40) Patching, S. G. *Biochimica et Biophysica Acta (BBA) - Biomembranes* **2014**, *1838*, 43.
(41) Sun, T.; Zhang, Y. S.; Pang, B.; Hyun, D. C.; Yang, M.; Xia, Y. *Angewandte Chemie International Edition* **2014**, *53*, 12320.
(42) Mudshinge, S. R.; Deore, A. B.; Patil, S.; Bhalgat, C. M. *Saudi Pharmaceutical Journal* **2011**, *19*, 129.
(43) Kumari, A.; Yadav, S. K.; Yadav, S. C. *Colloids and Surfaces B: Biointerfaces* **2010**, *75*, 1.

# Chapter 3 pH-sensitive glycopolymer-coated gold nanoparticles: Functional platforms for theranostic applications

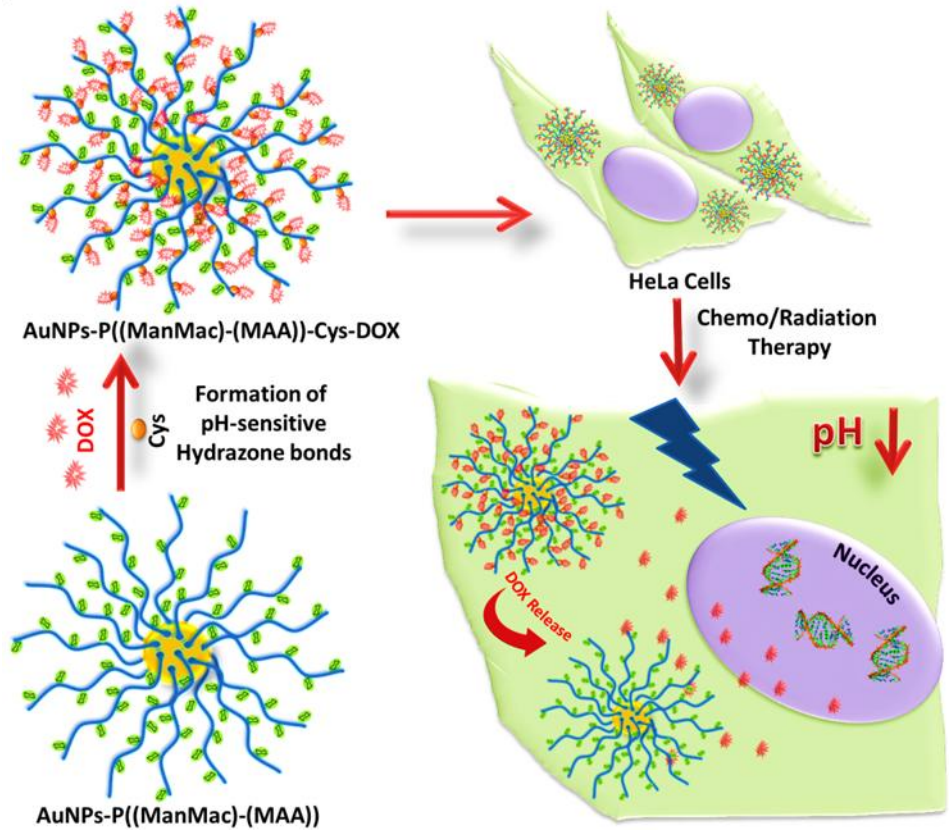


*The integration of drugs with nanomaterials has received significant interest in the efficient drug delivery systems. Conventional treatments with therapeutically active drugs may cause undesired side effects and thus, novel strategies to perform these treatments with a combinatorial approach of therapeutic modalities are required. In this chapter, pH-sensitive glycopolymer-coated gold nanoparticles (glyco-AuNPs), which were synthesized with reversible addition-fragmentation chain transfer (RAFT) polymerization were combined with doxorubicin (DOX) as a model anticancer drug by creating a pH-sensitive hydrazone linkage in the presence of cysteine (Cys) and a cross-linker. Further experiments under different pH conditions (pH 5.3 and 7.4) also showed that DOX conjugated glyco-AuNPs conjugate could release the DOX in a pH-sensitive way. Finally, cell studies demonstrated effective therapeutic impact of the final conjugate for both chemotherapy and radiation therapy by comparing free DOX and DOX-glyco-AuNPs independently.*

## 3.1 Introduction

Recently, the use of nanomaterials in drug delivery systems has gained a tremendous attraction in the research of the pharmaceutical industry.[1] Their usage in drug formulations is getting more important due to the limitation by poor penetration of drugs into tumor tissues and adverse effects on healthy cells. Since the conventional therapies including therapeutically active drug molecule may not generate a selective distribution for a certain location on the organism, undesirable impacts could have been observed in organs and healthy tissues. In order to prevent side effects, surface modification strategies become crucial because the attachment of targeting moieties to the drug carrier system makes it selective to the target tissue or cells.[2,3] There are two strategies for obtaining the targeted drug delivery; (i) passive targeting and (ii) active targeting. Passive targeting includes the transport of the nanocarriers, though leaky vasculature of the diseased tissues *via* convection or passive diffusion and this technique reveals the enhanced permeability and retention (EPR) effect of the drug carrier systems.[4] The use of passive targeting may cause the accumulation of the nanocarriers within long circulation time in solid tumors.[5] For being the appropriate candidate to use in passive targeting with EPR effect, the nanocarriers should include three important properties; first, they should be larger than 10 nm to avoid the filtration by the kidneys and should be about 100 nm to avoid the specific capture by the liver. Second, the nanocarriers should be non-ionic or anionic in order to avoid the renal elimination. Third, they should be recognized by the reticuloendothelial system for not to be phagocytosed.[6] Within this strategy, many drug delivery systems have been reported, especially with the use of metallic nanoparticles, polymers, lipid or surfactant based vesicular carriers.[7-11] Active targeting of nanoparticles contains peripherally conjugated targeting ligands for enhanced and selective delivery. The targeting ligands such as antibodies, folic acid, glycoconjugates or nucleic acids like aptamers are important to the mechanism of cellular uptake. Long circulation times will allow for effective transport of the nanoparticles to the tumor site through the EPR effect, and the targeting molecule is able to increase endocytosis of the

nanoparticles. The internalization of nanoparticle drug delivery systems has shown an increased therapeutic effect.[12,13]

Those drug delivery systems have been generally constructed for the cancer treatment which remains the major common cause of morbidity and mortality throughout the world.[14] In the treatment of cancers, a combination of several types of therapeutic modalities with distinct mechanisms is considered to be a potential strategy.[15] Chemotherapy is one of the most common therapies employed in oncology. Therefore, newly designed drug delivery systems are regarded as a new paradigm in cancer chemotherapy, particularly by creating pH-sensitive infrastructures thanks to the feature of lower acidic matrix of cancerous tissue.[16] By using this prominent information, numerous chemotherapeutic strategies were developed involving a pH-dependent conjugation approach.[17,18] Concomitantly, novel multifunctional carriers also offer combinatorial therapies with this approach. In a related study, Chen *et al.* designed a novel kind of intelligent nanogels which can spatiotemporally control the release of doxorubicin and photosensitizers to combine chemotherapy and photodynamic therapy.[19]

Gold nanoparticles (AuNPs) are emerging as an efficient platform for diagnostic and therapeutic purposes since they have several unique features such as chemical inertness, facile surface functionalizability, electronic structure amenable for plasmon resonance and optical properties suitable as imaging agents.[20] On the other hand, in spite of the synthesis of AuNPs is well-advanced, sometimes colloidal stability of NPs might create aggregation problems in the case of long-term stability. Furthermore, AuNPs are known as nontoxic, however, AuNPs with the size of 1.4 nm induced the toxicity of HeLa cells to a greater extent rather than 15 nm AuNPs.[21] Meanwhile, toxicity of colloidal NPs is also due to the surface chemistry. In regard of this situation, it has to be essential to control precisely the functional groups on the surface as well as remove residual contaminants, especially citrate, arising from the particle synthesis.[22,23] Therefore, polymer covered AuNPs are considerably in importance under favor of contribution of expanded functionalities, composition and charge. Additionally, AuNPs have an excellent capability in the radiation therapy. Radiotherapy, which is known as another commonly used

therapeutic tool for the treatment of half of the cancers is based on the cancer tissue damage with the generation of reactive oxygen species (ROS) like hydroxyl radical ($OH^{-}$) and superoxide anion ($O^{-2}$) upon illumination with X-rays. Beside, gold (atomic number, Z = 79) has a better radiation effect than other radiosensitive elements such as carbon (Z = 6), gadolinium (Z = 64), and platinum (Z = 78) due to the photoelectric effect of gold.[24] Also, PEG, polysaccharides, poloxamines or poloxamers covered AuNPs were introduced to radiation therapy.[25]

Glycopolymer-coated gold nanoparticles as carbohydrate-based systems can provide in a similar manner to mimic the behavior of naturally existing glycocalyx. Hence, they have attracted much attention to insert their biological properties into nanostructured materials due to their use for bio-mimetic purposes, their crucial role in bio-recognition processes at molecular level and their functional role in living systems.[26-28] The specific recognition properties of carbohydrates and unique physiochemical properties of gold nanoparticles could be a fantastic combination for the creation of multivalent nanoparticles for the treatment of chemotherapy/radiotherapy and fluorescence imaging. Inspired by this idea, we have developed the combined nanoplatforms involving both glycopolymer coated AuNPs and an anti-cancer drug doxorubicin. These DOX conjugated glyco-AuNPs were synthesized with a pH-sensitive hydrazone linkage between cysteine (Cys) modified glyco-AuNP and DOX. Following the successful preparation of DOX conjugated AuNPs, which was denoted as "AuNPs-polymer-Cys-DOX", spectroscopic and physicochemical characterizations and *in vitro* drug release studies were accomplished. The experiments with different pH conditions (pH 5.3 and 7.4) showed that DOX conjugated polymer-AuNPs conjugate could release the DOX in a pH-sensitive way. Furthermore, AuNPs-polymer-Cys-DOX conjugates were applied for the further cell culture studies including cytotoxicity, radiotherapy and cell imaging by using Human cervix adenocarcinoma cell line (HeLa). To evaluate the effectiveness of AuNPs-polymer-Cys-DOX platforms, polymer-AuNPs and free DOX were tested for the comprehensive comparison. The results represented effective therapeutic impact of the final conjugate for both chemotherapy and radiation therapy by comparing free DOX and AuNPs-polymer-Cys-DOX independently.

## 3.2 Results and Discussion

### 3.2.1 Synthesis of D-mannose methacrylate glycomonomer (ManMac)

The reversible addition-fragmentation chain transfer (RAFT) polymerization is very commonly used technique to polymerize methacrylates. Hence, mannose methacrylate glycomonomer was prepared to be polymerized *via* RAFT polymerization. The Copper-catalyzed azide-alkyne cycloaddition (CuAAC) was undertaken for the synthesis of mannose methacrylate. Azide functionalized methacrylate was clicked to mannose alkyne, successfully. As shown in Scheme 3.1, the CuAAC "*click*" reaction was carried out in the presence of $CuSO_4 \cdot 5H_2O$ and (+)-sodium L-ascorbate as a catalyst system in MeOH/$H_2O$ mixture at the room temperature for 24 h. This CuAAC "*click*" reaction was monitored and confirmed by $^{1}$H- NMR, $^{13}$C-NMR and ESI-MS.

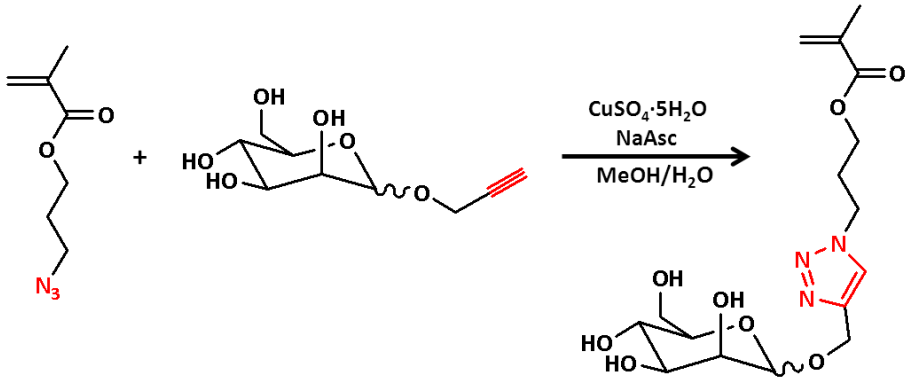


**Scheme 3.1.** Schematic representation of the synthesized D-Mannose methacrylate glycomonomer *via* CuAAC.

As depicted in Figure 3.1, the new peak at 8.02 ppm appeared according to the formation of triazole ring, which confirmed the "click" reaction between azide and alkyne groups. In addition, the existence of D-mannose C-1 peaks at 102.3 & 104.7 ppm revealed that the monomer is an anomeric mixture according to $^{13}$C-NMR. In the ESI-MS spectra, there is a clear peak at 387.4 m/z that corresponds to the molecular weight of the mannose glycomonomer with 387.2 m/z. The product was obtained as a white solid with a 43.9% yield. A possible reason behind of low yield is the poor solubility of 3-azidopropyl methacrylate in MeOH/$H_2O$ mixture and also the loss of some product during the column purification.

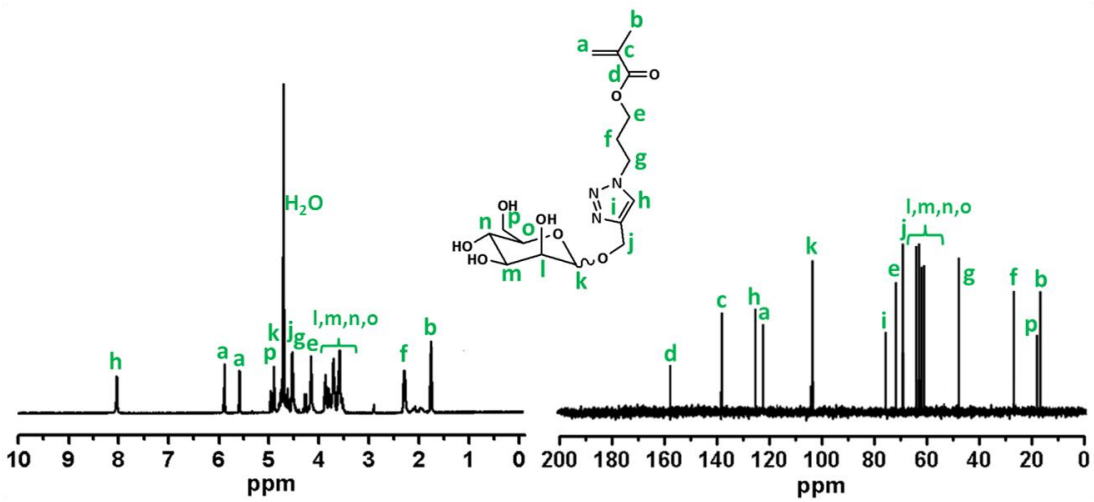


**Figure 3.1.** Details of $^{1}$H-NMR and $^{13}$C-NMR spectrum of D-mannose methacrylate glycomonomer.

### 3.2.2 Synthesis of homo/co-polymers *via* RAFT

RAFT polymerization of the homo/co-monomers was carried out in the presence of 2-cyano-2-propyl benzodithioate (CPDBT) as a RAFT agent, 4,4'-azobis-(2-methylpropionitrile) AIBN as an initiator in the methanol and water mixture (2:1) at 70 °C for 12 h. Briefly, a Schlenk tube was charged with targeted monomer or monomers (methacrylic acid (MAA), poly(ethylene glycol) methyl ether methacrylate (OEGMA) and D-mannose methacrylate (ManMac) (in total 100 eq), CPDBT (1 eq), AIBN (0.1 eq) and the solvent (3.0 mL) was degassed by gentle bubbling of argon gas for 30 min. The Schlenk tube was sealed properly and the mixed solution was allowed to polymerize. The RAFT homo/copolymerizations has been achieved with a good control due to a narrow dispersity index with high molar mass. After the purification, DMF SEC analysis based on PMMA standards revealed a single peak of each polymers without any considerable tailing or shoulder with an apparent $M_n$ = 12.1-32.7 kg/mol and $M_w/M_n$ = 1.18-1.21 (Table 3.1). However, some obtained polymers including carboxylic acid moieties showed a small amount of tailing at the low molar mass range in according to SEC analysis. The possible reason of that could be an interaction of carboxylic acid moieties of the polymers and SEC column packing materials. In addition, the obtained polymers containing

poly(ethylene glycol) methyl ether methacrylate (OEGMA) monomer represented a small shoulder due to some coupling reactions.

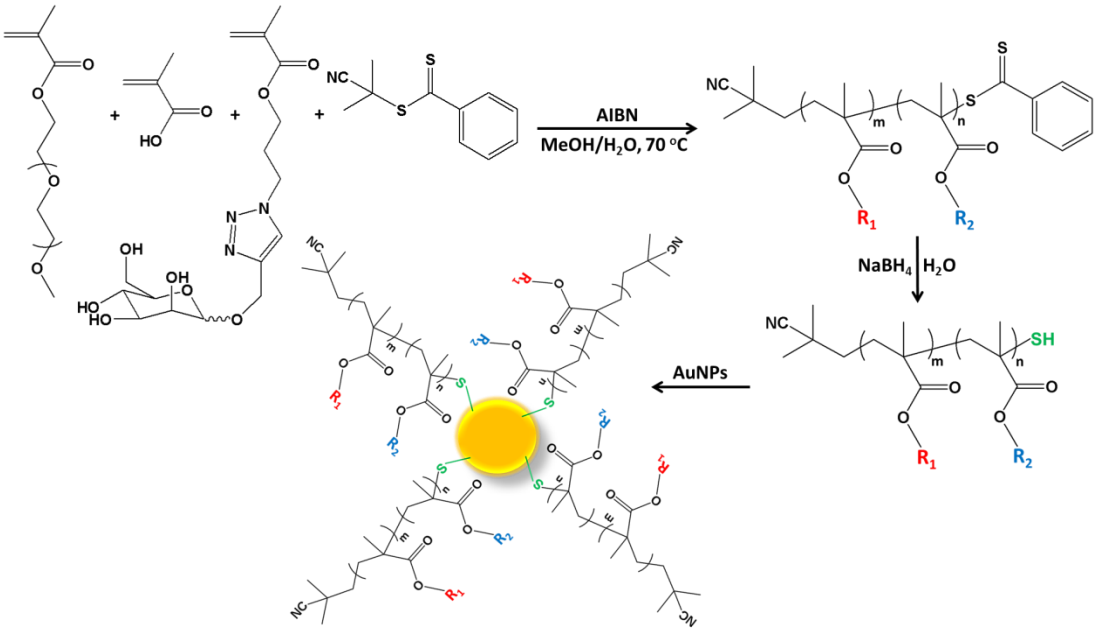


**Scheme 3.2.** Homo and co-polymerization using RAFT and formation of the stabilized AuNPs using synthesized polymers.

**Table 3.1.** Summary of RAFT polymerizations of ManMac, MAA and OEGMA; number average molar masses ($M_n$) and molar mass distributions ($Đ$) of all homo and random co-polymers.

| Code | Composition | $M_{n,Theo}$ (g.mol$^{-1}$) | $M_{n,GPC}$ (g.mol$^{-1}$) | $Đ$ |
|---|---|---|---|---|
| **P1** | P((ManMac)$_{94}$) | 37300 | 32700 | 1.20 |
| **P2** | P((MAA)$_{96}$) | 8400 | 12100 | 1.18 |
| **P3** | P((ManMac)$_{46}$-r-(MAA)$_{44}$) | 21800 | 24600 | 1.21 |
| **P4** | P((ManMac)$_{45}$-r-(OEGMA)$_{43}$) | 30500 | 29400 | 1.20 |
| **P5** | P((MAA)$_{42}$-r-(OEGMA)$_{40}$) | 15800 | 22100 | 1.19 |

The conversion values of monomers were calculated using GC and $^1$H NMR by comparing the integrated signal intensity due to the aromatic protons of the RAFT agent at 7.8–7.9 ppm with the vinyl protons of monomers at 5.8–6.2 ppm. Both characterizations revealed that quantitative conversions were achieved for each monomer. The $M_n$ by GPC is slightly higher or lower than the theoretical molar mass mainly due to the different structure of the obtained polymers according to

PMMA calibration standards. The theoretical number average molar masses of the synthesized polymers, $M_{n(Theo)}$, was calculated by using the equation ($M_{n(Theo)}$ = ($[M]_o/[RAFT]_o$ x conversion x $M_{mon}$) + $M_{RAFT}$) where $[RAFT]_o$ is the initial RAFT concentration, $[M]_o$ is the initial monomer concentration, $M_{mon}$ is the monomer molecular weight and $M_{RAFT}$ is the RAFT agent's molecular weight.

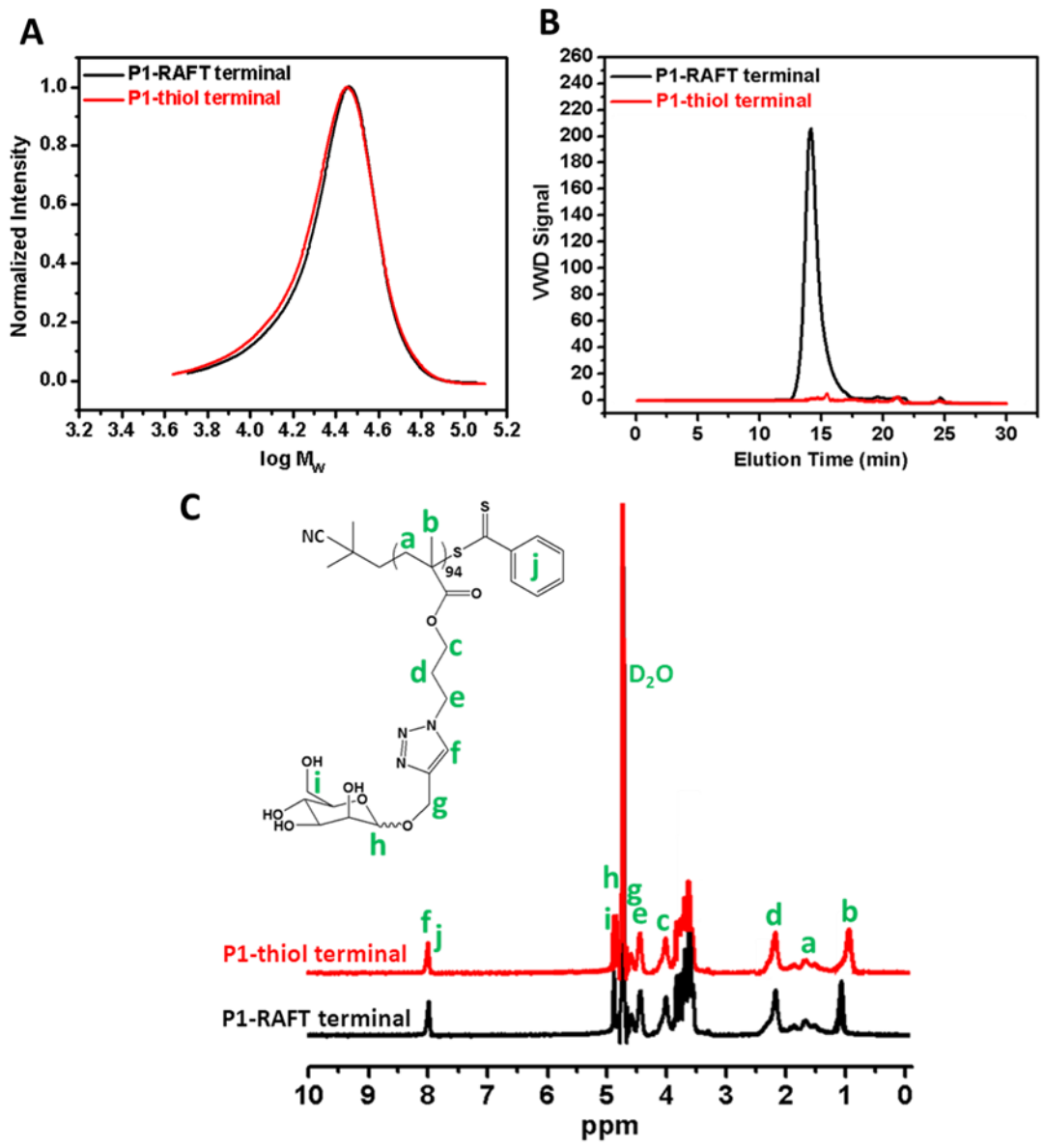


**Figure 3.2. A)** SEC analysis *via* RI detector; **B)** VWD; **C)** $^1$H NMR characterization of the synthesized **P1** homopolymer before and after the reduction of the RAFT terminal group.

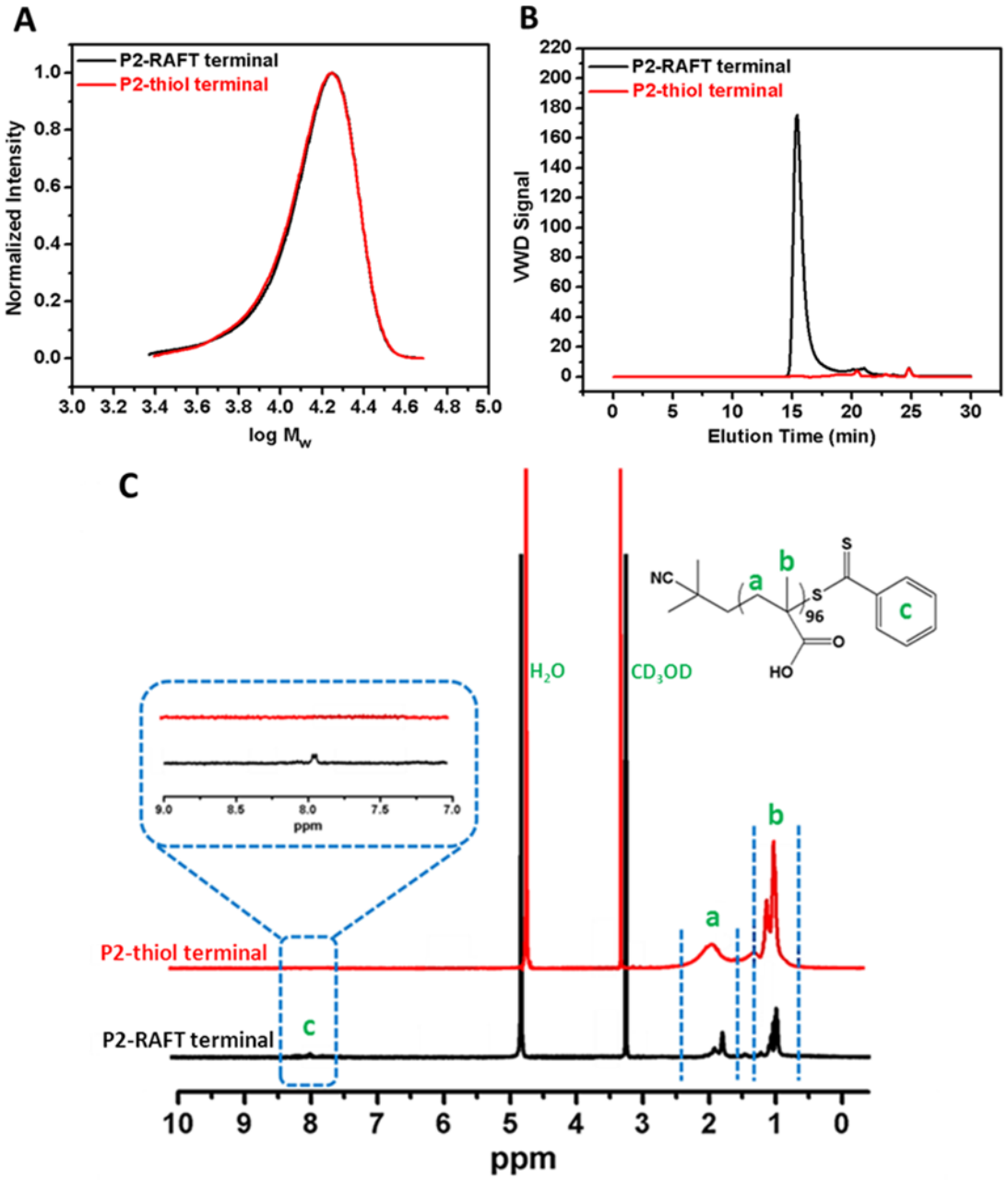


**Figure 3.3. A)** SEC analysis *via* RI detector; **B)** *via* VWD; **C)** $^{1}$H NMR characterization of the synthesized **P2** homopolymer before and after the reduction of the RAFT terminal group.

### 3.2.3 Reduction of the RAFT end group of homo/co-polymers

The RAFT agent terminal group of the obtained polymers was reduced to thiol-terminal one in order to immobilize the synthesized polymers onto gold nanoparticles in the presence of aqueous $NaBH_4$. $^{1}$H NMR and GPC were used to analyze the polymers before and after the reduction. The disappearance of the

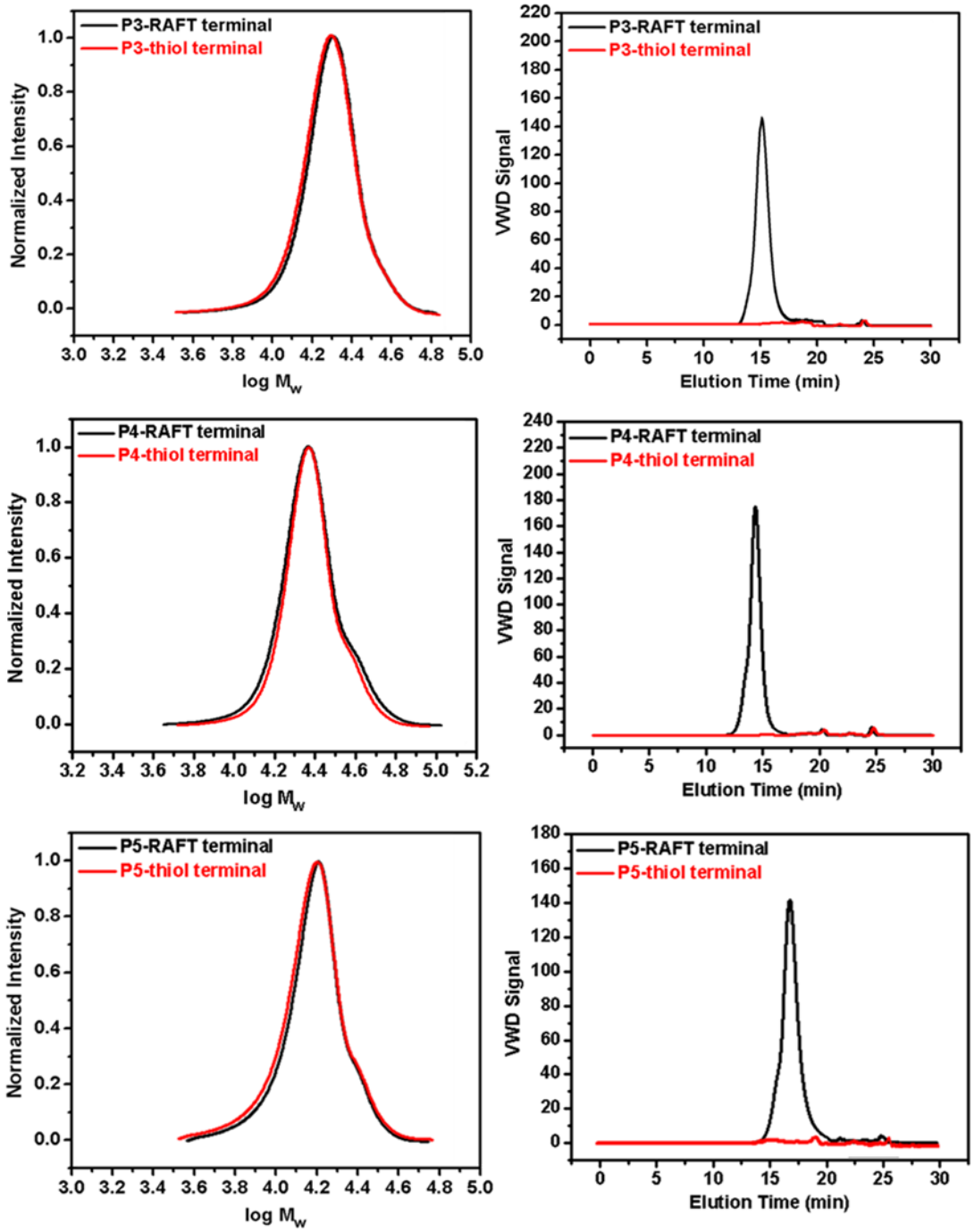


**Figure 3.4.** SEC analysis *via* RI and VWD detector before and after the reduction of the RAFT terminal group.

aromatic protons of the RAFT agent at 7.8–7.9 ppm after being treated indicated that all end groups in the CPDBT units have been reduced. As depicted in Figure 3.2, 3.3 and 3.4 no obvious change in the GPC traces was observed and the molar mass was exactly similar to that of before treatment according to RI detector of GPC. However, Variable Wavelength Detector (VWD) of GPC at 308 nm did not show any

significant peak after treatment suggesting that the polymer-SH chains were successfully obtained. In contrast, an intense UV signal associated with polymer-RAFT terminal elution was observed. Moreover, the color of the polymers that was provided by the RAFT terminal group changed from pink to white after the successful cleavage of the RAFT end group.

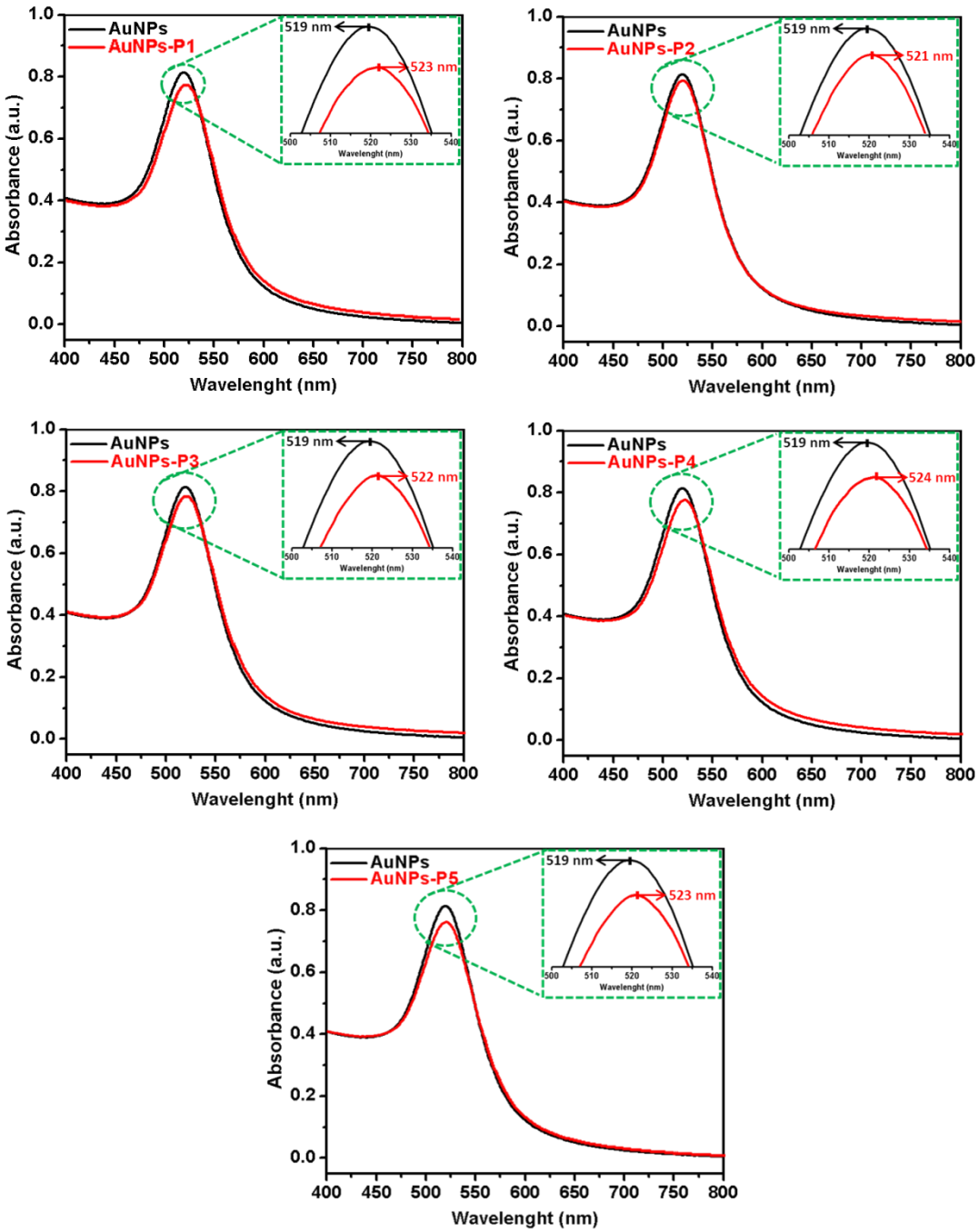


**Figure 3.5** UV/Vis spectroscopy characterization of AuNPs and the obtained polymer-coated AuNPs particles.

### 3.2.4 Preparation of polymer-substituted AuNPs

Prior to the polymer functionalization, the AuNPs solution was centrifuged. The supernatant was removed and replaced by the same volume of water. Then, the polymer coated gold nanoparticles were prepared by mixing polymer and AuNPs in the dark for overnight. Firstly, the obtained polymer-coated AuNPs were characterized *via* DLS and UV/Vis Spectroscopy in terms of the investigation of the size and surface plasmon resonance maximum band ($SPR_{max}$) value change. The $SPR_{max}$ band of AuNPs is usually in according to the nanoparticle size, shape, aggregation and also their dielectric environment. As seen in Figure 3.5, the position of the $SPR_{max}$ bands shifted to higher wavelength due to adsorption of the polymer on the surface. Moreover, UV absorbance peaks confirmed that the AuNPs coated with thiol-terminated polymers were still spherical in shape and also did not show any aggregation due to not any large broad shift in the UV absorbance. The general scheme of the reactions related to the synthesis of the synthesized polymers covered AuNPs was given in Scheme 3.2.

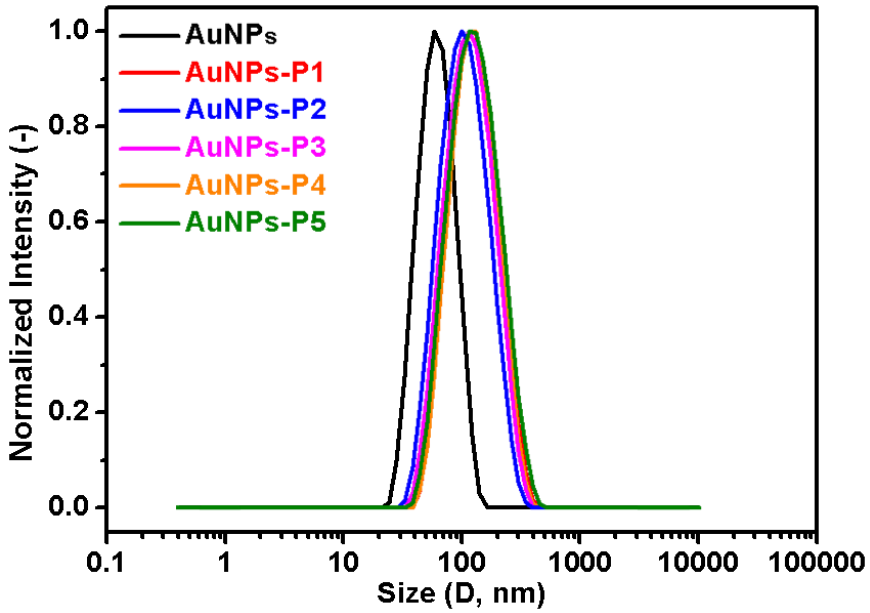


**Figure 3.6.** DLS measurements of the synthesized polymer-coated AuNPs particles.

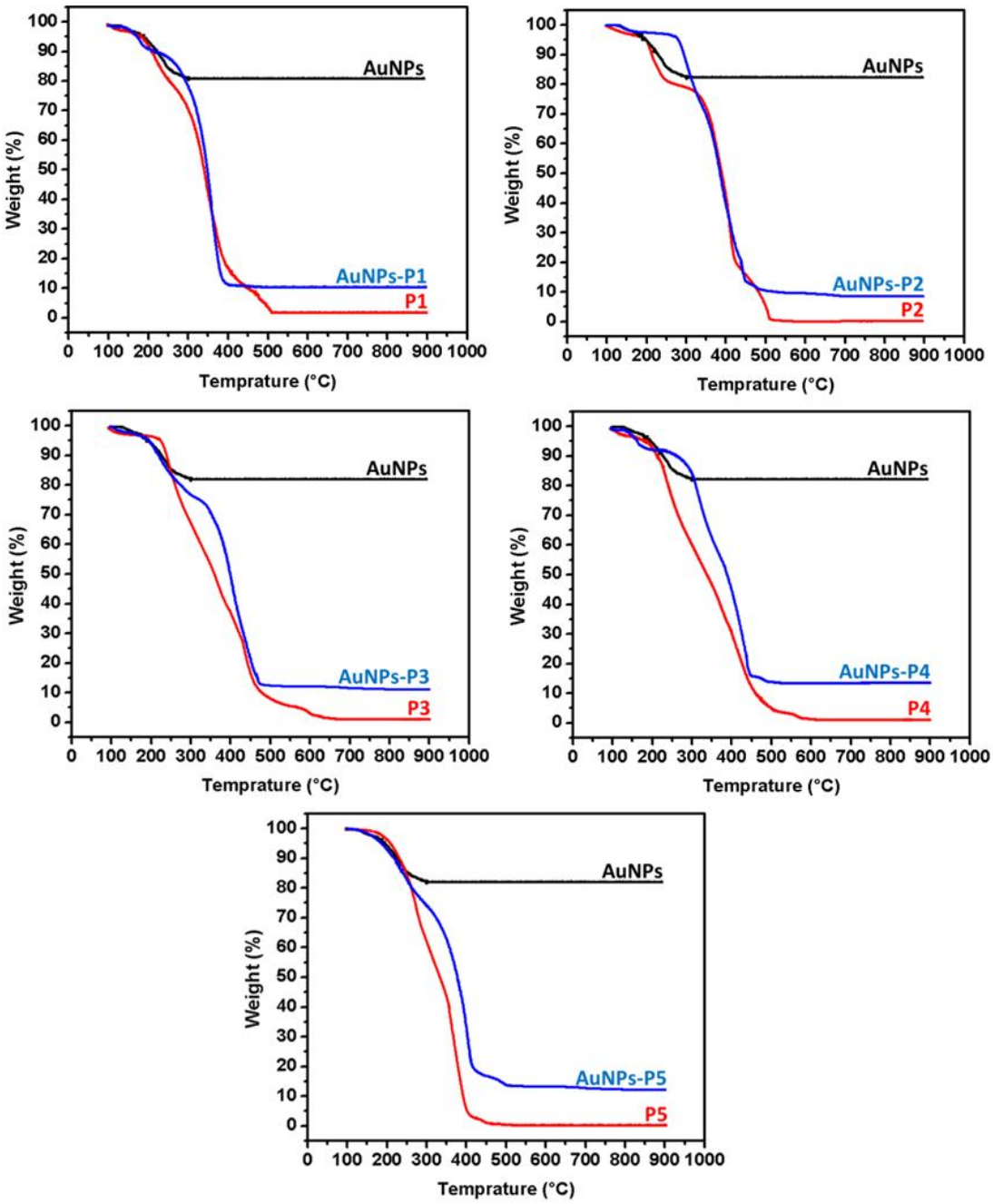


**Figure 3.7.** TGA measurements of AuNPs, all synthesized polymers and their substituted AuNPs.

Polymer-substituted AuNPs were characterized in terms of the size and zeta potential by using DLS. There were significant increases in the hydrodynamic volume between AuNPs and polymer-AuNPs, indicating successful immobilization of the polymers onto the surface. As depicted in Figure 3.6, the size of the gold nanoparticles after the coating with polymers increased from 55.7±0.2 nm to 104±0.7-107±1.2 nm with dispersity index (*Đ*) between 0.15 and 0.22, signifying a

narrow particle size distribution. Furthermore, the negative zeta potential of AuNPs increased or decreased depending on the polymer moieties, for example, even though the magnitude of the negative zeta potential of p(MAA)-coated AuNPs increased from -26.9±0.2 mV to -43.6±0.8 mV due to the deprotonation of the carboxyl group ($RCOOH \leftrightarrow RCOO^- + H^+$) in aqueous solution, the negative zeta potential of p(ManMac)-coated AuNPs decreased to -23.4±1.6 mV. According to transmission electron microscopy (TEM) images, the size of polymer-coated gold nanoparticles ranged between 53±2.4 and 64±1.8 nm. The average size of the monodisperse nanoparticles was summarized in Table 3.2.

**Table 3.2.** Summary of DLS, UV/Vis spectroscopy and TEM characterization results of the synthesized polymer-coated AuNPs particles.

| Sample | DLS | | TEM | Zeta Potential | $SPR_{band(max)}$ |
|---|---|---|---|---|---|
| | $D_h$ (nm) | Đ | Size (nm) | (mV) | (nm) |
| **AuNPs** | 55.7±0.2 | 0.11 | 43±1.2 | -26.9±0.2 | 519 |
| **AuNPs-P1** | 106±0.6 | 0.18 | 60±2.4 | -23.4±1.6 | 523 |
| **AuNPs-P2** | 104±0.7 | 0.15 | 57±1.8 | -43.6±0.8 | 521 |
| **AuNPs-P3** | 106±0.9 | 0.21 | 59±2.1 | -34.3±1.2 | 522 |
| **AuNPs-P4** | 107±1.2 | 0.22 | 61±1.7 | -22.7±0.9 | 524 |
| **AuNPs-P5** | 105±0.8 | 0.20 | 59±1.5 | -31.7±1.2 | 523 |

In order to determine the amount of the polymer immobilized onto AuNPs, thermal gravimetric analysis (TGA) was performed to analyze each materials thermal profile. As seen in Figure 3.7, each polymer-coated AuNPs exhibited mass loss until approximately 650 °C due to the decomposition of the polymer onto the surface and the remaining fraction was the Au core of the synthesized nanoparticles that was unaffected at temperature as high as 650 °C. It was observed that polymer-substituted AuNPs contained approximately 86.2-88.7% of the polymer.

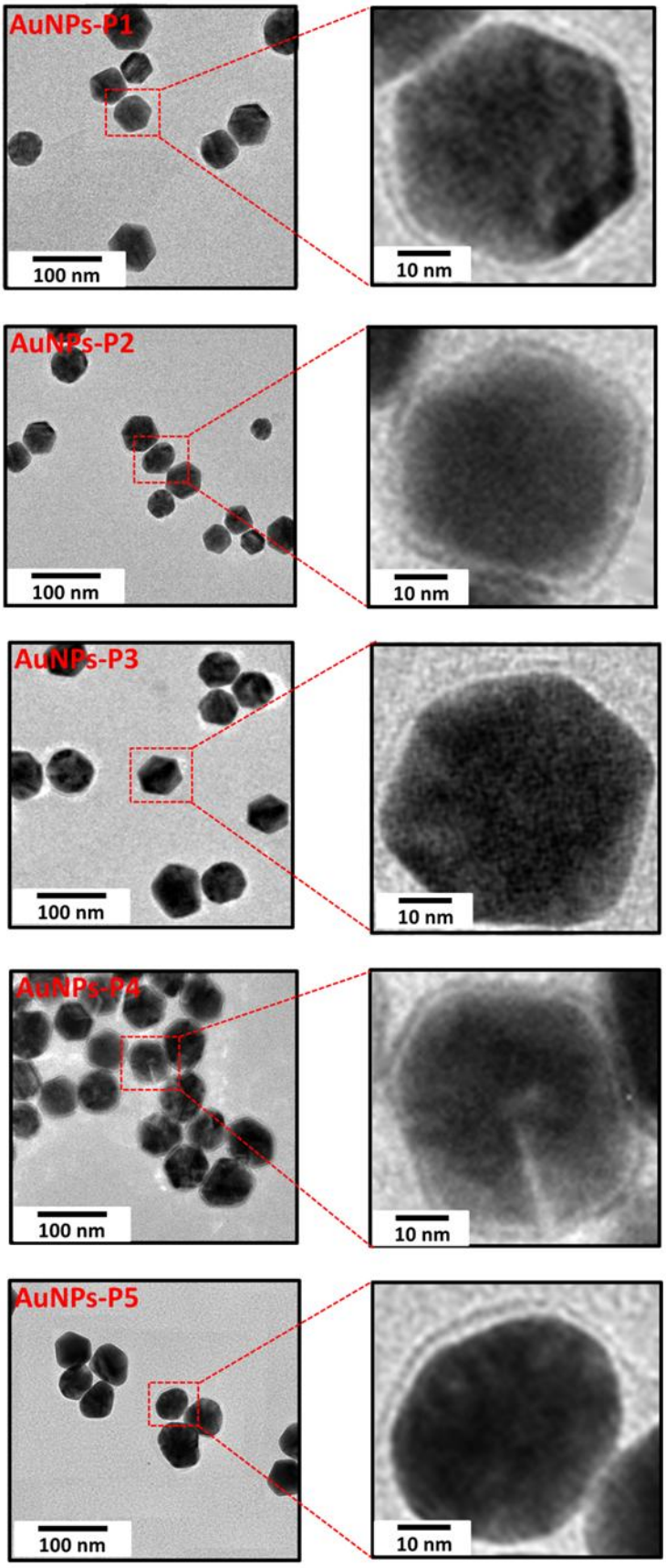


**Figure 3.8.** TEM iamges of the obtained polymer-coated AuNPs particles.

### 3.2.5 Synthesis and characterization of AuNPs-polymer-Cys-DOX

Following the successful synthesis of polymer coated AuNPs, a covalent binding strategy between AuNPs-polymer and Cys *via* EDC/NHS chemistry was applied to create a host structure for constructing a pH-sensitive bond between AuNPs-polymer-Cys and DOX in PBS and under ambient conditions. The conjugation steps for the formation of pH-sensitive hydrazone linkage in AuNPs-polymer-Cys-DOX were given in Scheme 3.3.

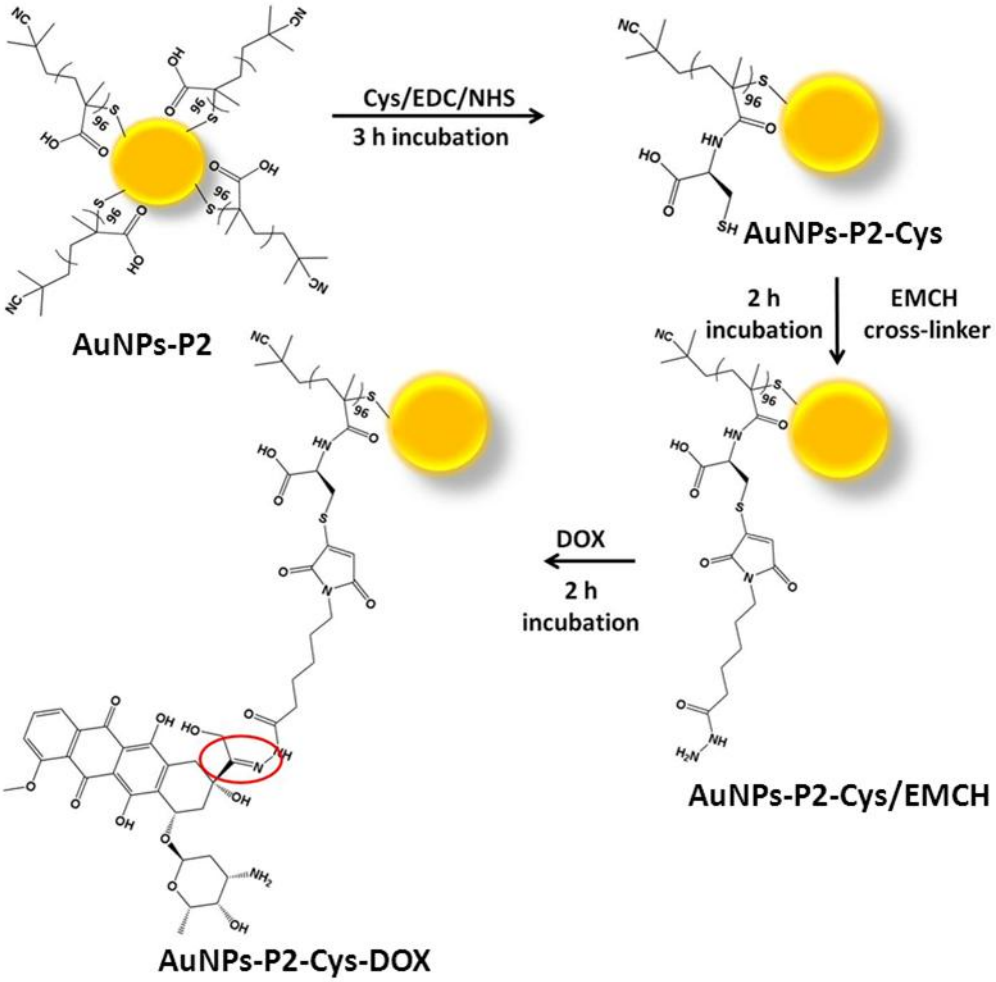


**Scheme 3.3.** The conjugation reactions of the AuNPs-P2-Cys-DOX particles.

As the initial characterization step of AuNPs-polymer-Cys-DOX conjugate, the spectrophotometric properties were investigated. The fluorescence and UV-vis spectra of conjugate were illustrated in Figure 3.9. To compare the spectral features of DOX before and after conjugation procedure, free DOX was also used at the

same concentration in AuNPs-polymer-Cys-DOX conjugate. As revealed in Figure 3.9A, DOX could show its fluorescence emission at 600 nm (ex: 480 nm) while it was conjugated to AuNP-polymer-Cys. Herein, the DOX conjugation was proved with the decrease of fluorescence intensity and absorption peaks, which were caused by the conjugation steps. In the other studies, similar cases showed up as demonstrated in Du *et al.* and Shantni *et al.* by conjugation of polymer-quantum dots and PEGylated palladium nanoparticles.[29,30] However, DOX could protect its spectral properties in the visible area, thereby this issue could be beneficial in calculating the binding efficiency (BE %) of DOX to polymer-coated AuNPs. Hence, a standard calibration curve was generated in the concentration range of 2.5-100 µM DOX at 480 nm. Then, the freshly synthesized 1.25 mg/mL AuNPs-polymer-Cys-DOX conjugate was measured and the repeatable results showed that Cys extended and polymer coated AuNPs could bind 25.5 µM of DOX. Therefore, the BE was calculated as 51% by using the following formula;

BE % = (DOX concentration in conjugate/ Total DOX concentration) x 100.

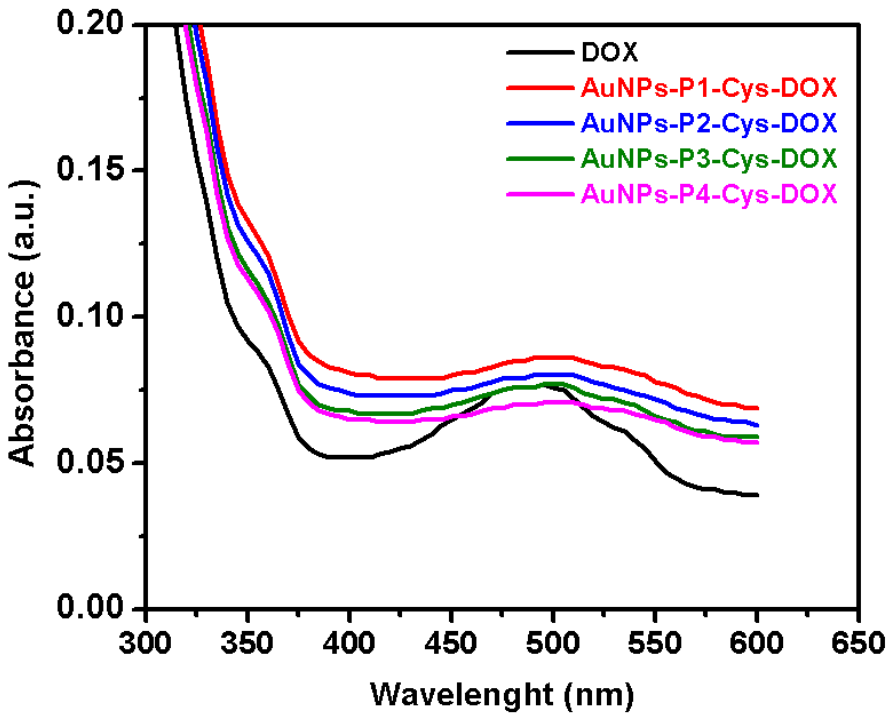


**Figure 3.9.** Spectrophotometric characterization of 1.25 mg/mL AuNPs-polymer-Cys-DOX bioconjugates containing 25 µM DOX) and 25 µM free DOX.

After the spectroscopic characterization of AuNPs-polymer-Cys-DOX conjugates, another physicochemical parameter was investigated in terms of particle size and zeta potential. The hydrodynamic particle size of AuNPs-polymer-Cys-DOX conjugates increased significantly after the conjugation around 40 nm. According to the subsequent zeta potential analysis, the negative surface charges of AuNPs-polymer-Cys-DOX conjugates decreased by covering the surface with Cys and DOX. It is known that negatively surface charged NPs demonstrate a reduced plasma protein adsorption and low rate of nonspecific cellular uptake.[13,31] Additionally, the charged NPs can repel one another to overcome the natural tendency of aggregation of NPs.[32] Hence, it can be claimed that newly synthesized polymer-coated AuNPs and their DOX conjugated forms could be suitable for the accumulation in the cancerous tissue by EPR effect thanks to their good dispersion stability, which was supported by *Đ* values.

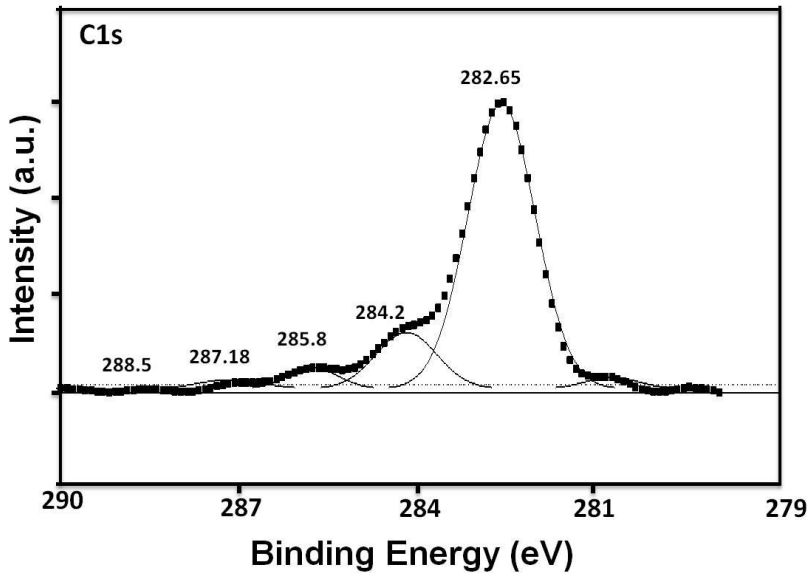


**Figure 3.10.** XPS scan of C1s of AuNPs-P2-Cys-DOX conjugation.

In addition to the physicochemical parameters, XPS of the AuNPs-polymer-Cys-DOX particles were employed to observe the demand typical bonds of the final conjugate *via* the binding energies. XPS spectrum in Figure 3.10 illustrates the detailed information about the crucial bonds, which were used in the conjugation steps, including an amide bond between carboxyl residues of polymer-coated AuNPs and amino group of Cys and hydrazone as the pH-sensitive linkage. In the

spectra, the binding energy of 282.65 eV reveals the typical C-C bonds. Normally, C-C binding energy shows itself approximately 284 eV.[33,34] However, it was proved that chemisorption of carbon over a surface could show its binding energy at 282.6 eV.[35] In addition, amide bond of O=C-N reveals itself at 287.18 eV with a shift and binding energy of 285.8 presents the typical hydrazone linkage (C=N) as detected in previous studies.[36,37] Furthermore, a small shoulder at 288.5 eV of binding energy shows the RCOO- groups which might come from the Cys residues or non-conjugated carboxyl group over p(MAA).[38]

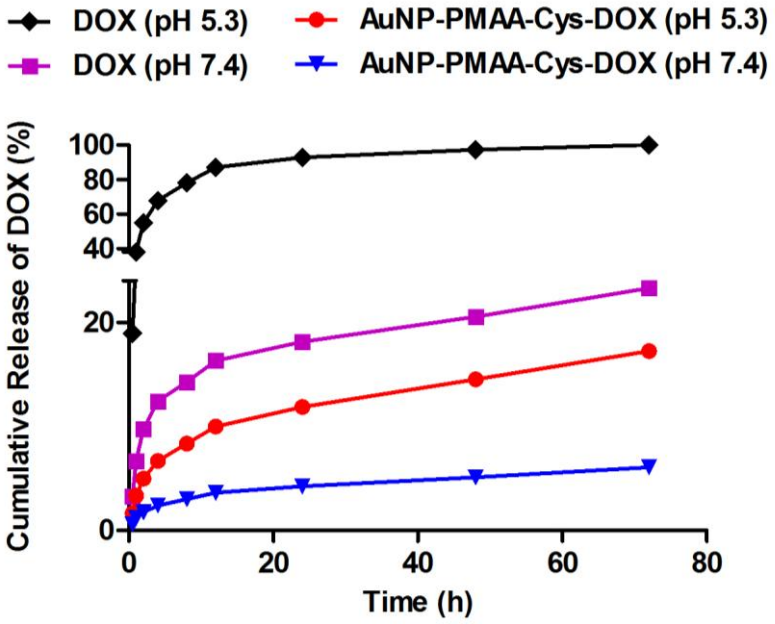


**Figure 3.11.** Cumulative drug release profiles of free DOX at pH 7.4 and AuNPs-P2-Cys-DOX bioconjugates at pH 5.3 and pH 7.4 for 72 h at 37 °C.

### 3.2.6 *In vitro* drug release studies

In addition to the characterization steps, *in vitro* release profiles of DOX-conjugated polymer coated AuNPs were generated in order to investigate the potential use of these particles as delivery carriers. One of the main characteristic feature of tumor sites is that having the slightly-acidic microenvironment.[39] Therefore, the current study was aimed to generate a pH-sensitive DOX conjugation using the polymer-coated AuNPs as a vehicle in the use of chemotherapeutic approaches. Many of the pH-sensitive bonds between a drug and a carrier which are formed from a typical hydrazone linkage were evaluated at pH 5.3 as modeling the extracellular pH

environment of cancer cells and at pH 7.4 as modeling the environment of healthy cells.[40] As depicted in Figure 3.11, free DOX was illustrated the typical release profile at pH 5.3 by reaching 100% release. On the other hand, it was seemed that the cumulative release profile of AuNPs-polymer-Cys-DOX conjugate was more controllable at pH 5.3 according to the free DOX release. Concomitantly, a similar case was also observed at pH 7.4. DOX release from the conjugate at pH 7.4 was about 6.0% up to 72 h. This valuable data demonstrated the potential of AuNPs-polymer-Cys-DOX with a slow and sustained release and usability for a long-time by keeping the formulation at lower temperatures.

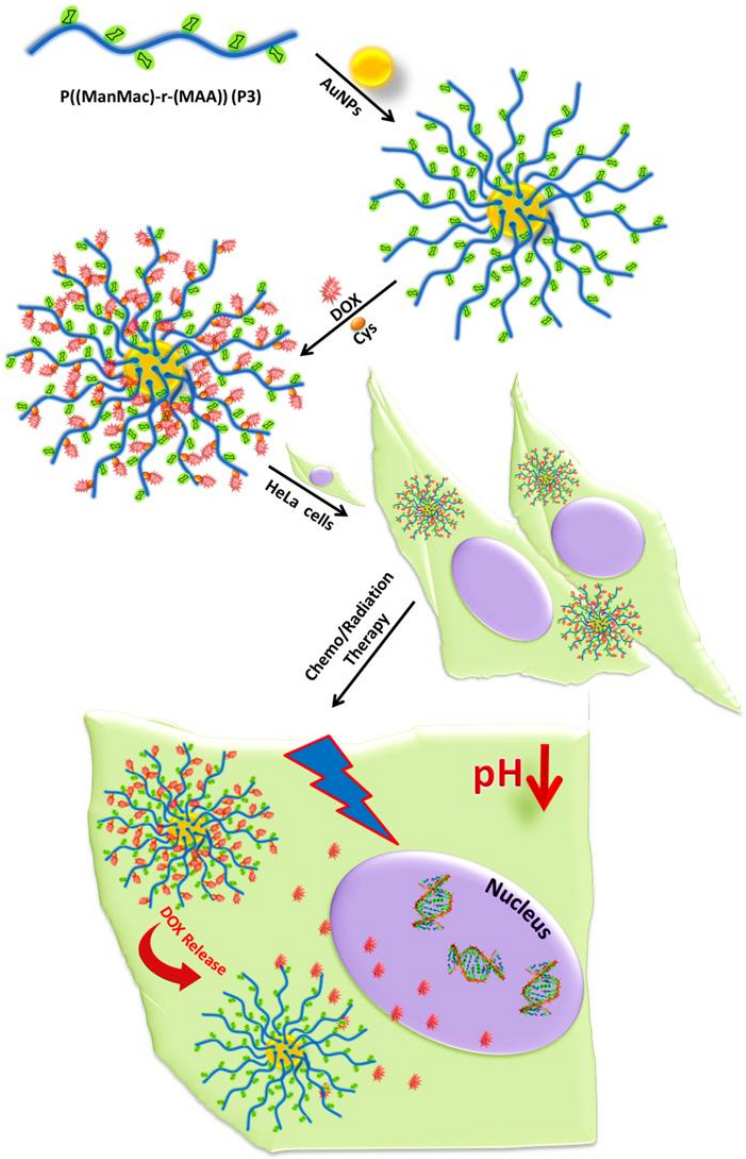


**Scheme 3.4.** Diagram of the synthesis of AuNPs-P3-Cys-DOX conjugate particles and their cell studies.

### 3.2.7 Cell culture studies

Following the successful characterization steps and defining the release profile of DOX *in vitro,* artificial media modeling the extracellular conditions of cancer cells, cell culture techniques were used to evaluate the effects of the final DOX conjugate by comparing free DOX and polymer-coated AuNPs alone with the same concentrations as conjugate. In this manner, cytotoxicity, radiosensitive effect and cell imaging studies were performed during cell culture experiments. Due to the therapeutic efficacy of DOX and unique radiosensitive activity of AuNPs, a combined modality, which is conducted with passive targeting strategy, was enabled within bioimaging of HeLa cells within the fluorescence properties of DOX molecule. The related results are given below by discussing the experiments, comparatively.

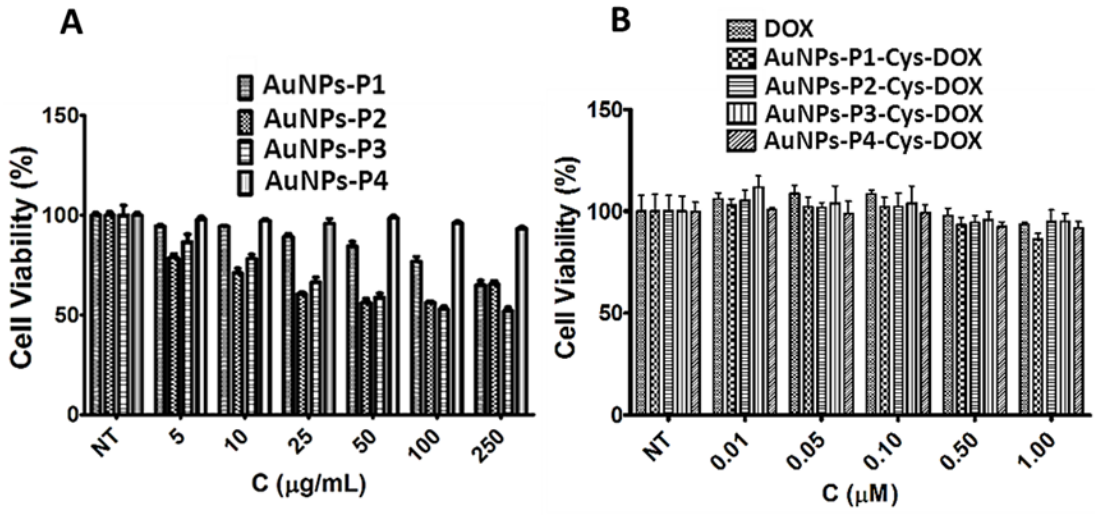


**Figure 3.12.** The dose-dependent toxicity of AuNPs-polymers (**A**), AuNPs-polymer-Cys-DOX particles and free DOX (**B**) for HeLa cells. Error bars mean ± standard deviation, (n = 4).

#### 3.2.7.1 Cytotoxicity

Before the evaluation of other parameters with HeLa cells as the model cancer cell line in this work, the dose-dependent viability of the cells were determined for polymer-coated AuNPs, DOX and AuNPs-polymer-Cys-DOX conjugates for 24 h at 37 °C and 5.0% $CO_2$ under humidified conditions. To date, it is known that AuNPs do

not have much toxic effect upon both cancer and healthy cell lines as illustrated in previous works.[41,42] In this step, polymer-AuNPs structures were initially tested for their influence upon the viability of HeLa cells. Figure 3.12 represents the effect of polymer coated AuNPs on cell viability. It can be clearly said that polymer coated AuNPs do not exhibit any toxic effect on HeLa cells up to 500 µg/mL particles (84%). As shown in the Figure 3.12B, the cell viability profile of free DOX is close to AuNPs-polymer-Cys-DOX up to 1.0 µM DOX (equivalent to 50 µg/mL polymer-coated AuNPs for conjugate). Although DOX was seemed more effective until 5.0 µM, there was a significant decrease between free DOX (47.11%) and AuNPs-polymer-Cys-DOX (25.6%) in the final concentration ($p<0.001$). It is known that the delivery of free DOX is based on simple diffusion across the cell membrane. Besides, the uptake of many nanocarriers are based on different endocytic pathways depending on the cell type and the physicochemical properties of nanocarrier.[43] After the uptake of the functional particles, the particles get cleaved in the cells and therapeutic molecules are delivered in the slightly acidic conditions. Since the *in vitro* DOX release profile presented the similar behavior like other studies, the effect of this profile also can give idea for the cytotoxicity. Moreover, it is showed that free DOX can release easily under acidic conditions in the cumulative drug release profiles. However, the nanocarrier systems get more effective in the 24 h toxicity tests. In our case, we have observed the effective concentration of the proposed theranostic platform as 5.0 µM DOX concentration. Hence, the constructed DOX conjugate with a pH-sensitive bond may be a good potential in the chemotherapy thanks to its sustained release and having non-toxic carrier architecture.

### 3.2.7.2 Radioactivity

Radiation therapy is one of the most commonly used treatment modality for cancer disease by giving ionizing radiation. It was reported that the effect of ionizing radiation could be enhanced within the addition of high-Z materials, including heavy elements such as gold, cis-platin *etc.*[44] Beside this, there may be some difficulties related to the radiotherapy resulting from the acquired radiation resistance. This limitation opens the doorway of the required multiple/combined

approaches such as simultaneous applications of drug formulations or treatment modalities like photodynamic therapy/radiotherapy as demonstrated in previous reports.[45] Accordingly, the combination of chemotherapy and radiotherapy by using the enhancers of both modalities, AuNPs and DOX were conjugated in a facile and efficient way by creating a pH-sensitive hydrazone linkage. To investigate the radiosensitive effects of AuNPs-polymer-Cys-DOX conjugations, HeLa cells were treated with three different ionizing radiation levels (2.5, 5.0 and 10 Gray). In addition, free DOX (5.0 µM), polymer-coated AuNPs and citrate coated AuNPs (as the same concentration with both AuNPs-polymers and AuNPs-polymer-Cys-DOX conjugations were compared, comprehensively.

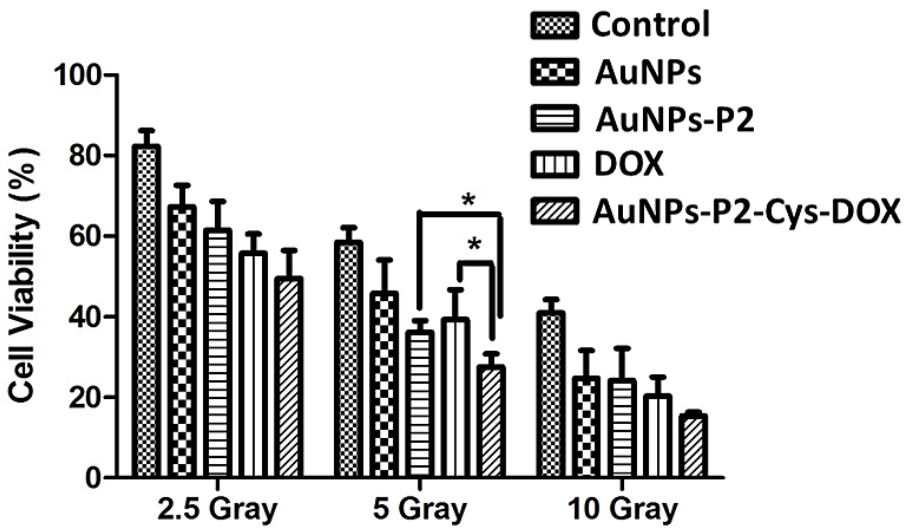


**Figure 3.13.** Radiosensitivity effect of uncoated AuNPs, AuNPs-P2, free DOX and AuNPs-P2-Cys-DOX at different ionizing radiations (2.5, 5.0 and 10 Grays).

As shown in Figure 3.13, 5.0 Gray of ionizing radiation for AuNPs-P2-Cys-DOX conjugations (27%) demonstrated a significant difference among free DOX (40%), AuNPs-P2 (36.3%) and also citrate coated AuNPs (46%) by comparing other doses ($p<0.05$). Meanwhile, DOX was applied to cancer cells in a reported work which supports our findings.[46] In the irradiation of 2.5 and 10 Grays, it is shown that the cell viabilities of the samples ranging from citrate capped AuNPs to AuNPs-polymer-Cys-DOX conjugates gave similar results. These results were also compared statistically; however, as can be seen from Figure 3.13, there is no dramatic change between applied samples for both irradiation doses. Furthermore, the free DOX

concentration of 5.0 µM did not present any additional therapeutic effect at 2.5 Gray. The cell viability of that sample is similar to cytotoxicity test. Within the increase of irradiation level, both polymer-coated AuNPs and DOX created a significant effect according to the control group. As mentioned in introduction part, the radiosensitive effect of AuNPs could demonstrate in this study, clearly. Expectedly, AuNPs-polymer-Cys-DOX particles were able to enhance the therapeutic efficacy comparable to free DOX upon HeLa cells under irradiation of 5 Gray. In other reported studies, DOX was used as a radiosensitizer for HeLa cells and V79 hamster cell line.[47,48] Jagetia and Nayak carried out their research for irradiation effect of DOX by introducing 10 µg/mL (equals to 5.8 µM) DOX to HeLa cells between the range of 0 - 3.0 Gray irradiation doses.[47] According to this study, increasing irradiation doses enabled a gradual decline in the cell survival compare to control cells without DOX. These results also support our findings related to the decrease in cell viabilities of free DOX group. As reported in those studies, the high irradiation doses like 10 gray might cause reduced cell viability for control groups without therapeutic molecules. However, samples could significantly show their toxicity upon HeLa cells at 10 Gray, when compare to control group only ($p<0.001$).

### 3.2.7.3 Cell imaging

As the final study for the synthesized AuNPs-polymer-Cys-DOX particles, nontoxic concentrations of conjugates were applied to HeLa cells for 2 h to monitor the internalization of DOX conjugates. As can be seen from Figure 3.14, DOX in conjugate could easily localize in the nucleus of HeLa cells as free DOX. Besides fluorescent imaging with the unique spectroscopic properties of DOX, phase-contrast images were taken to overlap the images and to show that AuNPs-polymer-Cys-DOX particles was also effective in monitoring the cells. This capability of the proposed conjugate reveals that it may be a suitable and beneficial candidate as a theranostically engineered nanoparticle. DOX conjugate for 2 h at 37 °C and 5.0% $CO_2$ atmosphere, under humidity. Images of samples were taken with a red filter of fluorescence set up with 100x magnification.

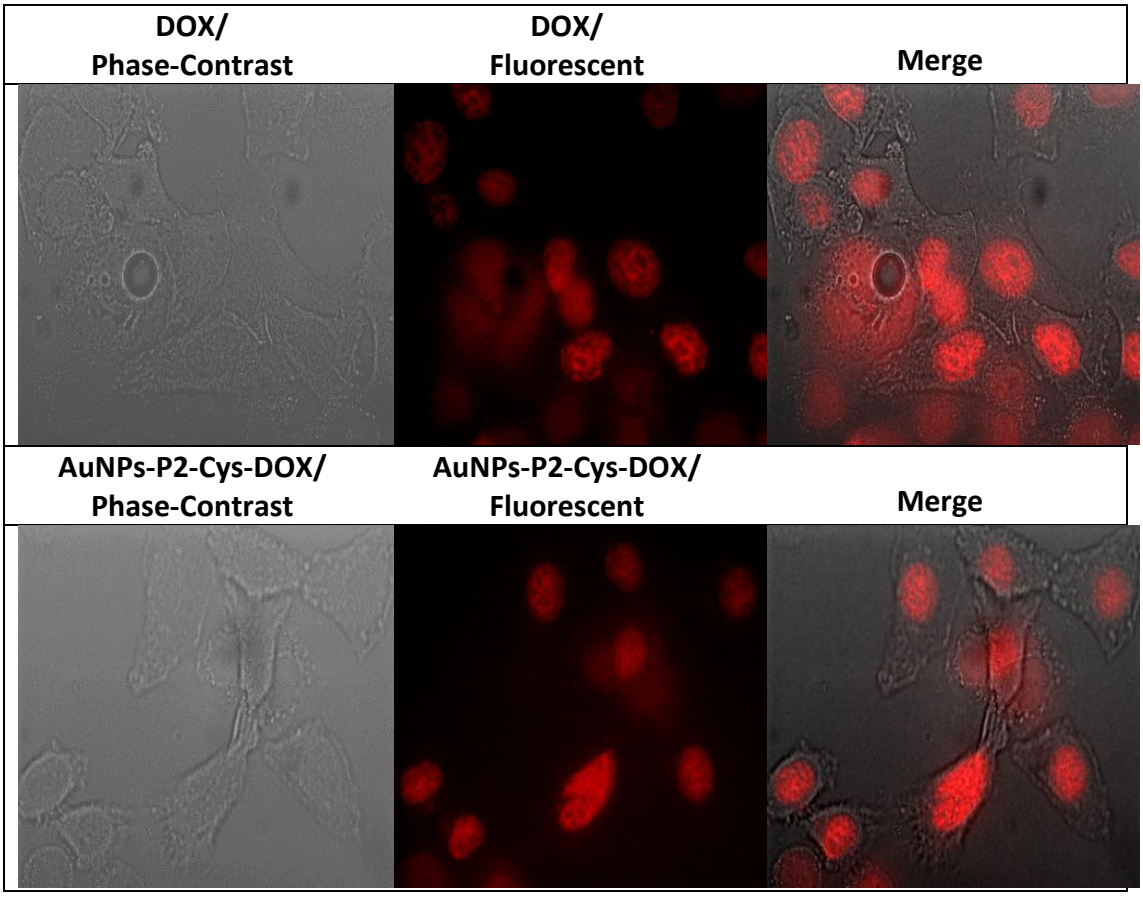


**Figure 3.14.** Imaging of HeLa cells with phase-contrast and fluorescence technique. Images were obtained after treatment of the cell with free DOX and AuNPs-P2-Cys-

## 3.3 Conclusion

Functional homo/co-polymers were synthesized by using RAFT polymerization to develop combined nanoplatforms involving both polymer-coated AuNPs and an anti-cancer drug doxorubicin *via* creating a pH-sensitive hydrazone linkage in the presence of cysteine and a cross-linker. The obtained AuNPs-polymer-Cys-DOX particles have shown a sustained drug release in the simulated extracellular matrix conditions by differentiating the pH to prove the pH-sensitive property of AuNPs-polymer-Cys-DOX conjugations. Another considerable influence of the AuNPs-polymer-Cys-DOX particles was that these novel platforms could be used effectively for the treatment of cancer with chemotherapy and radiotherapy modalities when compared only polymer covered AuNPs and DOX. In the final step, the capability of these conjugates for cell imaging was illustrated due to the fluorescence of DOX.

Thereby, AuNPs-polymer-Cys-DOX particles can be a satisfactory theranostic tool in the combined treatment of chemotherapy/radiotherapy and fluorescence imaging.

## 3.4 Experimental

### 3.4.1 Materials

Methacrylic acid (MAA, 99%, contains 250 ppm mono methyl ether hydroquinone (MEHQ) as inhibitor), poly(ethylene glycol) methyl ether methacrylate (OEGMA, average *Mn* ≈ 300 $g.mol^{-1}$, contains 100 ppm MEHQ and 300 ppm butylated hydroxytoluene (BHT) as inhibitor), 2-Cyano-2-propyl benzodithioate (CPBDT, 97%), sodium borohydride ($NaBH_4$, 98%, granular, 10-40 mesh) and gold nanoparticle suspension (40 nm) that stabilized with citrate were purchased from Sigma Aldrich Chemical Company (Dorset, UK). MAA and OEGMA was passed through a short column of basic alumina in order to remove MEHQ inhibitor prior to polymerization. 4,4'-azobis-(2-methylpropionitrile) (AIBN) and $H_2SO_4$-silica catalyst were previously synthesized within the group. All other reagents and solvents were obtained at the highest purity available from Sigma Aldrich Chemical Company (Dorset, UK) and used as received unless stated otherwise. Water ($H_2O$, HiPerSolv Chromanorm for HPLC from VWR International, UK) was used throughout the study. Dialysis tubes were purchased from Spectrum Laboratories (California, USA). Copper coated 3.05mm diameter square carbon film mesh grids were purchased from Agar Scientific (Essex, UK). Doxorubicin (DOX), Cysteine (Cys), N-(3-dimethylaminopropyl)-N'-ethylcarbodiimide hydrochloride (EDC), N-hydroxysuccinimide (NHS), 3-(4,5-dimethylthiazolyl-2)-2,5-diphenyltetrazolium bromide (MTT) and sodium dodecyl sulfate (SDS) were obtained from Sigma-Aldrich (St. Louis, USA). N-ε-maleimidocaproic acid hydrazide (EMCH) was obtained from Thermo Fischer Scientific (California, USA). Dulbecco's Modified Eagle Medium (DMEM), Penicillin/Streptomycin (10,000 UI/mL), L-Glutamine (200 mM). Trypsin/EDTA (0.05% Trypsin; 0.2 g/L EDTA), and Phosphate Buffered Saline (PBS) used in cell culture experiments were obtained from Lonza (Basel, Switzerland). Fetal Bovine Serum (FBS) was purchased from Biowest (Nuaillé, France).

### 3.4.2 Instruments and Analysis

Proton and carbon-13 ($^{1}$H-NMR and $^{13}$C-NMR) nuclear magnetic resonance spectroscopy (Bruker DPX-400/600) were used to determine the chemical structure of the synthesized polymers. Samples were dissolved at 5 mg/mL concentration in $D_2O$ or $(CD_3)_2SO$ solvents depending on the solubility of the samples.

Size-exclusion chromatography (SEC) measurements were conducted on an Agilent 1260 infinity system operating in DMF with 5.0 mM $NH_4BF_4$ and equipped with refractive index detector (RID) and variable wavelength detector (VWD), 2 PLgel 5 µm mixed-C columns (300×7.5mm), a PLgel 5 mm guard column (50x7.5mm) and an autosampler. The instrument was calibrated with linear poly(methyl methacrylate) standards in range of 550 to 46890 g.mol$^{-1}$. All samples were passed through 0.2 µm PTFE filter before analysis.

GC was used to measure monomer conversion for homopolymerization of MAA. GC analysis was performed using an Agilent Technologies 7820A. An Agilent J&W HP-5 capillary column of 30 m x 0.320 mm with a film thickness of 0.25 mm was used. The oven temperature was programmed as follows: 40 °C (hold for 1 min) increase at 30 °C/min to 300 °C (hold for 2.5 min). The injector was operated at 250 °C and the FID was operated at 320 °C. Nitrogen was used as carrier gas at flow rate of 6.5 mL/min and a split ratio of 1:1 was applied. Chromatographic data was processed using OpenLab CDS ChemStation Edition, version C.01.05.

Thermal gravimetric analysis (TGA) was conducted with a TA Instruments TGA Q500 under nitrogen atmosphere using approximately 5.0 mg of the respective sample for the analysis. Method settings: heating from 100 to 900 °C with a heating rate of 10 °C/min. UV measurements were performed on a PerkinElmer UV/Vis Spectrometer Lambda 35.

Transmission electron microscopy (TEM) analysis was carried out on a JEOL 1400 instrument operating at an acceleration voltage 100 kV. The TEM specimens were prepared by placing a drop of a nanoparticle water suspension on a carbon-coated copper grid.

UV-visible spectra were recorded on a PerkinElmer Lamda 25 UV/VIS spectrometer equipped with a (PTP-1) temperature control unit at a certain temperatures in the range of 200 nm and 600 nm using quartz microcuvettes.

The FT-IR spectra were recorded on a Bruker FT-IR spectrometer TENSOR II with Diamond-ATR module. The scanning range was 600-4000 $cm^{-1}$ and the resolution was 1 $cm^{-1}$.

Electrospray ionization-mass spectrometry (ESI-MS) spectra were recorded on a Thermo Finnigan LCQ Decaquadrupole ion trap mass spectrometer (Thermo Finnigan, San Jose, CA), equipped with an atmospheric pressure ionization source operating in the nebulizer assisted electrospray mode and was used in positive ion mode.

To confirm the conjugation of AuNP-PMAA particles to DOX, particle size, surface charge, spectrofluorimetric and X-ray photoelectron spectroscopy (XPS) analysis were carried out. Size distribution and zeta potential of AuNP-PMAA-Cys-DOX conjugates were measured by a dynamic light scattering (DLS) method with Zetasizer Nano ZS (Malvern Instruments Ltd., U.K.) at a scattering angle of 90 using a wavelength of 633 nm and at 25 °C. Prior to measurements, the samples (50 µL) were diluted to 1.0 mL with PBS and each sample was measured three times. Zeta potentials of samples were calculated by the device according to Smoluchowski equation. The samples were kept in +4 °C when not in use. Fluorimetric and spectroscopic properties of AuNP-PMAA-Cys-DOX were assessed *via* a Varioskan spectrofluorometer (Thermo, Fischer, U.S.A.). XPS analysis (PHI 5000 VersaProbe, Minnesota, USA) of the final drug-AuNP conjugate was accomplished, too. Prior to measurements, AuNP-PMAA-Cys-DOX solution was dried over an ultrasonically cleaned indium tin oxide surface.

### 3.4.3 Synthesis of D-mannose acrylate glycomonomer

1-(2'-propargyl) D-mannose (2.61 g, 12.1 mmol) and 3-azidopropyl methacrylate (2.00 g, 11.0 mmol) were dissolved in MeOH/$H_2O$ (3:1 vol/vol, 80 mL), aqueous solution of $CuSO_4 \cdot 5H_2O$ (240 mg, 0.97 mmol) and (+)-sodium L-ascorbate (250 mg,

1.22 mmol) were added into the reaction solution. The reaction mixture was stirred at ambient temperature for 24 h. Methanol was then removed under vacuum and the residue mixture was freeze dried to remove water. The obtained product was purified through silica gel column chromatography using dichloromethane-MeOH (8:1) as eluent. After removing of solvent, the product was obtained as white (1.94 g, yield: 43.9%).

$^{1}$H NMR ($D_2O$, 298 K, 400 MHz): δ =8.02 (s, 1 H, NCH=C), 5.96 (s, 1H, =$CH_2$), 5.58 (s, 1H, $CH_2$), 4.92-4.97 (m, 2H, $CH_2$-OH), 4.88-4.22 (m, CH-O-$CH_2$, H-1 of mannose , overlap with $H_2O$), 4.54 (t, 2 H, J=6.6 Hz, $CH_2$-N), 4.21 (t, 2 H, J=6.8 Hz, C=O-O-$CH_2$), 3.51-3.92 (m, H residues of mannose), 2.26 (m, 2H, $CH_2$-$CH_2$-$CH_2$), 1.84 (s, 3H, $CH_3$) ppm.

$^{13}$C NMR ($D_2O$, 298 K, 400 MHz): δ =158.4 (C=O), 134.6 (C-$CH_2$), 126.4 (N-CH=C), 123.7 ($CH_2$-C), 104.6 (β anomeric, C 1 of mannose), 103.2 (α anomeric, C 1 of mannose), 72.3 (N-CH=C), 71.6 (C=O-O-$CH_2$), 70.4 (C-$CH_2$-O), 66.8, 64.4, 63.5, 62.3 (carbons of anomeric mannose), 48.6 ($CH_2$-N), 29.7 ($CH_2$-$CH_2$-N), 19.4 ($CH_2$-OH), 18.6.5 ($CH_3$-C) ppm.

ESI-MS m/z: calculated for $C_{16}H_{25}N_3O_8$ ($M+H^+$), 387.2; found, 387.4.

### 3.4.4 General procedure for RAFT polymerization

RAFT polymerization reactions were carried out in the presence of CPDBT as a RAFT agent, AIBN as an initiator in the methanol and water mixture (2:1) at 70 °C for 12 h. A Schlenk tube was charged with targeted monomer or monomers (methacrylic acid (MAA), poly(ethylene glycol) methyl ether methacrylate (OEGMA) and D-mannose methacrylate (ManMac)) (in total 100 eq), CPDBT (1 eq), AIBN (0.1 eq) and the solvent (3.0 mL) was degassed by gentle bubbling of argon gas for 30 min. The Schlenk tube was sealed properly and the mixed solution was allowed to polymerize. After the confirmation of nearly full conversion according to GC and $^{1}$H NMR, the polymerization reaction was stopped by cooling down and exposure to the air. Subsequently, the reaction solution was diluted with 3.0 mL of MeOH and then purified by precipitation in diethyl ether twice. After the filtration, the

obtained polymer was dried *in vacuo* and characterized *via* $^{1}$H-NMR and DMF SEC analysis.

### 3.4.5 Reduction of the RAFT End Group of the obtained polymers

The RAFT end group of the obtained polymers was reduced by the addition of $NaBH_4$ as the reducing agent in distilled water. The homo/co-polymers were added into a 50-mL round-bottom flask with 10 mL water solution of 1.0 M $NaBH_4$ and the solution was bubbled for 15 min with argon (molar ratio of $NaBH_4$:dithioester end groups was 25:1). After that, the mixture was allowed to react for 2 h. Following reduction, the reaction solution was dialyzed against to water for 3 days, while changing the water at least three times. Finally, it was freeze dried to get the polymer with thiol end group. The product was characterized by $^{1}$H-NMR and DMF SEC analysis.

### 3.4.6 Preparation of PMAA-Substituted AuNPs

The AuNPs solution was centrifuged in order to remove the supernatant and then replaced by the same volume of water prior to the PMAA functionalization. The terminally thiolated polymers (10 mg) were dissolved in 1.0 mL AuNPs solution and then agitated in the dark for overnight. To remove excess polymer, the solution of the AuNPs-stabilized polymers were centrifuged (5470 rpm, 30 min). Following careful decantation of the supernatant, the nanoparticles were then redispersed in 1.0 mL of deionized water and then the centrifugation and resuspension process was repeated one more cycle. These synthesized polymers-substituted GNPs were characterized by DLS, UV/Vis Spectroscopy, TGA and TEM. The PMAA-coated AuNPs were stored at 4 °C for the further study.

### 3.4.7 Construction of pH-sensitive AuNPs-polymer-Cys-DOX bioconjugates

The bioconjugation of polymers capped AuNPs was carried out as three main steps. Initially, AuNPs which have pendant carboxylic acid (-COOH) groups were activated with EDC/NHS chemistry and covalent amide bonds were generated by adding Cys. For this purpose, the mixture of 25 µL polymer- coated AuNPs (100 mg/mL dissolved in 10 mM phosphate buffer, pH 7.4), 48.9 mg EDC, 7.2 mg NHS and 250 µL

Cys (from 1.0 mg/mL stock solution dissolved in pH 5.0 MES buffer) was prepared ($V_{total}$=1500 µL with the addition of MES buffer) and incubated for 3 h with 1000 rpm shaking under ambient conditions. After the incubation step, final mixture was dialyzed against pH 7.4 PBS for 2 h. The dialyzed bioconjugate solution was treated with DTT (1:0.9 molar ratio of Cys:DTT). This mixture was incubated overnight under 1000 rpm shaking and ambient conditions. After the reduction of S-S linkages between Cys residues, EMCH cross-linker was added as 3.2 mg and reacted for 2 h at 1000 rpm shaking at room temperature. After incubation, the mixture was dialyzed for 6 h against PBS pH 7.4. In the final step, DOX (50 µM as the final concentration) was added to the AuNPs-polymer-Cys (EMCH) solutions and incubated for 2 h at 1000 rpm shaking and room temperature and final solution was increased to 2.0 mL. The final AuNPs-poymer-Cys-DOX conjugates were dialyzed overnight against PBS, pH 7.4.

### 3.4.8 *In vitro* drug release studies

The *in vitro* release behavior of DOX-loaded nanoparticles was monitored by creating an artificial medium. pH 7.4 and pH 5.3 (PBS) were used to simulate the healthy and cancerous cellular environments, respectively. Dialysis bags containing 0.5 mL of sample were submerged in 5.0 mL buffer medium at 37 °C at 100 rpm. To investigate the in vitro release profiles of the samples, 0.5 mL of each of the samples was collected at several time intervals (0, 30 min and 1, 2, 4, 6, 8, 12, 24, 48, and 72 h) and replaced with an equal volume of fresh medium.

The concentration of DOX in the collected samples was determined by fluorescence spectroscopy using a standard curve that was generated by the fluorescence properties of DOX. Probing the released DOX, the cumulative drug release percentage (Er) was calculated according to the following equation:

$$E_r = \frac{Ve \sum_{1}^{n-1} Ci + Vo\, Cn}{M(Dox)}$$

Where M(Dox) represents the amount of DOX in the particles, Vo is the whole volume of the release media (Vo = 5.0 mL), Ve is the volume of the replace media (Ve = 0.5 mL), and Cn represents the concentration of DOX in the $n^{th}$ sample.

### 3.4.9 Cell culture studies

Human cervix adenocarcinoma cell line (HeLa), (American Type Culture Collection) was maintained in DMEM supplemented with 10% FBS, 100 UI/mL Penicillin/Streptomycin, and 2.0 mM, L-Glutamine at 37 °C in a humidified incubator with 5.0% $CO_2$. HeLa cells were sub-cultured at 80% confluency. Following the synthesis of AuNPs-polymer-Cys-DOX bioconjugates, cell culture studies including toxicity, cell imaging and radiosensitivity with HeLa cells were performed.

#### 3.4.9.1 Cytotoxicity studies

A cell proliferation assay kit (MTT reagent) was used to determine the changes in cell viability of cells treated with samples. To perform the MTT assay, HeLa cells were seeded into 96 well plates and incubated until reaching confluence with normal morphology. The samples of AuNPs-polymer, DOX and AuNPs-poymer-Cys-DOX particles with varying concentrations were added to wells and then the cell culture plates were placed in a $CO_2$ incubator for incubation at 37 °C for 2 h. After incubation, the cells were washed to remove culture medium. MTT assay on the cell lines was carried out according to standard procedure. The dose-dependent cell viability of bioconjugates was reported as cell viabilities relative to the control (untreated) cells.

#### 3.4.9.2 Cell imaging studies

In order to observe the interactions of the constructed AuNPs-polymer-Cys-DOX bioconjugates and free DOX with HeLa cells, 100 µL of samples were introduced into the cells grown in a chamber slide for two days. The cell images were taken by a fluorescence microscope (Olympus BX53F) equipped with a CCD camera (Olympus DP72). Following the treatment for 2 h at 37 °C in $CO_2$ incubator, the cells were rinsed twice with PBS. Cell images were given by merging with phase-contrast images of cells and fluorimetric images of free DOX and bioconjugates.

#### 3.4.9.3 Radioactivity studies

In the radiotherapy study, HeLa cells were treated with commercial AuNPs (40 nm), AuNPs-polymer, free DOX and AuNPs-polymer-Cys-DOX particles for 24 h, followed by irradiation with 2.5, 5.0 and 10 Gray (Gy) using a 6 MV linear accelerator system (LINAC, Siemens Primus, Germany). 4,000 cells/well were incubated at 96-well cell culture plate for 24 h under standard culture conditions. Then, medium was removed and AuNPs, AuNP-polymer and AuNPs-polymer-Cys-DOX particles (250 µg/mL and the equivalent of 5.0 µM DOX for the final conjugate), free DOX (5.0 µM) were applied for 2 h. A control group was added with no sample treatment for the comparison. After radiation treatment, cells were incubated for 72 h and cell viability was assessed *via* the MTT method described above.

## 3.5 References

(1) Doane, T. L.; Burda, C. *Chemical Society Reviews* **2012**, *41*, 2885.
(2) Khan, I. U.; Serra, C. A.; Anton, N.; Vandamme, T. *J Control Release* **2013**, *172*, 1065.
(3) Yamashita, F.; Hashida, M. *Advanced Drug Delivery Reviews* **2013**, *65*, 139.
(4) Pissuwan, D.; Valenzuela, S. M.; Cortie, M. B. *Trends in Biotechnology*, *24*, 62.
(5) Geyik, C.; Ciftci, M.; Demir, B.; Guler, B.; Ozkaya, A. B.; Gumus, Z. P.; Barlas, F. B.; Odaci Demirkol, D.; Coskunol, H.; Timur, S.; Yagci, Y. *Polymer Chemistry* **2015**, *6*, 5470.
(6) Gullotti, E.; Yeo, Y. *Molecular pharmaceutics* **2009**, *6*, 1041.
(7) Song, W.; Tang, Z.; Li, M.; Lv, S.; Yu, H.; Ma, L.; Zhuang, X.; Huang, Y.; Chen, X. *Macromolecular Bioscience* **2012**, *12*, 1375.
(8) Zhang, Y.; Xiao, C.; Li, M.; Chen, J.; Ding, J.; He, C.; Zhuang, X.; Chen, X. *Macromolecular Bioscience* **2013**, *13*, 584.
(9) Seleci, M.; Seleci, D. A.; Ciftci, M.; Odaci Demirkol, D.; Stahl, F.; Timur, S.; Scheper, T.; Yagci, Y. *Langmuir* **2015**, *31*, 4542.
(10) Cai, S.; Zhang, Q.; Bagby, T.; Forrest, M. L. *Advanced drug delivery reviews* **2011**, *63*, 901.
(11) Her, S.; Jaffray, D. A.; Allen, C. *Advanced Drug Delivery Reviews*.
(12) Byrne, J. D.; Betancourt, T.; Brannon-Peppas, L. *Advanced Drug Delivery Reviews* **2008**, *60*, 1615.
(13) Alexis, F.; Pridgen, E.; Molnar, L. K.; Farokhzad, O. C. *Molecular Pharmaceutics* **2008**, *5*, 505.

(14) Gu, L.; Mooney, D. J. *Nat Rev Cancer* **2016**, *16*, 56.
(15) Greco, F.; Vicent, M. J. *Advanced Drug Delivery Reviews* **2009**, *61*, 1203.
(16) Simon, S.; Roy, D.; Schindler, M. *Proceedings of the National Academy of Sciences of the United States of America* **1994**, *91*, 1128.
(17) Du, J.-Z.; Mao, C.-Q.; Yuan, Y.-Y.; Yang, X.-Z.; Wang, J. *Biotechnology Advances* **2014**, *32*, 789.
(18) Shi, J.; Liu, Y.; Wang, L.; Gao, J.; Zhang, J.; Yu, X.; Ma, R.; Liu, R.; Zhang, Z. *Acta Biomaterialia* **2014**, *10*, 1280.
(19) Chen, X.; Yao, X.; Chen, L.; Chen, X. *Macromolecular Bioscience* **2015**, *15*, 1563.
(20) Li, X.; Takashima, M.; Yuba, E.; Harada, A.; Kono, K. *Biomaterials* **2014**, *35*, 6576.
(21) Pan, Y.; Neuss, S.; Leifert, A.; Fischler, M.; Wen, F.; Simon, U.; Schmid, G.; Brandau, W.; Jahnen-Dechent, W. *Small* **2007**, *3*, 1941.
(22) Niidome, T.; Yamagata, M.; Okamoto, Y.; Akiyama, Y.; Takahashi, H.; Kawano, T.; Katayama, Y.; Niidome, Y. *Journal of Controlled Release* **2006**, *114*, 343.
(23) Hauck, T. S.; Ghazani, A. A.; Chan, W. C. W. *Small* **2008**, *4*, 153.
(24) Muddineti, O. S.; Ghosh, B.; Biswas, S. *International Journal of Pharmaceutics* **2015**, *484*, 252.
(25) Jiao, P. F.; Zhou, H. Y.; Chen, L. X.; Yan, B. *Current Medicinal Chemistry* **2011**, *18*, 2086.
(26) Barrientos, Á. G.; de la Fuente, J. M.; Rojas, T. C.; Fernández, A.; Penadés, S. *Chemistry – A European Journal* **2003**, *9*, 1909.
(27) de la Fuente, J. M.; Barrientos, A. G.; Rojas, T. C.; Rojo, J.; Cañada, J.; Fernández, A.; Penadés, S. *Angewandte Chemie International Edition* **2001**, *40*, 2257.
(28) Sun, T.; Zhang, Y. S.; Pang, B.; Hyun, D. C.; Yang, M.; Xia, Y. *Angewandte Chemie International Edition* **2014**, *53*, 12320.
(29) Du, W.; Yuan, Y.; Wang, L.; Cui, Y.; Wang, H.; Xu, H.; Liang, G. *Bioconjugate Chemistry* **2015**, *26*, 2571.
(30) Shanthi, K.; Vimala, K.; Gopi, D.; Kannan, S. *RSC Advances* **2015**, *5*, 44998.
(31) He, C.; Hu, Y.; Yin, L.; Tang, C.; Yin, C. *Biomaterials* **2010**, *31*, 3657.
(32) Aggarwal, P.; Hall, J. B.; McLeland, C. B.; Dobrovolskaia, M. A.; McNeil, S. E. *Advanced Drug Delivery Reviews* **2009**, *61*, 428.
(33) Rück-Braun, K.; Petersen, M. Å.; Michalik, F.; Hebert, A.; Przyrembel, D.; Weber, C.; Ahmed, S. A.; Kowarik, S.; Weinelt, M. *Langmuir* **2013**, *29*, 11758.
(34) Ma, W.; Xu, S.; Li, J.; Guo, J.; Lin, Y.; Wang, C. *Journal of Polymer Science Part A: Polymer Chemistry* **2011**, *49*, 2725.
(35) Mattevi, C.; Hofmann, S.; Cantoro, M.; Ferrari, A. C.; Robertson, J.; Castellarin-Cudia, C.; Dolafi, S.; Goldoni, A.; Cepek, C. *Physica E: Low-dimensional Systems and Nanostructures* **2008**, *40*, 2238.

(36) Beverly, S.; Seal, S.; Hong, S. *Journal of Vacuum Science & Technology A* **2000**, *18*, 1107.
(37) Yuan-Li, H.; Avinash, B.; Hsi-Wen, T.; Ying-Kui, Y.; Shin-Yi, Y.; Chen-Chi, M. M.; Hong-Yuan, L.; Yiu-Wing, M.; Nian-Hau, W. *Nanotechnology* **2011**, *22*, 475603.
(38) Casaletto, M. P.; Kaciulis, S.; Mattogno, G.; Mezzi, A.; Ambrosio, L.; Branda, F. *Surface and Interface Analysis* **2002**, *34*, 45.
(39) Wong, L.; Kavallaris, M.; Bulmus, V. *Polymer Chemistry* **2011**, *2*, 385.
(40) Strambi, A.; De Milito, A. In *Tumor Cell Metabolism: Pathways, Regulation and Biology*; Mazurek, S., Shoshan, M., Eds.; Springer Vienna: Vienna, 2015, p 173.
(41) Unak, G.; Ozkaya, F.; Ilker Medine, E.; Kozgus, O.; Sakarya, S.; Bekis, R.; Unak, P.; Timur, S. *Colloids and Surfaces B: Biointerfaces* **2012**, *90*, 217.
(42) Demir, B.; Barlas, F. B.; Guler, E.; Gumus, P. Z.; Can, M.; Yavuz, M.; Coskunol, H.; Timur, S. *RSC Advances* **2014**, *4*, 34687.
(43) Shuai, X.; Ai, H.; Nasongkla, N.; Kim, S.; Gao, J. *Journal of Controlled Release* **2004**, *98*, 415.
(44) Cooper, D. R.; Bekah, D.; Nadeau, J. L. *Frontiers in Chemistry* **2014**, *2*.
(45) Barlas, F. B.; Demir, B.; Guler, E.; Senisik, A. M.; Arican, H. A.; Unak, P.; Timur, S. *RSC Advances* **2016**, *6*, 30217.
(46) Xu, W.-H.; Han, M.; Dong, Q.; Fu, Z.-X.; Diao, Y.-Y.; Liu, H.; Xu, J.; Jiang, H.-L.; Zhang, S.-Z.; Zheng, S.; Gao, J.-Q.; Wei, Q.-C. *International Journal of Nanomedicine* **2012**, *7*, 2661.
(47) Jagetia, C. G.; Nayak, V. *Strahlentherapie und Onkologie* **2000**, *176*, 422.
(48) Bonner, J. A.; Lawrence, T. S. *International Journal of Radiation Biology* **1990**, *57*, 55.

# Chapter 4 Reversible single-chain glycopolymer folding *via* host-quest interaction and its effect on lectin binding

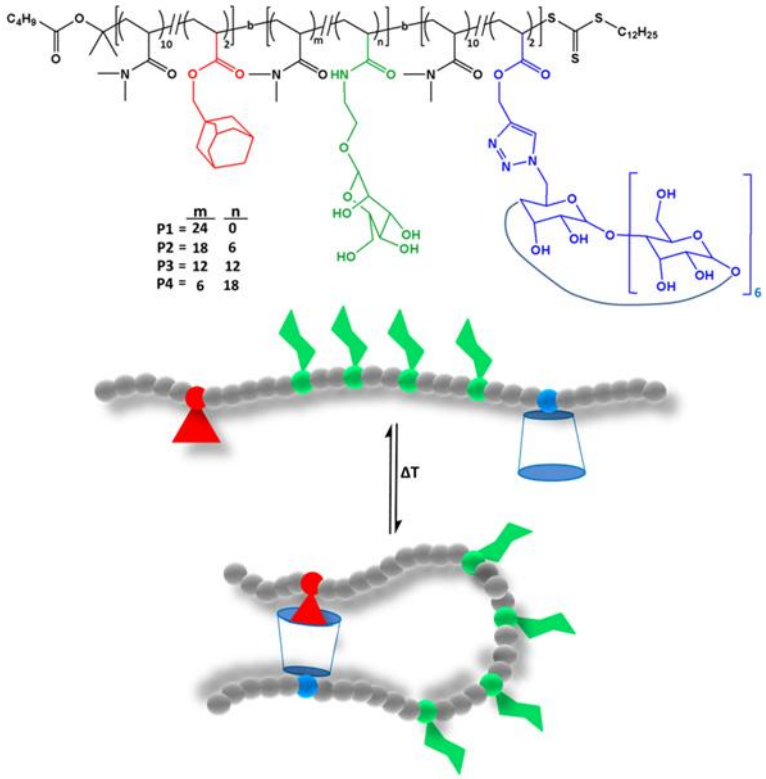


*The reversible self-folding actions of natural biomacromolecules play very important roles for their specific and unique biological functions in nature. Hence, the single-chain folding inspired by nature has attracted significant attention in recent years. Herein, the reversible single-chain glycopolymer folding structures in α-shape with different sugar moieties were created to investigate the influence of this folded collapse on the binding capability with different lectins. The synthesis of triblock co-glycopolymers bearing β-CD and adamantane for the host-quest interaction and also mannose residues for the lectin interaction was achieved via reversible addition-fragmentation chain transfer (RAFT) polymerization. The reversible single-chain folding of glycopolymers was created in a highly diluted aqueous solution and monitored by 2D nuclear overhauser enhancement spectroscopy (NOESY) NMR and dynamic light scattering (DLS). The binding results showed that the single-chain folded structures enhanced greatly the binding ability, in comparison to the unfolded structures.*

## 4.1 Introduction

Nowadays, “single chain technology” has been elucidated for a deep understanding of the multivalent functions and the precise mechanism of naturally occurring single-chain architectures of macromolecules in biological systems (such as tertiary structure of proteins or enzymes).[1-3] In nature, many biomolecules exhibit reversible self-folding processes that are necessary for interfacial molecular recognition. Therefore, the introduction of precision synthetic single polymer chain folding into supramolecular chemistry is an important step forward in order to create more complex macromolecules with good functionality and properties to imitate the complicated biological systems. Recent advances in the control polymerization techniques have allowed polymer chemists to produce precision polymers with a sufficient control in chain length, architecture, monomer sequence, chain folding, and tertiary structures.[4-7] It is not only polymer chemists that are interested in single-chain collapse, but also researchers from other areas, especially in the biological area, that are drawn into this field by the opportunities to create the controlled folding single-chain polymers with specific biological functions. However, it has still some setbacks to synthesize well-defined macromolecules that can fold into structures with the precision of naturally occurring polymers. Single-chain folded polymer structures can be generated *via* selective point folding or repeat unit folding routes.[8-14] The selective point folding approach can be achieved by metal-ligand complexation, host-guest chemistry, hydrogen bonding, and covalent bonding that enable polymer chains to be folded into relatively controlled architectures with a good accuracy.[15-17] In contrast, even though the repeat unit folding approach provides less-defined folding structures due to random distribution of functional groups along the polymer chains it provides a much easier synthesis route to obtain foldable polymer chains.[18-21] A few elegant reports were published on these methodologies in the last five years. For example, Lutz and collaborators have developed a very efficient strategy for fabricating different polymer chain folding architectures (such as P, Q, 8 and α shaped folding origamis).[13] *N*-substituted maleimides were polymerized with styrene using atom transfer radical polymerization (ATRP) to achieve a controlled primary polymer

structures. Intramolecular covalent bridges *via* functional groups positioned on the polymer chain provided a controlled single-chain folding.

Host-quest interaction is another versatile useful approach for constructing selective single-chain folding structures.[22-25] In general, host molecules contain a large cavity volume such as cyclodextrins (CD), cucurbiturils (CB) and calixarenes. Guest molecules typically have both a complementary shape and interaction with the host molecules. Hence, the selective noncovalent interaction between the host and the guest molecules can be created in terms of molecular recognition. The cyclodextrins are cyclic oligosaccharides consisting of 6-8 glucopyranose units. Adamantane is one of the most important guest molecules for CD due to its effective inclusion entrapment and high binding affinity. Recently, Barner-Kowollik and coworkers succeeded to create reversible single-chain selective point polymer folding using β-cyclodextrin driven host-quest interaction with adamantane in water.[11] Water soluble poly(*N,N*-dimethylacrylamide) carrying β-CD) and adamantyl moiety at the chain ends was synthesized *via* reversible addition-fragmentation chain transfer (RAFT) polymerization. The reversible single-chain folding was followed by dynamic light scattering (DLS) and nuclear overhauser enhancement spectroscopy (NOESY) spectroscopy in diluted aqueous solution at elevated temperatures.

Inspired by these studies, we herein developed the reversible single-chain glycopolymer folding structures in α-shape with different sugar moieties. The obtained glycopolymers synthesized by RAFT have the same chain length carrying β-CD and adamantane for the host-quest interactions. Well-defined triblock glycocopolymers carrying different mannose moieties were synthesized with the desired molar masses and low distributions. Single-chain folding structures were obtained in a highly diluted aqueous solution and were monitored by using 2D NOESY NMR and DLS techniques. It is commonly known that glycopolymer architecture, valency, size and density of binding elements can affect their binding activities significantly. Therefore, the investigation of the binding ability of the fabricated single-chain glycopolymer folding structures was carried out in the presence of different types of lectins, namely, dendritic cell-specific intercellular

adhesion molecule-3-grabbing non-integrin (DC-SIGN), concanavalin A (ConA), wheat germ agglutinin (WGA), ricinus communis agglutinin ($RCA_{120}$) and peanut agglutinin (PNA) *via* the turbidity assay, quantitative precipitation and also SPR method. The results showed that these folded glycomaterials can mimic biological functions in Nature according to their multivalent interaction with different lectins.

## 4.2 Results and Discussion

### 4.2.1 Synthesis of D-mannose acrylamide glycomonomer (ManAcm)

Acrylamide derivatives can be polymerized *via* RAFT process to create complex high-order multiblock copolymers in a short polymerization time in one-pot reaction. Perrier and collaborators have recently reported the preparation of a large number of multiblock copolymers *via* RAFT polymerization of various acrylamide monomers. Acrylamide monomers have a high propagation rate coefficient in aqueous solutions. In this thesis, *N,N*-dimethylacrylamide (DMA) was chosen to design triblock copolymers where each block bearing different functional moieties. Therefore, D-mannose acrylamide glycomonomer was synthesized according to previously published reports and used further for the copolymerization with DMA. Mannosylated monomer tetra-O-acetyl-D-1-mannopyranosyl hydroxylethyl acrylamide was prepared by the reaction of *N*-hydroxyethyl acrylamide with D-mannose pentaacetate using boron trifluoride diethyl etherate ($BF_3$-$OEt_2$) as the activating agent.

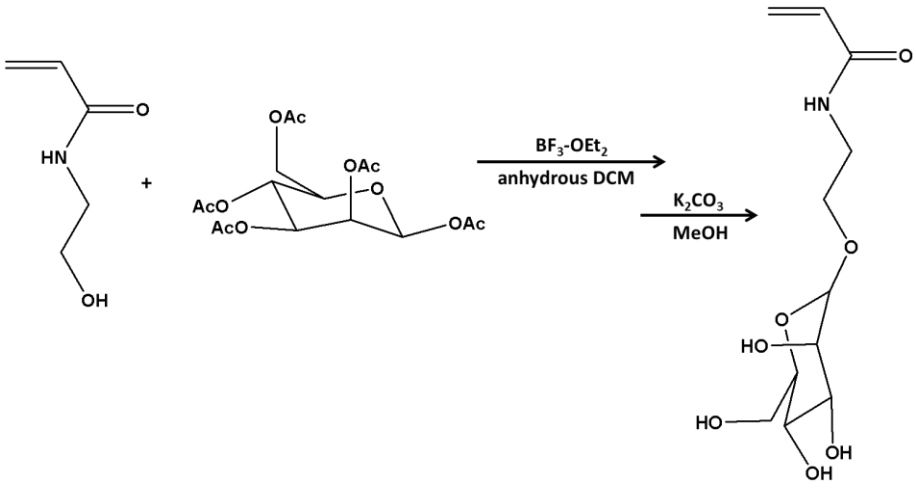


**Scheme 4.1.** Schematic representation of the synthesis of D-mannose acrylamide.

Firstly, D-mannose pentaacetate was synthesized successfully and then used for the reaction with *N*-hydroxyethyl acrylamide. The reaction solution was sonicated for 90 min. After washing with brine, the solvent was removed under reduced pressure to obtain a yellowish gummy crude product, which was used directly without any further purification to synthesize 2-(D-manosyloxy) hydroxylethyl acrylamide. The protection of acetyl groups was carried out in the presence potassium carbonate ($K_2CO_3$) in methanol (MeOH). The reaction was followed by thin-layer chromatography (TLC). After the neutralization of the reaction solution using Amberjet 1200H ($H^+$) cation exchange resin, the crude product was purified by column chromatography with 32% yield.

As seen in Figure 4.1, the synthesized D-mannose acrylamide glycomonomer (ManAcm) structure was confirmed by $^1$H-NMR and $^{13}$C-NMR. Moreover, ESI-MS spectra showed a clear peak at 277.15 m/z that corresponds to the molecular weight of the ManAcm glycomonomer with 277.12 m/z.

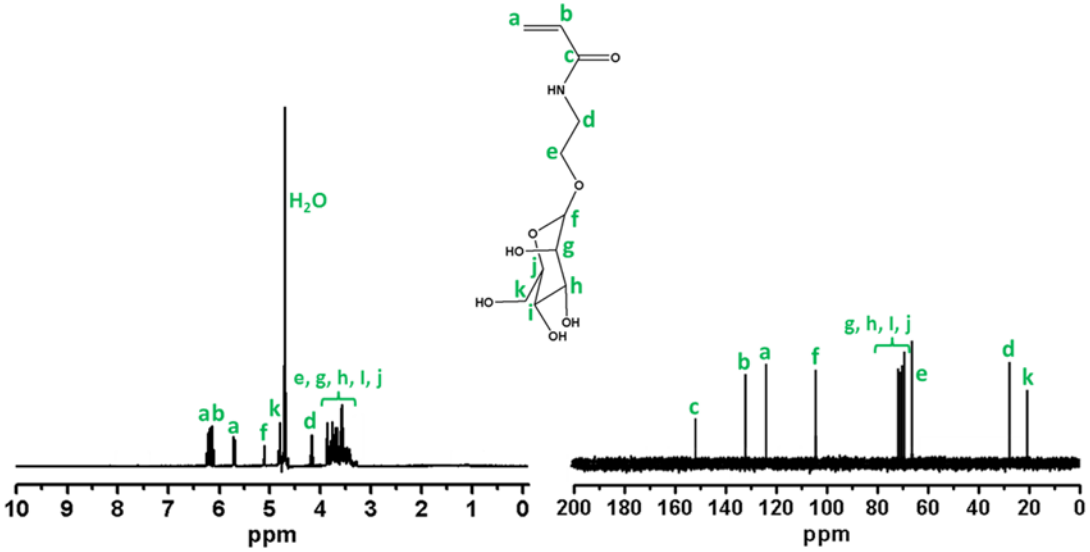


**Figure 4.1.** Details of $^1$H-NMR and $^{13}$C-NMR spectrum of the synthesized D-mannose acrylamide.

### 4.2.2 Synthesis of adamantane acrylate monomer (AdAc)

As mentioned before, adamantane is one of the guest molecules due to its effective inclusion entrapment and high binding affinity. Therefore, adamantyl groups can

form strong inclusion stable complexes not only with CD but also with cyclodextrin-containing polymers. In order to incorporate adamantly functional groups into the polymers, adamantane acrylate was synthesized *via* esterification of 1-adamantane methanol with acryloyl chloride. As shown in scheme 4.2, the reaction was performed in THF for overnight in the presence of triethlyamine ($Et_3N$).

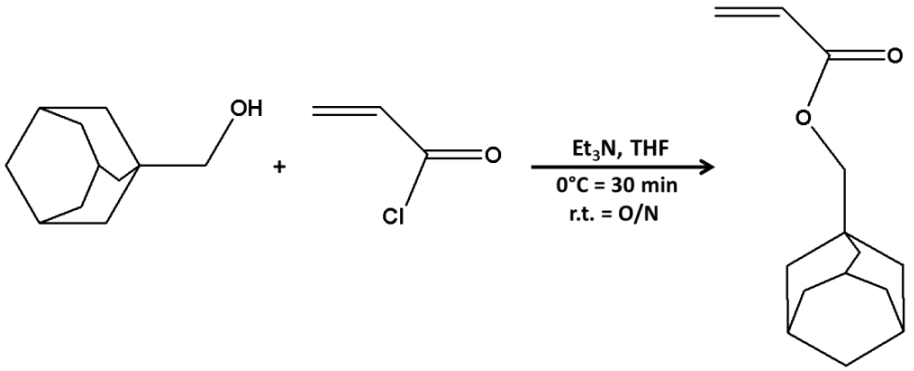


**Scheme 4.2.** Schematic representation of the synthesis of adamantane acrylate.

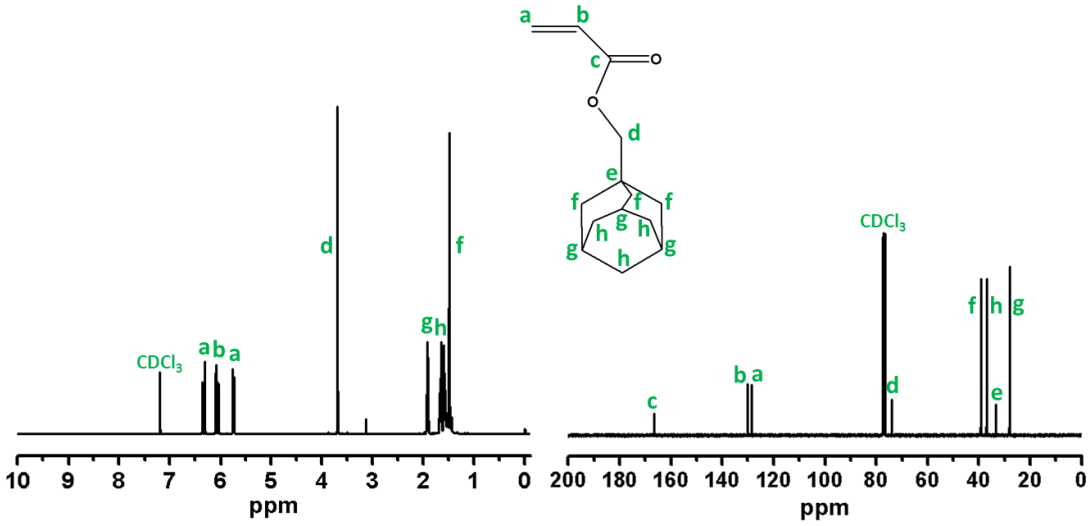


**Figure 4.2.** Details of $^{1}$H-NMR and $^{13}$C-NMR spectrum of the synthesized adamantane acrylate.

The reaction was monitored by $^{1}$H-NMR and the esterification was confirmed by the appearance of the vinyl groups at 5.8-6.4 ppm and also formation of ester protons were observed at 3.8 ppm.

### 4.2.3 Synthesis of β-cyclodextrin azide (β-CD-$N_3$)

In order to synthesize β-cyclodextrin acrylate *via* Cu-catalyzed azide-alkyne click (CuAAC) reaction of propargyl acrylate, mono azide functional cyclodextrin was prepared according to previously developed method.

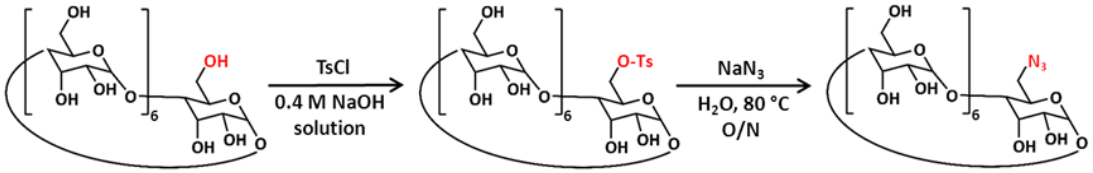


**Scheme 4.3.** Schematic representation of the synthesis of β-CD-$N_3$.

As illustrated in scheme 4.3, mono-6-deoxy-6-(p-tolylsulfonyl)-β-cyclodextrin (β-CD-OTs) was firstly synthesized successfully and then this only one TsCl functionalized hydroxyl group of the β-CD ring was converted to azide group. The $^1$H NMR spectrum of β-CD-OTs confirmed that only one TsCl is reacted with the 6-positioned hydroxyl group of the β-CD ring according to integration ratio of the phenyl protons at 7.42 and 7.75 ppm with 2,3-positioned hydroxyl groups of the β-CD ring. Furthermore, azide functionalization reaction was carried out in water at 80°C for overnight. The reaction was monitored by $^1$H NMR and FT-IR. The characteristic phenyl protons in β-CD-OTs disappeared completely according to $^1$H NMR spectrum and also FITR showed the peak of azide appeared at 2095 $cm^{-1}$ after reaction.

### 4.2.4 Synthesis of β-cyclodextrin acrylate monomer (CDAc)

Ritter and coworkers achieved to synthesize β-cyclodextrin methacrylate using CuAAC "*click*" chemistry before and also they polymerized it *via* free-radical polymerization technique successfully. As illustrated Scheme 4.4, the CuAAC "*click*" reaction between β-CD-$N_3$ and propargyl acrylate was carried out in the presence of $CuSO_4 \cdot 5H_2O$ and (+)-sodium L-ascorbate as a catalyst system in DMF mixture. The reaction solution was irradiated in the microwave at 120 °C for an hour and it was monitored and confirmed by $^1$H NMR, FT-IR and MALDI-TOF.

As shown in Figure 4.3, the appearance of the new peak at 7.9 ppm according to formation of triazole ring confirmed the new structure in $^1$H NMR spectrum.

According to FT-IR, azide stretch at 2095 $cm^{-1}$ disappeared following the click reaction. Moreover, the MALDI-ToF MS spectrum showed peaks corresponding to the fully substituted product at ≈ 1309 (m/z). All these data support the synthesis of pure β-cyclodextrin acrylate successfully.

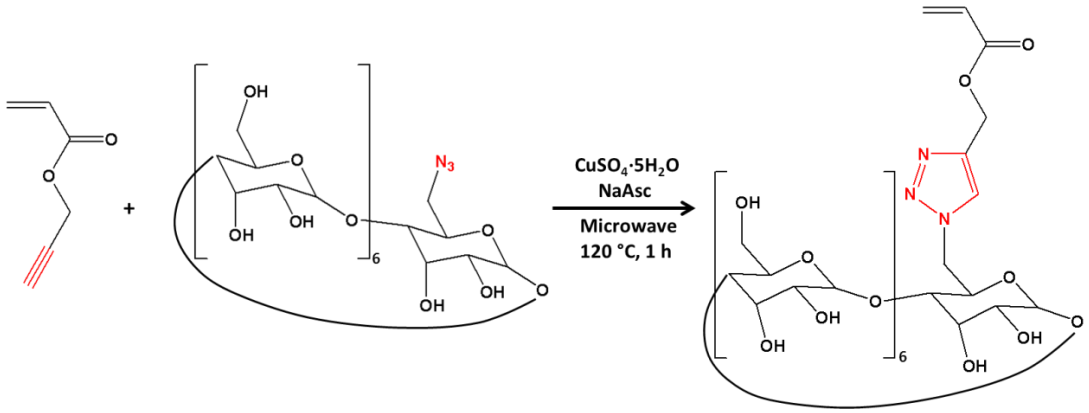


**Scheme 4.4.** Schematic representation of the synthesis of β-cyclodextrin acrylate.

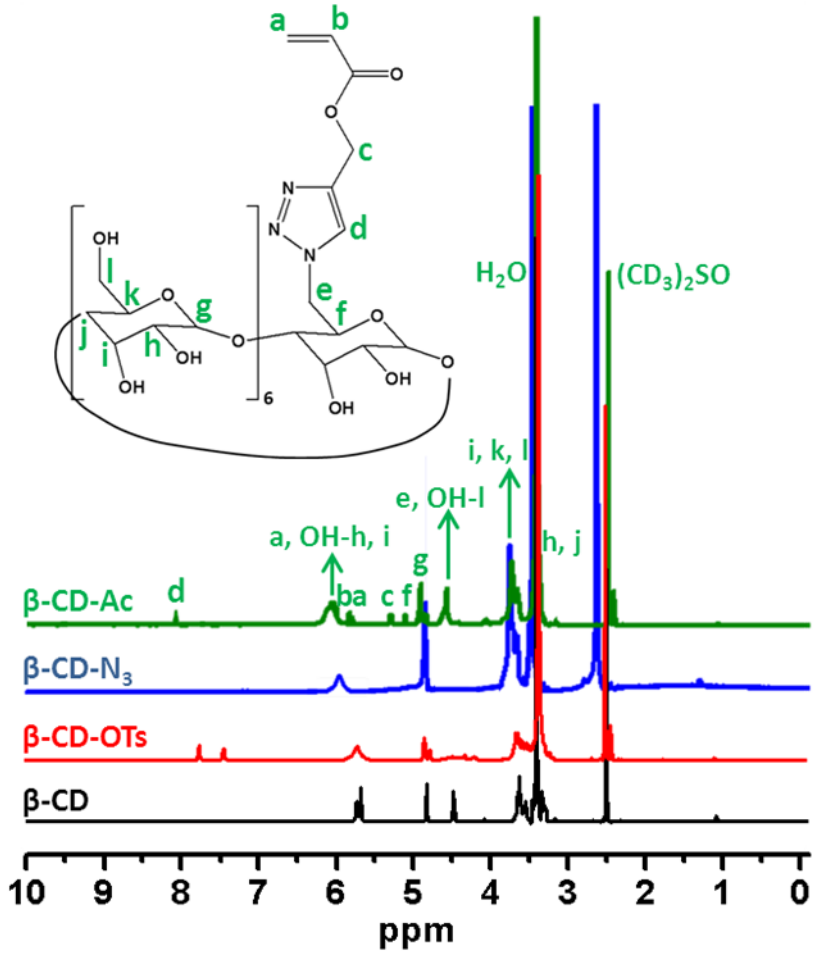


**Figure 4.3.** $^{1}$H NMR spectrum for step-by-step synthesis of β-cyclodextrin acrylate.

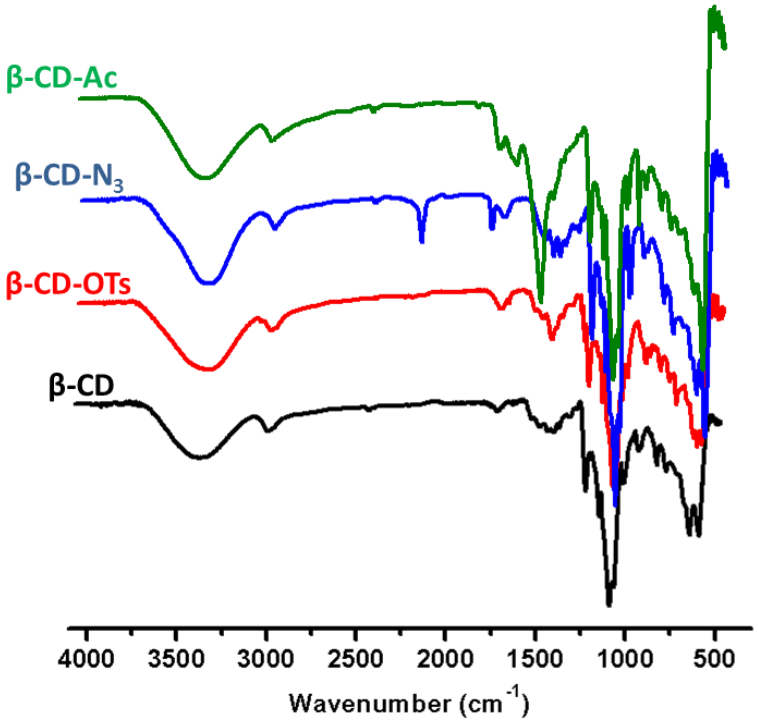


**Figure 4.4.** FT-IR spectrum of each step of the synthesis of β-cyclodextrin acrylate.

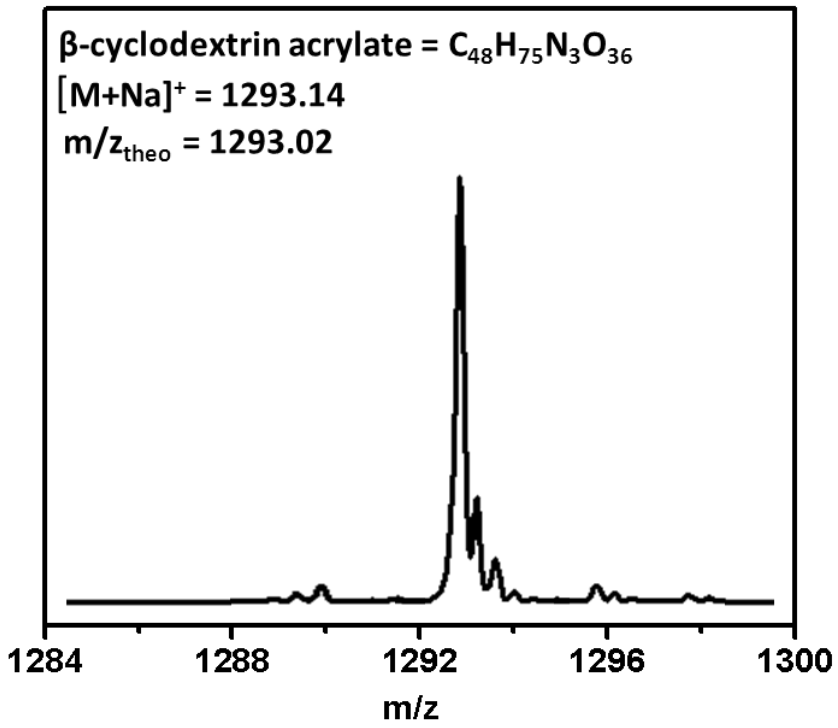


**Figure 4.5.** MALDI-ToF MS spectrum of the obtained β-cyclodextrin acrylate.

### 4.2.5 Synthesis of p((DMA)$_{10}$-r-(AdAc)$_2$) macro-RAFT agent

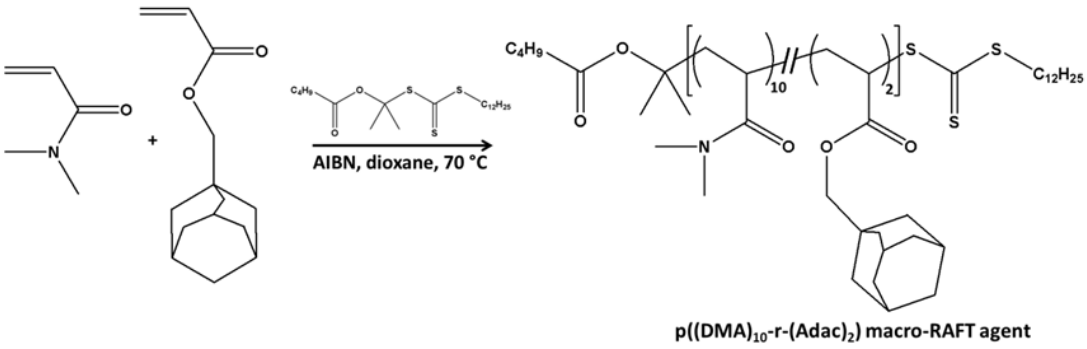


**Scheme 4.5.** The synthesis of p((DMA)$_{10}$-r-(AdAc)$_2$) macro-RAFT agent *via* RAFT polymerization.

Random copolymerization of DMA and AdAc was performed to prepare water-soluble macro-RAFT agent for the further polymerization reactions. As seen scheme 4.4,2-(((dodecylthio)carbonothioyl)thio)propan-2-yl pentanoate and 2,2'-azobis(2-methyl-propionitrile) (AIBN) were used as chain transfer agent (CTA) and radical initiator, respectively. The polymerization was carried out in 1,4-dioxane at 70 °C. Briefly, a Schlenk tube was charged with targeted monomers (DMA:AdAc = 10:2), CTA (1 eq), AIBN (0.01 eq) and the solvent was degassed by gentle bubbling of argon gas for 30 min. Schlenk tube was sealed properly and the mixed solution was allowed to polymerize. After the monomers reached full conversion in 2 h according to GC, the tube was subsequently cooled with liquid nitrogen to stop the reaction. The polymer was precipitated in cold hexane for two times before the DMF SEC and $^1$H NMR characterization. The SEC trace of the obtained polymer did not show any shoulder or tailing with an apparent $M_n$ = 1500 g.mol$^{-1}$ and $Đ$ = 1.14 according to PMMA calibration. Moreover, $^1$H NMR spectrum revealed the identification of the synthesized copolymer qualitatively after purification.

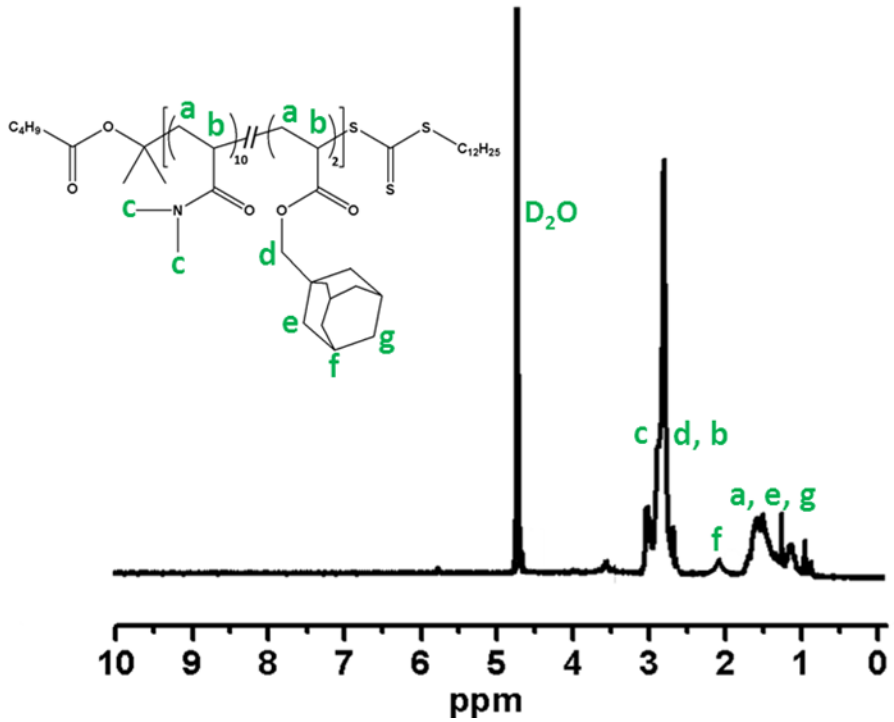


**Figure 4.6.** $^{1}$H NMR spectrum of the obtained p((DMA)$_{10}$-r-(Adac)$_2$) macro-RAFT agent.

### 4.2.6 Synthesis of well-defined tri-block copolymers

The obtained p((DMA)$_{10}$-r-(AdAc)$_2$) was employed as macro-RAFT agent to synthesize tri-block co-glycopolymers. The RAFT polymerization of second and third blocks was performed in one-pot reaction *via* chain extension. While the second block of the synthesized polymers consisted of DMA and ManAcm monomers with different ratios, the third blocks contained the same ratio of DMA and CDAc monomers (DMA:CDAc = 10:2) for each triblock copolymers. The RAFT polymerization of second block was carried out in the presence of water-soluble 4,4'-Azobis(4-cyanopentanoic acid) (V-501) radical initiator in water at 70 °C. The necessary time to achieve nearly full monomer conversion, especially for glycomonomer, increased with increase of molar ratio of ManAcm. After nearly full conversion of both monomers, the chain extension of the third block was carried out in DMF:$H_2O$ mixture. The mixture of degassed DMA and CDAc monomers, initiator and solvent was added *via* gastight syringe to the polymerization medium. Long reaction times were employed to ensure that conversion of each monomer

was close to full conversion. The necessary amount of initiator added for the third block polymerization was calculated according to the following formula;

$$m_{V\text{-}501\ remaining} = m_{V\text{-}501\ total} \times 2fe^{-kdt} \times (1\text{-}f_c/2) \text{ with}$$

where $f = 0.5$, $f_c = 0$, $k_d = 1.9\ 10^{-5} s^{-1}$ and t = polymerization time.

$[\text{Macro-RAFT agent}]_0/[\text{V-501}]_0$ ratio was kept the same as 100:1 to avoid dead-end polymerization. If the V-501 concentration is lowered, the polymerization reaction requires a longer reaction time to reach full conversion.

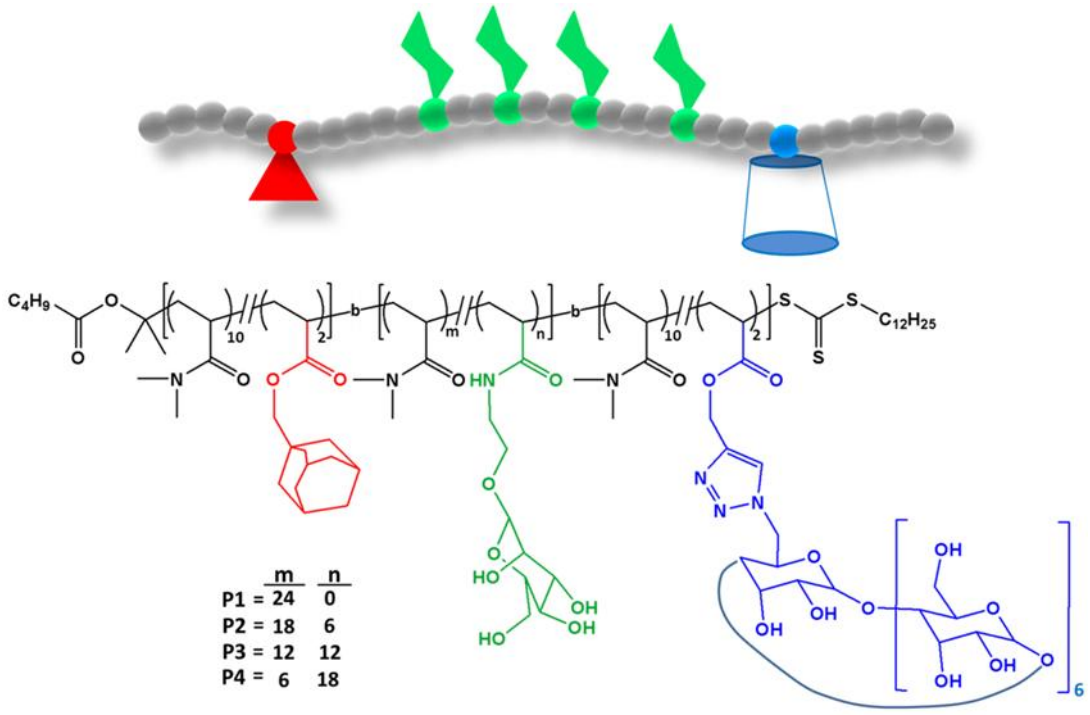


**Scheme 4.6.** Illustration of the formation of the reversible single-chain folding in highly diluted aqueous solution.

Even though full consumption of monomers for each block was achieved, the conversion CDAc remained lower than 76%. The possible reason behind of it could be the bulky cyclodextrin ring. However, DMF SEC traces showed the successful chain growing as revealed clear shifts to higher molar masses with each block addition. (Figure 4.7) Despite of the fact that small amount tailing in low molar mass range was obtained after the third block polymerization due to some dead polymer chains, the final dispersity of the obtained tri-block copolymers was still relatively narrow ($Đ$ = 1.18-1.24). Expectedly, the measured molar masses by SEC

were higher than theoretical molar mass mainly due to the different structure of copolymer with PMMA calibration standard, which would cause a significant difference of hydrodynamic volume of polymer in DMF.

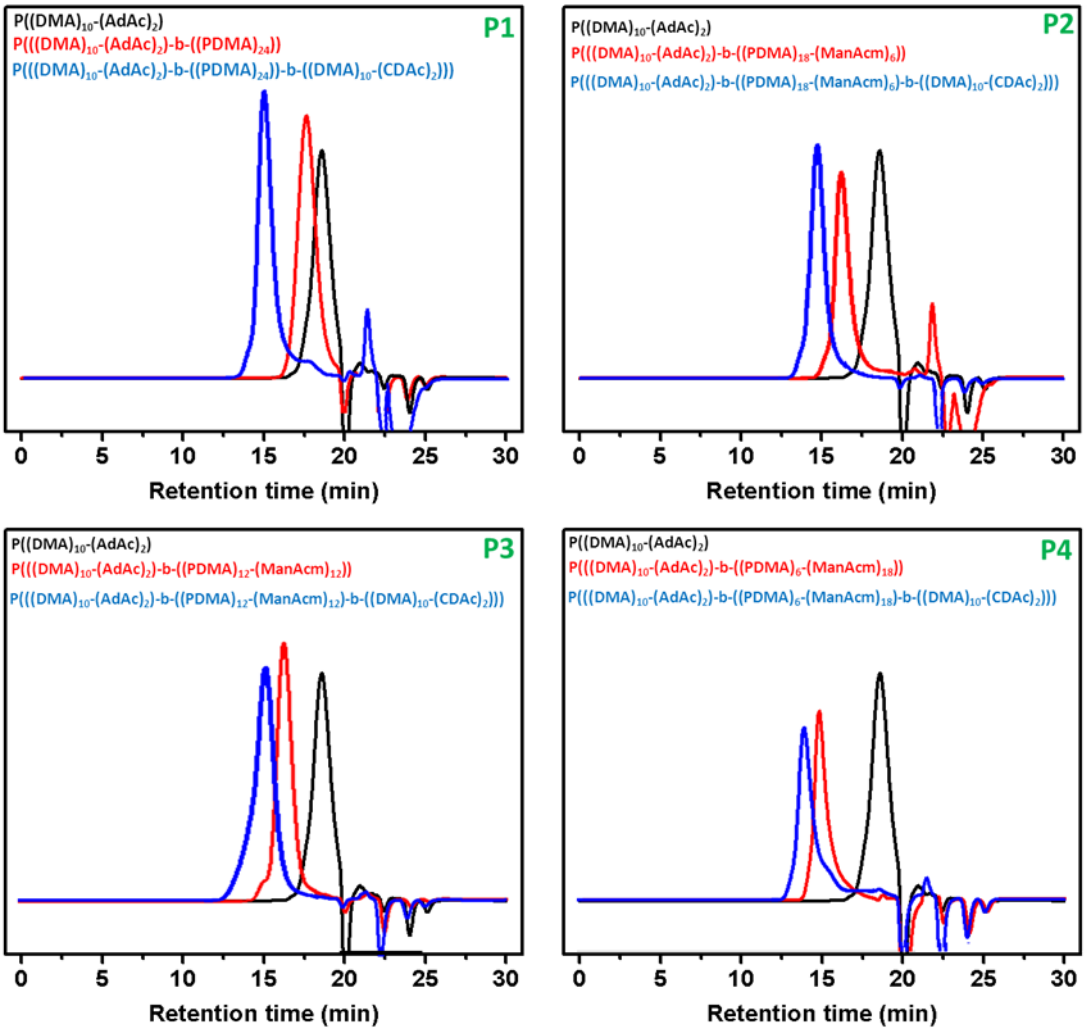


**Figure 4.7.** SEC traces of the synthesized triblock copolymer using RI detector.

**Table 4.1.** Summary of monomer conversions, number average molar masses ($M_n$) and molar mass distributions ($Đ$) of tri-block co-glycopolymers.

| Code | Polymer | $\rho^a$ (%) | | | | $M_{n,Theo}{}^b$ | $M_{n,SEC}{}^c$ | $Đ$ |
|---|---|---|---|---|---|---|---|---|
| | | DMA | AdAc | ManAcm | CDAc | (g.mol$^{-1}$) | (g.mol$^{-1}$) | |
| **P1** | P(((DMA)$_{10}$-(AdAc)$_2$)-*b*- | 99 | 96 | - | - | 1850 | 1500 | 1.14 |
| | ((PDMA)$_{24}$)-*b*- | 98 | - | - | - | 4200 | 4500 | 1.16 |
| | ((DMA)$_{10}$-(CDAc)$_2$)) | 97 | - | - | 76 | 7750 | 9600 | 1.18 |
| **P2** | P(((DMA)$_{10}$-(AdAc)$_2$)-*b*- | 98 | 96 | - | - | 1850 | 1500 | 1.14 |
| | ((PDMA)$_{18}$-(ManAcm)$_6$)-*b*- | 98 | - | 97 | - | 5300 | 6400 | 1.17 |
| | ((DMA)$_{10}$-(CDAc)$_2$)) | 96 | - | - | 73 | 8800 | 11200 | 1.21 |
| **P3** | P(((DMA)$_{10}$-(AdAc)$_2$)-*b*- | 99 | 96 | - | - | 1850 | 1500 | 1.14 |
| | ((PDMA)$_{12}$-(ManAcm)$_{12}$)-*b*- | 98 | - | 94 | - | 6300 | 8100 | 1.17 |
| | ((DMA)$_{10}$-(CDAc)$_2$)) | 96 | | | 72 | 9800 | 12500 | 1.21 |
| **P4** | P(((DMA)$_{10}$-(AdAc)$_2$)-*b*- | 99 | 96 | - | - | 1850 | 1500 | 1.14 |
| | ((PDMA)$_6$-(ManAcm)$_{18}$)-*b*- | 97 | - | 92 | - | 7350 | 8900 | 1.18 |
| | ((DMA)$_{10}$-(CDAc)$_2$)) | 95 | - | - | 71 | 10900 | 12800 | 1.24 |

**[a] Conversion ($\rho$) obtained from $^1$H NMR and GC analysis; [b] $M_{n(Theo)}$ = ([M]$_o$/[RAFT]$_o$ x conversion x M$_{mon}$) + M$_{RAFT}$; [c] Determined by DMF GPC (relative to PMMA stn.).**

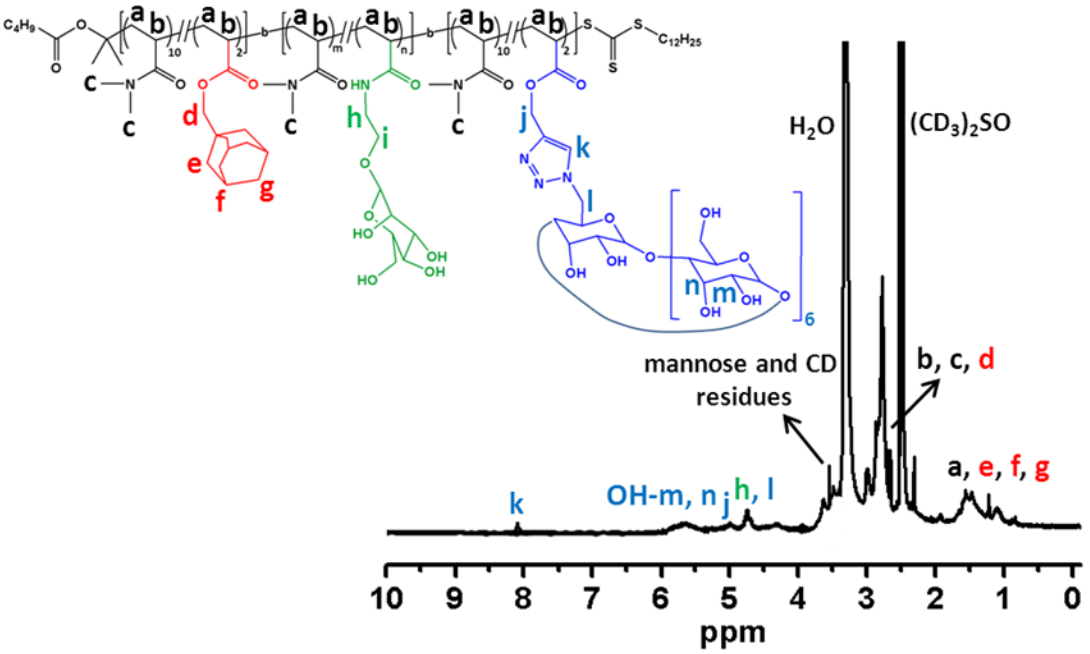


**Figure 4.8.** $^1$H NMR spectrum of the synthesized tribock copolymers.

### 4.2.7 Reversible single-chain folding studies of the obtained glycopolymers

As mentioned in the introduction part, single-chain folded architectures can be created using selective point folding or repeat unit folding approach. The selective point folding approach that can be achieved by metal-ligand complexation, host-guest chemistry and hydrogen bonds as well as covalent bonds enables polymer chains to be folded into relatively controlled shapes with good accuracy. In contrast, the repeat unit folding approach provides less-defined folding structures than selective point folding due to random distributed in the polymer chains. However, it is much easier to achieve repeat unit folding collapses than selective point folding collapses.

Herein, reversible selective point single-chain glycopolymer folding driven by host-quest interaction between cyclodextrin and adamantane was achieved in water. It is known that CD and Ad can form strong inclusion stable complexes in different solvents. However, only few studies of single-chain folded structures in aqueous solution have been reported so far. To the best of our knowledge, this is the first study on single-chain folding of glycopolymer to investigate the influence of folded architecture on the recognition with different lectins.

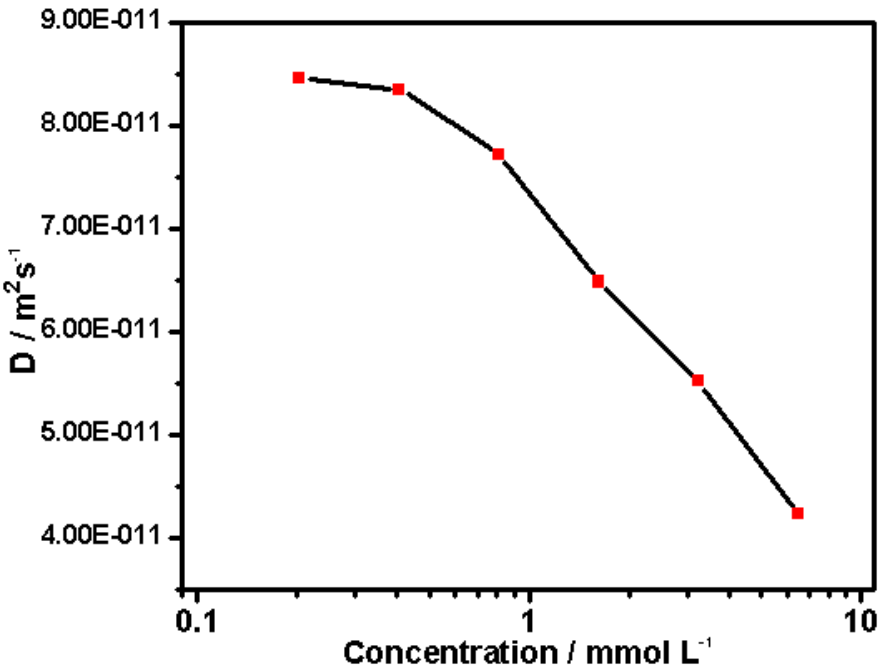


**Figure 4.9.** Averaged diffusion coefficient *D* plotted against the concentration of **P1** in $D_2O$.

Firstly, the diffusion coefficient of the obtained glycopolymers was measured using diffusion ordered spectroscopy (DOSY) NMR at different concentrations in order to determine the necessary concentration for the single-chain regime. As depicted in Figure 4.9, the diffusion coefficient decreases with increasing concentration, which can be interpreted to the open chain or the formation intermolecular inclusion complexes. Theoretically, diffusion coefficient depends on size and shape of molecule, interaction with solvent and viscosity of solvent. In particular, molecular shape is an important property in determining the value of diffusion coefficient for large molecules. According to DOSY NMR results, the single-chain folding of the obtained copolymers was achieved in a highly diluted aqueous solution. The single-chain conformation was reached below a concentration of 0.45 mM approximately. Moreover, the diffusion coefficient showed an increase with increase of sugar moieties on the polymer. It may be due to better solubility of sugar moieties than DMA moieties in the water.

After the determination of the necessary concentration for single-chain folding, the NMR samples were prepared in $D_2O$ at the same concentration. The conformation architecture of the glycopolymers was monitored *via* 2D nuclear overhauser enhancement spectroscopy (NOESY) NMR and dynamic light scattering (DLS). As depicted in Figure 4.10, the 2D NOESY NMR spectrums confirmed the cross-correlation signals between the protons of the CD cavity and the adamantane protons. The Ad protons between 1.62-2.02 ppm and the inner CD protons between 3.65-3.82 ppm represented clearly the cross-correlation signals. However, 2D NOESY NMR spectroscopy is not enough to confirm single-chain folding structure unambiguously due to intra- or intermolecular nature of the complexes. Therefore, DLS measurements were performed to ensure the formation of intra-chain folded structure. DLS is a powerful tool for the measurement of the size distribution profile of small particles in suspension or polymers in solution from a few nanometres to several micrometres. In particular, the mean hydrodynamic diameter ($D_{h,}$ the volume weight diameter of the distribution) measurements can provide an accurate evidence for the single-chain folded polymers.

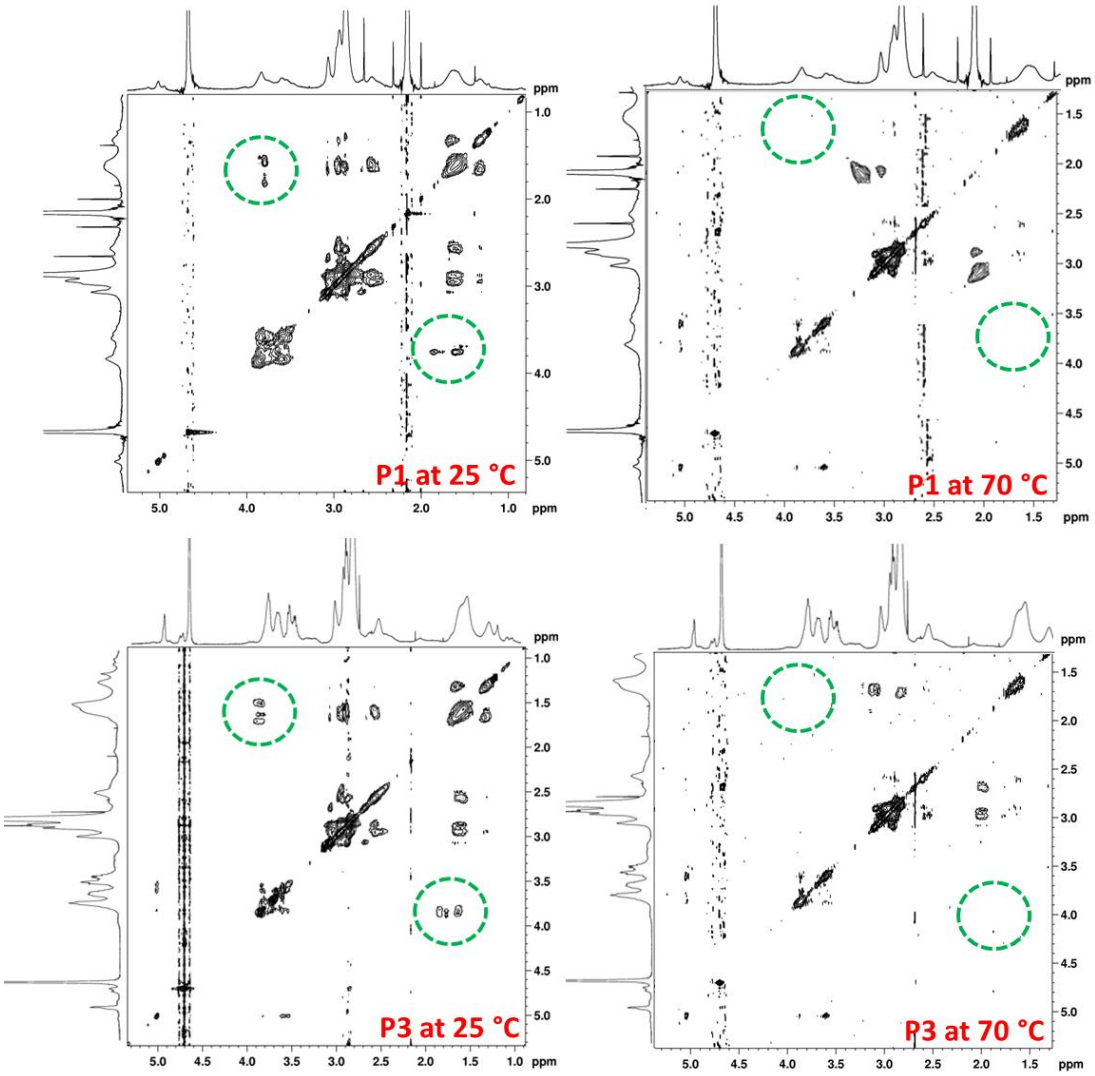


**Figure 4.10.** 2D NOESY NMR spectrums of P1 and P3 at 25 and 70 °C.

The $D_h$ values of the single-chain folded glycopolymers were measured to be 5.4-6.2 nm at same low concentration at 25 °C. As seen in Table 4.2, while **P1** illustrated the biggest size (6.2 nm), **P4** was obtained as smallest size (5.4 nm). Additionally, DLS experiments were carried out at different concentrations for each copolymer, as well. The results showed that the $D_h$ increased dramatically with increasing concentrations, which revealed the formation of inter-chain assemblies of polymers or aggregations. According to previous studies, the host-guest interaction between CD and Ad can reversibly be opened at high temperatures of 70 °C. Therefore, the reversible self-folding process of the obtained copolymers was analyzed at 70 °C. As shown in Figure 4.11, the $D_h$ values increased to approximately 11.3-12.2 nm after the temperature increase. These unfolded

structures of the copolymers were also followed *via* 2D NOESY NMR due to the absence of cross-correlation signals between the protons of the CD cavity and the adamantane protons. (Figure 4.10) Furthermore, the inter-chain assemblies of polymers and also aggregations at high concentrations were shifted to unfolded polymer chains at 70 °C according to the DLS observations. When the solution was cooled it down to ambient temperature again in 24 h, the $D_h$ of the triblock copolymers decreased to between 5.2-6.6 nm, which is in good agreement with the initial single-chain folded structure values. This is important, because it suggests that we can control this reversible single-chain folding behavior of glycopolymers efficiently. (Figure 4.11)

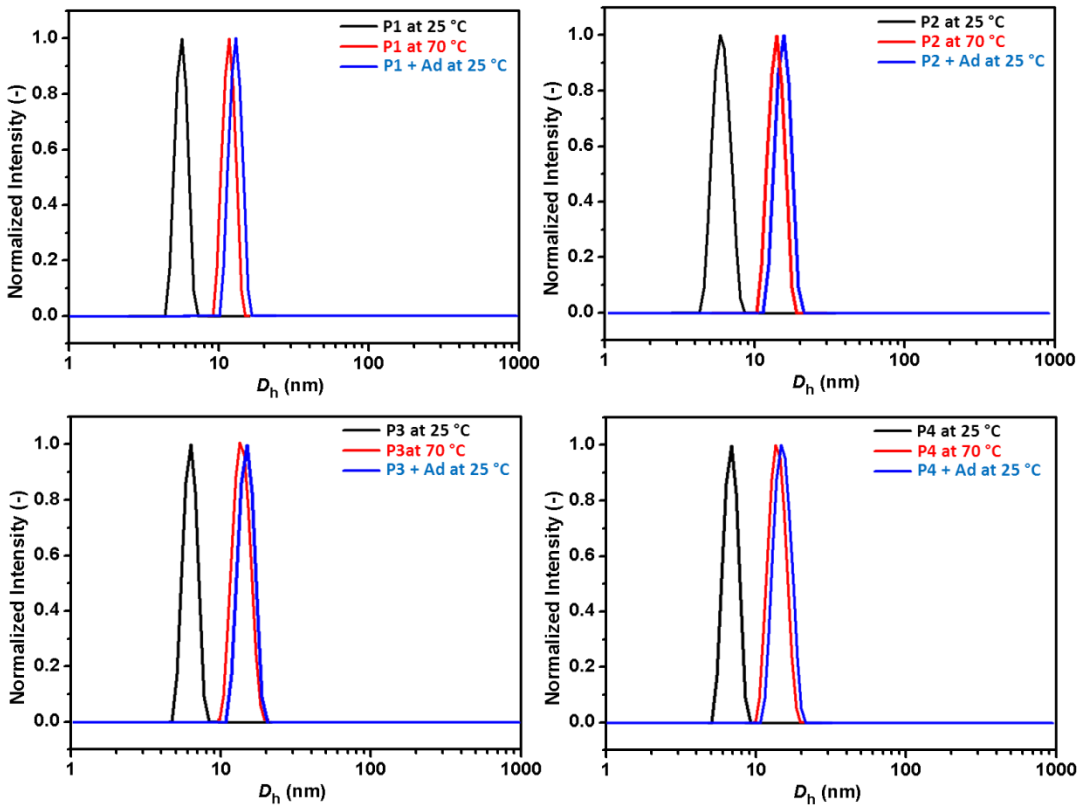


**Figure 4.11.** Number-weighted size distributions of the obtained copolymers in aqueous solution (0.45 mM) at 25 and 70 °C.

Barner-Kowollik and coworkers have also demonstrated to displace adamantane molecules by providing competitive guest molecules in the environment and heating up to 70 °C.[11] It was also utilized for our systems and the DLS results

confirmed that the mean hydrodynamic diameter of the single-chain folding glycopolymers increased to 12.5-14.1 nm. It was noted that the copolymer chains were opened successfully.

Consequently, the reversible single-chain glycopolymer folding structures were achieved in diluted aqueous solution at low temperatures. The results evidenced that this reversible behaviour can be controlled by changing temperature and concentration.

**Table 4.2** DLS characterization of the folded and unfolded structures.

| Code | $D_h$ (nm) @ 25 °C | $D_h$ (nm) @ 70 °C | $D_h$[a] (nm) @ 25 °C | $D_h$[b] (nm) @ 25 °C |
|---|---|---|---|---|
| **P1** | 6.2 | 12.2 | 6.1 | 13.6 |
| **P2** | 5.9 | 12.1 | 6.6 | 12.5 |
| **P3** | 5.8 | 11.3 | 5.2 | 12.9 |
| **P4** | 5.4 | 11.7 | 5.7 | 14.1 |

**[a] The mean hydrodynamic diameter was measured after cooling to room temperature; [b] after the addition of 1-Adamantane methanol.**

### 4.2.8 Lectin binding studies

Carbohydrate-binding proteins (lectins) that are complicated and important molecules for many biological process and living organisms open the doors of biological entities to glycans. Although there are a wide variety of lectins in terms of their structure and size, all these different lectins are highly specific for sugar moieties. In here, the investigation of the binding ability of the fabricated single-chain glycopolymer folding structures was carried out in the presence of different types of lectins, namely, concanavalin A (ConA), wheat germ agglutinin (WGA), ricinus communis agglutinin ($RCA_{120}$) and peanut agglutinin (PNA). Plant lectins are very common used lectins for the examination of the multivalent binding of carbohydrates. They play important roles in external and internal activities of plants. ConA that is a tetramer at neutral pH with four subunits has high binding affinity with mannose and glucose. Therefore, it is usually used as a model lectin to investigate the multivalent binding of glycopolymers. PNA that is another legume PNA binds to galactose, preferably to galactosyl (β,1-3) *N*-acetylgalactosamine, and

has wide applications. Moreover, a partially unfolded intermediate of PNA retains carbohydrate binding ability with affinities that are 75–85% of those of native PNA.WGA is in Gramineae family and a dimeric lectin with eight binding sites for GlcNAc. WGA has the ability to recognise specifically the pathogen for plant defence mechanisms. Ricin is a ribosome-inactivating protein and also used for generating immunotoxins. $RCA_{120}$ that is a ribosome-inactivating protein are closely related to be one of the most toxic lectins and can cause rapid death.

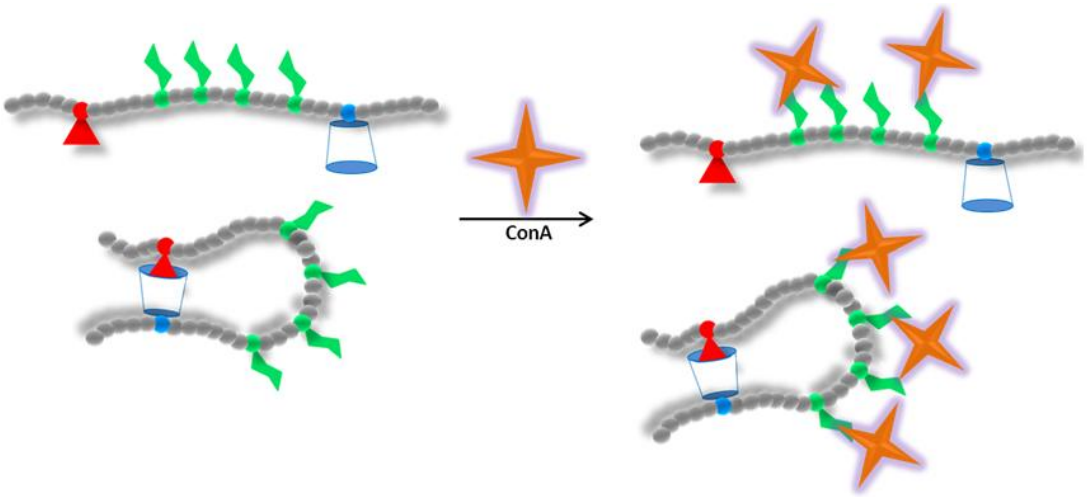


**Scheme 4.7.** Illustration of the interaction between single-chain folded/unfolded glycopolymers and ConA.

The most widely applied and the oldest technique is turbidimetry that is based on the determination of the turbidity of the solution upon aggregation of lectin and polymer chains. UV-vis spectrometer is a simple and versatile tool to determine the turbidity of the solution at varying ratio of lectin to glycopolymers. Haddleton and collaborators have reported a library of well-defined glycopolymers with different sugar azides (mannose, galactose, and glucose) and their ability to form cluster with ConA *via* UV-vis spectrometer.[26] ConA was chosen as a model lectin due to the interactions with a wide range of saccharides, especially mannose and glucose. The influence of the nature and densities of different sugars residues on the stoichiometry of the cluster, the rate of the cluster formation, the inhibitory potency of the glycopolymers, and the stability of the turbidity were investigated *via* using different assays. Therefore, the binding ability of the obtained single-chain

glycopolymer folded structures with different lectins was investigated using turbidimetry and quantitative precipitation assays *via* UV-vis spectrometer.

### 4.2.8.1 Turbidimetry assay

Turbidimetry assay is to measure the loss of intensity of transmitted light due to the scattering effect of protein-carbohydrate complex formation suspended in the solution. It was carried out according to a previously described procedure.[27] All lectins were fully dissolved in HBS buffer (approximately 60 μM) and then transferred into a dry quartz microcuvette. The dry quartz microcuvette was placed in the UV spectrometer. A solution of the copolymers in HBS buffer (320 μM) was added into solution and then the absorbance of the mixture was quickly recorded at 420 nm for 15 min every 0.12 s.

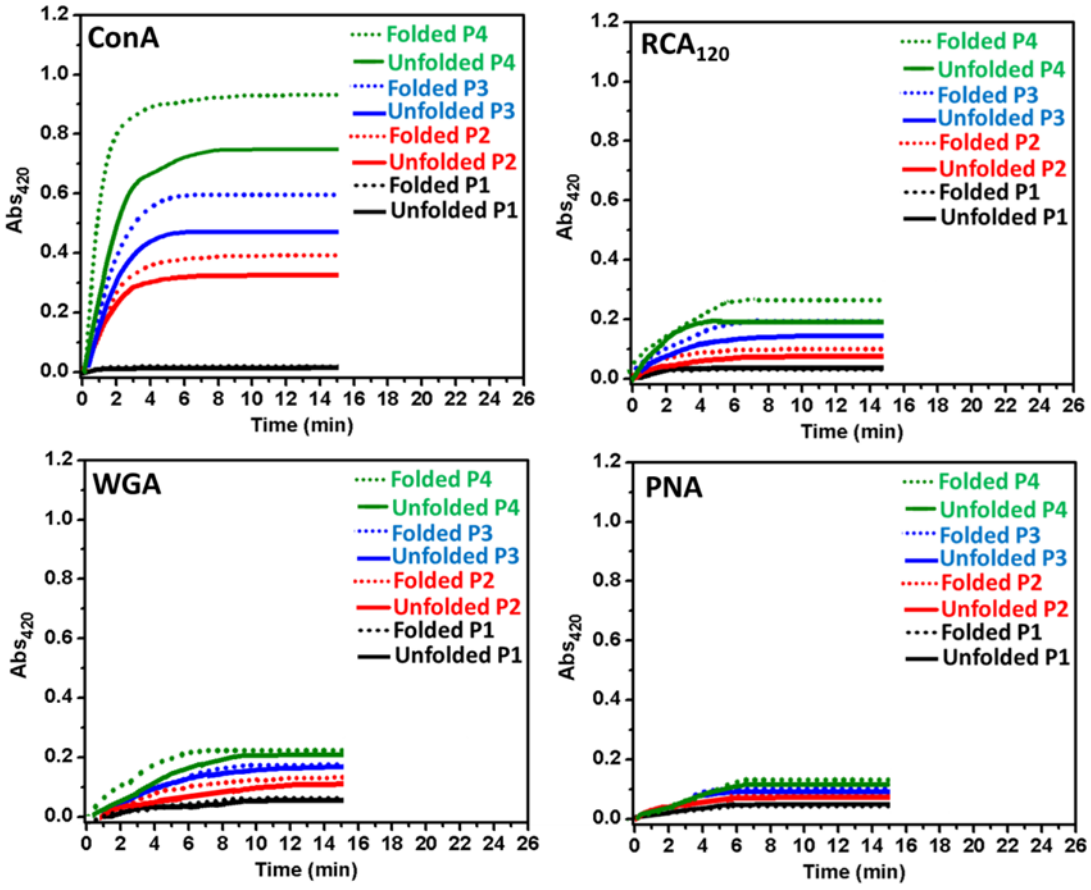


**Figure 4.12.** Turbidity measurements to monitor the influence of folded structure on the lectin interactions.

**P1** not bearing mannose moieties was used to control for the binding system of lectins. Expectedly, it did not show any binding through lectins. (Figure 4.12) While ConA that binds mannose specifically illustrated the highest binding with all glycopolymers, WGA and PNA lectins showed the lowest binding affinity through glycopolymers. The rest of lectins represented similar or equal binding avidity. Additionally, **P4** that has the highest density of mannose residues showed the highest binding with all lectins. All single-chain folded glycopolymers interacted strongly with lectins, leading to the rapid formation of aggregates.

In order to investigate the binding difference between single-chain folded and unfolded structure, unfolded solution was prepared at same concentration by addition of 1-Adamantane methanol and then heating up to 70 °C. When it was cooled down to 25 °C again, it was used immediately for the binding measurement. As depicted in Figure 4.12, single-chain folded structure of the obtained glycopolymers enhanced the specific binding significantly. Especially for ConA, the single-chain folded structure provided dramatic benefit for the binding affinity. **P4** folded structure showed the highest specific binding and also the biggest difference with unfolded structure. Moreover, the enhanced binding capability was obtained for other lectins as well when it was compared with that of the unfolded structure. These results indicated that the single-chain folding structure has a crucial and natural influence on the binding with proteins.

#### 4.2.8.2 Quantitative Precipitation Assay

Quantitative precipitation assay was also employed to investigate the capability of the single-chain folding glycopolymers to bind different lectins. 60 μM lectin solutions were prepared in HBS buffer. The glycopolymer solutions were also prepared at a series of different concentration and then mixed with lectin solutions. Subsequently, these solutions were incubated for 5 h at 25 °C. White precipitated particles were separated by centrifugation and washed with cold buffer solution several times. Lastly, the obtained particles were dissolved in a buffer solution of methyl-α-D-mannopyranoside (1 mL, 100 mM).

The results showed that **P4** represented the most lectin binding among all of the glycopolymers while **P1** not containing any binding element did not precipitate with any lectin. Additionally, it was reasonable because of the high sugar density of **P4**. As seen in Figure 4.13, the binding of the glycopolymers agreed with the concentration dependence, as well. Even though the concentration of the glycopolymers was high, there was not any considerable binding capability for $RCA_{120}$, WGA, PNA. Hence, the glycopolymers were associated with the binding properties of the relative monosaccharaides to lectins.

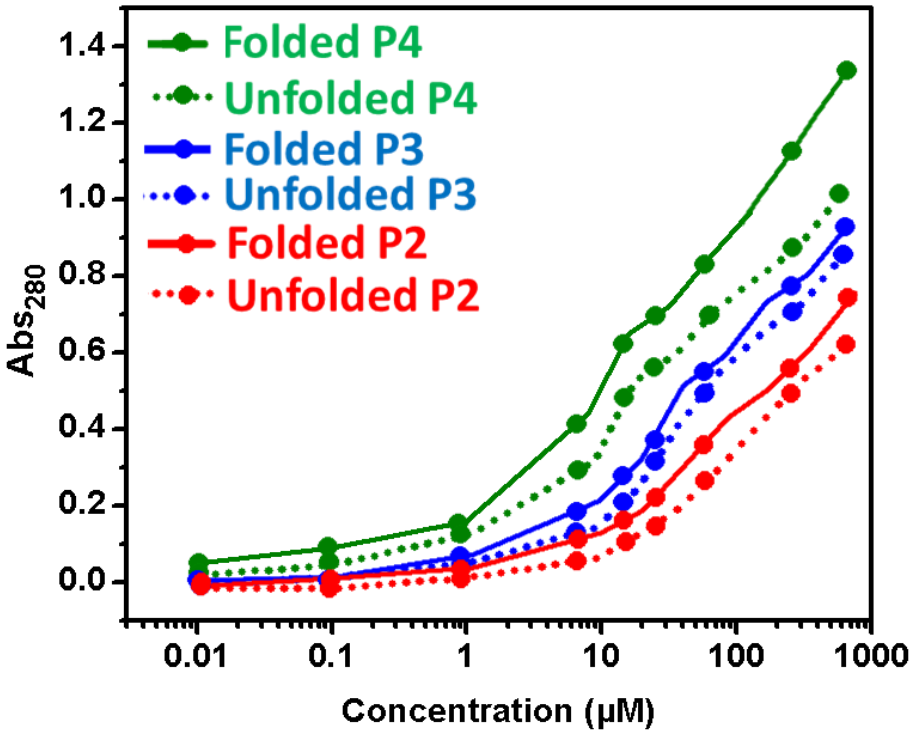


**Figure 4.13.** Quantitative assay results of the interaction of folded/unfolded glycopolymers with ConA.

The influence of the single-chain folding structure on the binding capability was examined using this method, as well. 1-Adamantane methanol was added into all glycopolymer solutions (512 μM) and then heated up to 70 °C in order to open the polymer chains. After the cooling down to 25 °C, the rest of the glycopolymer solutions were prepared and mixed with lectin solutions. The obtained results are quite promising again for the evidence of folded structure effect on the clustering of lectins. In particular, the binding between glycopolymers and ConA was greatly

enhanced by folded structure. Therefore, it is obvious that the folding shape is one of the dominant control factors on the binding capability. **P4** showed the biggest difference again because of its high mannose density. It was obviously noticed that the folding shape of ligand has an important influence on its binding activity. The reason could be that the folded structure provides more flexibility and accessibility for the mannose moieties, which allows better recognition between the mannose residues and the specific binding sites of lectins.

#### 4.2.8.3 Surface Plasmon Resonance (SPR) measurements

As a further investigation, the interaction of these folded and unfolded glycopolymer structures with DC-SIGN, a mannose-specific lectin, was then analyzed by using SPR. SPR which is one of the most sensitive technique can be used to detect association of glycoproteins or glycopolymers in pico-molar concentrations. DC-SIGN that is a member of C-type lectins binds to microorganisms and host molecules by recognizing surface rich mannose containing glycans through multivalent glycan-protein interactions and notably serves a target molecule for several viruses such as human immunodeficiency virus (HIV). C-type lectins that are one of the largest families of the animal lectins need $Ca^{+2}$ ions for their interaction with carbohydrates. Commonly, they consist of complex structures with carbohydrate recognition domains of about 120 amino acids and can have a variable number of subunits with 1-8 specific binding sites.

As depicted in Figure 4.14, the synthesized glycopolymers were bound to DC-SIGN selectively and specifically according to their mannose units. Even though **P4** represented the highest interaction with DC-SIGN, **P1** not bearing mannose moieties did not show any binding. Additionally, the SPR results also confirmed that single-chain folded structure enhanced the selective and specific interaction notably. We observed a considerable binding difference between the single-chain folded and unfolded structure. **P4** folded structure exhibited the highest selective and specific binding with DC-SIGN. These results indicated that the single-chain folding structure can create a great enhancement on the binding with proteins

since this folded shape and structure may provide more flexibility and accessibility for the mannose units hydrodynamically.

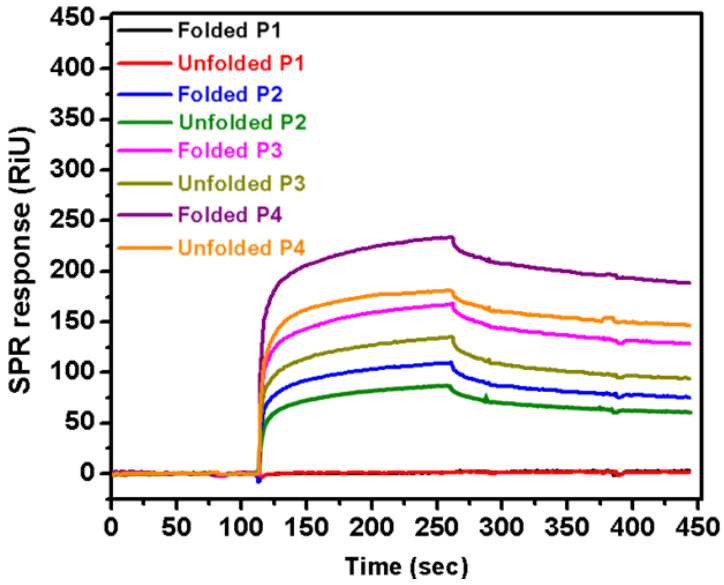


**Figure 4.14.** SPR analysis results of the interaction of folded and unfolded glycopolymers with DC-SIGN.

## 4.3 Conclusion

In this chapter, the well-defined triblock co-glycopolymers bearing β-CD and adamantane for the host-quest interaction and also mannose residues for the interaction with lectins were synthesized *via* RAFT polymerization. The single-chain folding of glycopolymers and their reversion ability were monitored by 2D NOESY NMR and DLS. These single-chain folding structures were achieved in very high diluted aqueous solution. The sufficient control was obtained for the conformation of glycopolymers. The single-chain folding structures were opened at high temperature and also by addition of a competitive guest. Moreover, intermolecular complexes existed at high concentration. The binding capability of the created single-chain glycopolymer folding structures was carried out in the presence of different types of lectins by UV-vis spectrometer. The results evidenced that these single-chain folded structures enhanced greatly the multivalent interaction, compared to the unfolded structures. This study can be a good example to develop new materials with different structures that may mimic the natural biological systems.

## 4.4 Experimental

### 4.4.1 Materials

*N,N*-Dimethylacrylamide (DMA, 99%, contains 250 ppm mono methyl ether hydroquinone (MEHQ) as inhibitor), *N*-hydroxylethyl acrylamide (97%, contains 1000 ppm MEHQ as inhibitor), β-cyclodextrin (β-CD, 97%), 1-adamantanemethanol (Ad, 99%), *p*-toluenesulfonyl chloride (TsCl, ≥99%), sodium azide ($NaN_3$, ≥99.5%), propargyl alcohol (99%), propargyl acrylate (98%), D-(+)-mannose (≥99%), sodium methoxide ($CH_3Ona$, 25 wt. % in methanol) were purchased from Sigma Aldrich Chemical Company (Dorset, UK). DMA was passed through a short column of basic alumina in order to remove MEHQ inhibitor prior to polymerization. 4,4'-azobis-(2-methylpropionitrile) (AIBN), 4,4'-Azobis(4-cyanopentanoic acid) (V-501) and $H_2SO_4$-silica catalyst were previously synthesized within the group. The RAFT agent, 2-(((dodecylthio)carbonothioyl)thio)propan-2-yl pentanoate, kindly provided by Lubrizol. ConcanavalinA (ConA), wheat germ agglutinin (WGA), ricinus communis agglutinin ($RCA_{120}$) and peanut agglutinin (PNA) were also purchased Sigma Aldrich Chemical Company (Dorset, UK). All other reagents and solvents were obtained at the highest purity available from Sigma Aldrich Chemical Company (Dorset, UK) and used as received unless stated otherwise. Water ($H_2O$, HiPerSolv Chromanorm for HPLC from VWR International, UK) was used throughout the study. Dialysis tubes were purchased from Spectrum Laboratories (California, USA).

### 4.4.2 Instruments and Analysis

Proton and carbon-13 ($^1$H-NMR and $^{13}$C-NMR) nuclear magnetic resonance spectroscopy (Bruker DPX-400/600) were used to determine the chemical structure of the synthesized polymers. Samples were dissolved at 5 mg/mL concentration in $D_2O$, $(CD_3)_2SO$ and $CDCl_3$ solvents depending on the solubility of the samples.

DOSY experiments were performed on a 400 MHz Bruker Avance III spectrometer equipped with a broadband $^1$H decoupling probe (PABBO) using an Eddy current compensated bipolar gradient pulse sequence (BPLED) at a temperature of 298 K. Proton pulse lengths were determined to be 11.15 µs and bipolar gradients of δ=

4.8–6.4 ms. 8 scans with 12k complex data points were recorded for each increment with 8 dummy scans per experiment, leading to an overall experiment time of 20 minutes and 31 seconds per sample. The diffusion delay Δ was set to 100 ms. Corresponding diffusion coefficients *D* of the polymer signals and the solvent are the result of the fitting procedure, which was performed by using Topspin 3.1 software.

2D NOESY NMR experiments were performed on a 600 MHz Bruker Avance III spectrometer at a temperature of 295 K or 340 K. The mixing time was set to 200 µs. The 90° pulse was determined to be 8.7 µs. Spectra were recorded with 4k × 1k complex data points using 16 or 20 scans per t1 increment and 16 dummy scans at 25 °C and 70 °C. The spectral width was set to 5 × 5 ppm which leads to a total experiment time of between 5 and 7 h. After zero filling to 4k × 2k points and apodization, using a 90°-phase shifted squared sine function, the spectra were Fourier transformed.

Size-exclusion chromatography (SEC) measurements were conducted on an Agilent 1260 infinity system operating in DMF with 5.0 mM $NH_4BF_4$ and equipped with refractive index detector (RID) and variable wavelength detector (VWD), 2 PLgel 5 µm mixed-C columns (300×7.5mm), a PLgel 5 mm guard column (50x7.5mm) and an autosampler. The instrument was calibrated with linear poly(methyl methacrylate) standards in range of 550 to 46890 $g.mol^{-1}$. All samples were passed through 0.2 µm PTFE filter before analysis.

The mean hydrodynamic diameters ($D_{h,}$ the volume weight diameter of the distribution) were determined by using a Malvern Zetasizer Nano ZS instrument equipped with a He-Ne laser at 633 nm. DLS measurements were performed by taking 1mL of nanoparticle solution from the dialysed solution directly. All measurements were carried out at 25 and 70 °C and repeated three times.

UV-visible spectra were recorded on a PerkinElmer Lamda 25 UV/VIS spectrometer equipped with a (PTP-1) temperature control unit at a certain temperatures in the range of 200 nm and 600 nm using quartz microcuvettes.

GC was used to measure monomer conversion of DMA and AdAc. GC analysis was performed using an Agilent Technologies 7820A. An Agilent J&W HP-5 capillary column of 30 m x 0.320 mm with a film thickness of 0.25 mm was used. The oven temperature was programmed as follows: 40 °C (hold for 1 min) increase at 30 °C/min to 300 °C (hold for 2.5 min). The injector was operated at 250 °C and the FID was operated at 320 °C. Nitrogen was used as carrier gas at flow rate of 6.5 mL/min and a split ratio of 1:1 was applied. Chromatographic data was processed using OpenLab CDS ChemStation Edition, version C.01.05.

The FT-IR spectra were recorded on a Bruker FT-IR spectrometer TENSOR II with Diamond-ATR module. The scanning range was 600-4000 $cm^{-1}$ and the resolution was 1 $cm^{-1}$.

Matrix assisted laser desorption/ionisation-time of flight mass spectroscopy (MALDI-ToF MS) was performed using a Bruker Daltonics Autoflex MALDIToF mass spectrometer, equipped with a nitrogen laser at 337 nm with positive ion ToF detection. *Trans*-2-[3-(4-tert-Butylphenyl)-2-methyl-2-propenylidene]malononitrile (DCTB, ≥98%) and potassium trifluoroacetate (KTFA) were used as matrix and cationisation agent, respectively. Spectra were recorded in reflectron mode and the mass spectrometer was calibrated with a peptide mixture up to 6000 Da.

### 4.4.3 Synthesis of D-mannose acrylamide glycomonomer

Firstly, D-mannose pentaacetate was synthesized according to previous reported procedure.[28] The obtained D-mannose pentaacetate (6.73 g, 0.017 mol) and *N*-hydroxylethyl acrylamide (2.22 g, 0.019 mol) were dissolved in anhydrous dichloromethane (25 mL) and then degassed by argon gas for 10 min. Subsequently, boron trifluoride diethyl etherate (8.63 g, 0,060 mol) was added *via* syringe and the solution was sonicated for 90 min. The reaction solution was washed with brine for 3 times (30 mL). After the organic layer was dried over $MgSO_4$, the solvent was removed under reduced pressure to obtain a yellowish gummy crude product. The obtained crude product was used directly without any further purification to synthesize 2-(D-manosyloxy) hydroxylethylacrylamide. The protection of acetyl groups was carried out in the presence potassium carbonate (1.0 g, 7.2 mmol) in

methanol (25 ml). The reaction was followed by thin-layer chromatography (TLC). After the neutralization of the reaction solution using Amberjet 1200H ($H^+$) cation exchange resin. The resin was removed by filtration and the solvent was removed under reduced pressure. The obtained crude product was purified by column chromatography (chloroform:MeOH), gradient elution) to yield a white amorphous solid upon lyophilizing. (0.67 g, yield: 32.6%).

$^1$H NMR ($D_2O$, 298 K, 400 MHz): δ =6.32 (dd, 1H, J=14.6 Hz, $CH_2$), 6.30 (dd, 1H, J=14.2 Hz, CH), 5.82 (dd, 1H, J=14.4 Hz, CH), 5.12 (m, 1 H, H-1 of mannose), 4.82 (t, 2H, $CH_2$-OH), 4.22 (m, 2 H, $CH_2$-NH), 3.82 (t, 2H, $CH_2$-$CH_2$), 3.40-3.82 (m, H residues of mannose) ppm.

$^{13}$C NMR ($D_2O$, 298 K, 400 MHz): δ =152.3 (C=O), 134.7 (C-$CH_2$), 126.5 (N-CH=C), 105.9 (C 1 of mannose), 72.3, 71.1, 69.6, 68.3 (carbons of anomeric mannose), 64.7 ($CH_2$-NH), 28.3 ($CH_2$-$CH_2$), 19.7 ($CH_2$-OH) ppm.

ESI-MS m/z: calculated for $C_{11}H_{19}NO_7$ ($M+H^+$), 277.2; found, 277.1.

**4.4.4 Synthesis of adamantane acrylate monomer**

1-Adamantane methanol (3.0 g, 18.0 mmol) as dissolved in 80 mL of THF and $Et_3N$ (6.3 mL, 45.0 mmol) was added. The reaction mixture was then cooled to 0 °C. Acryloyl chloride (1.7 mL, 21.6 mmol) in THF (20 mL) was added dropwise within 30 minutes. The reaction mixture was stirred for 15 min at 0 °C then over night at room temperature. The reaction was filtered off, solvent evaporated and was added $CH_2Cl_2$, then extracted with HCl (1 M, 2×30 mL), deionized water (2×30 mL) in sequence. After removing the solvents by a rotary evaporator, the crude product was purified by column chromatography over silica gel eluting with hexane/EtOAc (9/1). (Yield=2.9 g, 73%).

$^1$H NMR ($CDCl_3$, 298 K, 400 MHz): δ =6.33 (d, 1H, J=16.9 Hz, $CH_2$), 6.06 (dd, 1H, J=17.3 Hz, CH), 5.74 (d, *J* = 10.4 Hz, 1H, $CH_2$), 3.89 (s, 2H, $CH_2O$) 1.92 (m, 3H, CH), 1.70 and 1.65 (d, 6H, $CH_2$), 1.60 (d, 6H, CH) ppm.

$^{13}$C NMR ($CDCl_3$, 298 K, 400 MHz): δ =167.2 (C=O), 131.4 (C-$CH_2$), 128 (CH=C), 72.4 ($CH_2O$), 39.6 (CH), 38.1 ($CH_{2)}$, 33.5, 26 ($CH_2$) ppm.

### 4.4.5 Synthesis of mono-6-deoxy-6-azido-β-cyclodextrin

In a 500 mL round bottom flask β-cyclodextrin (20.0 g, 17.6 mmol) was suspended in 250 mL 0.4 M sodium hydroxide (NaOH) aqueous solution. The flask was cooled to 0°C in ice bath. TsCl (13.4 g, 70.3 mmol) was added in slow portions over 10 min. After 45 min of stirring at 0°C, the precipitate was removed by filtration and the pH of the filtrate was adjusted to 8.5 by dropping HCl aqueous solution. Then the mixture was stirred for 1 h at room temperature. The resulting white precipitate was recovered by filtration and washed three times with water. The final product was used to synthesize β-CD-$N_3$ directly after drying in a vacuum oven at 60 °C. β-CD-OTs (8.0 g, 6.2 mmol) was suspended in 100 mL water. After heating to 80°C, $NaN_3$ (2.0 g, 31.0 mmol) was added. The reaction mixture was stirred at 80°C for overnight. The reaction solution was cooled to room temperature and precipitated in 800 mL acetone. The resulting white precipitate was recovered by filtration and redissolved in 50 mL of water and precipitated again in acetone. The white solid was dried under vacuum at 60°C for 2 days (6.8 g, yield: 95%).

$^1$H NMR ($(CD_3)_2SO$), 298 K, 400 MHz): δ =5.72 (br, 14H, OH-2,3), 4.88 (s, H, H-1), 4.83 (d, 6H, H-1), 4.57-4.40 (br, 6H, OH-6), 3.86-3.50 (br, 28H, H-3,5,6,6'), 3.32 (br, 14H, H-2,4 overlap with $H_2O$) ppm.

FT-IR v: 3316 (OH), 2924 (CH), 2160 (C-C), 2102 (N=N), 1644 (C=C), 1364 (OH), 1152 (CN), 1077 (OH), 1025 (CH), 945, 853, 756 (NH), 704 (CH) $cm^{-1}$.

### 4.4.6 Synthesis of β-cyclodextrin acrylate monomer

The "*click*" reaction was carried out *via* a previously described procedure by Ritter et al.[29] Mono-6-deoxy-6-azido-β-cyclodextrin (1 g, 0.86 mmol) and propargyl acrylate (0.19 g, 1.72 mmol) were dissolved in DMF (6 ml), a DMF solution of $CuSO_4 \cdot 5H_2O$ (21.47 mg, 0.086 mmol) and (+)-sodium L-ascorbate (34.1 mg, 0.172 mmol) were added into the reaction solution. The reaction solution was transferred into a microwave tube and then irradiated in the microwave at 120 °C for 1 h. After precipitating the reaction mixture with acetone, 0.76 g of product was isolated (69% yield).

$^1$H NMR ($(CD_3)_2SO$), 298 K, 400 MHz): δ =8.11 (1H, CH), 6.12 (H,-CH), 5.83 (br, 14H, OH-2,3), 5.22 (H, -CH), 5.06 (2H,-$CH_2$), 4.78 (d, 6H, H-1), 4.51 (br, 6H, OH-6), 3.62 (br, 28H, H-3,5,6), 3.31 (br, 14H, H-2,4) ppm.

FT-IR v: 3320 (OH), 2924 ($CH_2$), 1720 (CdO), 1652 (CdC), 1160 (C-O-C), 1075 (OH), 1023 (C-O).

MALDI-TOF m/z: calculated for $C_{48}H_{75}N_3O_{36}$ ($M+Na^+$), 1293.02; found, 1293.14.

### 4.4.7 Synthesis of p((DMA)$_{10}$-r-(Adac)$_2$) macro-RAFT agent

2-(((dodecylthio)carbonothioyl)thio)propan-2-yl pentanoate (1 eq), DMA (10 eq), Adac (2 eq), AIBN (0.01 eq) and solvent ( 5 mL) were introduced in a Schlenk tube equipped with a magnetic stirrer and sealed with a rubber septum. The reaction solution was degassed by gentle bubbling of argon gas for 30 min and then the schlenk tube was sealed properly and the mixed solution was allowed to polymerize. After the confirmation of nearly full conversion according to GC, the polymerization reaction was stopped by cooling down and exposure to air. Subsequently, the reaction solution was diluted with 2.0 mL of THF and then purified by precipitation in cold diethyl ether twice. After the filtration, the obtained polymer was dried *in vacuo* and characterized *via* $^1$H-NMR and DMF SEC analysis.

### 4.4.8 Synthesis of well-defined triblock copolymers

RAFT polymerization reactions were carried out in the presence of p((DMA)$_{10}$-r-(Adac)$_2$) as a RAFT agent, V-501 as an initiator in the water-DMF mixture at 70 °C. In order to polymerize second block, a Schlenk tube was charged with DMA and ManAcm monomers (in total 24 eq), macro-RAFT agent (1 eq), V-501 (0.01 eq) and water (2.0 mL) was degassed by gentle bubbling of argon gas for 30 min. During the polymerization, samples were withdrawn from the polymerization medium using a degassed syringe for GC and $^1$H NMR to determine monomer conversions. When both monomer reached to nearly full conversion, pre-degassed solution of DMA and CDAc (DMA:CDAc = 10:2) in DMF was added into the Schlenk tube. The reaction was stopped by cooling down and then the reaction mixture was dialyzed

against a mixture of distilled water and methanol for 3 days, while changing the water at least three times. The final product was freeze-dried under vacuum and characterized by $^{1}$H NMR and DMF SEC.

### 4.4.9 Single-chain folding studies

The diffusion coefficient of the obtained glycopolymers was measured using DOSY NMR at different concentrations in order to determine the necessary concentration for the single-chain regime. 2D NOESY NMR and DLS experiments at 25 and 70 °C were carried out at the calculated concentration. In order to open the single-chain folding structure, 1-adamantanemethanol (1mg) was added into solutions and then heated up 70 °C. Subsequently, it was allowed to cool down again and DLS was measured at 25 °C.

### 4.4.10 Lectin binding studies

All experiments were conducted with HEPES-buffered saline (HBS) (0.10 M HEPES, 0.9 M NaCl, 1 mM $MgCl_2$, 1 mM $CaCl_2$, and 1 mM $MnCl_2$ adjusted to pH 7.4 and filtered with 0.2 µm regenerated cellulose syringe filter.

#### 4.4.10.1 Turbidimetry assay

The assay was followed a modified procedure.[27] A solution of 60 µM ConA in HBS buffer solution was prepared fresh before the assay. Turbidity measurements were performed by adding 350 µL of the ConA solution to a dry quartz microcuvette and put into the holder of UV-visible spectrophotometry at a certain temperature for 1 min. A solution of the ligand in HBS buffer (350 µL at 320 µM) was added into into the cuvette *via* a pipette, the absorbance of the mixture was quickly recorded at 420 nm for 15 min every 0.12 s.

#### 4.4.10.2 Quantitative Precipitation Assay

Con A was dissolved in the HBS buffer solution to make fresh stock solution and the concentration was 60 µM (assuming Con A tetramers with a molecular weight of 104 kDa.) Glycopolymers in HBS buffer (512 µM) were also prepared with a series of different concentration. Then Con A solution and the glycopolymer solutions were

mixed (1:1, v/v) and ten incubated for 5 h at 25 °C. White precipitated particles were separated from solution by centrifugation at 5000 x *g* for 10 min, followed by removal of the supernatants very carefully using pipette. Then the pellets were washed in cold buffer solution for three times. After removal of the supernatants, the precipitates were dissolved in a HBS buffer solution of methyl-α-D-mannopyranoside (1 mL, 100 mM). With complete dissolution, the Con A content was determined by measuring the absorbance at 280 nm.

#### 4.4.10.3 Surface Plasmon Resonance

Interactions between the glycopolymers and DC-SIGN were measured using SPR in a high-throughput multichannel mode. In the concentration experiments, all glyconanoparticles were measured at 3 different concentrations, in which the buffer was flowed over the chip alone before (90 s) and after (650 s) injection of the analyte (900 s). Buffer solution was prepared in 25 mM HEPES pH 7.4, 150 mM NaCl, 5 mM $CaCl_2$, 0.01% Tween-20. Regeneration of the sensor chip surfaces was performed using 10 mM glycine pH 2.5. Before measurements, star-shaped (8 arms) glycopolymer at different concentrations was used as control for binding. It showed higher affinities during binding with DC-SIGN due to higher mannose content.

## 4.5 References

(1) Dobson, C. M. *Nature* **2003**, *426*, 884.
(2) Dill, K. A.; MacCallum, J. L. *Science* **2012**, *338*, 1042.
(3) Perrier, S. *Nat Chem* **2011**, *3*, 194.
(4) Matyjaszewski, K.; Xia, J. *Chemical Reviews* **2001**, *101*, 2921.
(5) Chiefari, J.; Chong, Y. K.; Ercole, F.; Krstina, J.; Jeffery, J.; Le, T. P. T.; Mayadunne, R. T. A.; Meijs, G. F.; Moad, C. L.; Moad, G.; Rizzardo, E.; Thang, S. H. *Macromolecules* **1998**, *31*, 5559.
(6) Barner-Kowollik, C.; Perrier, S. *Journal of Polymer Science Part A: Polymer Chemistry* **2008**, *46*, 5715.
(7) Percec, V.; Guliashvili, T.; Ladislaw, J. S.; Wistrand, A.; Stjerndahl, A.; Sienkowska, M. J.; Monteiro, M. J.; Sahoo, S. *Journal of the American Chemical Society* **2006**, *128*, 14156.
(8) Altintas, O.; Gerstel, P.; Dingenouts, N.; Barner-Kowollik, C. *Chemical Communications* **2010**, *46*, 6291.
(9) Altintas, O.; Rudolph, T.; Barner-Kowollik, C. *Journal of Polymer Science Part A: Polymer Chemistry* **2011**, *49*, 2566.

(10) Willenbacher, J.; Altintas, O.; Roesky, P. W.; Barner-Kowollik, C. *Macromolecular Rapid Communications* **2014**, *35*, 45.
(11) Willenbacher, J.; Schmidt, B. V. K. J.; Schulze-Suenninghausen, D.; Altintas, O.; Luy, B.; Delaittre, G.; Barner-Kowollik, C. *Chemical Communications* **2014**, *50*, 7056.
(12) Lutz, J.-F. *Polymer Chemistry* **2010**, *1*, 55.
(13) Schmidt, B. V. K. J.; Fechler, N.; Falkenhagen, J.; Lutz, J.-F. *Nat Chem* **2011**, *3*, 234.
(14) Shishkan, O.; Zamfir, M.; Gauthier, M. A.; Borner, H. G.; Lutz, J.-F. *Chemical Communications* **2014**, *50*, 1570.
(15) Inoue, Y.; Kuad, P.; Okumura, Y.; Takashima, Y.; Yamaguchi, H.; Harada, A. *Journal of the American Chemical Society* **2007**, *129*, 6396.
(16) Altintas, O.; Krolla-Sidenstein, P.; Gliemann, H.; Barner-Kowollik, C. *Macromolecules* **2014**, *47*, 5877.
(17) Altintas, O.; Lejeune, E.; Gerstel, P.; Barner-Kowollik, C. *Polymer Chemistry* **2012**, *3*, 640.
(18) Fan, W.; Tong, X.; Yan, Q.; Fu, S.; Zhao, Y. *Chemical Communications* **2014**, *50*, 13492.
(19) Glassner, M.; Oehlenschlaeger, K. K.; Gruendling, T.; Barner-Kowollik, C. *Macromolecules* **2011**, *44*, 4681.
(20) Song, W.; Wang, Y.; Qu, J.; Lin, Q. *Journal of the American Chemical Society* **2008**, *130*, 9654.
(21) Mueller, J. O.; Guimard, N. K.; Oehlenschlaeger, K. K.; Schmidt, F. G.; Barner-Kowollik, C. *Polymer Chemistry* **2014**, *5*, 1447.
(22) Yang, H.; Yuan, B.; Zhang, X.; Scherman, O. A. *Accounts of Chemical Research* **2014**, *47*, 2106.
(23) Schmidt, B. V. K. J.; Hetzer, M.; Ritter, H.; Barner-Kowollik, C. *Progress in Polymer Science* **2014**, *39*, 235.
(24) Séon, L.; Parat, A.; Gaudière, F.; Voegel, J.-C.; Auzély-Velty, R.; Lorchat, P.; Coche-Guérente, L.; Senger, B.; Schaaf, P.; Jierry, L.; Boulmedais, F. *Langmuir* **2014**, *30*, 6479.
(25) Zhang, Y.; Tu, Q.; Wang, D.-E.; Chen, Y.; Lu, B.; Yuan, M.-S.; Wang, J. *New Journal of Chemistry* **2013**, *37*, 2358.
(26) Gou, Y.; Geng, J.; Richards, S.-J.; Burns, J.; Remzi Becer, C.; Haddleton, D. M. *Journal of Polymer Science Part A: Polymer Chemistry* **2013**, *51*, 2588.
(27) Cairo, C. W.; Gestwicki, J. E.; Kanai, M.; Kiessling, L. L. *Journal of the American Chemical Society* **2002**, *124*, 1615.
(28) Slavin, S.; Burns, J.; Haddleton, D. M.; Becer, C. R. *European Polymer Journal* **2011**, *47*, 435.
(29) Munteanu, M.; Choi, S.; Ritter, H. *Macromolecules* **2008**, *41*, 9619.

# Chapter 5 *S*-glucosyl substituted 2-oxazolines and their binding to lectins

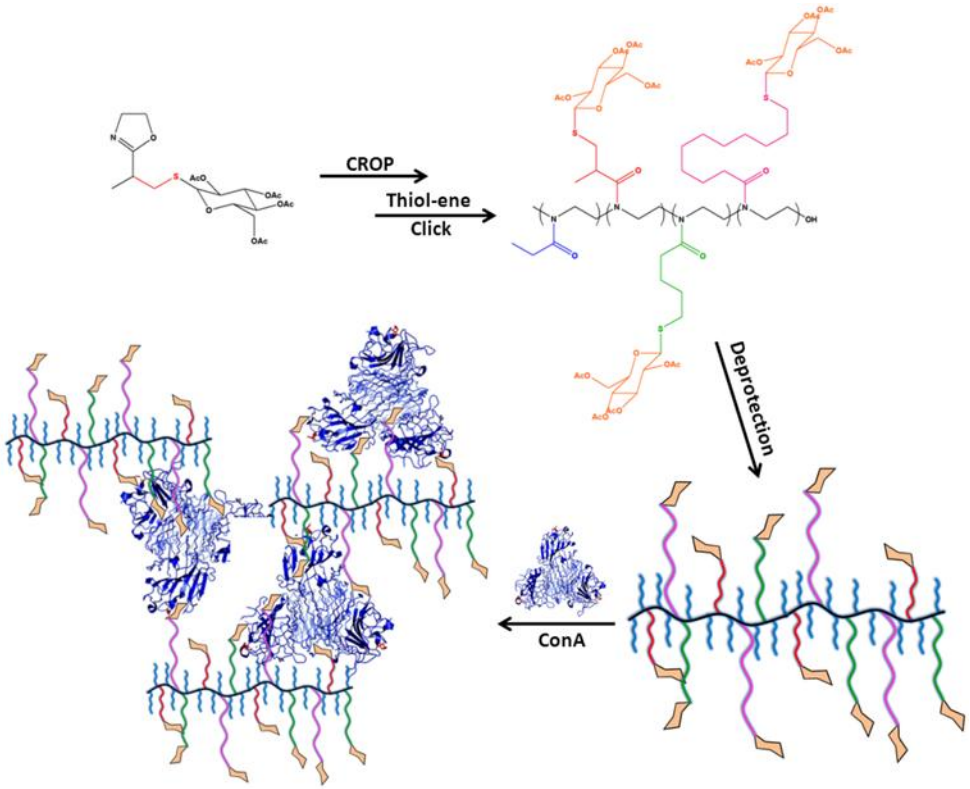


*A new monomer, 2-[2-(2,3,4,6-Tetra-O-acetyl-β-D-glucopyranosylthio) propyl)]-2-oxazoline ($Ac_4Glc$-S-Ox) , was synthesized by direct addition of 2,3,4,6-Tetra-O-acetyl-1-thio-β-D-glucopyranose ($Ac_4Glc$-SH) to 2-Isopropenyl-2-oxazoline (iPOx) in the presence of solid butyl amine resin via thiol-ene "click" reaction. This new glycomonomer structure was confirmed by $^{1}H$ NMR, $^{13}C$ NMR and GC-MS. The living cationic ring-opening polymerization (CROP) was performed to prepare copolymers of $Ac_4Glc$-S-Ox with 2-ethyl-2-oxazoline (EtOx). In order to investigate the effect of S-glucosyl substituent linker length to the polymer backbone on the cloud point and the binding ability systematically, copolymers of 2-decenyl-2-oxazoline (DecenOx) and 2-butenyl-2-oxazoline (ButenOx) with EtOx were prepared and then treated with $Ac_4Glc$-SH to yield the respective glycopolymers. The obtained glycopolymers exhibited a lower critical solution temperature behavior (LCST) that could be changed significantly according to alkyl linker length of glucose to polymer backbone. Moreover, ConA was used to investigate the influence of sugar linker length to the polymer backbone on the bioactivity and bioavailability of the synthesized glycopolymers.*

## 5.1 Introduction

The multivalent carbohydrate-protein interactions play a crucial role in a wide range of complex biological processes, such as intercellular recognition, signal transmission and infection of pathogens.[1-4] Carbohydrates could exhibit a great interaction capacity with their specific binding lectins according to their monomeric units and their ability to be highly branched molecules.[5] This interaction could also be enhanced by "glycocluster effect".[6] Glycopolymers that are essentially synthetic carbohydrate containing macromolecules could display similar structural and functional features with oligosaccharides due to the variations in anomeric status, linkage positions, branching, and introduction of site specific substitutions.[7,8] Therefore, even though there has been a great development on the synthesis of well-defined glyco-polymers/nanoparticles for different bio-related applications such as drug delivery purposes, biomaterials, biotechnologies over the last decade, it is still demanding to provide a precision control on chain lengths, monomer sequences, compositions, and architectures in order to understand this high selectivity, strength and specific interaction between glycomaterials and lectins in more detail.[9]

The cationic ring opening polymerization (CROP) that is one of the earliest developed controlled radical polymerization technique has only been performed few times in glycopolymer synthesis because the direct polymerization of carbohydrate-containing cyclic monomers is still very limited.[10-12] Therefore, it is necessary to develop new strategies to prepare different types of glycopolymers with various tunable properties *via* CROP. 2-Alkyl-2-oxazolines are the most commonly used monomers for CROP and they are promising candidates for biological applications due to their biocompatibility, low biotoxicity and incorporation with different functionalities and properties.[13-17] In general, there are two advanced synthesis strategies to prepare glycopolymers: either the direct polymerization of carbohydrate-bearing monomers or the synthesis of polymeric backbone bearing pendant reactive sites subsequently functionalized by carbohydrate moieties by using the combination of controlled/living polymerization techniques and "*click*" chemistry.

There are only two reports dealing with the direct cationic ring opening polymerization of a sugar-functionalized 2-oxazoline so far. The first study was performed in 2010 by Kojima *et. al.* and two different *S*-galactosyl substituted oxazolines were prepared in three step reaction and polymerized *via* CROP.[12] After the deprotection, the obtained poly(2-oxazoline)s having pendant sugar showed specific interaction with $RCA_{120}$ (*Ricinus communis* agglutinin). After a very short time, Schubert and coworkers reported the synthesis of glucose-substituted 2-oxazoline monomer and its co-polymerization by CROP in the presence of 2-oxazoline-based monomers.[11] This new glucose-substituted 2-oxazoline monomer was prepared by using the copper-catalyzed azide-alkyne cycloaddition (CuAAC) click chemistry after a multi-step reaction. A series of well-defined block glycocopolymers with different chain lengths was prepared in acetonitrile at 120 °C. In this chapter, we describe the synthesis and cationic ring opening polymerization of 2-[2-(2,3,4,6-Tetra-*O*-acetyl-β-D-glucopyranosylthio) propyl)]-2-oxazoline ($Ac_4$Glc-S-Ox) glycomonomers for the first time. To the best of our knowledge, this is third report published that discusses the synthesis and the direct polymerization of a carbohydrate bearing 2-oxazoline monomer. However, our glycomonomer synthesis method is easier and more efficient than previous methods as being one-pot reaction and requires no further purification. The thiol-ene "*click*" reaction was performed to prepare $Ac_4$Glc-S-Ox by the addition of 2,3,4,6-Tetra-*O*-acetyl-1-thio-β-D-glucopyranose ($Ac_4$Glc-SH) to 2-isopropenyl-2-oxazoline (iPOx) with 1 to 1 molar ratio in the presence of solid butyl amine resin at 365 nm UV lamp for overnight. As mentioned above, in order to achieve effective and selective lectin binding and signal transduction, some glycopolymer features influencing activity need to be considered. The flexibility of linker that connects the carbohydrate to the backbone is one of these features that has a strong impact on the interaction between glycopolymer and accessible binding sites of lectins. From this perspective, in order to investigate the effect of carbohydrate substituents linker length to the polymer backbone on the binding ability, copolymers of 2-decenyl-2-oxazoline (DecenOx) and 2-butenyl-2-oxazoline (ButenOx) with 2-ethyl-2-oxazoline (EtOx) were prepared and then modified with $Ac_4$Glc-SH to yield the respective glycopolymers. In this way, a series of glyco-copolymers were prepared by polymer

post-modification exploiting the photoaddition of thiols onto pendant alkene functionalities. Furthermore, the lower critical solution temperature (LCST) behavior of the obtained glyco-copolymers are determined to discuss the influence of sugar content and also sugar linker length to the backbone on the cloud points. In general, a reversible phase transition from soluble to insoluble was observed for all glycopolymers when their solution temperature was raised above their LCST values due to the disruption of hydrogen bonds between polar groups of the glycopolymers and water. In addition, the bioactivity and bioavailability of the synthesized glyco-copolymers were investigated by the interaction with concanavalin A (ConA). ConA that is a tetramer at neutral pH with four subunits has high binding affinity with mannose and glucose. Therefore, it is usually used as a model lectin to investigate the multivalent binding of glycopolymers.[18] The obtained results showed that glycopolymers carrying long sugar linker to backbone provided higher binding capability than those bearing short linker. This observation is so important to confirm the "glycocluster effect" for the multivalent interaction.

## 5.2 Results and Discussion

### 5.2.1 Synthesis of *S*-glucosyl substituted 2-oxazoline glycomonomer ($Ac_4$Glc-S-Ox)

Thiol-ene "click" chemistry, which is one of the most popular click reactions, is known for over 100 years. The potential of this reaction is huge since thiol and alkene components can be incorporated in an easy and versatile way into a wide range of substituents.[19,20] The addition of a thiol to an ene bond can proceed *via* two different mechanistic pathways, namely a radical and an anionic pathway.[21,22] In this contribution, we firstly reported a simple, one-pot, efficient and versatile synthetic strategy to prepare a new *S*-glucosyl substituted 2-oxazoline glycomonomer *via* thiol-ene "*click*" chemistry. This new glycomonomer can undergo controlled cationic ring opening polymerization *via* 2-oxazoline moiety. As depicted in Scheme 4.1, the thiol groups of $Ac_4$Glc-SH were reacted with the double bonds of iPOx in the presence of solid butyl amine resin as a catalyst in dry acetonitrile at 365 nm UV lamp overnight. This thiol-ene "*click*" reaction was monitored and confirmed by $^{1}$H- NMR, $^{13}$C-NMR and ESI-MS. The conversion of the

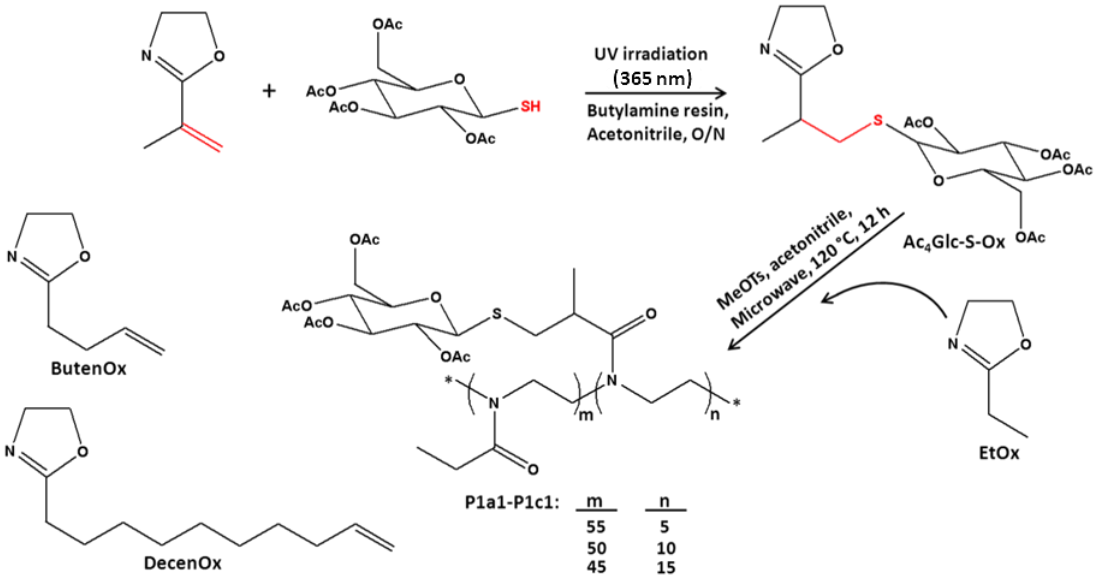


**Scheme 5.1.** Schematic representation of the synthesis of $Ac_4$Glc-S-Ox and the cationic ring-opening copolymerization of $Ac_4$Glc-S-Ox with EtOx; Graphical illustration of the other monomers (ButenOx and DecenOx) used for the copolymerization.

reaction is more than 98% for each time. As seen in Figure 5.1, the new glycomonomer structure was confirmed by the disappearance of the double bound peaks at 5.5 and 5.7 ppm of iPOx, the appearance of the new peaks at 2.6-2.8 and 3.0-3.1 ppm according to formation of the corresponding thioether structure and also the chemical shift of $–CH_3$ protons of iPOx after the reaction due to difference chemical environment. In the ESI-MS spectra, there is a clear peak at 475.16 m/z that corresponds to the molecular weight of the new *S*-glucosyl substituted 2-oxazoline glycomonomer with 475.15 m/z. The product was obtained as a pale white gummy material with a 97% yield.

Here, the thiol-ene *"click"* reaction between $Ac_4$Glc-SH and iPOx yielded the corresponding thiolether glycomonomer product in essentially and excellent yields. Hence, there was no need to make any rigorous and intensive purification that usually causes a loss of product. The another important advantage of this *S*-glucosyl substituted 2-oxazoline glycomonomer is that the previous reports included multi-step reactions causing time-consuming and high-cost chemical usage to prepare a carbohydrate substituted 2-oxazoline , but in this case a simple, one-pot, efficient

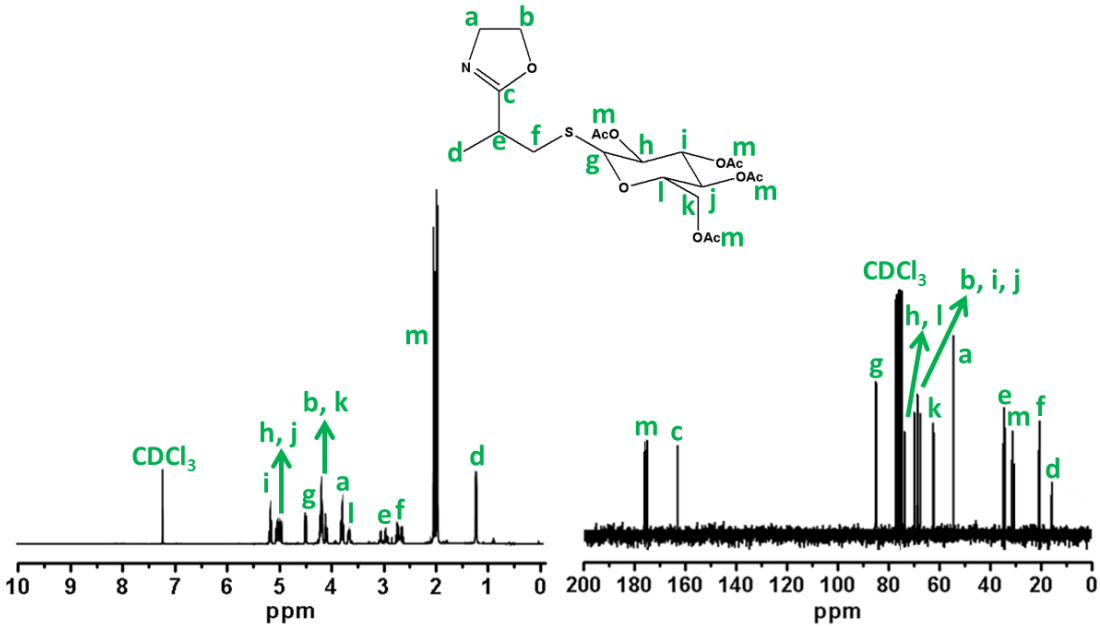


**Figure 5.1.** Details of $^{1}$H-NMR and $^{13}$C-NMR spectrum of $Ac_4$Glc-S-Ox.

and robust synthetic strategy was achieved. According to our observations, the presence of oxygen in the reaction environment had no significant negative effect on the conversion, however, when the reaction was scaled up, the reaction never reached to high conversion even if it was allowed to react for a couple of days.

### 5.2.2 Synthesis of ButenOx and DecenOx

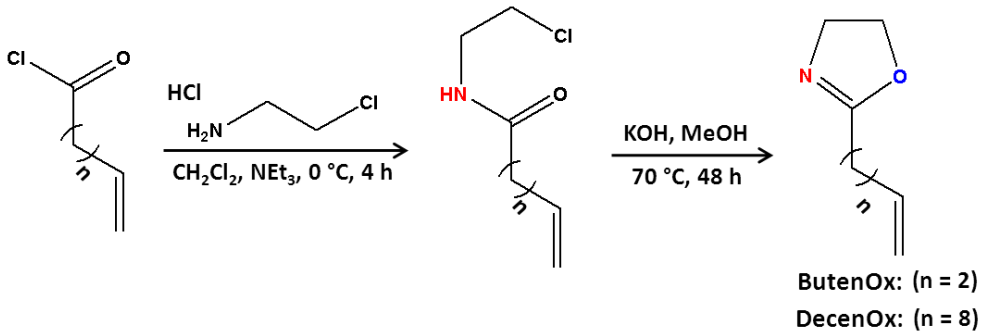


**Scheme 5.2.** Reaction scheme for the synthesis of 2-butenyl-2-oxazoline (ButenOx) and 2-decenyl-2-oxazoline (DecenOx).

ButenOx and DecenOx monomers were prepared in aaccording to a two-step procedure reported previously by Kempe and co-workers.[17] ButenOx and DecenOx were synthesized from commercially available acid chlorides, namely, 4-pentenoyl chloride and 10-undecenoylchloride, respectively.

As shown in Scheme 5.2, the first step is the nucleophilic substitution reaction and it was monitored by using GC-MS measurements as well as $^{1}$H-NMR spectroscopy. Both measurements confirmed a partial formation of the desired 2-oxazoline already after the first step and, therefore, the second reaction was carried out without any further purification of the intermediate product. The ring closure to 2-butenyl-2-oxazoline and 2-decenyl-2-oxazoline was achieved with KOH in dry MeOH at 70 °C. The pure products were obtained after vacuum distillation with a yield of 42% for ButenOx and 72% for DecenOx. The chemical structure of the final products was confirmed by $^{1}$H-NMR, $^{13}$C-NMR and ESI-MS.

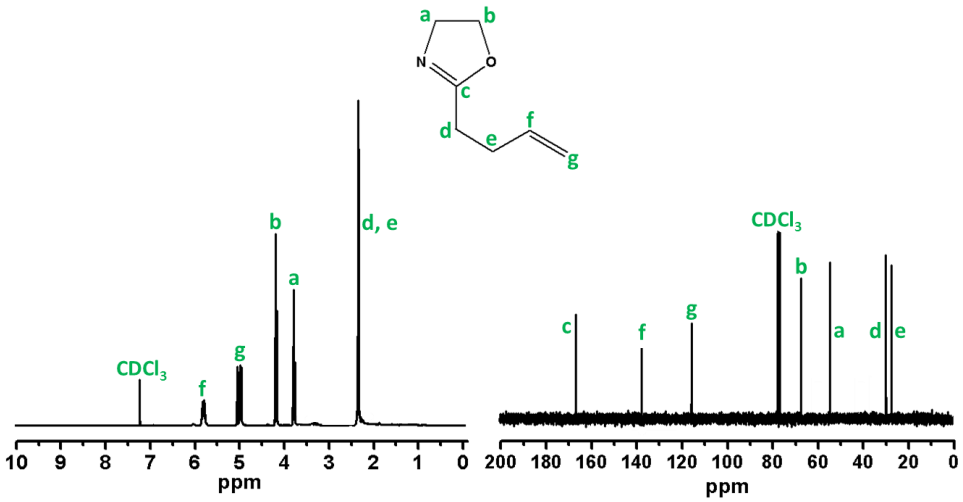


**Figure 5.2.** Details of $^{1}$H-NMR and $^{13}$C-NMR spectrum of ButenOx.

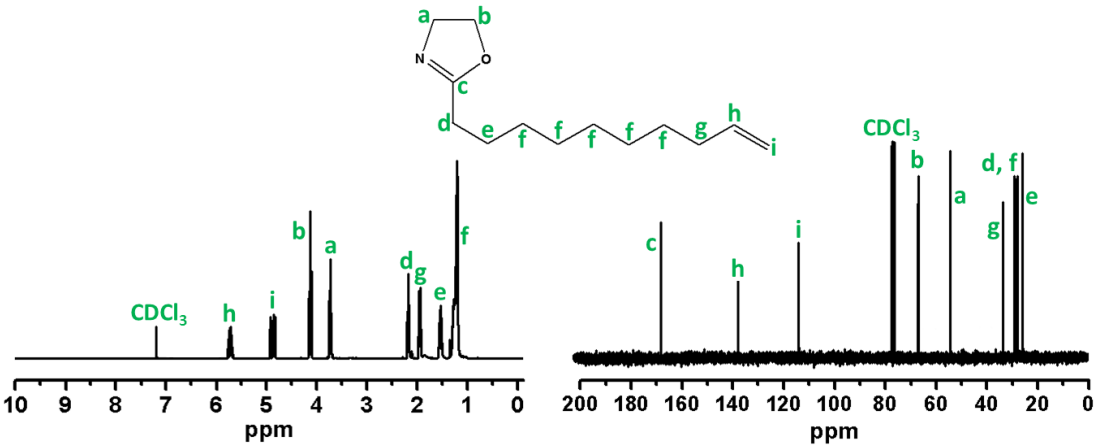


**Figure 5.3.** Details of $^{1}$H-NMR and $^{13}$C-NMR spectrum of DecenOx.

### 5.2.3 Microwave-assisted copolymerization

The cationic ring opening polymerization using favourable oxazoline monomers can be effected significantly by polymerization solvent, monomer concentration, temperature and also air or moisture in the polymerization mixture.[23-25] Any changes in these parameters will deteriorate the polymerization results and obtained polymers. Therefore, several optimization polymerization reactions were performed to find out the best system for the copolymerization of EtOx and $Ac_4$Glc-S-Ox according to previous studies. Briefly, when the polymerization reaction was carried out at 140 °C or high monomer concentration, the polymer was obtained with high dispersity because of a shoulder at higher molar mass observed by GPC analysis. The possible reason behind of this could be the degradation of the sugar moiety or some coupling of polymer chains. In the case of low temperature polymerization, the conversion of $Ac_4$Glc-S-Ox remained at undesired low rate. According to these results, the optimal temperature and monomer concentration were determined as a 120 °C and 1M, respectively for the further copolymerizations.

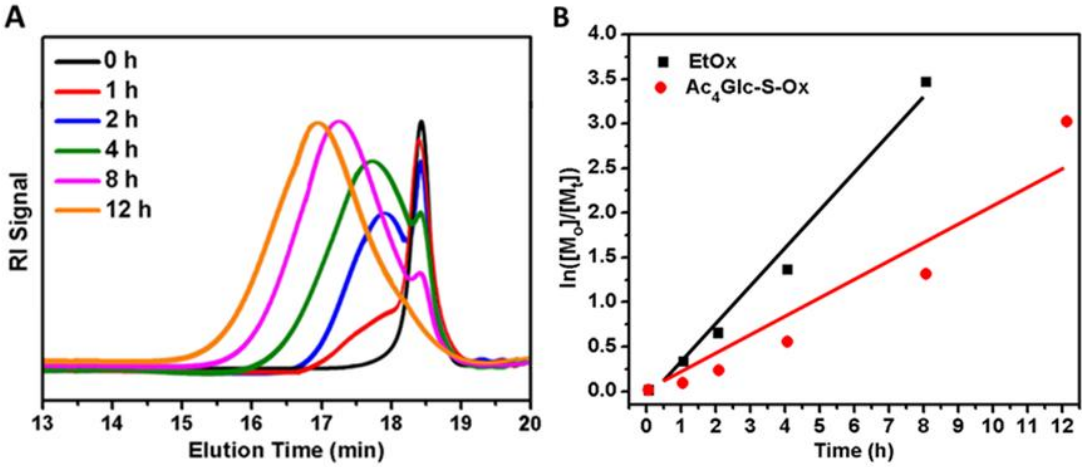


**Figure 5.4. A)** GPC traces of the microwave-assisted copolymerization of EtOx and $Ac_4$Glc-S-Ox ([M]/[I] = 60, EtOx 50, $Ac_4$Glc-S-Ox 10) after different polymerization times at 120 °C; **B)** Monomer conversion, represented by the ratio, plotted against time.

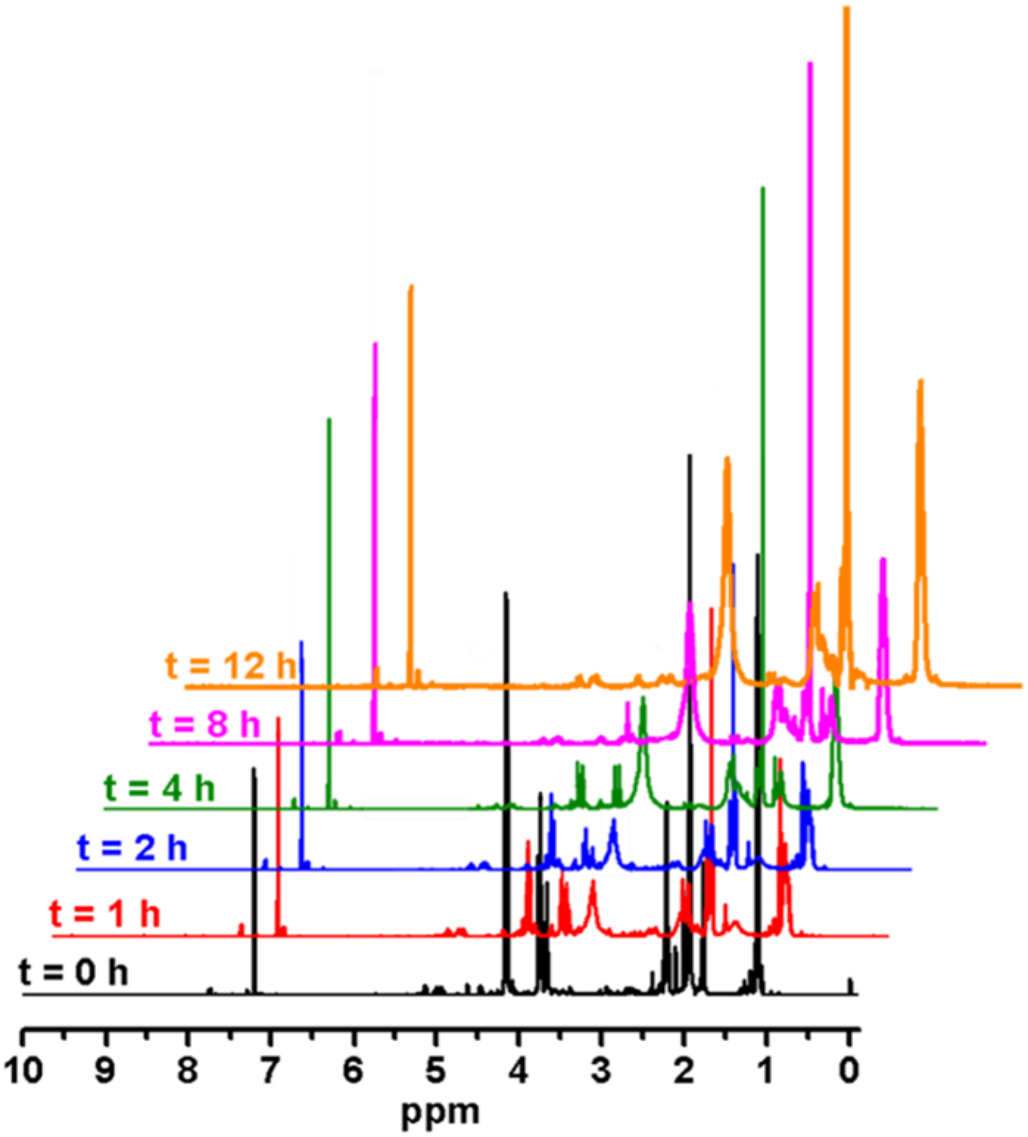


**Figure 5.5.** $^{1}$H-NMR spectra in $CDCl_3$ displaying monomer conversion of EtOx and $Ac_4$Glc-S-Ox at different polymerization time.

In order to obtain further and more detailed investigations, the kinetic study of the statistical copolymerization of EtOx and $Ac_4$Glc-S-Ox was performed with a degree polymerization of 60 (EtOx 50, $Ac_4$Glc-S-Ox 10) and 1M monomer concentration at 120 °C for 12 h in in the microwave synthesizer. Even though the polymerization conversion of EtOx was followed by GC, the sugar substituted 2-oxazoline conversion could not be monitored by GC or $^{1}$H-NMR because of an overlapping of sugar signals with the oxazoline ring signals at 3.8 and 4.2 ppm. Therefore, the conversion of $Ac_4$Glc-S-Ox was estimated roughly from the GPC analysis. As depicted in Figure 5.4, semi-logarithmic kinetic plots of both monomers displayed

displayed a linear increase of conversion with time as expected for both monomers, showing the livingness of the polymerization and the absence of termination reactions. The increase in the molar mass with conversion over time demonstrated the formation of close to ideal random copolymers.

Obviously, the copolymerization of EtOx and $Ac_4$Glc-S-Ox has been achieved with a good control and living characteristics throughout the whole polymerization. Full conversion of both monomers could be obtained after 12 h according to GC and GPC analysis. The polymerization of EtOx proceeded significantly faster than that of $Ac_4$Glc-S-Ox. In particular, the composition of the polymer changed dramatically from a random copolymer to a gradient copolymer structure after 8 h. The number average molar mass ($M_n$), by DMF GPC, generally increased linearly with monomer conversion. However, the $M_n$ by GPC is higher than theoretical molar mass mainly due to the different structure of copolymer with PS calibration standard, which would cause a significant difference of hydrodynamic volume of polymer in DMF. The molar mass distribution kept low ($Đ$ < 1.23) through the whole polymerization. This living/controlled copolymerization process allowed us to prepare a series of well-defined glyco-copolymers (**P1a1-P1c1**) by using EtOx and $Ac_4$Glc-S-Ox monomers with a same degree of polymerization adjusting to 8.3 mol% decrement and increment of $Ac_4$Glc-S-Ox.

As mentioned above, in order to study the effect of sugar substituent alkyl linker length to backbone on the binding ability, copolymers of DecenOx and ButenOx with EtOx were synthesized to prepare glycopolymers by using the polymer post-modification exploiting the photoaddition of $Ac_4$Glc-SH onto pendant alkene functionalities according to previously published reports. Therefore, these copolymerizations were not studied in detail. Each copolymerization was carried out at 120 °C for 12 h in the microwave synthesizer with 1M monomer concentration, as well. Full conversion of monomers was obtained according to GC and $^1$H-NMR. As seen in Table 5.1, it is obvious that the copolymerizations of DecenOx and ButenOx with EtOx have been achieved with a good control due to narrow dispersities with high molar masses.

**Table 5.1.** Summary of monomer conversions, number average molar masses ($M_n$) and molar mass distributions ($Đ$) of cationic ring opening polymerization of the statistical copolymers.

| Polymer Code | [EtOx]:[Targeted Mon]:[I][a] | $\rho$[b] (%) | | $M_{n,GPC}$[c] (g.mol$^{-1}$) | $Đ$ |
|---|---|---|---|---|---|
| | | EtOx | Targeted Mon | | |
| P1a1 = P($(EtOx)_{55}$-co-( $Ac_4$Glc-S-Ox)$_5$) | 55:5:1 | 99 | 98 | 8400 | 1.19 |
| P1b1 = P($(EtOx)_{50}$-co-( $Ac_4$Glc-S-Ox)$_{10}$) | 50:10:1 | 98 | 97 | 10900 | 1.21 |
| P1c1 = P($(EtOx)_{45}$-co-( $Ac_4$Glc-S-Ox)$_{15}$) | 45:15:1 | 98 | 97 | 12800 | 1.23 |
| P2a1 = P($(EtOx)_{55}$-co-(ButenOx)$_5$) | 55:5:1 | 99 | 99 | 7600 | 1.15 |
| P2b1 = P($(EtOx)_{50}$-co-(ButenOx)$_{10}$) | 50:10:1 | 99 | 99 | 7400 | 1.16 |
| P2c1 = P($(EtOx)_{45}$-co-(ButenOx)$_{15}$) | 45:15:1 | 98 | 98 | 7800 | 1.16 |
| P3a1 = P($(EtOx)_{55}$-co-(DecenOx)$_5$) | 55:5:1 | 99 | 99 | 7900 | 1.15 |
| P3b1 = P($(EtOx)_{50}$-co-(DecenOx)$_{10}$) | 50:10:1 | 98 | 98 | 8600 | 1.15 |
| P3c1 = P($(EtOx)_{45}$-co-(DecenOx)$_{15}$) | 45:15:1 | 98 | 97 | 9700 | 1.16 |

[a] Initial molar ratio of monomers to initiator; [b] Conversion ($\rho$) obtained from $^1$H NMR and GC analysis; [c] Determined by DMF GPC (relative to PS stn.)

The more complex copolymer, **P4a1**, containing monomers, namely, EtOx, ButenOx, DecenOx and $Ac_4$Glc-S-Ox was synthesized to compare its LCST behaviour and lectin binding ability with other obtained glyco-copolymers. Hence, the total degree of polymerization was kept same (DP=60) with same amount of ButenOx, DecenOx and $Ac_4$Glc-S-Ox (8.3 mol%, DP=5). All monomers were mixed in the presence of MeOTs as an initiator and acetonitrile as a solvent and then irradiated in the microwave at 120 °C. Full consumption was reached for each monomer after 12 h. The molar mass of the synthesized copolymer obtained by GPC was expectedly higher than the theoretical molar mass with the slight increase in the $Đ$ value due to the broad peak. However, this result is reasonable because of some possible side reaction between monomers.

### 5.2.4 Thiol-ene Photoaddition Reactions of copoly(EtOx-ButenOx)s, copoly(EtOx-DecenOx)s and copoly(EtOx-ButenOx-DecenOx-$Ac_4$Glc-S-Ox) using $Ac_4$Glc-SH

Thiol-ene "*click*" reactions have been gained interest since a wide range of enes and thiols can be clicked. The post-polymerization modification of ene-containing polymers with a thiol functional sugar is one of the most popular and efficient strategy employed to prepare well-defined glycopolymers with different chain

lengths, architectures and functionalities.[26,27] From this perspective, the obtained copoly(EtOx-ButenOx)s, copoly(EtOx-DecenOx)s and copoly(EtOx-ButenOx-DecenOx-$Ac_4$Glc-S-Ox) were modified with $Ac_4$Glc-SH under UV irradiation at ambient temperature in the presence of an UV-labile radical initiator (DMPA) overnight. DMPA was employed to accelerate the reaction. $Ac_4$Glc-SH was used in slight excess (1.2 equivalent with respect to the amount of double bonds) to ensure a complete conversion of the ene groups as investigated by $^1$H NMR spectroscopy and GPC analysis.

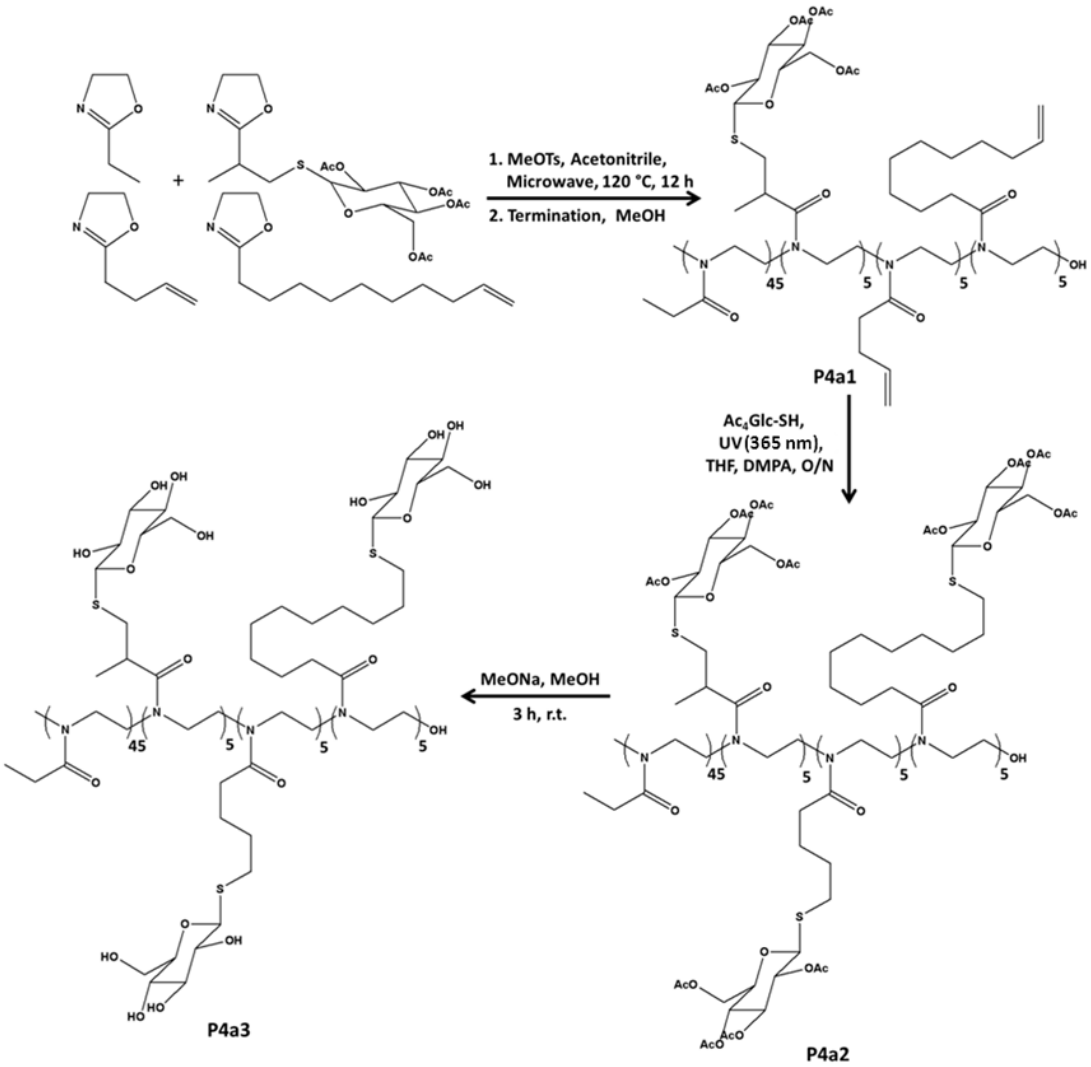


**Scheme 5.3.** Schematic representation of the cationic ring-opening copolymerization of EtOx, $Ac_4$Glc-S-Ox, ButenOx and DecenOx ([M]/[I] = 60, EtOx 45, $Ac_4$Glc-S-Ox 5, ButenOx 5 and DecenOx 5); Thiol-ene reaction and also the deprotection reaction of the copolymer (**P4a1**).

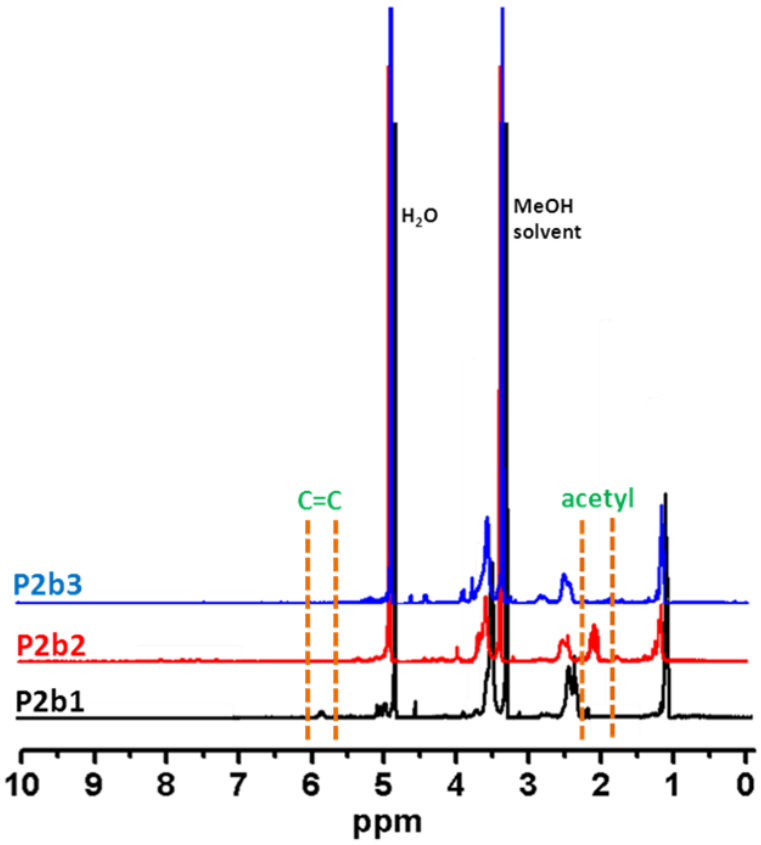


**Figure 5.6.** $^{1}$H NMR characterization (400 MHz, $CD_3OD$) of the obtained copolymers **P2b1**, **P2b2** (thiol-ene product) and **P2b3** (after deacetylation).

As shown in Figure 5.6, the peaks of the alkene groups of copolymers at 5.8-6.0 ppm disappeared and the acetyl protecting groups of sugar appeared at 2.0 ppm according to the completion of the thiol–ene reaction. The GPC traces of copolymers also showed a significant shift due to increase of molar mass after the thio-ene photoaddition reaction with $Ac_4$Glc-SH.

Moreover, there was not any considerable increase in *Đ* values. The FT-IR spectrum revealed the appearance of the stretch at 1745 $cm^{-1}$ originated from the ester bond of acetyl protecting groups, as well.

### 5.2.5 Deprotection of the obtained copolymers

The deprotection of the all copolymers bearing protected sugar moieties was performed by treatment with sodium methoxide solution in MeOH for 3 h at room

temperature. The successful deprotection could be followed by $^{1}$H NMR and FT-IR due to the disappearance of the acetyl protecting groups of sugar. As seen in Figure

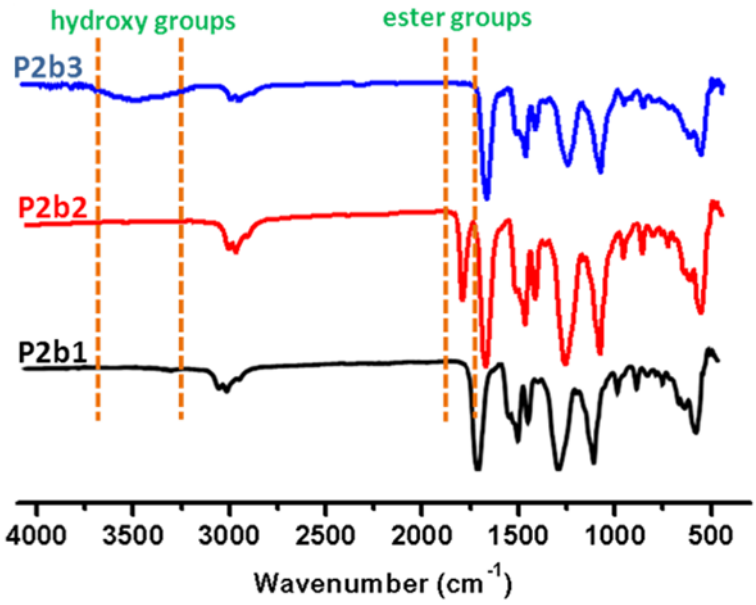


**Figure 5.7.** FT-IR spectra of **P2b1, P2b2** (thiol-ene product) and **P2b3** (after deacetylation) demonstrating successful addition of acetyl-protected glucose units (ester band at 1755 cm$^{-1}$ onto the polymer precursor. The disappearance of the ester band as well as the appearance of a broad band between 3100 cm$^{-1}$ and 3600 cm$^{-1}$ confirms the successful deprotection of the sugar moieties.

5.6 and 5.7, the peak of the acetate groups at 2.0 ppm disappeared in the $^{1}$H NMR spectra and also the signal at 1745 cm$^{-1}$ disappeared after the deacetylation of the protected sugar residues producing free hydroxyl groups that cause a broad stretch at about 3350 cm$^{-1}$ in FT-IR spectrum.

Furthermore, DMF GPC analysis revealed the shift of elution traces after the deprotection reaction due to the change of hydrodynamic volume (Figure 5.8). Even if the theoretical molar mass decreased after the reaction, the $M_n$ by GPC increased because of the clear shift to lower elution volume due to high solubility of the free hydroxyl groups of the sugar moieties with a larger hydrodynamic volume. However, the elution time of GPC traces are in good agreement with the theoretical molecular value of the synthesized glycopolymers (Figure 5.9).

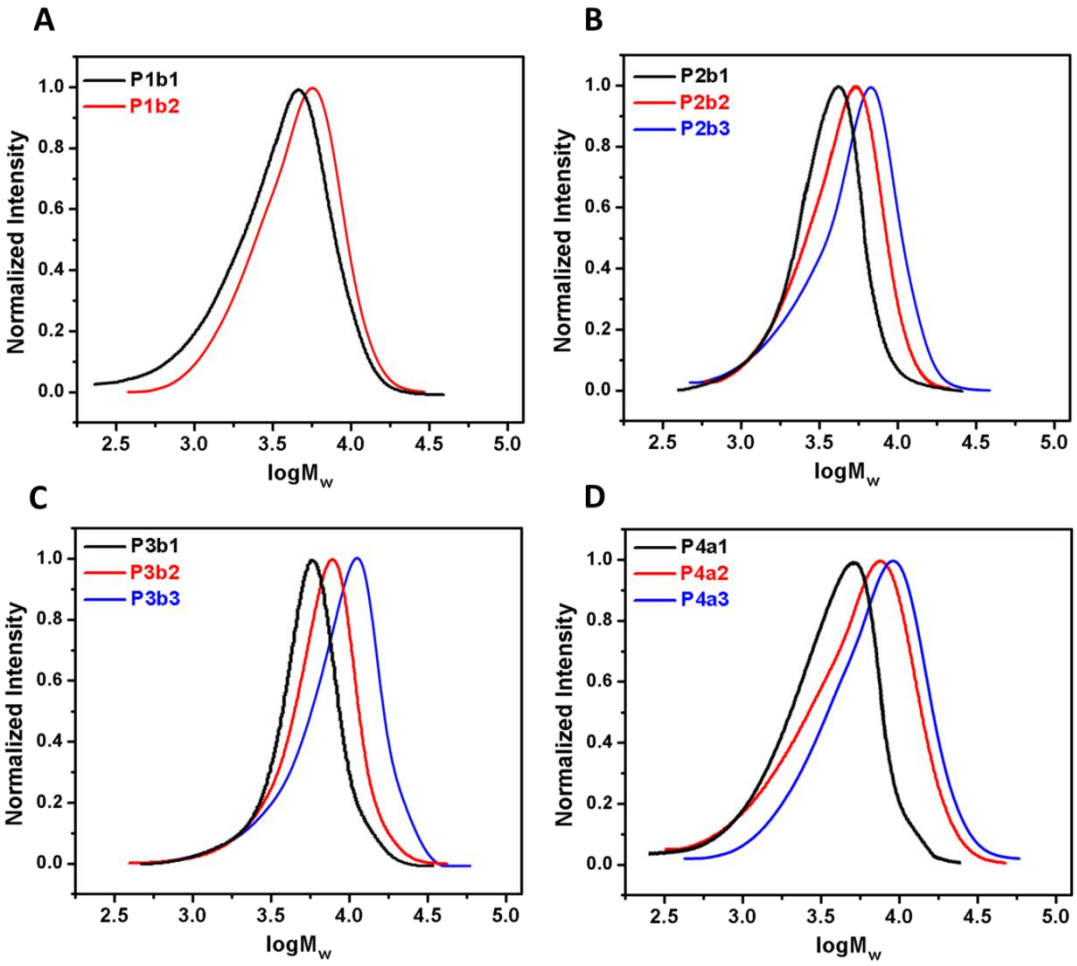


**Figure 5.8.** GPC traces of the copolymers of each series before and after thiol-ene and deprotection reaction; **A**) poly(EtOx-co-$Ac_4$Glc-S-Ox)s; **B)** poly(EtOx-co-ButenOx)s; **C)** poly(EtOx-co-DecenOx)s; **D)** copoly(EtOx-ButenOx-DecenOx-$Ac_4$Glc-S-Ox).

**Table 5.2.** GPC summary ($M_n$ and $Đ$ values; PS calibration) of the obtained deprotected glyco-copolymers.

| | P1a2 | P1b2 | P1c2 | P2a3 | P2b3 | P2c3 | P3a3 | P3b3 | P3c3 | P4a3 |
|---|---|---|---|---|---|---|---|---|---|---|
| $M_{n,GPC}$ (g.mol$^{-1}$) | 9500 | 11400 | 13300 | 9900 | 11700 | 13800 | 10800 | 12900 | 14600 | 13100 |
| $Đ$ | 1.21 | 1.20 | 1.21 | 1.14 | 1.16 | 1.15 | 1.16 | 1.16 | 1.17 | 1.24 |

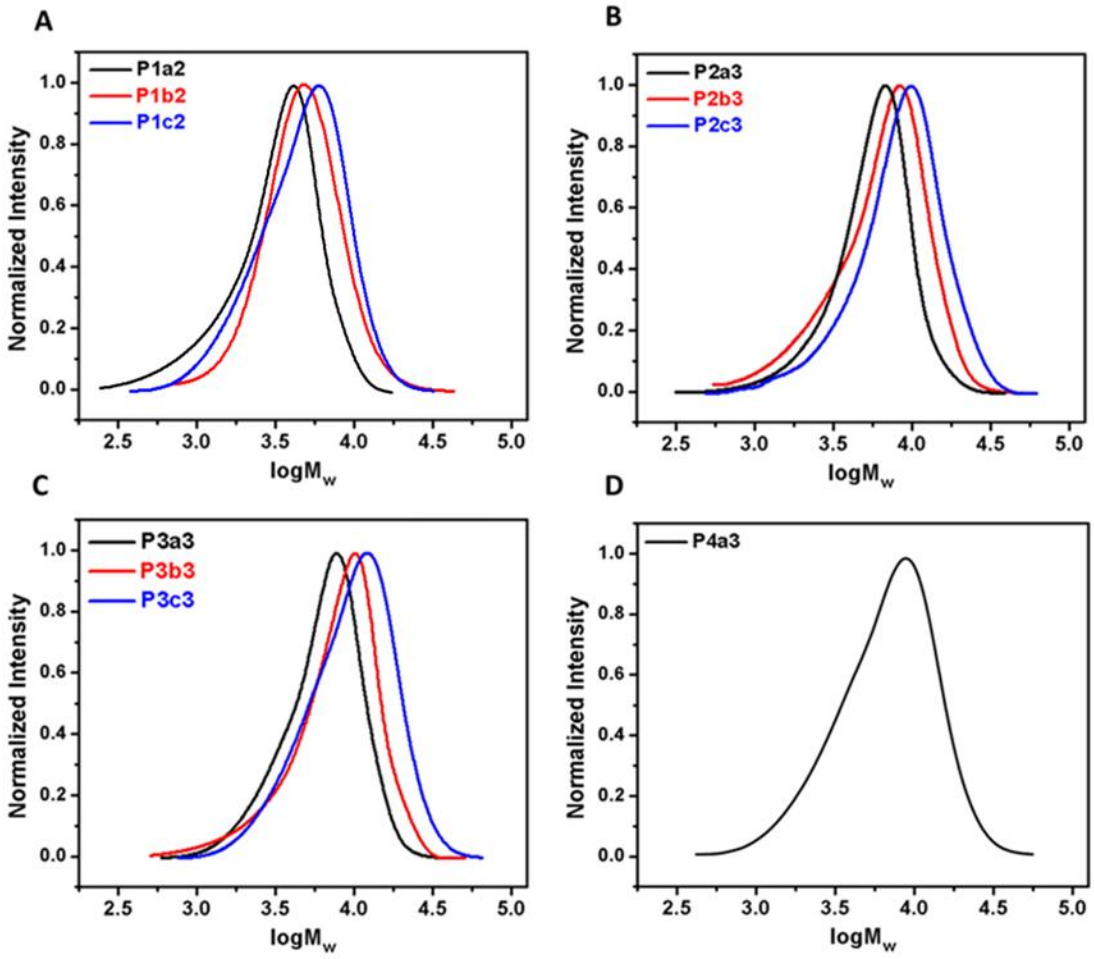


**Figure 5.9.** GPC traces of the (deprotected) glyco-copolymers of each series; **A**) poly(EtOx-co-$Ac_4$Glc-S-Ox)s; **B)** poly(EtOx-co-ButenOx)s; **C)** poly(EtOx-co-DecenOx)s; **D)** copoly(EtOx-ButenOx-DecenOx-$Ac_4$Glc-S-Ox).

### 5.2.6 Solubility of the glycopolymers in aqueous media

Thermal phase transition temperature of the glyco-copolymers was measured as a function of temperature at a polymer concentration of 5 mg/mL in the temperature range from 20 °C and 80 °C in order to investigate the effect of the spacer length between the polymer backbone and the sugar residues and also the ratio of sugar content on the cloud points. In general, the LCST behaviour can be influenced by several properties, such as, the chain length, architecture, hydrophilic-hydrophobic balance and also concentration of the polymers.[28-30] In some cases, the intramolecular interaction could be effective as much as intermolecular interaction on the thermo-responsive behaviour of the polymer. A couple of reports recently published highlighted the LCST behavior of the poly(oxazoline)-based

glycopolymers with different carbohydrate content.[11,26,27] In here, the cloud points of the glyco-copolymers including different alkyl linker lengths of sugar to the polymer backbone and sugar moieties were studied in systematic way to discuss how to provide a sufficient control on the thermo-responsive glycopolymers for specific targeted applications.

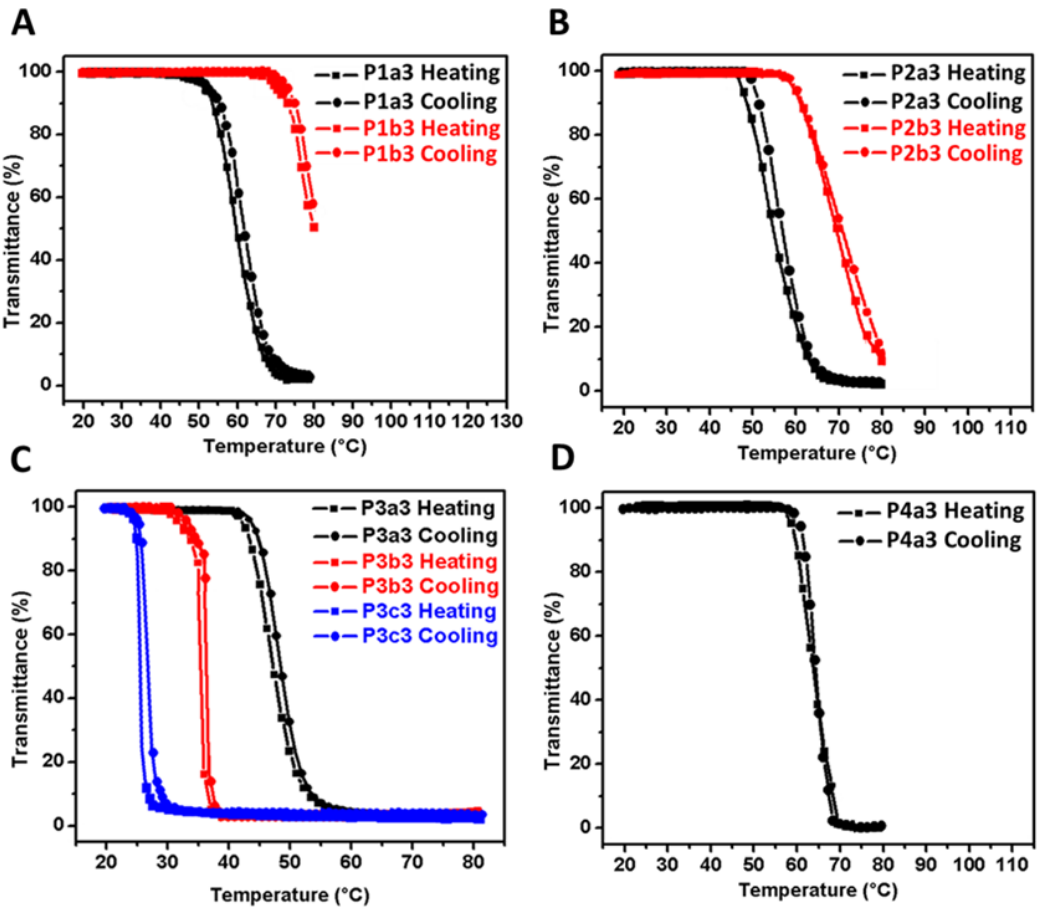


**Figure 5.10.** Turbidity curves for the determination of the cloud points of the (deprotected) glyco-copolymers of each series; **A**) poly(EtOx-co-$Ac_4$Glc-S-Ox)s; **B)** poly(EtOx-co-ButenOx)s; **C)** poly(EtOx-co-DecenOx)s; **D)** copoly(EtOx-ButenOx-DecenOx-$Ac_4$Glc-S-Ox).

As seen in Figure 5.10, the amount of sugar content has a dramatic effect on the LCST value of the glycopolymers. For **P1a2-P1c2** and **P2a3-P2c3**, an increasing the amount of sugar moieties results an increase in the cloud point temperature of the copolymers. In general, the LCST values of all glycopolymers revealed successively phase transitions with a small hysteresis. It is very obvious that there is a

considerable difference on the LCST value between the glycopolymers with the same amount of sugar content. It means that the spacer length between the polymer backbone and the sugar residues has a significant influence on the cloud point of the glycopolymers due to the increase in hydrophobicity of the copolymers with longer alkyl chain sugar substituents.

**Table 5.3.** Cloud point temperatures (°C; heating and cooling cycles) obtained for the corresponding deprotected glycopolymers [not det. = not determined].

| | P1a2 | P1b2 | P1c2 | P2a3 | P2b3 | P2c3 | P3a3 | P3b3 | P3c3 | P4a3 |
|---|---|---|---|---|---|---|---|---|---|---|
| Heating | 61.4 | 80.8 | not det. | 54.3 | 75.9 | not det. | 47.8 | 36.5 | 27.2 | 64.3 |
| Cooling | 62.3 | 81.2 | not det. | 55.7 | 76.3 | not det. | 48.7 | 37.3 | 28.4 | 64.7 |

As can be seen in Table 5.3, the cloud points of the glycopolymers having the shortest alkyl linker of sugar substituents (**P1a2-P1c2**) were found higher than that of other glycopolymers. **P1c2** including a highest degree of glucose has higher LCST value than the investigated temperature range. In contrast, the cloud points of the glycopolymers bearing decenyl chain sugar substituent (**P3a3-P3c3**) exhibited the lowest cloud points between the glyco-copolymers due to the long DecenOx alkyl chains. Furthermore, even though the fraction of the sugar content increased, the cloud point temperature of the glycopolymers decreased as observed by Schubert and co-workers.[26] The series of the glycopolymers bearing decenyl chain sugar substituents displayed the LCST values in the temperature range between 27 °C (**P3c3**) and 47 °C (**P3a3**). The cloud points of ButenOx modified glycopolymers (**P2a3-P2c3**) were found to vary over a temperature range of 15 degrees. The LCST values of glycopolymers with $Ac_4$Glc-S-Ox were observed to be 8 °C higher than that of ButenOx modified glycopolymers for the each same fraction of glucose. For more advanced glycopolymer **P4a3**, the cloud point was obtained like 64 °C which is logical according to the relative results. Therefore, these investigations showed that it is possible to provide an efficient control on the thermo-responsive behavior of the synthesized glycopolymers with the targeted LCST value for different applications. Moreover, it is noteworthy to state that the spacer length between

the polymer backbone and the sugar residues could influence the cloud point of the glycopolymers significantly.

### 5.2.7 Lectin binding studies

Carbohydrate-binding proteins (lectins) that are complicated and important molecules for many biological process and living organisms open the doors of biological entities to glycans.[31,32] ConA that is known to specifically bind to mannosyl and glucosyl moieties represents four binding sites enabling the interaction of up to for sugar residues.

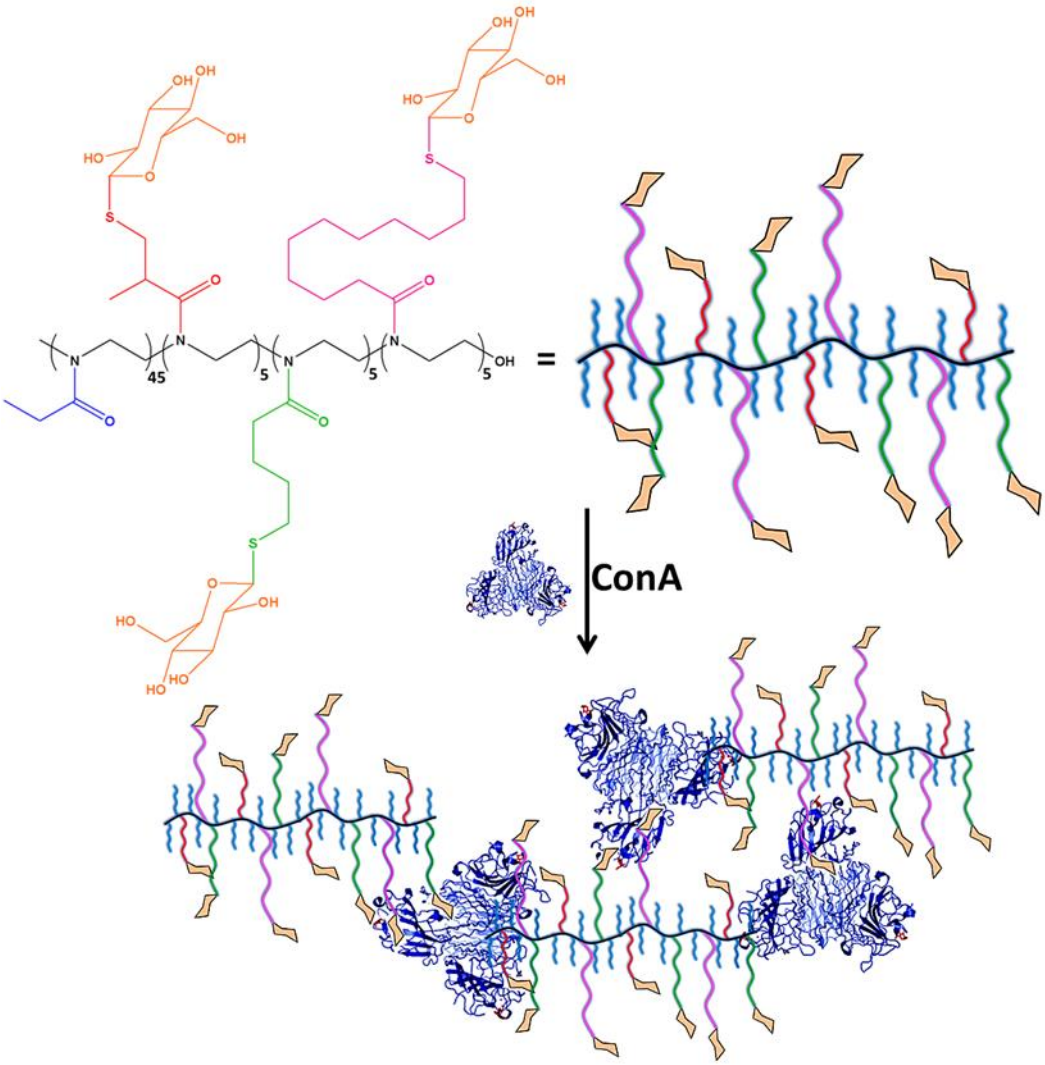


**Scheme 5.4.** Illustration of the interaction between **P4a3** glycopolymer and ConA.

The formation of aggregates created by the binding of glycopolymers with lectin can be monitored by UV-vis spectrometer due to the loss of intensity of

transmitted light.[33] Turbidimetry is the most common used techniques to determine the turbidity of the solution at varying ratio of lectin to glycopolymers. Hence, this approach was performed to analyze the binding capability of the obtained glycopolymers with ConA.

Turbidimetry assay was followed a modified procedure.[33] All glycopolymers were dissolved in a freshly prepared HBS buffer solution (320 μM) and then added into ConA solution (60 μM), which was placed in the UV spectrometer. The absorbance of the mixture was quickly recorded at 420 nm for 15 min every 0.12 s.

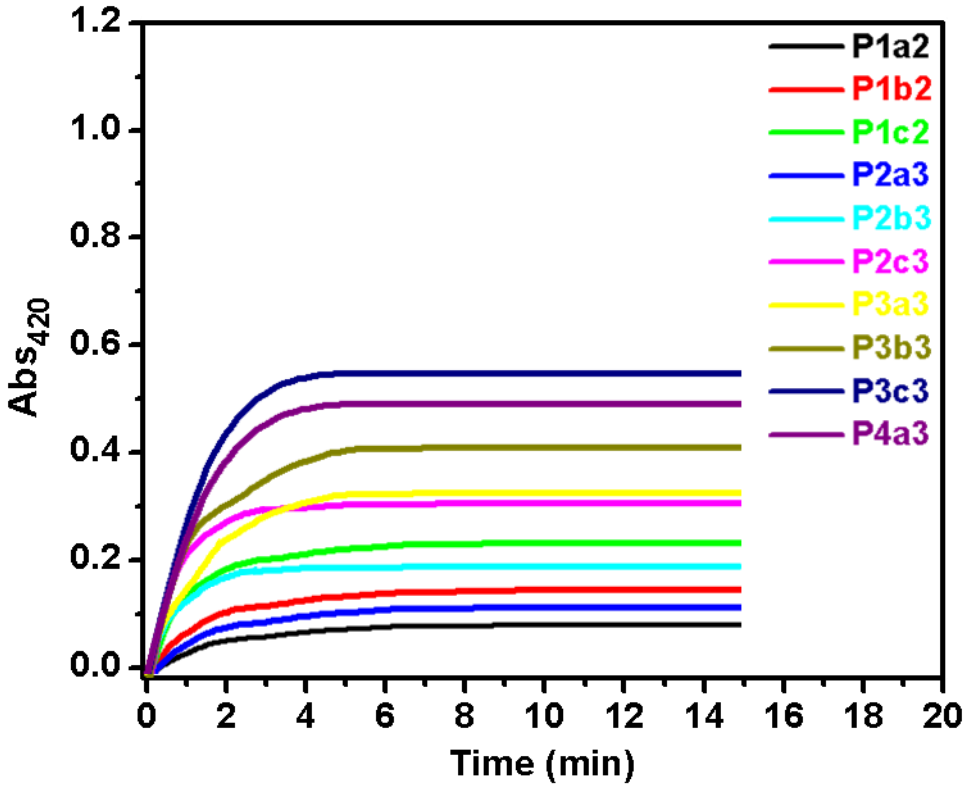


**Figure 5.11.** Turbidity measurements of the obtained glycopolymers with ConA.

**P3c3** containing the longest linker space showed the highest binding affinity through glycopolymers. However, the more complex glycopolymer, **P4a3**, represented the similar high binding capability, as well. Additionally, the binding ability of the obtained glycopolymers showed the relationship with the sugar density. Expectedly, **P1a2** interacted weakly with ConA due to its low sugar density and also short linker space because it decreases the accessibility of sugar residues. As seen in Figure 5.11, while there is not big difference between the glycopolymers

bearing short linker space (**P1a2-P1c2**), **P3** series showed a significant increase on the binding capability with ConA. The obtained results confirmed that the interaction between glycopolymers and lectins can be enhanced dramatically by changing the polymer structure. In particular, the binding between glycopolymers and ConA was greatly enhanced by longer linker space. Hence, it is obvious that the length of linker space has an important influence on its binding activity due to its more flexibility. This flexibility provides more accessibility and avidity to carbohydrate moieties.

## 5.3 Conclusion

In summary, glyco copoly(oxazoline)s containing different glucose substituents alkyl linker length to the polymer backbones were synthesized *via* cationic ring opening polymerization successfully. A simple, one-pot, easy and versatile synthetic strategy was firstly described to prepare a new *S*-glucosyl substituted 2-oxazoline glycomonomer *via* thiol-ene "*click*" chemistry without any rigorous *and* intensive purification. This new glycomonomer was characterized by $^{1}$H NMR, $^{13}$C NMR and ESI-MS. A systematical study of the cloud points of the obtained glycol copoly(oxazoline)s was performed to examine the effect of the spacer length between the polymer backbone and the sugar residues and also the ratio of sugar content. The results showed that it is possible to provide an efficient control on the thermo-responsive behaviour of the synthesized glycopolymers with the targeted LCST value for different applications. Moreover, ConA was used to investigate the influence of sugar linker length to the polymer backbone on the bioactivity and bioavailability of the synthesized glycopolymers. The results showed that the length of linker space has a significant effect on the binding capability.

## 5.4 Experimental

### 5.4.1 Materials

4-pentenoyl chloride (98%), 10-undecenoyl chloride (97%), acetonitrile (anhydrous, 99.8%, ACN), (2-chloroethyl)trimethylammonium chloride (98%), sodium methoxide (95%, powder), 2,3,4,6-tetra-*O*-acetyl-1-thio-β-D-glucopyranose ($Ac_4$Glc-SH, 97%),

2-ethyl-2-oxazoline (EtOx, ≥99%), 2-Isopropenyl-2-oxazoline (iPOx, 98%) and methyl *p*-toluenesulfonate (MeOTs, 98%), 2,2-dimethoxy-2-phenylacetophenone (DMPA, 98%), Merrifield's peptide resin (1% cross-linked), butylamine (99.5%) were purchased from Sigma Aldrich Chemical Company (Dorset, UK). EtOx, iPOx and methyl *p*-toluenesulfonate were distilled and stored over activated *4Å* molecular sieves under an argon atmosphere. All other reagents and solvents were obtained at the highest purity available from Sigma Aldrich Chemical Company (Dorset, UK) and used as received unless stated otherwise. Dialysis tube (1kDa MWCO) was purchased from Spectrum Laboratories (California, USA).

### 5.4.2 Instruments and Analysis

The Emrys Liberator single-mode microwave synthesizer from Biotage equipped with a non-invasive IR sensor (accuracy: ± 2%) was used for the microwave assisted cationic ring-opening polymerization. All polymerizations were performed with temperature control. Microwave vials were firstly heated to 120 °C and then allowed to cool to room temperature under an argon atmosphere before usage.

Proton and carbon-13 ($^{1}$H-NMR and $^{13}$C-NMR) nuclear magnetic resonance spectroscopy (Bruker DPX-400/600) were used to determine the chemical structure of the synthesized polymers. Samples were dissolved at 5 mg/mL concentration in $CDCl_3$ or MeOH-$d_4$ solvents depending on the solubility of the samples.

Size-exclusion chromatography (SEC) measurements were conducted on an Agilent 1260 infinity system operating in DMF with 5.0 mM $NH_4BF_4$ and equipped with refractive index detector (RID) and variable wavelength detector (VWD), 2 PLgel 5 µm mixed-C columns (300×7.5mm), a PLgel 5 mm guard column (50x7.5mm) and an autosampler. The instrument was calibrated with linear narrow poly(styrene) standards in range of 575 to 281,700 g.mol$^{-1}$. All samples were passed through 0.2 µm PTFE filter before analysis.

Gas Chromatography (GC) was used to measure monomer conversion for polymerizations. GC analysis was performed using an Agilent Technologies 7820A. An Agilent J&W HP-5 capillary column of 30 m x 0.320 mm with a film thickness of

0.25 mm was used. The oven temperature was programmed as follows: 40 °C (hold for 1 min) increase at 30 °C/min to 300 °C (hold for 2.5 min). The injector was operated at 250 °C and the FID was operated at 320 °C. Nitrogen was used as carrier gas at flow rate of 6.5 mL/min and a split ratio of 1:1 was applied. Chromatographic data was processed using OpenLab CDS ChemStation Edition, version C.01.05.

Beckman DU Series 700 UV/Vis Scanning Spectrophotometer was used to analyze the binding ability of the nanoparticles. SPR Sensorgrams were recorded in a Biorad ProteOn XPR36 SPR biosensor (Biorad, Hercules CA). Soluble DC-SIGN was immobilized to 6000 response units (RU) on discrete channels within Biorad GMC sensor chips *via* amine coupling. Soluble-phase analytes were prepared in 25 mM HEPES pH 7.4, 150 mM NaCl, 5 mM $CaCl_2$, 0.01% Tween-20 and flowed over the immobilized materials at a rate of 25 µL/min at 25 °C. Regeneration of the sensor chip surfaces was performed using 10 mM glycine pH 2.5.

The FT-IR spectra were recorded on a Bruker FT-IR spectrometer TENSOR II with Diamond-ATR module. The scanning range was 600-4000 $cm^{-1}$ and the resolution was 1 $cm^{-1}$.

LCST and turbidimetry measurements were performed on a Cary 100 UV-Vis spectrophotometer (Agilent) at a wavelength of 500 nm. Solutions of polymers were prepared in water (HPLC grade) at a concentration of 5 mg/mL and stirred until fully dissolved. The samples were thermostatted at 20 °C for 15 minutes prior to measurement. The transmittance was measured between 20 °C and 80 °C at a rate of 1 °C $min^{-1}$ in a heating and cooling cycle. The cloud points reported were determined as the 50% transmittance point during the heating cycle.

Electrospray ionization-mass spectrometry (ESI-MS) spectra were recorded on a Thermo Finnigan LCQ Decaquadrupole ion trap mass spectrometer (Thermo Finnigan, San Jose, CA), equipped with an atmospheric pressure ionization source operating in the nebulizer assisted electrospray mode and was used in positive ion mode.

### 5.4.3 Synthesis of the solid butylamine resin

Based on a literature procedure, in a 250 mL round-bottom containing a magnetic stir bar butylamine (15 g, 200 mmol) was dissolved in DMF (50 mL).[34] Merrifield's peptide resin (10 g, 40 mmol) was added into the reaction flask and refluxed overnight. The solid resin was filtered and then washed with 150 mL of dichloromethane two times until unreacted butylamine was removed. Subsequently, the obtained butylamine solid resin was dried under vacuum at ambient temperature overnight and analyzed by FT-IR.

### 5.4.4 Synthesis of 2-[2-(2,3,4,6-Tetra-*O*-acetyl-β-D-glucopyranosylthio) propyl)]-2-oxazoline ($Ac_4$Glc-S-Ox) glycomonomer

This new glycomonomer, $Ac_4$Glc-S-Ox, was synthesized by using photo-induced thiol-ene coupling reaction of the ene bond of iPOx *with* $Ac_4$Glc-SH. This easy and one-pot strategy used to synthesize *S*-glycosyl substituted 2-oxazoline is depicted in Scheme 1. The thiol-ene "*click*" reaction was carried out in anhydrous acetonitrile (ACN) at 365 nm UV lamp under an argon atmosphere. $Ac_4$Glc-SH (437.3 mg, 1.2 mmol) and iPOx *(*133.4 mg, 1.2 mmol) were dissolved in 1.2 mL anhydrous acetonitrile and then the solid butylamine resin (203.7 mg, 0.64 mmol) as a catalyst was added into the reaction solution under an argon. After degassing the solution for 15 min, the reaction solution was irradiated at 365 nm UV lamp overnight. The reaction was followed by $^1$H-NMR and GC. The solid butyl amine resin was filtered and the proposal chemical structure of the product was confirmed by $^1$H-NMR, $^{13}$C-NMR and ESI-MS after removing of the solvent by a rotary evaporator. The product was obtained as a pale white gummy material. (553.5 mg, yield: 97%) The obtained product was used directly for co-polymerization without any further purification.

$^1$H-NMR (400 MHz, $CDCl_3$, 298 K, ppm): δ = 5.24 (1H, m, H-3), 5.00-5.11 (1H, m, H-4), 4.57-5.01 (1H, m, H-2), 4.51 (1H, dd, J= 9.9 Hz, H-1), 4.24 (2H, t, J= 9.6 Hz, $NCH_2CH_2O$), 4.08–4.19 (2H, m, H-6), 3.83 (2H, t, J= 9.6 Hz, $NCH_2CH_2O$), 3.72 (1H, m, H-5), 2.92–3.08 (1H, m, $CH2CH_3CHCN(O)$), 2.63 (2H, m, $CH2CH_3CHCN(O)$), 1.99, 2.04, 2.09, 2.16 (12H, 4s, $COCH_3$ ), 1.22 (3H, dd, J= 9.4 Hz, $CHCH_3$).

$^{13}$C-NMR (400 MHz, $CDCl_3$, 298 K, ppm): δ = 173.45-174.17, 161.26, 84.78, 76.81, 74.36, 69.49, 68.71, 67.54, 53.67, 32.83, 31.23, 19.89, 17.47.

ESI-MS m/z: calculated for $C_{20}H_{29}NO_{10}S$ ($M+H^+$), 475.15; found, 475.16.

### 5.4.5 Synthesis of 2-butenyl-2-oxazoline (ButenOx)

ButenOx and DecenOx were prepared according to the procedure reported by Kempe *et al*.[17] 4-pentenoyl chloride (5.37 g, 0.045 mol) and 2-chloroethylammonium chloride (5.33 g, 0.046 mol) were suspended in 100 mL anhydrous dichloromethane and then the reaction solution was cooled to 0 °C. Subsequently, triethylamine ($Et_3N$) (14.6 mL, 0.104 mol) were added dropwise within one hour and the reaction mixture was stirred for three more hours at room temperature. The reaction was terminated by adding 30 mL water. The aqueous phase was extracted 3 times with 25 mL dichloromethane and then the combined organic phases were washed with water and brine, respectively. After drying over magnesium sulfate (MgSO4), the solvent was removed by a rotary evaporator and then the obtained crude product was dissolved in methanol and used for next step without any further purification. A 25 wt% solution of potassium hydroxide (KOH) in methanol (MeOH) was added dropwise into the solution and the reaction solution was heated to 70 °C and stirred for 48 h. After removing of MeOH under reduced pressure, 30 mL was added and extracted 3 times with diethyl ether and then the combined organic phases were washed with water and brine again. After drying over magnesium sulfate (MgSO4), the solvent was removed by a rotary evaporator and then the obtained crude product was purified by distillation (55 °C, $1.2 \times 10^{-2}$ mbar) to give 2.26 g (0.018 mol) of ButenOx in 42% yield (relative to the 4-pentenoyl chloride).

$^{1}$H-NMR (400 MHz, $CDCl_3$, 298 K, ppm): δ = 5.76-5.88 (m, 1H, CHCH2), 4.96-5.10 (m, 2H, CHCH2), 4.21 (t, 2H, *J* = 9.0 Hz, OCH2), 3.82 (t, 2H, *J* = 9.0 Hz, NCH2), 2.34-2.42 (m, 4H, CH2).

$^{13}$C-NMR (400 MHz, $CDCl_3$, 298 K, ppm): δ = 167.76, 138.97, 118.61, 67.35, 54.52, 29.37, 27.44.

ESI-MS m/z: calculated for $C_7H_{11}NO$ ($M+H^+$), 125.08; found, 125.10.

### 5.4.6 Synthesis of 2-decenyl-2-oxazoline (DecenOx)

10-undecenoylchloride (10 g, 0.084 mol) and 2-chloroethylammonium chloride (9.86 g, 0.085 mol) were suspended in 200 mL anhydrous dichloromethane and then the reaction solution was cooled to 0 °C. Subsequently, $Et_3N$ (27 mL, 0.193 mol) were added dropwise within one hour and the reaction mixture was stirred for three more hours at room temperature. The reaction was terminated by adding 60 mL water. The aqueous phase was extracted 3 times with 50 mL dichloromethane and then the combined organic phases were washed with water and brine, respectively. After drying over MgSO4, the solvent was removed by a rotary evaporator and then the obtained crude product was dissolved in methanol and used for next step without any further purification. A 25 wt% solution of KOH in MeOH was added dropwise into the solution and the reaction solution was heated to 70 °C and stirred for 48 h. After removing of MeOH under reduced pressure, 60 mL was added and extracted 3 times with diethyl ether and then the combined organic phases were washed with water and brine again. After drying over MgSO4, the solvent was removed by a rotary evaporator and then the obtained crude product was purified by distillation (85 °C, $1.2 \times 10^{-2}$ mbar) to give 7.2 g (0.034 mol) of ButenOx in 72% yield (relative to the 10-undecenoylchloride).

$^1$H-NMR (400 MHz, $CDCl_3$, 298 K, ppm): δ = 5.80 (m, 1H, CH2), 4.95 (m, 2H, CH), 4.21 (t, 2H, *J* = 9.6 Hz, CH2), 3.81 (t, 2H, *J* = 9.6 Hz, CH2), 2.26 (t, 2H, *J* = 7.6 Hz, CH2), 2.03 (m, 2H, CH2), 1.61 (m, 2H, CH2), 1.31 (m, 10H, CH2).

$^{13}$C-NMR (400 MHz, $CDCl_3$, 298 K, ppm): δ = 169.63, 138.26, 114.91, 68.65, 54.19, 33.85, 29.83, 29.21, 29.10, 28.92, 25.87, 24.94, 23.67.

ESI-MS m/z: calculated for $C_{13}H_{23}NO$ ($M+H^+$), 209.18; found, 209.23.

### 5.4.7 Microwave-assisted copolymerization of EtOx with $Ac_4$Glc-S-Ox, ButenOx and DecenOx

As a general procedure, a polymerization solution of initiator (methyl *p*-toluenesulfonate), monomers (EtOx, $Ac_4$Glc-S-Ox, ButenOx and DecenOx) and solvent (acetonitrile) was prepared. The total monomer concentration was adjusted to 1 M with a [EtOx]:[targeting monomer]:[I] = 55:5:1, 50:10:1, 45:15:1 for each targeting monomer, respectively. Preheated to 150 $^0$C microwave vials were allowed to cool to room temperature under an argon atmosphere before the polymerization solutions was transferred into vials. Vials were capped and the solutions were allowed to polymerize at 120 °C for 12 h in the microwave synthesizer. After cooling, the reaction was quenched by the addition of 25 µL MeOH. Samples were taken for GC, $^1$H NMR and GPC analysis to determine the monomer conversions and the molar mass and dispersity (*Đ*) of the polymers. For the calculations of the monomer conversions, the polymerization solvent was used as internal standard. The obtained copolymers were purified by precipitation in ice-cold diethyl ether for twice and then dried in a vacuum oven at 40 $^0$C for 3 h.

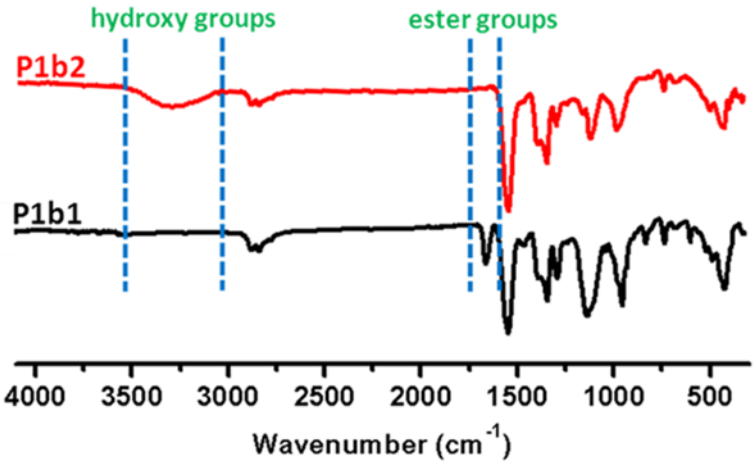


**Figure 5.12.** FT-IR spectra of the synthesized glyco-copolymer (EtOx and $Ac_4$Glc-S-Ox), **P1b1** and **P1b2** (after deacetylation) demonstrating acetyl-protected glucose units (ester band at 1755 cm$^{-1}$ onto the polymer precursor. The disappearance of the ester band as well as the appearance of a broad band between 3100 cm$^{-1}$ and 3600 cm$^{-1}$ confirms the successful deprotection of the sugar moieties.

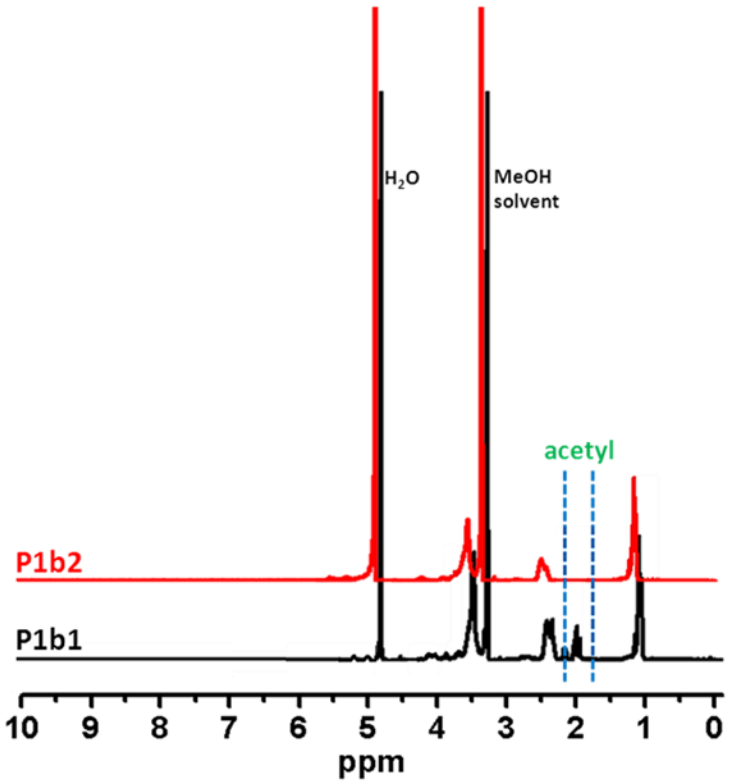


**Figure 5.13.** $^{1}$H NMR characterization of the synthesized glyco-copolymer (EtOx and $Ac_4$Glc-S-Ox), before (**P1b1**) and after (**P1b2**) the deprotection of the acetyl groups.

### 5.4.8 Preparation of the copoly(EtOx-ButenOx-DecenOx-$Ac_4$Glc-S-Ox) P4a1

A solution containing initiator, monomers (EtOx, ButenOx, DecenOx and $Ac_4$Glc-S-Ox), and solvent (acetonitrile) was polymerized at 120 °C for 12 h in the microwave synthesizer. The total monomer concentration was 1.0 M again and a total monomer to initiator ([M]/[I]) ratio of 60 was applied containing same mole ratio (8.3%) for ButenOx, DecenOx and $Ac_4$Glc-S-Ox (EtOx 45, ButenOx 5, DecenOx 5 and $Ac_4$Glc-S-Ox 5). The conversion of monomers was followed GC and $^{1}$H NMR. The obtained copolymer was purified by precipitation in ice-cold diethyl ether for twice and then dried in a vacuum oven at 40 $^{0}$C for 3 h.

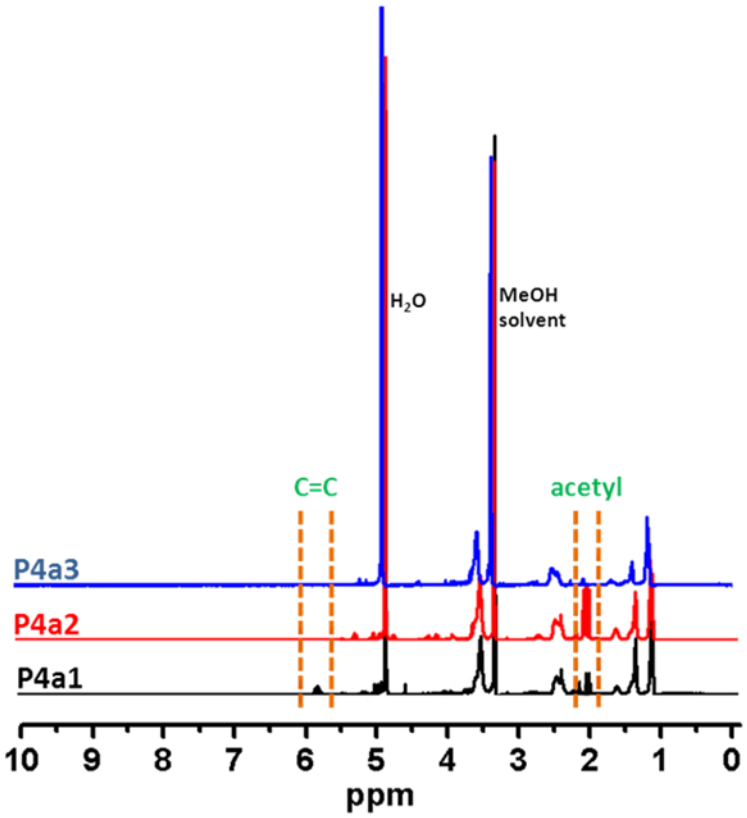


**Figure 5.14.** $^{1}H$ NMR characterization (400 MHz, $CD_3OD$) of the obtained copolymers **P4a1**, **P4a2** (thiol-ene product) and **P4a3** (after deacetylation).

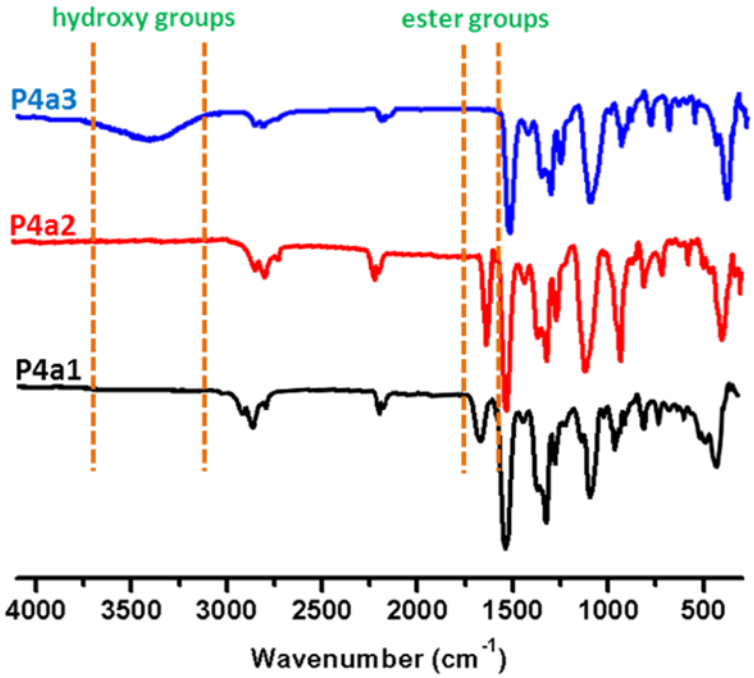


**Figure 5.15.** FT-IR spectra of **P4a1, P4a2** (thiol-ene product) and **P4a3** (after deacetylation) demonstrating successful addition of acetyl-protected glucose units

(ester band at 1755 $cm^{-1}$ onto the polymer precursor. The disappearance of the ester band as well as the appearance of a broad band between 3100 $cm^{-1}$ and 3600 $cm^{-1}$ confirms the successful deprotection of the sugar moieties.

### 5.4.9 Thiol-ene Photoaddition Reactions of poly(EtOx-co-ButenOx)s and poly(EtOx-co-DecenOx)s using $Ac_4$Glc-SH

The synthesized copolymers (75-100 mg) were dissolved in 3 mL dry THF and $Ac_4$Glc-SH was added in 1.2-fold excess with respect to the double bonds. After the addition of 2,2-dimethoxy-2-phenylacetophenone (DMPA), the reaction solutions were degassed for 30 min and then irradiated at 365 nm UV lamp overnight. The resulting copolymers were purified by precipitation in ice-cold diethyl ether for twice and then dried in a vacuum oven at 40 $^0$C for 3 h.

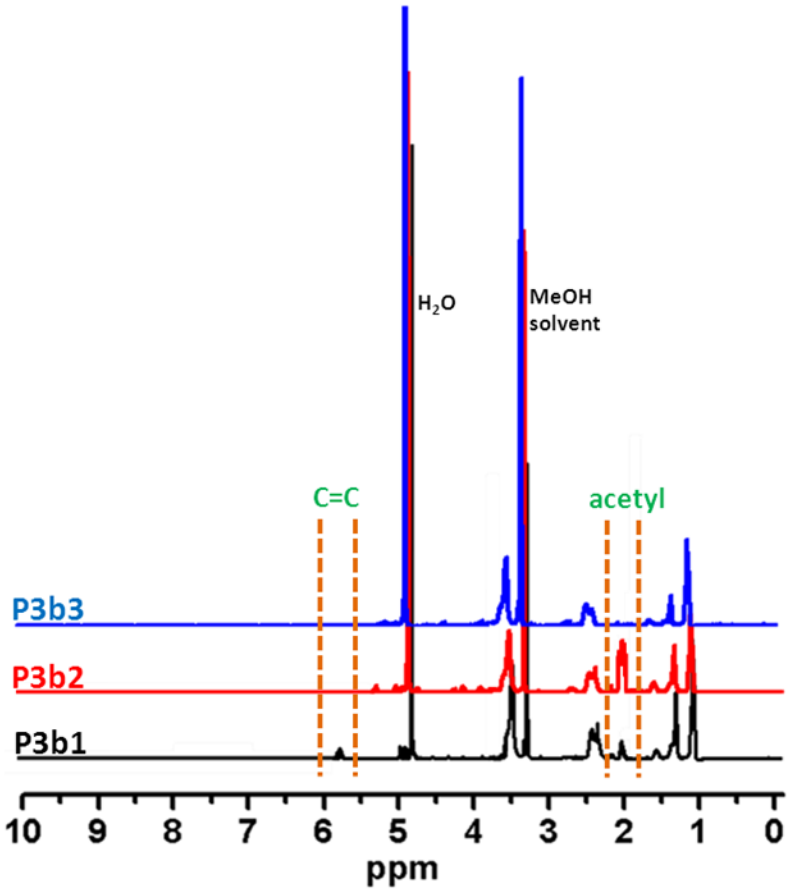


**Figure 5.16.** $^1$H NMR characterization (400 MHz, $CD_3OD$) of the obtained copolymers **P3b1**, **P3b2** (thiol-ene product) and **P3b3** (after deacetylation).

### 5.4.10 Deprotection of the synthesized acetyl-protected glyco-copolymers

The obtained protected glycopolymers (100-150 mg) were dissolved in 5 mL MeOH. 1 mL of 2.0 M sodium methoxide solution was added and the reaction solution was stirred for 3 h. After the removal of MeOH *via* rotary evaporator, the obtained polymer re-dissolved in water and neutralized with diluted HCl solution. Subsequently, the mixture was directly transferred to one dialysis tubing and dialyzed against water for 3 days after which the glycopolymer could be recovered by freeze drying.

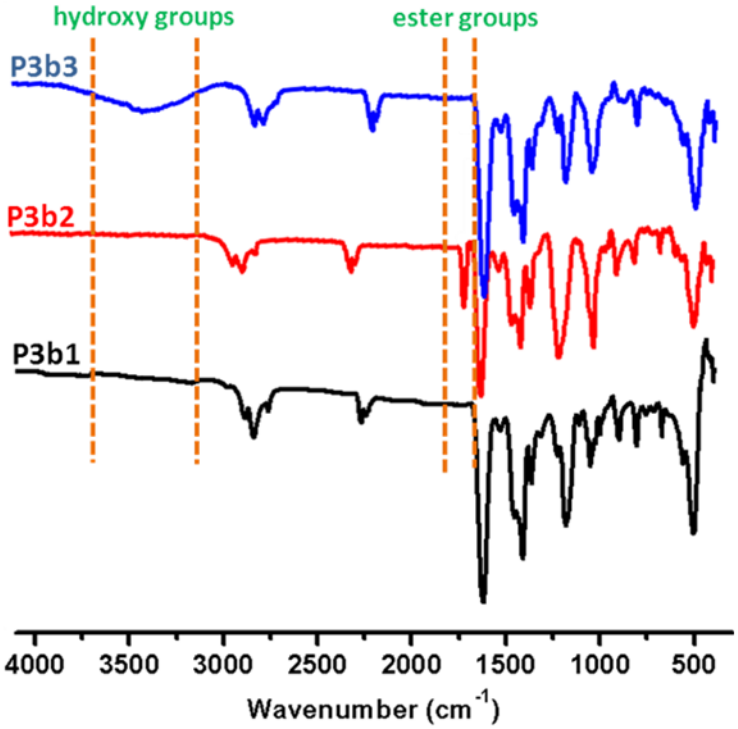


**Figure 5.17.** FT-IR spectra of **P3b1, P3b2** (thiol-ene product) and **P3b3** (after deacetylation) demonstrating successful addition of acetyl-protected glucose units (ester band at 1755 $cm^{-1}$ onto the polymer precursor. The disappearance of the ester band as well as the appearance of a broad band between 3100 $cm^{-1}$ and 3600 $cm^{-1}$ confirms the successful deprotection of the sugar moieties.

### 5.4.11 Cloud point measurements

The glyco-copolymers were dissolved in HPLC grade water at a constant concentration of 5 mg/mL. The turbidity of the solutions was determined in two temperature cycles ranging from 20 to 80 °C at a rate of 1 °C $min^{-1}$ in a heating and

cooling cycle. The cloud point temperatures were determined at 50% transmittance.

### 5.4.12 Lectin binding studies

All experiments were conducted with HEPES-buffered saline (HBS) (0.10 M HEPES, 0.9 M NaCl, 1 mM $MgCl_2$, 1 mM $CaCl_2$, and 1 mM $MnCl_2$ adjusted to pH 7.4 and filtered with 0.2 µm regenerated cellulose syringe filter. A solution of 60 µM ConA in HBS buffer solution was prepared fresh before the assay. Turbidity measurements were performed by adding 350 µL of the ConA solution to a dry quartz microcuvette and put into the holder of UV-visible spectrophotometry at a certain temperature for 1 min. A solution of the ligand in HBS buffer (350 µL at 320 µM) was added into into the cuvette *via* a pipette, the absorbance of the mixture was quickly recorded at 420 nm for 15 min every 0.12 s.

## 5.5 References

(1) Gamblin, D. P.; Scanlan, E. M.; Davis, B. G. *Chemical Reviews* **2009**, *109*, 131.
(2) Ting, S. R. S.; Chen, G.; Stenzel, M. H. *Polymer Chemistry* **2011**, *2*, 2917.
(3) Geng, J.; Biedermann, F.; Zayed, J. M.; Tian, F.; Scherman, O. A. *Macromolecules* **2011**, *44*, 4276.
(4) Pieters, R. J. *Org. Biomol. Chem.* **2009**, *7*, 2013.
(5) Kiessling, L. L.; Splain, R. A. *Annual Review of Biochemistry* **2010**, *79*, 619.
(6) Ahmed, M.; Wattanaarsakit, P.; Narain, R. *European Polymer Journal* **2013**, *49*, 3010.
(7) Yilmaz, G.; Becer, C. R. *Frontiers in Bioengineering and Biotechnology* **2014**, *2*.
(8) Yilmaz, G.; Becer, C. R. *European Polymer Journal* **2013**, *49*, 3046.
(9) Yilmaz, G.; Becer, C. R. *Polymer Chemistry* **2015**, *6*, 5503.
(10) Makino, A.; Kobayashi, S. *Journal of Polymer Science Part A: Polymer Chemistry* **2010**, *48*, 1251.
(11) Kempe, K.; Weber, C.; Babiuch, K.; Gottschaldt, M.; Hoogenboom, R.; Schubert, U. S. *Biomacromolecules* **2011**, *12*, 2591.
(12) Takasu, A.; Kojima, H. *Journal of Polymer Science Part A: Polymer Chemistry* **2010**, *48*, 5953.
(13) Rossegger, E.; Schenk, V.; Wiesbrock, F. *Polymers* **2013**, *5*, 956.
(14) Kempe, K.; Lobert, M.; Hoogenboom, R.; Schubert, U. S. *Journal of Combinatorial Chemistry* **2009**, *11*, 274.
(15) Hoogenboom, R. *Angewandte Chemie International Edition* **2009**, *48*, 7978.

(16) Diehl, C.; Schlaad, H. *Chemistry – A European Journal* **2009**, *15*, 11469.
(17) Kempe, K.; Vollrath, A.; Schaefer, H. W.; Poehlmann, T. G.; Biskup, C.; Hoogenboom, R.; Hornig, S.; Schubert, U. S. *Macromolecular Rapid Communications* **2010**, *31*, 1869.
(18) Ting, S. R. S.; Chen, G.; Stenzel, M. H. *Polymer Chemistry* **2010**, *1*, 1392.
(19) Lowe, A. B. *Polymer Chemistry* **2010**, *1*, 17.
(20) Slavin, S.; Burns, J.; Haddleton, D. M.; Becer, C. R. *European Polymer Journal* **2011**, *47*, 435.
(21) Koo, S. P. S.; Stamenović, M. M.; Prasath, R. A.; Inglis, A. J.; Du Prez, F. E.; Barner-Kowollik, C.; Van Camp, W.; Junkers, T. *Journal of Polymer Science Part A: Polymer Chemistry* **2010**, *48*, 1699.
(22) Acosta Ortiz, R.; García Valdez, A. E.; Navarro Tovar, A. G.; Hilario de la Cruz, A. A.; González Sánchez, L. F.; García Trejo, J. H.; Espinoza Muñoz, J. F.; Sangermano, M. *Journal of Polymer Research* **2014**, *21*, 1.
(23) Nuyken, O.; Pask, S. *Polymers* **2013**, *5*, 361.
(24) Wiesbrock, F.; Hoogenboom, R.; Leenen, M. A. M.; Meier, M. A. R.; Schubert, U. S. *Macromolecules* **2005**, *38*, 5025.
(25) Hoogenboom, R.; Wiesbrock, F.; Huang, H.; Leenen, M. A. M.; Thijs, H. M. L.; van Nispen, S. F. G. M.; van der Loop, M.; Fustin, C.-A.; Jonas, A. M.; Gohy, J.-F.; Schubert, U. S. *Macromolecules* **2006**, *39*, 4719.
(26) Kempe, K.; Neuwirth, T.; Czaplewska, J.; Gottschaldt, M.; Hoogenboom, R.; Schubert, U. S. *Polymer Chemistry* **2011**, *2*, 1737.
(27) Gress, A.; Völkel, A.; Schlaad, H. *Macromolecules* **2007**, *40*, 7928.
(28) Lambermont-Thijs, H. M. L.; Hoogenboom, R.; Fustin, C.-A.; Bomal-D'Haese, C.; Gohy, J.-F.; Schubert, U. S. *Journal of Polymer Science Part A: Polymer Chemistry* **2009**, *47*, 515.
(29) Jaksch, S.; Schulz, A.; Kyriakos, K.; Zhang, J.; Grillo, I.; Pipich, V.; Jordan, R.; Papadakis, C. M. *Colloid and Polymer Science* **2014**, *292*, 2413.
(30) Weber, C.; Becer, C. R.; Hoogenboom, R.; Schubert, U. S. *Macromolecules* **2009**, *42*, 2965.
(31) Ghazarian, H.; Idoni, B.; Oppenheimer, S. B. *Acta histochemica* **2011**, *113*, 236.
(32) Kumar, K.; Chandra, K.; Sumanthi, J.; Reddy, G.; Shekar, P.; Reddy, B. *Journal of Orofacial Sciences* **2012**, *4*, 20.
(33) Cairo, C. W.; Gestwicki, J. E.; Kanai, M.; Kiessling, L. L. *Journal of the American Chemical Society* **2002**, *124*, 1615.
(34) Cortez, M. A.; Grayson, S. M. *Macromolecules* **2010**, *43*, 4081.

# Chapter 6 Overview and Prospect

The synthesis of the various well-defined glyco-polymer/particle architectures and their interaction with corresponding lectins for different biorelated applications such as drug delivery purposes, biomaterials, bio- and nanotechnologies and gene therapy were highlighted. Very recent and elegant synthetic routes have allowed polymer chemists to prepare a wide range of glyco-polymers/particles that show really excellent and significant recognition properties towards lectins. These novel methodologies for synthesizing and studying well-defined glycopolymers have a potential for future investigations to enhance their unique recognition properties and develop therapeutic agents and biological probes. It is likely that a forthcoming close interdisciplinary collaboration between glycol-polymer/particle synthesis and the medical/pharmaceutical research area for therapeutic purposes and for many more bio-related devices.

Amphiphilic block glycocopolymers with optimal molecular weights and relatively narrow molecular weight distributions were synthesized *via* SET-LRP to prepare different glyconanostructures. These synthesized amphiphilic glycopolymers with the same number of mannose units self-assembled in water to generate glyconanoparticles with different morphologies such as spherical and worm-like micelles as well as spherical vesicles. Moreover, the obtained glyconanoparticles can be potentially utilized in biological applications.

Functional glycopolymers were synthesized by using RAFT polymerization to develop combined nanoplatforms involving both polymer-coated gold nanoparticles and an anti-cancer drug doxorubicin *via* creating a pH-sensitive hydrazone linkage in the presence of cysteine and a cross-linker. The obtained gold-glycopolymer-Cys-DOX particles have shown a sustained drug release in the simulated extracellular matrix conditions by differentiating the pH to prove the pH-sensitive property of gold-glycopolymer-Cys-DOX conjugations.

Well-defined triblock co-glycopolymers bearing β-CD and adamantane for the host-quest interaction and also mannose residues for the interaction with lectins were synthesized via RAFT polymerization. The single-chain folding structures were

achieved in very high diluted aqueous solution. The sufficient control was obtained for the conformation of glycopolymers. The binding results showed that these single-chain folded structures enhanced greatly the multivalent interaction.

Glyco copoly(oxazoline)s containing different glucose substituents alkyl linker length to the polymer backbones were synthesized via cationic ring opening polymerization successfully. A simple, one-pot, easy and versatile synthetic strategy was firstly described to prepare a new S-glucosyl substituted 2-oxazoline glycomonomer via thiol-ene “click” chemistry without any rigorous and intensive purification. A systematical study of the cloud points and binding capabilities of the obtained glyco copoly(oxazoline)s showed that the length of linker space has a significant effect on both properties.

The development of carbohydrate-based systems can open a new avenue to create more complex scaffolds that exhibit excellent and significant recognition properties towards lectins. The multivalent lectin-carbohydrate interactions could be succeeded by the integration of biologically significant carbohydrates into more complex materials to develop versatile functions and the medical or pharmaceutical applications.